Distributed Hybrid Quantum Computing

PhD Thesis, The Graduate University for Advanced studies

Author:
Sebastien G.R. Louis

Supervisor:
Prof. Kae Nemoto

October 28, 2008

Abstract

There are numerous proposals for the physical realization of a quantum computer. However, distributed approaches, making use both of flying and stationary qubits, seem to constitute the most promising route towards a truly scalable device. Such systems guarantee extendibility, they incorporate the interface with communication applications and relax the physical realization of the device, allowing for defect tolerance. Flying qubits are included in the more general concept of a quantum bus, a mediating system which can be of higher dimension. Such a quantum bus can be used in the straightforward preparation of a standard multi-qubit resource enabling measurement based quantum computation, the cluster state. This constitutes the framework for the results presented in this thesis.

We begin by investigating the effects of dissipation in the continuous variable bus scheme known as the qubus scheme. By considering loss in the bus as it mediates interactions between the stationary qubits, we obtain analytical results for the effective action of the induced quantum gate. We find that a particular two-qubit gate operates with high fidelity in the presence of moderate loss and give a simple iteration scheme to simplify the effects of loss on the qubits. We then attempt to reduce these effects by preparing the bus in more elaborate state, however no improvements are observed.

We then apply the qubus scheme to the probabilistic generation of cluster states and develop an entangling gate working with high success probability. This allows us to produce cluster states far more efficiently than other proposals. Investigating new methods to analyze the performance of different generation strategies constitutes the second part of this set of results. We begin by making the large flow approximation, used in queuing theory, to obtain the optimal strategy in a regime with large resources. After what we take the other more familiar limit of single cluster growth and introduce absorbing Markov chains as a key mathematical tool.

Finally we look at the transmission of composite quantum systems via a single higher dimensional bus. We provide generalized protocols and interactions guaranteeing a full transfer of the information from one composite system to another. These protocols can also serve information processing tasks, as useful logical operations can be applied to the data as it is transfered. We notice lastly that the qubus scheme constitutes a potential physical realization.

Publications

Journal Articles

- Sebastien G. R. Louis, Kae Nemoto, W. J. Munro, and T. P. Spiller, *Weak nonlinearities and cluster states*, Physical Review A **75**, 042323 (5 pages, 2007).
- Sebastien G. R. Louis, Kae Nemoto, W. J. Munro, and T. P. Spiller, *The efficiencies of generating cluster states with weak nonlinearities*, New Journal of Physics **9**, 193 (20 pages, 2007).
- Sebastien G. R. Louis, W. J. Munro, T. P. Spiller, and Kae Nemoto, *Loss in hybrid qubit-bus couplings and gates*, Physical Review A **78**, 022326 (11 pages, 2008).
- W. J. Munro, R. Van Meter, Sebastien G. R. Louis, and Kae Nemoto, *High-bandwidth hybrid quantum repeater*, Phys. Rev. Lett. **101**, 040502 (4 pages, 2008).
- Sebastien G. R. Louis, Andrew D. Greentree, W. J. Munro and Kae Nemoto, *Teleportation of composite systems for communication and information processing*, accepted for publication in the journal for Quantum Information and Computation, available on arxiv.org, quant-ph/0803.1342 (15 pages, 2008).

Conference Proceedings

- Sebastien G. R. Louis, Kae Nemoto, W. J. Munro and T. P. Spiller, *The efficiencies of building cluster states with weak-nonlinearities*, Proceedings of the 8th International Conference on Quantum Communication, Measurement and Computing (4 pages, 2007).
- W. J. Munro, Samuel L. Braunstein, T. D. Ladd, Sebastien G.R. Louis, G. J. Milburn, C. R. Myers, Kae Nemoto, Marcus Silva, T. P. Spiller, R. Van Meter, P. van Loock and Y. Yamamoto, *Qubus Computation*, Proceedings of the 8th International Conference on Quantum Communication, Measurement and Computing (6 pages, 2007).

Acknowledgements

First I would like to thank my supervisor Kae Nemoto for giving me the opportunity to come and do my PhD thesis here in Tokyo, generously supported by the Japanese government with a Monbukagakusho scholarship. Professor Nemoto's patience, support, careful and thought-provoking guidance have permitted me to grow in my research and pursue my own interests.

I am deeply grateful to Bill Munro for his constant encouragement. He has been an inspiration through time and together with Tim Spiller whom I also thank, has invited me for stimulating studentship visits in their Quantum Information Processing group at Hewlett-Packard Laboratories in Bristol.

I thank Tokishiro Karasawa, Peter van Loock, Rod van Meter, Casey Myers, Simon Devitt, Todd Tilma and Jun Suzuki in the QIST group here at NII, for valuable support and discussions. I also acknowledge the hard work of Yukiko Nakano who helps us organize our trips and our funding.

I am grateful to Andrew Greentree for his infectious enthusiasm and to Norbert Lütkenhaus for his receptiveness and wit, which led to stimulating interactions. Both of their collaborations have played a significant role in developing what now makes up the contents of my thesis.

I would like to thank Mio Murao for her kind support and advice, and for allowing me to partake in enlightening activities with her Quantum Information group at the University of Tokyo. I acknowledge the highly informative quantum information and computation lectures given by Keiji Matsumoto here at the Graduate University for Advanced Studies.

I am grateful to Sandu Popescu without whom I wouldn't be where I stand now. His enthrawling fascination for the world we live in triggered my interest in the field and first conveyed to me the excitement involved in research and discovery. His conceptual openness will always be an inspiration.

For useful discussions and interactions during the course of my PhD I thank Peter Rohde, Thaddeus Ladd, Jens Eisert, Konrad Kieling, Krishna Dovzhik, Julian Grond, Pieter Kok, Radu Ionicioiu, Anthony Chefles, Chun-Hsu Su, Marcus Silva, Patrick Leung, Dimitris Tsomokos, Yoshihisa Yamamoto, Rob Thew, Christian Sommer and Sebastien Duval.

I thank Alex, Juan, Andre, Albert and Carl for their unshakable friendship throughout my student years.

I am grateful to my parents Janet and Patrick and my precious sister Krystelle, for their love and support since my early days. I would also like

to thank my grandmother Sylvia for her invariant care and her memorable pasties, as well as my grandfather Roland and his companion Andrée for bringing me countless smiles, laughs and delicious 'tartes aux pommes'.

I will always be grateful to Ogawa-san ('oniisan') for his precious friendship and rare frankness.

Finally I want to thank my beloved Marvia with all my heart. Her unconditional love has provided me with a secure footing through this journey. Her understanding and advice have been crucial both to this work and to my personal growth.

Contents

Chapter 1

Introduction

1.1 Historical background

Understanding the context in which quantum information and computation arose requires us to look at the different fields which contributed to its development.

A good starting point is the field of physics and its state at the end of the 19th century. At this point in time, physicists were confronted with different phenomena observed experimentally, lacking an explanation based on the known theories of gravitation, thermodynamics and electromagnetism. One such phenomenon was black-body radiation. The problem was initiated in 1858, when Kirchhoff showed that the energy emitted from a black body (an object that absorbs all the light that falls upon it, reflecting none and thus appearing black to an observer when cold) depended solely on the temperature T of that body and the wavelength $\lambda = 2\pi/\omega$ of the emitted radiation. He challenged the physicists of the time to find the mathematical expression characterizing this emission spectrum. In the following two decades, a fourth power dependence on temperature T^4 of the spectrum was proposed. First by Stefan on experimental grounds and then by Boltzmann from theoretical considerations based on Maxwell's theory of electromagnetism. The result known as the Stefan-Boltzmann law did not however provide a full characterization of the spectrum at all wavelengths. A subsequent expression by Wien matched the experimental data well but only for small wavelengths. The problem subsided until 1900 when Planck wrote down his expression, now know as Planck's law of black-body radiation, fitting experimental data at all wavelengths [1]. In order to arrive at this result, Planck assumed that the total energy was made up of indistinguish-

able elements - quanta of energy $\hbar\omega$ (where $\hbar$ is Planck's constant) - thus discretizing for the first time a physical quantity and going against the wave nature of light as defined by Maxwell's theory. This brilliant result earned him the Nobel Prize for physics in 1918.

Another set of experimental observations which didn't fit with the electromagnetic theory of the time came from the photoelectric effect. This physical process consists in electrons being emitted from matter through the absorption of energy from electromagnetic radiation. In 1905, inspired by Planck's work, Einstein postulated that light itself consisted of individual quanta (now known as photons), to successfully characterize the photoelectric effect [2], more precisely to account for the fact that energy of the emitted electrons does not depend on the intensity of the incoming light, but on the energy (frequency) of the individual photons. He was in turn awarded the 1921 physics Nobel Prize for this experimentally verified theory which now further concretised the wave-particle duality of light, displaying both wave-like and particle-like properties. This result, combined with the quantum theory of the atom proposed by Bohr in 1913 [3, 4] to overcome the problematic classical definition of electron orbitals triggered the rapid development of a full blown quantum theory of light and matter. Some initial elements of this development were the extension to all particles of the wave-particle duality by de Broglie [5] and the exclusion principle stated by Pauli providing theoretical foundations to the periodic table. Heisenberg then derived a matrix mechanics formulation of quantum theory [6] before Schrödinger gave an equivalent wave-mechanical formulation [7]. Finally special relativity was brought into the quantum picture by Dirac, providing a relativistic quantum theory of the electron [8]. From quantum mechanics was later born the field of quantum electro-dynamics (QED), the most accurately verified physical theory of all times.

The above physicists and their discoveries are part of what constituted a great scientific revolution, in which many familiar concepts about Nature were overturned. The rules of quantum mechanics are hard, if not impossible, to grasp intuitively. Wave-particle duality is one of them, best illustrated by Young's double slit experiment. Interference effects have been observed for various particles and even large molecules such as C_{60} [9], no matter how small the intensity of the incoming beam. This means that particles can interfere with themselves although at the time of the measurement, when they hit the screen, they are localized. Trying to check which slit each particle comes through will in turn destroy the interference pattern. These observations are accounted for by the wave function. This wave function which fully characterizes a physical system, contains complex

probability amplitudes, leading to interference effects. From them we can obtain the probabilities of finding the system at different locations. Once we physically measure where the system is, the wave function collapses to a particular location with a certain probability, yielding a localization of the system. However the interpretation of the quantum measurement has been an open question ever since the rules were written down. The intrinsically probabilistic aspect of the wave function representation in quantum mechanics is also hard to accept; no matter how much we know about a physical system, there are circumstances in which we can only assign probabilities to different outcomes. In other words determinism cannot hold any longer.

One consequence of these single system properties is the possibility for nonlocal correlations to arise when we move to composite systems. This was first pointed out by Einstein, Podolsky and Rosen in their famous 1935 paper [10]. The thought experiment they conducted is now known as the EPR paradox and underlines a 'spooky action at a distance', which refutes the principle of locality they proposed. Attempts at resolving the paradox through locally hidden variables (shared randomness which we do not have access to) were cut short when a lot later in 1964, Bell showed very elegantly that no hidden variable theory could possibly reproduce the measurement statistics predicted by quantum theory [11]. Since then many experiments have verified these predictions, the most famous of which were led by Aspect and collaborators in the 1980s [12]. We will leave the field of quantum physics at this exciting point before returning to it later, to quickly outline the progress in another all important field of the 20th century.

Modern computer science was initiated by Turing in 1936, when he defined an abstract machine, now referred to the Turing Machine, which performs algorithmic tasks in a very general way, providing a model for computing [13]. He also conceptualized at the time a Universal Turing Machine (UTM), capable of simulating any other Turing machine. This was formulated more rigorously in joint work with a mathematician to the name of Church, becoming the Church-Turing thesis. The thesis states that given an algorithm being run on any form of hardware, there always exists an equivalent algorithm completing the same task on a UTM. In the 1940s, two great minds focused their attention on computation and information. One was von Neumann who created the field of cellular automata [14], but more to the point proposed a computer architecture [15] in which data and program memory are mapped into the same address space. This architecture is widely used today. The other great mind was Shannon who defined communication in a mathematical context, producing the two fundamental noiseless and noisy channel coding theorems [16], the latter setting the maximum

attainable efficiency of an error-correcting scheme. These vital theoretical advances were accompanied by the development of hardware systems, in particular the creation of the transistor in 1947 by Bardeen, Brattain and Shockley. Since then the processing power of computers hasn't ceased to increase, deeply affecting society and tremendously amplifying scientific progress.

The growth in processing power of devices successfully projected by Moore in 1965 [17], leads us to the first factor that triggered the field of quantum computation. Moore's law states that the number of transistors that can inexpensively be placed on an integrated circuit is increasing exponentially, doubling approximately every two years. However this exponential growth in power is not sustainable, as eventually the components will reach the scale of the atom, at which quantum mechanical effects come into the picture, making them inoperable in a classical sense. Another version of Moore's law illustrating this point is that the number of electrons contained in each memory element will halve every two years, eventually reaching the single electron regime. In addition to this there is the financial cost, which depending on the technological advances may blow up once we reach a certain scale. In any case, at this point there are two options. One is to develop a whole arsenal of techniques to fight quantum effects and preserve the information in the classical form of bits. The other is to use quantum effects to process information, that is to encode the information in quantum systems which we let behave in a quantum fashion. This direction had already started to be paved in the 1970s by physicists who managed little by little to isolate single quantum systems and observe their behavior. Here quantum physics comes back into our picture.

This triggering factor arose from a technological challenge lying ahead, however there was also a shift of mindset amongst physicists. They had been struggling with the interpretation of quantum mechanical rules for decades and now some of them decided to just accept those rules and see what interesting things could be done in this new framework. Illustrating this line of thought, Feynman asked in 1986 [18] whether it would be possible to efficiently simulate quantum systems on a classical computer. It is believed that the answer is negative although there is no rigorous proof of the conjecture. He also pointed out that in contrast, an information processor using quantum effects may be able to efficiently do this simulation. The observation was later shown to be true by Lloyd [19] and represents one of the strongest incentives to the realization of quantum information processing (QIP) devices. Such a technology could potentially accelerate other areas of scientific research would accelerate progress in all kinds of fields across

medical, chemical and life sciences.

At the same time as Feynman made his observations, Deutsch tried to understand and extend the Church-Turing thesis from a physical point of view. In so doing he was led to consider quantum theory and defined a Universal Quantum Computer [20], providing an even more powerful computational model. The units of memory in this computer are quantum bits (qubits). In 1992, in collaboration with Jozsa, he devised a quantum algorithm [21] to estimate whether a given function is constant (returns 0 on all inputs or 1 on all inputs) or balanced (returns 1 for half of the inputs and 0 for the other half). Although initially this algorithm was of little use, it showed very simply how some tasks could be realized more efficiently on a quantum computer. The algorithm was rapidly generalized and a couple of years later inspired one of the central breakthroughs of the field. In 1994, Shor revealed two quantum algorithms [22] efficiently solving important problems for which no efficient classical algorithm has been found. The first one consists in finding the prime factors of an integer and the second is referred to as the discrete logarithm problem. These results were followed by a search algorithm devised by Grover in 1995 [23], which provides a quadratic speedup over known classical algorithms.

Advances in quantum computing were accompanied by equally important developments in quantum communication. The concept of quantum cryptography goes all the way back to the 1960s and Stephen Wiesner. However the first result to be accepted was only proposed in 1984 by Charles Bennett and Gilles Brassard [24]. They constructed a communication protocol using quantum systems with which two parties, commonly known as Alice and Bob, can generate a shared random bit string only known by them, without the possibility of an eavesdropper gaining any information. This bit string constitutes a one time pad with which Alice and Bob can communicate securely over a public channel. It is worth noting here that some classical public key ciphers, including the algorithm developed by Rivest, Shamir and Adleman (RSA), rely on the hardness to factor large integers. Quantum key distributions in contrast is in theory 100% secure, independent of the eavesdroppers information processing power. The use of the nonlocal correlations mentioned earlier was made clear first in 1992 when Bennett and Wiesner invented superdense coding [25]. In this protocol, Alice and Bob can communicate two bits of information while only transmitting one qubit. Then in 1993 these correlations were employed in a famous theoretical scheme to teleport (transmit via quantum correlations and classical information) an unknown quantum state [26].

Quantum teleportation and quantum key distribution have since then

been implemented experimentally using single photons and even single atoms. There are already commercial quantum cryptography devices being sold and fabrication costs will rapidly decrease. However skeptics at the time of the theoretical breakthroughs in QIP may have judged the physical realization of a quantum computer to be fundamentally limited by the presence of noise. This argument was overcome in 1995 at which point Shor [27], Andrew Steane [28], and Robert Calderbank [29] initiated the field of quantum error correction by providing the first quantum error correction codes. These results comforted scientists in their search for a physical realization of a quantum computer. They include ion traps [30], nuclear magnetic resonance [31], quantum dots [32], silicon based implementations [33] and linear optical implementations [34]. Many experiments have been undertaken in which single qubit control or few qubit controlled interactions were realized. Scaling up these few qubit achievements is one of the main challenges of the exciting field of quantum computation and information. Along with physical realizations, research is stretching out in many directions, from quantum complexity theory to the foundations of quantum physics.

1.2 Motivation and outline

As just mentioned, the field focusing on the implementation of quantum computing is at a crucial point. Many different physical realizations have been proposed but we are still lacking a truly scalable approach. Distributed architectures, in which qubits communicate via a shared quantum bus or mediating system, seem to be the most promising. They insure well isolated memory regions with low decoherence, allowing for straightforward extendibility of the processor. Another key feature of this approach is that the interface with communication applications is incorporated into the processor and does not constitute an extra technological challenge. Distributed architectures are also compatible with the measurement-based model of quantum computing, a powerful model relying solely on the gradual measurement of a multi-qubit state (cluster state), which relaxes several implementation constraints. The results obtained in this thesis lie within this framework of quantum buses and cluster states. They are organized as follows.

In chapter two we provide an overall background study of the fields relevant to the work presented. The first section of this chapter introduces the mathematical framework of quantum mechanics, presenting the notion of quantum information and underlining some striking features of the theory itself. With these tools in hand we describe two different models for

quantum computing, the circuit and measurement-based models. The next section focuses on quantum optics, starting from the quantization of the classical theory and ending with irreversible processes. Along the way we also consider light-matter interactions. These two sections lead naturally to an overview of optical quantum computing. The final section of this background chapter introduces the continuous variable quantum bus (qubus) and it's applications. This scheme constitutes one of the main tools in the results to be presented.

Chapter three marks the beginning of the original work with an investigation into the effects of bus loss on qubus gates. We first characterize loss during the interaction between the continuous variable bus and a discrete subsystem. The we proceed to adding loss in between interactions with different subsystems so as to fully characterize the impact on logical gates themselves. Having understood the process by which the subsystems undergo decoherence we propose a bus engineering scheme so as to boost the fidelity of a particular logical gate.

In the first section of chapter four we provide some results on the generation of cluster states using the qubus scheme. Achieving a higher logical gate efficiency enables us to achieve true scalability in the generation of cluster states and makes it possible for us to consider new growth strategies. In the second section we introduce two frameworks in which to characterize the growth of cluster states via probabilistic logical gates. The first one makes a flow approximation of the resources, converting the problem of finding the optimal strategy into a simple linear programming problem. The second introduces the concept of absorbing Markov chains to calculate production rates and compare a range of different strategies.

The fifth and last chapter of the thesis goes over some work involving the transfer of information held by composite systems via a single higher dimensional bus. We propose two protocols and find interactions allowing a deterministic transfer of the information. The protocols can then serve data transfer as well as QIP roles.

Chapter 2

Background

2.1 Quantum information and computation

In this chapter we introduce some basic concepts in quantum information and computation. To do so we first go over the mathematical framework of quantum theory by recounting the so called postulates of quantum mechanics. This will provide us with the tools necessary to understand the main ideas involved in quantum computation. Two different models are then introduced, the circuit model and the cluster state model. There are other models such as adiabatic or topological quantum computing which we do not consider here. Interested readers can find good reviews on these in [35, 36].

2.1.1 Quantum states, measurements and evolution

All the results in different branches of quantum theory have their roots in a set of fundamental postulates. We will go over them so as to provide the basic tools needed in the present work. The first postulate of quantum mechanics states that any quantum system corresponds to a Hilbert space $\mathcal{H}$ and that any state of an isolated system (without any correlation to other systems) can be represented by a unit vector in this Hilbert space. This unit vector is referred to as the state vector and in the simplest case of a two-dimensional Hilbert space can be written in the orthonormal basis $\{|0\rangle, |1\rangle\}$ as

$$|\psi\rangle = c_0|0\rangle + c_1|1\rangle. \tag{2.1}$$

Here we are using the Dirac notation [37], where the 'bra' $\langle\psi|$ in dual space, represents the conjugate transpose of the the 'ket' $|\psi\rangle$. For $|\psi\rangle$ to be a unit

vector we require

$$\langle\psi|\psi\rangle = (c_0^*, c_1^*).\begin{pmatrix} c_0 \\ c_1 \end{pmatrix} = |c_0|^2 + |c_1|^2 = 1. \tag{2.2}$$

Thus the inner product defined on the Hilbert space, between two states $\langle\psi|\phi\rangle$, maps an ordered pair of vectors to a complex number. It is often referred to as the overlap between a pair of quantum states. This two dimensional state $|\psi\rangle$ constitutes the most fundamental unit in quantum information, the qubit. Unlike its classical analogue, the bit, a qubit can be in a coherent superposition of two binary states. Being in a superposition where $|c_0|, |c_1| > 0$, it is not possible to say whether the qubit is in state $|0\rangle$ or in state $|1\rangle$ with certainty, as it is fully characterized by $|\psi\rangle$. This is to be contrasted with a classical uncertainty and will become clearer as we go on. Now extending the size of the Hilbert space to d dimensions, we obtain what is called a qudit

$$|\psi\rangle = \sum_{n=0}^{d-1} c_n|n\rangle, \text{ with } \langle\psi|\psi\rangle = \sum_{n=0}^{d-1} |c_n|^2 = 1. \tag{2.3}$$

Such states are also of interest to quantum information applications and qubits are often obtained experimentally by restricting ourselves to the dynamics of a subspace of a higher dimensional system.

Having defined the representation of quantum states we move on to another postulate of quantum mechanics, that of observables and measurements. An observable is a property of a system that can be observed and in quantum mechanics it takes the form of a Hermitian operator acting on the state space of the system. It is convenient to define a linear operator via the outer-product, for example the rank-one operator $M = |\phi\rangle\langle\varphi|$, mapping state vectors to state vectors as $M|\psi\rangle = \langle\varphi|\psi\rangle|\phi\rangle$ with $|\psi\rangle$,$|\phi\rangle$,$|\varphi\rangle \in \mathcal{H}$. For an operator M to be Hermitian means that it is self-adjoint $M^\dagger = M$. All self adjoint operators in Hilbert space have a spectral decomposition

$$M = \sum_n a_n A_n, \tag{2.4}$$

where a_n are eigenvalues of the operator M and A_n is the corresponding orthogonal projection on onto all eigenstates with eigenvalue a_n. If the eigenvalues are non-degenerate then the A_n become projectors $|n\rangle\langle n|$ where $|n\rangle$ is an eigenvector with eigenvalue a_n. Given a state $|\psi\rangle$, the probability of obtaining the result a_n when measuring M precisely is given by

$$p(a_n) = \langle\psi|A_n|\psi\rangle, \tag{2.5}$$

and the state of the system right after this particular measurement outcome is

$$|\psi\rangle \overset{a_n}{\rightarrow} \frac{A_n|\psi\rangle}{\sqrt{\langle\psi|A_n|\psi\rangle}}. \tag{2.6}$$

We note here that $|\psi\rangle$ and $e^{i\lambda}|\psi\rangle$ represent the same physical state as they cannot be distinguished, with $|e^{i\lambda}| = 1$ representing a global phase. The A_n projectors satisfy $\sum_n A_n^\dagger A_n = I$ as a consequence of normalization, where I is the identity operator. They are orthogonal following $A_n A_m = \delta_{nm} A_n$ and Hermitian $A_n = A_n^\dagger$. Now the average result of the measurement can simply be written as

$$\langle M\rangle = \sum_n a_n p(a_n) = \langle\psi|M|\psi\rangle. \tag{2.7}$$

To illustrate these expressions, let us come back to our qubit $|\psi\rangle = c_0|0\rangle + c_1|1\rangle$ and measure the valid observable $M = |0\rangle\langle 0| - |1\rangle\langle 1|$, where we identify $A_0 = |0\rangle\langle 0|$ and $A_1 = |1\rangle\langle 1|$ with associated eigenvalues $a_0 = 1$ and $a_1 = -1$. This corresponds to a measurement in the computational basis $\{|0\rangle, |1\rangle\}$. The probability of measuring the qubit in the state $|0\rangle$ is given by $\langle\psi|0\rangle\langle 0|\psi\rangle = |a_0|^2$ and similarly measuring it in the state $|1\rangle$, corresponding to the eigenvalue -1, is $|a_1|^2$. Now we see how the modulus squared of the probability amplitudes c_0 and c_1 give rise to the actual probabilities of finding the qubit in either state. Setting $c_0 = c_1 = 1/\sqrt{2}$ yields an average measurement outcome $\langle\psi|M|\psi\rangle = 0$, meaning that there is a 50% chance of finding the qubit in either state. There are more general forms of measurements but projective measurements will be sufficient for the work presented herein.

In addition to measurements, the axioms of quantum mechanics tell us that quantum systems evolve unitarily in time. The statement can be arrived to through the Schrödinger equation describing the time evolution of a closed quantum system

$$i\hbar\frac{\partial|\psi(t)\rangle}{\partial t} = H|\psi(t)\rangle, \tag{2.8}$$

where H is the Hamiltonian of the closed system and $\hbar$ is Planck's constant, as we saw in the introduction. Taking an infinitesimal time step dt,the above equation becomes

$$|\psi(t+dt)\rangle = (1 - \frac{i}{\hbar}Hdt)|\psi(t)\rangle. \tag{2.9}$$

Now identifying the operator $U(dt) = 1 - \frac{i}{\hbar}Hdt$, we find that it is unitary ($U^\dagger U = 1$) to linear order in dt because H is Hermitian ($H^\dagger = H$), corresponding to the total energy. Thus the quantum state of a system at a given time t is related to the state at an earlier time $t = 0$ by a unitary operator U such that

$$|\psi(t)\rangle = U(t)|\psi(0)\rangle. \tag{2.10}$$

In the case that the Hamiltonian is time independent, we have $U = e^{-iHt/\hbar}$. One fascinating consequence of the last two postulates is that the evolution of a closed system is deterministic, as can be seen from Schrödinger's equation, while the measurement process and the collapse of the wave function is probabilistic. The interpretation of the quantum measurement is one of the many conceptual challenges posed by quantum theory.

The last postulate we have to consider is that of composite systems. It holds that the state space of a composite system is generated through the tensor product of the state spaces of the individual systems composing it. Thus supposing $\mathcal{H}_A$ is the Hilbert space of system A and $\mathcal{H}_B$ the Hilbert space of system B, then the Hilbert space of the composite system is given by $\mathcal{H}_A \otimes \mathcal{H}_B$. Taking the example of two qubits $|\psi\rangle_A = c_0|0\rangle_A + c_1|1\rangle_A$ and $|\psi\rangle_B = d_0|0\rangle_B + d_1|1\rangle_B$, with $|\psi\rangle_A \in \mathcal{H}_A$ and $|\psi\rangle_B \in \mathcal{H}_B$, the state of the combined system is

$$\begin{aligned} |\psi\rangle_{AB} = |\psi\rangle_A \otimes |\psi\rangle_B &= c_0 d_0 |0\rangle_A \otimes |0\rangle_B + c_0 d_1 |0\rangle_A \otimes |1\rangle_B \\ &+ c_1 d_0 |1\rangle_A \otimes |0\rangle_B + c_1 d_1 |1\rangle_A \otimes |1\rangle_B. \end{aligned} \tag{2.11}$$

When the combined state of two systems cannot be written in the tensor product form $|\psi\rangle_A \otimes |\phi\rangle_B$, we call them inseparable or entangled. The two systems exhibit quantum correlations. For example the state $c|0\rangle_A \otimes |0\rangle_B + d|1\rangle_A \otimes |1\rangle_B$ is clearly entangled for $c, d \neq 0$. This is the type of state Einstein and his collaborators alluded to in the EPR paradox and we will see that they are a very useful resource for quantum communication and computation. It is also important to note that any operator M acting on the Hilbert space of system A is identified by $M \otimes I$ on $\mathcal{H}_A \otimes \mathcal{H}_B$, where I corresponds to the identity. From now on we will only use the tensor product symbol when clarity is needed but will omit it otherwise.

So far we have only discussed pure states, states which only exhibit coherent superposition. However the probability amplitudes arising from these states are, as I announced earlier, different from classical probabilities. That is we may be given one of two pure states with a certain probability, representing an incoherent superposition. Characterizing the resulting state requires the density matrix (or equivalently density operator) representation.

2.1.2 The density matrix

Let us suppose that a quantum system is in one of a number of pure state $|\psi_i\rangle$ with a certain probability p_i associated to each one. The state of that system now consists in a statistical ensemble of pure states $\{p_i, |\psi_i\rangle\}$ and the density operator has the form

$$\rho = \sum_i p_i |\psi_i\rangle\langle\psi_i|, \tag{2.12}$$

with $\sum_i p_i = 1$ (meaning $\mathrm{tr}[\rho] = 1$). As ρ is a Hermitian matrix, it can always be diagonalized such that $\langle\psi_i|\psi_j\rangle = \delta_{ij}$. If the state is pure, there is only one term in the summation so $\rho^2 = \rho$ and $\mathrm{tr}[\rho^2] = 1$. If there is more than a single term in the above summation then we call the state mixed. For a mixed state $\rho^2 \neq \rho$ and $\mathrm{tr}[\rho^2] = \sum_i p_i^2 < 1$.

Measurement in the density matrix representation can be understood by looking back at expression (2.5) and using the fact that $\langle\psi_i|A_n|\psi_i\rangle = \mathrm{tr}[A_n|\psi_i\rangle\langle\psi_i|]$ to obtain the average over the different pure states

$$p(a_n) = \mathrm{tr}[A_n\rho]. \tag{2.13}$$

The density operator after the above measurement then becomes

$$\rho \xrightarrow{a_n} \frac{A_n\rho A_n}{\mathrm{tr}[A_n\rho]}. \tag{2.14}$$

It is also possible to obtain the evolution of a mixed state from the evolution of each one of the possible pure states $|\psi_i(t)\rangle = U(t)|\psi_i(0)\rangle$ such that

$$\rho(t) = U(t)\rho(0)U^\dagger(t). \tag{2.15}$$

The density matrix is very useful when dealing with a composite system, as one can define a reduced density matrix for each subsystem. For example in the case of a bipartite system represented by ρ^{AB} we have

$$\rho^A = \mathrm{tr}_B[\rho^{AB}], \tag{2.16}$$

where tr_B is the partial trace over system B. This reduced density operator provides us with the measurement statistics for subsystem A alone. As for pure states, the ability to write the composite system density operator in the form $\rho^{AB} = \rho^A \otimes \rho^B$ means that the two systems are separable. In that case $\mathrm{tr}_B[\rho^{AB}] = \rho^A$ simply, meaning that the measurement statistics of A and B do not contain quantum correlations. However if we take an entangled state of the form $|\psi\rangle_{AB} = c|0\rangle_A|0\rangle_B + d|1\rangle_A|1\rangle_B$, tracing out system B leads to

$$\rho^A = \mathrm{tr}_B[\rho^{AB}] = \mathrm{tr}_B[|\psi\rangle_{AB}\langle\psi|] = |c|^2|0\rangle_A\langle 0| + |d|^2|1\rangle_A\langle 1|. \tag{2.17}$$

What we observe is that even though the two qubit state is pure, the reduced states (in this case $\rho^A = \rho^B$) for each qubit are mixed: $\mathrm{tr}[\rho^A] = \mathrm{tr}[\rho^B] = |c|^4 + |d|^4 < 1$. That is we have full knowledge of the whole state but somehow we do not have full knowledge of the subsystems. This is again a striking feature of quantum mechanics and quantum correlations. For $|c|^2 = |d|^2 = 1/2$ we have what is referred to as a maximally entangled state of two qubits (such states were used by Bell in his work on non-locality and hidden variables), at which point the quantum correlations are strongest and at which point the reduced states of subsystems are maximally mixed.

Now that we have defined quantum systems, the measurement of observables and unitary evolution, we can move on to the basic concepts of QIP in the circuit model.

2.1.3 The circuit model of quantum information processing

The Hilbert space of a quantum computer containing n qubits is spanned by 2^N vectors each holding a complex amplitude. For moderate n, following all these amplitudes on a classical computer would not be conceivable. A quantum computer holds all of them simultaneously because of the ability of the qubits to be in coherent superpositions. However Alexander Holevo [38] showed in the early days of quantum information theory that one cannot extract more than n bits of information from n qubits. The result is known as the Holevo bound. Given this fact, the challenge of quantum computation is to extract useful information or global information, through interference effects taking place at the level of the amplitudes.

The execution of an algorithm on a quantum computer in the circuit model consists in three phases (see Fig. 2.1). In the first the qubits (the input register) are initialized in a particular state. The second phase consists in the execution of the algorithm which itself is a unitary operation over the whole set of qubits. This unitarity requirement means that the computation

has to be reversible. This is to be contrasted with classical computation in which irreversible gates are used such as the AND gate, whose inputs cannot be recovered given the output, meaning that information was lost. Another distinguishing feature is the impossibility to perfectly clone an unknown quantum state [39]. Finally the third phase is the measurement of the resulting qubit states (the output register) in a chosen orthonormal basis $\{|0\rangle, |1\rangle\}$, referred to as the computational basis.

The operation representing the algorithm may be decomposed into a set of individual operations or gates acting on subsets of the qubits only. A universal set of gates is a set to which any possible operation on a quantum computer can be reduced, meaning any unitary operation can be expressed as a finite sequence of gates from the set. There exists a variety of universal gate sets, containing single and two qubit gates, and even three qubit gates (see Fig. 2.1).

Single qubit operations are described by 2×2 unitary matrices, of which the Pauli matrices

$$X = \begin{pmatrix} 0 & 1 \\ 1 & 0 \end{pmatrix}, \qquad Y = \begin{pmatrix} 0 & -i \\ i & 0 \end{pmatrix}, \qquad Z = \begin{pmatrix} 1 & 0 \\ 0 & -1 \end{pmatrix}, \tag{2.18}$$

are particularly useful. The X operation can be assimilated to a bit flip gate acting as $X|j\rangle = |j \oplus 1\rangle$ (where $j = 0$, 1, and $\oplus$ represents the addition modulo two), switching one basis state to another. However the Z operation already has no classical analogue, flipping the sign of the basis states as $Z|j\rangle = (-1)^j|j\rangle$, generating a relative phase between basis states. The Y operation acts as a combination of the two $Y = iXZ$. Any unitary operation on a qubit can be parametrized (up to a global phase) by a three dimensional vector $\mathbf{n} = (n_x, n_y, n_z)$ and an angle θ, leading to a decomposition into Pauli matrices [40]

$$U(\mathbf{n}, \theta) = e^{-i\frac{\theta}{2}(n_x X + n_y Y + n_z Z)} = \cos\frac{\theta}{2} I - i\sin\frac{\theta}{2}(n_x X + n_y Y + n_z Z), \tag{2.19}$$

where we have used the fact that $X^2 = Y^2 = Z^2 = I$. Moreover any 2×2 unitary matrix is of the form $e^{i\gamma Z} e^{i\beta Y} e^{i\alpha X}$ up to a global irrelevant phase, meaning the ability to set the system Hamiltonian to X, Y and Z for fixed amounts of time enables one to implement arbitrary unitary operations on the qubit. This then provides us with the first element in our universal gate set. One of these gates which we will encounter corresponds to the Hadamard transformation

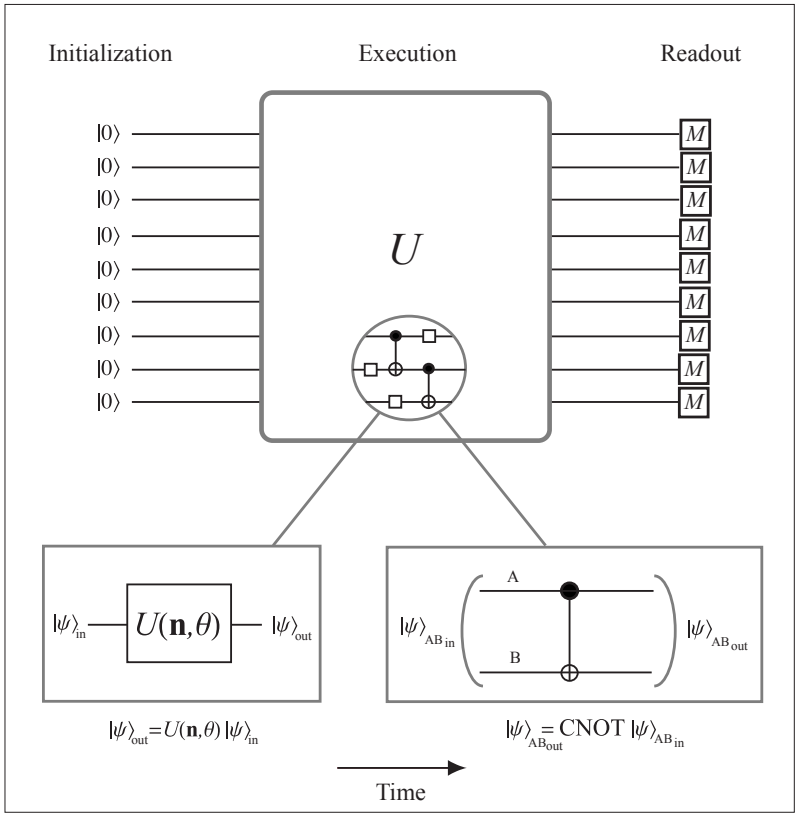

Figure 2.1: The three stages of a quantum computation in the circuit model. First the qubits are initialized in a standard state such as $|00...\rangle$. The algorithm, represented by a big unitary operation U over all qubits, is executed through a set of single and two qubit gates from a universal gate set. We have chosen here arbitrary single qubit operations and the two-qubit CNOT gate, as defined in the text. The final stage is the readout of the qubits to extract the classical information needed.

$$H = \frac{X+Z}{\sqrt{2}} = \frac{1}{\sqrt{2}} \begin{pmatrix} 1 & 1 \\ 1 & -1 \end{pmatrix}, \tag{2.20}$$

mapping the computational basis states to $H|j\rangle = (|0\rangle + (-1)^j|1\rangle)/\sqrt{2}$. We will be referring to this basis as the $|\pm\rangle$ basis, with $|\pm\rangle = (|0\rangle \pm |1\rangle)/\sqrt{2}$.

Now the CNOT gate acts on a pair qubits such that if the control qubit (A) is in the $|1\rangle$ state, the target qubit (B) is flipped (the X operator is applied to it)

$$\begin{aligned} & c_0|0\rangle_A|0\rangle_B + c_1|0\rangle_A|1\rangle_B + c_2|1\rangle_A|0\rangle_B + c_3|1\rangle_A|1\rangle_B \\ \overset{\text{CNOT}}{\rightarrow}\ & c_0|0\rangle_A|0\rangle_B + c_1|0\rangle_A|1\rangle_B + c_2|1\rangle_A|1\rangle_B + c_3|1\rangle_A|0\rangle_B. \end{aligned} \tag{2.21}$$

The corresponding matrix representation of the CNOT operation is

$$\text{CNOT} = \begin{pmatrix} 1 & 0 & 0 & 0 \\ 0 & 1 & 0 & 0 \\ 0 & 0 & 0 & 1 \\ 0 & 0 & 1 & 0 \end{pmatrix}. \tag{2.22}$$

We can also use projectors and write $\text{CNOT} = |0\rangle_A\langle 0| \otimes I_B + |1\rangle_A\langle 1| \otimes X_B$, allowing us to see that the gate is an instance of a more general conditional unitary gate $\text{CU} = |0\rangle_A\langle 0| \otimes I_B + |1\rangle_A\langle 1| \otimes U_B$. Another useful instance is the CZ gate in which $U = Z$ which acts on a two-qubit state as

$$\begin{aligned} & c_0|0\rangle_A|0\rangle_B + c_1|0\rangle_A|1\rangle_B + c_2|1\rangle_A|0\rangle_B + c_3|1\rangle_A|1\rangle_B \\ \overset{\text{CZ}}{\rightarrow}\ & c_0|0\rangle_A|0\rangle_B + c_1|0\rangle_A|1\rangle_B + c_2|1\rangle_A|0\rangle_B - c_3|1\rangle_A|1\rangle_B. \end{aligned} \tag{2.23}$$

Now we see that although this is a controlled unitary operation, there is no control and target qubit, it is symmetrical. It is worth pointing out that the CNOT gate is equivalent to the CZ gate up to Hadamard transformations on the target qubit before and after the gate.

Having described a universal set of gates for the circuit model of quantum computation, we will now move on to consider another very different model.

2.1.4 The cluster state model of quantum information processing

The cluster state model for quantum computation was first proposed in 2001 by Raussendorf and Briegel in a much acclaimed paper [41]. They showed

that a particular highly entangled multi-qubit state, the cluster state, combined with single qubit operations, feed forward and measurements are sufficient for universal quantum computation. A general graph state is prepared by first initializing all the qubit in the $|+\rangle$ state and then proceeding to apply CZ gates between pairs of neighboring qubits (see [42] for a detailed review). Then any regular two-dimensional lattice is a cluster state whose schematic representation is shown in Fig. 2.2. The quantum algorithm is specified by the measurements themselves, that is the basis in which the qubits are individually measured.

The input to the computation is represented by the qubits along one side of the lattice and the output qubits will become the qubits on the opposing side, once all the qubits in between have been measured out. The choice of basis of each measurement depends on previous measurement outcomes. Not all measurements can be made at once. To illustrate the basic workings of cluster state computing, we will consider a couple of simple examples simulating a quantum circuit. The first example will simulate a single qubit rotation and requires a two-quit cluster state see (Fig. 2.2)

$$\begin{aligned} |C2\rangle = \mathrm{CZ}|+\rangle_1|+\rangle_2 &= \frac{1}{2}(|0\rangle|0\rangle + |0\rangle|1\rangle + |1\rangle|0\rangle - |1\rangle|1\rangle) \\ &= \frac{1}{\sqrt{2}}(|0\rangle|+\rangle + |1\rangle|-\rangle). \end{aligned} \tag{2.24}$$

The first qubit constitutes the input and the second the output. Now the input is prepared by applying some $U(\mathbf{n},\theta)_1$ so that the above state becomes $(c_0|0\rangle|+\rangle + c_1|1\rangle|-\rangle)/\sqrt{2}$. This is equivalent to having prepared the input qubit in the state $|\psi\rangle_1 = c_0|0\rangle + c_1|1\rangle$ before applying the CZ gate. Next the input qubit is measured in the $\{(|0\rangle \pm e^{-i\theta}|1\rangle)/\sqrt{2}\}$ basis, that is the measurement operator is now given by $M = |\theta^+\rangle\langle\theta^+| - |\theta^-\rangle\langle\theta^-|$ with $|\theta^\pm\rangle = (|0\rangle \pm e^{-i\theta}|1\rangle)/\sqrt{2}$. The resulting state after the measurement is given by

$$\begin{aligned} &|\theta^\pm\rangle\langle\theta^\pm|\frac{1}{\sqrt{2}}(c_0|0\rangle|+\rangle + c_1|1\rangle|-\rangle) \\ &\qquad = |\theta^\pm\rangle(c_0|+\rangle \pm c_1 e^{i\theta}|1\rangle. \end{aligned} \tag{2.25}$$

The output qubit is now in one of two states $c_0|+\rangle \pm c_1 e^{i\theta}|-\rangle$ each occurring with probability $|c_0 \pm c_1 e^{i\theta}|^2/2$ corresponding to the ± 1 eigenvalues of the measurement. Representing the measurement outcome as a binary $m = 0, 1$ where 0 and 1 correspond to +1 and -1 respectively, this output state can be written as $X^m H R_Z(\theta)|\psi\rangle$ where $|\psi\rangle$ was the input and $R_\Sigma(\theta) = e^{i\Sigma\theta/2}$ for

$\Sigma = X$, Y and Z. In effect we have teleported the input state and applied the operation $R_Z(\theta)$ to it in the process. Repeating the procedure three times on a linear cluster of four qubits, by choosing an orthogonal basis for each measurement and remembering the measurement outcomes, enables one to simulate an arbitrary unitary operations $U = R_X(\theta_x)R_Y(\theta_y)R_Z(\theta_z)$ on the input qubit. For example the measurement basis corresponding to a desired $R_X(\theta_x)$ operation on the transmitted qubit will be $\{|+\rangle \pm e^{-i\theta_z}|-\rangle\}$. Alternatively one can apply $R_X(\theta_x)$ to the qubit before measuring it in the computational basis.

The simplest example of an entangling gate using the cluster state model is of course the CZ gate. In this case we encode the two input qubits on the qubits forming a two-dimensional cluster state. However this isn't very insightful. The implementation of a CNOT gate, element of the universal set discussed in the previous section, is a little more interesting and can be done with a four-qubit cluster state (see Fig. 2.2) in the shape of star. It turns out that this state is locally equivalent to the four qubit Greenberger-Horne-Zeilinger (GHZ) state $(|0000\rangle + |1111\rangle)/\sqrt{2}$ and as a matter of fact all star shaped cluster states are locally equivalent to GHZ states (of the form $(|0..0\rangle + |1..1\rangle)/\sqrt{2}$). The control qubit ($A$) will not be measured and teleported but the target qubit (B) will. The reason for this comes from the equivalence between the CZ gate and the CNOT gate up to Hadamard transformations on the target qubit before and after the gate (see Fig. 2.2). We use here a convenient notation by Barrett and Kok [43] to express qubit states after the application of a CZ gates. For example a CZ gate on a pair of qubits C and D initially unentangled is written as

$$\mathrm{CZ}(c_0|0\rangle_C + c_1|1\rangle_C)(d_0|0\rangle_D + d_1|1\rangle_D) = (c_0|0\rangle_C + c_1|1\rangle_C Z_D)(d_0|0\rangle_D + d_1|1\rangle_D). \tag{2.26}$$

Now the initial four-qubit cluster state of interest reads

$$(c_0|0\rangle_A + c_1|1\rangle_A Z_{B2})(d_0|0\rangle_{B1} + d_1|1\rangle_{B1} Z_{B2})(|0\rangle_{B2} + |1\rangle_{B2} Z_{B3})|+\rangle_{B3}, \tag{2.27}$$

where $B1$ serves as the input for qubit B, corresponding to an two qubit input

$$|\psi\rangle_{AB} = c_0 d_0|0\rangle_A|0\rangle_B + c_0 d_1|0\rangle_A|1\rangle_B + c_1 d_0|1\rangle_A|1\rangle_B + c_1 d_1|1\rangle_A|0\rangle_B. \tag{2.28}$$

Now in (2.26) a measurement of $B1$ in the $|\pm\rangle$ basis will leave us with a combined state

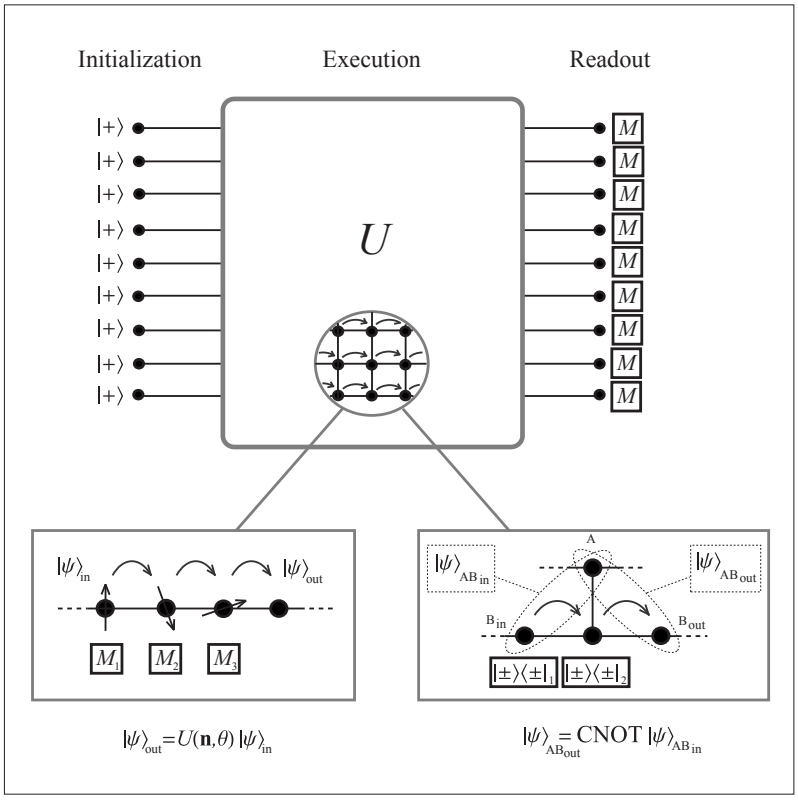

Figure 2.2: The two stages of a quantum computation in the measurement based model. The initialization here consists both in the preparation of the whole cluster state and the rotations on the input qubits, if necessary. Each vertex corresponds to a qubit initially prepared in the $|+\rangle$ state and each edge to the application of a CZ gate between the two adjacent vertices. The execution and the readout merge into one phase as they both consist in measurements. Each horizontal line can be assimilated to a single logical qubit being teleported along the chain. Logical operations are imprinted onto the logical qubits as they are teleported, through the adapted choice of the measurement basis. Three measurements along the chain are sufficient to implement an arbitrary single qubit operation. Vertical edges play the role of entangling gates between logical qubits and the simulation of a CNOT gate involves two measurements in the $|\pm\rangle$ basis on the target qubit as it crosses a vertical link.

$$(c_0|0\rangle_A + c_1|1\rangle_A Z_{B2})\,(d_0(|0\rangle_{B2} + |1\rangle_{B2}Z_{B3}) + (-1)^{m_1} d_1(|0\rangle_{B2} - |1\rangle_{B2}Z_{B3}))\,|+\rangle_{B3}. \tag{2.29}$$

As before m_1 represents the measurement outcome eigenvalue in binary form. Expanding the above expression we have

$$c_0|0\rangle_A\,(d_0(|0\rangle_{B2} + |1\rangle_{B2}Z_{B3}) + (-1)^{m_1} d_1(|0\rangle_{B2} - |1\rangle_{B2}Z_{B3}))\,|+\rangle_{B3}$$

$$+c_1|1\rangle_A\,(d_0(|0\rangle_{B2} - |1\rangle_{B2}Z_{B3}) + (-1)^{m_1} d_1(|0\rangle_{B2} + |1\rangle_{B2}Z_{B3}))\,|+\rangle_{B3}. \tag{2.30}$$

Then we measure $B2$ again in the $|\pm\rangle$ basis leaving us with the qubits A and $B3$ in the state

$$c_0|0\rangle_A\,(d_0(1 + (-1)^{m_2}Z_{B3}) + (-1)^{m_1} d_1(1 - (-1)^{m_2}Z_{B3}))\,|+\rangle_{B3}$$

$$+c_1|1\rangle_A\,(d_0(1 - (-1)^{m_2}Z_{B3}) + (-1)^{m_1}(1 + (-1)^{m_2}Z_{B3}))\,|+\rangle_{B3}. \tag{2.31}$$

Replacing B for $B3$ and simplifying, we obtain

$$X_B^{m_2} Z_B^{m_1} Z_A^{m_1}(c_0 d_0|0\rangle_A|0\rangle_B + c_0 d_1|0\rangle_A|1\rangle_B + c_1 d_0|1\rangle_A|1\rangle_B + c_1 d_1|1\rangle_A|0\rangle_B)$$

$$= X_B^{m_2} Z_B^{m_1} Z_A^{m_1}\mathrm{CNOT}|\psi\rangle_{AB}. \tag{2.32}$$

We have in effect simulated a CNOT gate on the two qubit input state, through two measurements in the $|\pm\rangle$ basis. The first measurement served to teleport the target qubit and simulate a Hadamard gate on it. Then the CZ gate with the control was imprinted onto it, before it was teleported again to the output qubit with a Hadamard transformation, exactly mimicking the circuit version of the CNOT gate using a CZ gate.

Having seen how to simulate quantum circuits we now introduce a very useful tool to further understand cluster states. They can also be characterized through the powerful stabilizer formalism developed by Gottesman [44]. In this framework, states are described by sets of operators which leave them unchanged, enabling a more compact representation. That is, an operator K is a stabilizer for $|\varphi\rangle$ if

$$K|\varphi\rangle = |\varphi\rangle. \tag{2.33}$$

We see that in fact $|\varphi\rangle$ is an eigenstate of operator K with eigenvalue $+1$. For example the four Bell states

$$|\phi^{\pm}\rangle = \frac{1}{\sqrt{2}}(|0\rangle|0\rangle \pm |1\rangle|1\rangle),$$
$$|\psi^{\pm}\rangle = \frac{1}{\sqrt{2}}(|0\rangle|1\rangle \pm |1\rangle|0\rangle), \tag{2.34}$$

can be entirely characterized by their stabilizers

$$\{ZZ, \pm XX\}_{\phi^{\pm}}$$
$$\{-ZZ, \pm XX\}_{\psi^{\pm}}. \tag{2.35}$$

Stabilizers have become the standard formalism to express quantum error correction codes. The main issue is to find a set of stabilizers for which a given state $|\varphi\rangle$ is the only eigenstate with eigenvalue $+1$, so that the stabilizers uniquely define the state. We note here that not all quantum states are stabilizer states, as is the case for the three-qubit state $(|001\rangle + |010\rangle + |100\rangle)/\sqrt{3}$. This is the case because we are only focusing on qubit operators within the Pauli group $G_1 = \{\pm I, \pm iI, \pm X, \pm iX, \pm Y, \pm iY, \pm Z, \pm iZ\}$.

The product of two stabilizers yields another valid stabilizer, meaning the set of stabilizers stabilizing a particular subspace have a group structure. The group, which we will from now on call the stabilizer, can be compactly expressed from the products of a set of generators. For cluster states, the stabilizer generators are given by

$$K_i = X_i \prod_{j \in N_i} Z_j, \tag{2.36}$$

one for each qubit i where all the qubits j share an edge with it in the graphical representation (see Fig 2.2). In other words the cluster state of n qubits is uniquely defined by as set of n generators, significantly more compact than the 2^n vector states required in the state notation. One advantage of this notation is that it allows us to investigate the effects of measurements on the cluster, in particular the measurement of Pauli operators. If the operator being measured commutes with all the generators, then the state is left unchanged. However if it anticommutes with one of the generators, that particular generator is removed from the group. These simple guide lines hold, up to -1 factors which can simply be taken into account or corrected for [40]. To illustrate this let us consider an X measurement on a qubit embedded in a linear cluster or chain (see Fig. 2.3). Given five qubits within a chain, the stabilizer generators read

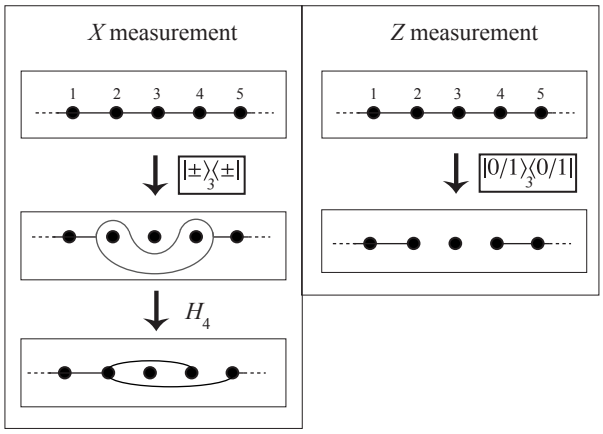

Figure 2.3: The effect of Pauli X and Z measurements on qubits with a cluster state. An X measurement removes the qubit from the cluster but does not break up the chain. A dangling bond can be generated through a Hadamard transformation on qubit 4. A Z measurement simply removes the qubit and breaks up the chain.

$$\left\{\begin{array}{cccccc} (1) & X & Z & I & I & I \\ (2) & Z & X & Z & I & I \\ (3) & I & Z & X & Z & I \\ (4) & I & I & Z & X & Z \\ (5) & I & I & I & Z & X \end{array}\right\} \tag{2.37}$$

An X measurement on the center qubit corresponds to the measurement of operator $IIXII$. As indicated above, all generators anticommuting with the measured operator will be removed from the set. Those are the ones with a Z on the third qubit, i.e. (2) and (4). Before removing them we generate the commuting operator $ZXIXZ$ by taking their product and we also generate $IZXIX$ by multiplying (3) with (5) (the latter can be done after the removal). Proceeding with the removal we have

$$\left\{\begin{array}{cccccc}(1) & X & Z & I & I & I\\ (2) & Z & X & I & X & Z\\ (3) & I & Z & X & Z & I\\ (4) & I & I & X & I & I\\ (5) & I & Z & X & I & X\end{array}\right\} \tag{2.38}$$

$$\overset{(3)\times(4)\&(4)\times(5)}{\longrightarrow}\left\{\begin{array}{cccccc}(1) & X & Z & I & I & I\\ (2) & Z & X & I & X & Z\\ (3) & I & Z & I & Z & I\\ (4) & I & Z & I & I & X\end{array}\right\} \tag{2.39}$$

$$\overset{IIIHI}{\longrightarrow}\left\{\begin{array}{cccccc}(1) & X & Z & I & I & I\\ (2) & Z & X & I & Z & Z\\ (3) & I & Z & I & X & I\\ (4) & I & Z & I & I & X\end{array}\right\} \quad . \tag{2.40}$$

In the first step we remove the now irrelevant qubit which has been measured by multiplying in the measured operator (if applying $IIXII$ leaves the state unchanged then the Xs on the third qubit can simply be replaced by Is). At this point qubits 2 and 4 form an embedded Bell pair. In the second step we apply a Hadamard transformation to the fourth qubit, affecting the concerned operators as $HXH = Z$ and $HZH = X$, and recover the modified cluster state. We see that the measured qubit has been removed from the cluster but the chain has not be broken up, instead it shrunk in length by one qubit and now has a 'dangling bond', represented by the fourth qubit which has only one connection to the chain. Following the same methods it can easily be shown that a Z measurement on an embedded qubit will remove it from the cluster along with all adjacent edges, breaking up the chain.

The circuit and the measurement based models differ on several points. The most obvious is the time at which entangling operations are performed. In the circuit model they occur during the computation in an online fashion. However in the cluster state approach all entangling operations are performed before the computation (the measurements) begins, in an offline fashion. This is a clear attribute when one considers applications in which entangling operations only work with a certain heralded success probability. For such applications the cluster state can be built efficiently before the computation is undertaken deterministically through local measurements and feed forward. This however comes at a price, that of resources, in terms of qubit usage and time taken. Such issues are crucial to the feasibility of

a useful measurement-based quantum computer, as the physical space containing the devices and qubits, as well as the coherence time of the qubits are finite. These vital issues will be discussed in chapter 4.

2.2 Quantum optics

Quantum optics is central to the work recounted in this thesis. In this subsection we provide an introductory overview of the field which includes relevant mathematical tools and concepts.

2.2.1 The quantized electromagnetic field

The standard starting point for the quantization the electromagnetic field is Maxwell's classical field equations [45]. The field in the vacuum, without charges or currents obeys the free space equations

$$\nabla.\mathbf{E} = 0, \tag{2.41}$$

$$\nabla.\mathbf{B} = 0, \tag{2.42}$$

$$\nabla \times \mathbf{E} = -\frac{\partial \mathbf{B}}{\partial t}, \tag{2.43}$$

$$\nabla \times \mathbf{B} = \mu_0 \epsilon_0 \frac{\partial \mathbf{B}}{\partial t}, \tag{2.44}$$

where μ_0 and ϵ_0 are the magnetic permeability and electric permittivity of the vacuum. From the above equations it is easy to show that $\mathbf{E}$ (and $\mathbf{B}$) obeys the wave equation

$$\nabla^2 \mathbf{E} = \mu_0 \epsilon_0 \frac{\partial^2 \mathbf{E}}{\partial t}. \tag{2.45}$$

The solution is a plane wave propagating at the speed of light $c = 1/\sqrt{\mu_0 \epsilon_0}$. It's full form is given by [46]

$$\mathbf{E}(\mathbf{r}, t) = i \sum_k \left(\frac{\hbar w_k}{2\epsilon_0} \right)^{1/2} \left[a_k \mathbf{u}_k(\mathbf{r}) e^{-iw_k t} - a_k^* \mathbf{u}_k^*(\mathbf{r}) e^{iw_k t} \right], \tag{2.46}$$

where ω_k is the frequency of each mode k. The $\mathbf{u}_k$ functions are plane wave mode functions of the form $\mathbf{u}_k(r) = V^{-1/2} \mathbf{e}^\lambda e^{i\mathbf{k}\cdot\mathbf{r}}$ where $\mathbf{e}^\lambda$ is the unit polarization vector and $\lambda = 1, 2$ is the polarization index. The dimensionless complex numbers a_k and a_k^* correspond to the amplitude of the classical

field. Now the transition to a quantum representation of the field is made by replacing these amplitudes with the operator $\hat{a}_k$ and its adjoint $\hat{a}_k^\dagger$. They obey the bosonic commutation relations

$$\left[\hat{a}_k, \hat{a}_{k'}^\dagger\right] = \delta_{k,k'}. \tag{2.47}$$

The energy of the electromagnetic field, initially given by the Hamiltonian

$$H = \frac{1}{2}\int (\epsilon_0 \mathbf{E}^2 + \frac{\mathbf{B}^2}{\mu_0}) d\mathbf{r}, \tag{2.48}$$

can now be rewritten in terms of the $\hat{a}_k$ and $\hat{a}^\dagger$ operators as

$$\hat{H} = \sum_k \hbar\omega_k \left(\hat{a}_k^\dagger \hat{a}_k + \frac{1}{2}\right). \tag{2.49}$$

Focusing on a single mode, if we denote by $|n\rangle$ the energy eigenstates of the above Hamiltonian, the eigenvalue equation reads

$$\hbar\omega(\hat{a}^\dagger\hat{a} + \frac{1}{2})|n\rangle = E_n|n\rangle. \tag{2.50}$$

One finds that the energy eigenvalues are given by $E_n = \hbar\omega(n+1/2)$, where n is the number of photons in the mode. We naturally define the number operator $\hat{n} = \hat{a}^\dagger\hat{a}$ of which the $|n\rangle$ are also eigenstates. They are termed number or Fock states and obey the eigenvalue equation $\hat{n}|n\rangle = n|n\rangle$. The individual operators $\hat{a}$ and $\hat{a}^\dagger$ are the raising and lowering operators of the harmonic oscillator eigenstates and their application leads to

$$\hat{a}|n\rangle = \sqrt{n}|n-1\rangle, \tag{2.51}$$
$$\hat{a}^\dagger|n\rangle = \sqrt{n+1}|n+1\rangle. \tag{2.52}$$

In view of this they are referred to as the annihilation and creation operators respectively. We see that the ground state of the oscillator is defined by $\hat{a}|0\rangle = 0$. The corresponding energy (zero point energy) $\hbar\omega/2$ represents the vacuum energy fluctuations. Successive applications of the creation operator on this vacuum state generates all higher energy number states

$$|n\rangle = \frac{(\hat{a}^\dagger)^n}{\sqrt{n!}}|0\rangle. \tag{2.53}$$

The number states are orthogonal and form a complete basis

$$\langle n|m\rangle = \delta_{nm}, \tag{2.54}$$

$$\sum_{n=0}^{\infty} |n\rangle\langle n| = I, \tag{2.55}$$

where I is the identity operator. The number state basis provides a representation for all optical fields, from single photons to thermal fields. As expected, superpositions of number states are of particular interest in quantum information. One such superposition, which is of particular interest to us, is the coherent state.

2.2.2 Coherent states

The coherent state $|\alpha\rangle$ is defined as the eigenstate of the annihilation operator

$$\hat{a}|\alpha\rangle = \alpha|\alpha\rangle. \tag{2.56}$$

Expanding in the number state basis and solving the above eigenvalue equation leads to

$$|\alpha\rangle = e^{-|\alpha|^2/2} \sum_{n=0}^{\infty} \frac{\alpha^n}{\sqrt{n!}}|n\rangle. \tag{2.57}$$

So the coherent state contains an indefinite number of photons averaging at $\langle\alpha|\hat{n}|\alpha\rangle = |\alpha|^2$, giving it a well defined phase for large α, in contrast to number states which have a perfectly well defined number of photons and in consequence a random phase. This is due to an uncertainty relation between the conjugate operators that are the number and phase operators, $\Delta\hat{n}\Delta\hat{\theta} \geq 1/2$. However, as there is no well defined phase operator in quantum optics [47], this is not a formal relation. We will see the same uncertainty relation arise for the field quadratures in a formal way. The coherent state can also be defined through the displacement operator $D(\alpha)$ acting on the vacuum as

$$D(\alpha)|0\rangle = |\alpha\rangle, \tag{2.58}$$

with

$$D(\alpha) = \exp\left[\alpha\hat{a}^\dagger - \alpha^*\hat{a}\right]. \tag{2.59}$$

The adjoint of the displacement operator is simply $D^\dagger(\alpha) = D(-\alpha)$. Successive displacements generate a geometrical phase which we will find to be very useful

$$D(\beta)D(\alpha) = e^{i\mathrm{Im}[\alpha^*\beta]}D(\alpha+\beta). \tag{2.60}$$

One important feature of coherent states comes from the fact that all their number state components are non-zero, meaning that two coherent states cannot be orthogonal

$$\langle\beta|\alpha\rangle = \exp\left[-\frac{1}{2}(|\alpha|^2+|\beta|^2)+\alpha\beta^*\right], \tag{2.61}$$

$$|\langle\beta|\alpha\rangle|^2 = \exp\left[-|\alpha-\beta|^2\right]. \tag{2.62}$$

However they can be made near orthogonal with a suitable choice of α and β. Coherent states form an overcomplete set

$$\int |\alpha\rangle\langle\alpha| d^2\alpha = \pi, \tag{2.63}$$

where the integral is taken over the real and imaginary components of α ($d^2\alpha = d\mathrm{Im}[\alpha]d\mathrm{Re}[\alpha]$). To some degree, the coherent state has properties which are relatively close to a classical state of the electromagnetic field. With the exception of some superimposed quantum noise which is small for large photon numbers, it resembles a classical oscillation of the electromagnetic field.

Having defined the relevant optical states, we now look at how they evolve through linear and nonlinear media.

2.2.3 Linear optics

Linear optical applications make use of passive optical elements such as phase shifters and beam splitters which conserve photon number, to prepare particular states through interference effects. In these elements, the annihilation operators on different input modes are transformed to operators on output modes only linearly, that is [48–50]

$$\hat{a}_i^{out} = \sum_j U_{ij}\hat{a}_j^{in}, \quad \text{and} \quad \hat{a}_i^{\dagger out} = \sum_j U_{ij}^*\hat{a}_j^{\dagger in} \tag{2.64}$$

where U is a unitary matrix. The phase shifter is based on a Hamiltonian proportional to the number operator $H_{ps} = -\hbar\chi\hat{a}^\dagger\hat{a}$ and applies a number dependent phase (time delay) on a particular mode

$$U_{ps}|n\rangle = e^{-iH_{ps}t/\hbar}|n\rangle = e^{i\phi\hat{a}^\dagger\hat{a}}|n\rangle = e^{in\phi}|n\rangle, \tag{2.65}$$

with $\phi = \chi t$. The action of a phase shifter on a coherent state is simply given by $e^{i\phi\hat{a}^\dagger\hat{a}}|\alpha\rangle = |\alpha e^{i\phi}\rangle$. The other essential device for linear optics is the beam splitter which in a general sense acts on the annihilation operators of a pair of incoming modes as

$$\begin{pmatrix} a_1^{out} \\ a_2^{out} \end{pmatrix} = U_{bs} \begin{pmatrix} a_1^{in} \\ a_2^{in} \end{pmatrix}. \tag{2.66}$$

U_{bs} is again a unitary 2×2 matrix and for an ideal phase-free beam splitter we have

$$\begin{pmatrix} a_1^{out} \\ a_2^{out} \end{pmatrix} = \begin{pmatrix} \sin\theta & \cos\theta \\ \cos\theta & -\sin\theta \end{pmatrix} \begin{pmatrix} a_1^{in} \\ a_2^{in} \end{pmatrix}. \tag{2.67}$$

It is worth noting here that there is another convention of the beam splitter operation involving a different relative phase between transmission and reflection amplitudes [50]. The effect of the above transformation (2.67) is to reflect or transmit an incoming photon with associated probability amplitudes $\pm\sin\theta$ (reflectivity) and $\cos\theta$ (transmittivity). Setting $\theta = \pi/4$ leads to the 50:50 beam splitter, which maps the incoming creation operators to

$$\hat{a}_1^{\dagger out} \rightarrow \frac{1}{\sqrt{2}}\left(\hat{a}_1^{\dagger in} + \hat{a}_2^{\dagger in}\right), \tag{2.68}$$

$$\hat{a}_2^{\dagger out} \rightarrow \frac{1}{\sqrt{2}}\left(\hat{a}_1^{\dagger in} - \hat{a}_2^{\dagger in}\right), \tag{2.69}$$

generating superpositions of number states. This particular transformation leads to the striking photon bunching effect, in which the incoming pair of modes each contain a single photon while the outgoing modes become entangled, with either zero or two photons per mode

$$|1\rangle_1|1\rangle_2 \rightarrow \frac{1}{\sqrt{2}}\left(|2\rangle_1|0\rangle_2 + |0\rangle_1|2\rangle_2\right). \tag{2.70}$$

As well as the path degree of freedom of photons, their polarization degree of freedom is often used in linear optics. Two orthogonal polarizations are contained in the solutions to the free space Maxwell equations and so

individual photons can be horizontally polarized ($|H\rangle$) and vertically polarized ($|V\rangle$). The circular polarization basis consists in the superpositions $(|H\rangle \pm |V\rangle)/\sqrt{2}$. A similar toolbox can be used in this setting, containing polarizers (realizing arbitrary unitary operations on a single photon polarization) and polarizing beam splitters which reflect a given polarization and transmit the orthogonal polarization. We will be seeing how this toolbox can be used to process quantum information in section 2.3.

2.2.4 The field quadratures and homodyne measurements

Coming back to the expression for the Hamiltonian of an single mode optical field (2.49), one can reexpress it in terms of the Hermitian $\hat{x}$ and $\hat{p}$ quadrature operators

$$\hat{H} = \frac{1}{2}\left(\hat{p}^2 + \omega^2 \hat{x}^2\right), \tag{2.71}$$

with

$$\hat{x} = \sqrt{\frac{\hbar}{2\omega}}\left(\hat{a} + \hat{a}^\dagger\right), \tag{2.72}$$

$$\hat{p} = -i\sqrt{\frac{\hbar}{2\omega}}\left(\hat{a} - \hat{a}^\dagger\right). \tag{2.73}$$

From these observables one defines the pair of dimensionless conjugate variables

$$\hat{X} = \frac{1}{2}\left(\hat{a} + \hat{a}^\dagger\right), \tag{2.74}$$

$$\hat{P} = \frac{1}{2i}\left(\hat{a} - \hat{a}^\dagger\right), \tag{2.75}$$

obeying the commutation relation $\left[\hat{X}, \hat{P}\right] = i/2$. The generalized quadrature operator can be written as

$$\hat{X}(\phi) = \frac{\hat{a}e^{-i\phi} + \hat{a}^\dagger e^{i\phi}}{2}, \tag{2.76}$$

then we have $\hat{X} = \hat{X}(0)$ and $\hat{P} = \hat{X}(\pi/2)$. From the Heisenberg uncertainty principle we have

$$\langle(\Delta\hat{X})^2\rangle\langle(\Delta\hat{P})^2\rangle \geq \frac{1}{16}. \tag{2.77}$$

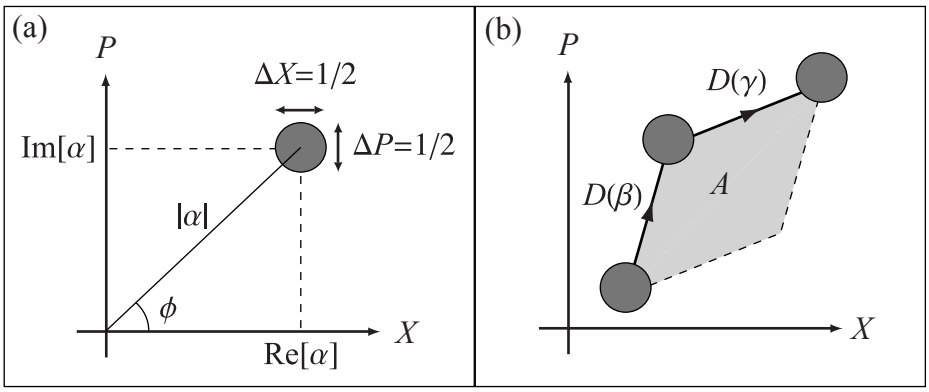

Figure 2.4: (a) A schematic representation of a coherent state $|\alpha\rangle$ in phase space. The X and P quadratures represent the real and imaginary parts of α. The uncertainty relation leads to a symmetrical phase space distribution of width $\Delta X = \Delta P = 1/2$. (b) Two consecutive displacements in phase space lead to a geometrical phase proportional to the area A traced out: $D(\gamma)D(\beta) = e^{i\mathrm{Im}[\beta^*\gamma]}D(\beta+\gamma) = e^{iA}D(\beta+\gamma)$.

$\langle(\Delta\hat{A})^2\rangle = \langle\hat{A}^2\rangle - \langle\hat{A}\rangle^2$ represents the variance of the operator $\hat{A}$ and calculating this variance for a coherent state (or the vacuum) $|\alpha\rangle$ we find $\langle(\Delta\hat{X})^2\rangle_\alpha = \langle(\Delta\hat{P})^2\rangle_\alpha = 1/4$. In other words the above expression becomes an equality and for this reason the coherent state is called a minimum uncertainty state.

The phase space representation of optical states will be very useful to us in this work. Due to the fact that the canonical variables $\hat{X}$ and $\hat{P}$ do not commute, optical states do not have a well defined position in phase space. In the case of a coherent state, the expectation values of $\hat{X}$ and $\hat{P}$ are

$$\langle\alpha|\hat{X}|\alpha\rangle = \frac{1}{2}(\alpha+\alpha^*) = \mathrm{Re}[\alpha], \tag{2.78}$$

$$\langle\alpha|\hat{P}|\alpha\rangle = \frac{1}{2}(\alpha-\alpha^*) = \mathrm{Im}[\alpha]. \tag{2.79}$$

Thus in this case, the pictorial representation of a coherent state of amplitude $\alpha = |\alpha|e^{i\theta}$ in phase space becomes very intuitive, as illustrated in Fig. 2.4. The phase space distribution of a coherent state is a Gaussian distribution, which we schematically represent in the plane by a disc with width $\Delta\hat{X} = \Delta\hat{P} = 1/2$, the center of the distribution at a distance $|\alpha|$ from the

origin and forming an angle θ with the real axis. The corresponding representation for the number state would be a circle around the origin, with a perfectly well defined number of photons but a completely random phase.

Now we describe the setup for a homodyne measurement, which allows us to detect a particular quadrature of a given mode. To do so, the mode must be combined on a 50:50 beam splitter with a intense 'local oscillator' assumed to be in a coherent state $|\alpha_{\rm LO}\rangle$ with large average photon number (see Fig. 2.5). With the local oscillator in mode 1 and the signal state in mode 2, the beam splitter output is

$$\hat{a}_1^{\rm out} = \frac{1}{\sqrt{2}}(\hat{a}_{\rm LO}^{\rm in} + \hat{a}_{\rm sig}^{\rm in}), \quad \hat{a}_2^{\rm out} = \frac{1}{\sqrt{2}}(\hat{a}_{\rm LO}^{\rm in} - \hat{a}_{\rm sig}^{\rm in}). \tag{2.80}$$

Assuming an intense local oscillator allows us to describe it classically through the complex amplitude $\alpha_{\rm LO}$ instead of using the annihilation and creation operators. A photodetector placed in each outgoing mode converts the photons into electrons, generating a measurable photocurrent $\hat{i}$. This photocurrent is directly proportional to the number photons and so we can write $\hat{i} = \lambda\hat{n}$, where λ is a constant. Thus the photodectors in each mode will measure photocurrents [48]

$$\hat{i}_1 = \lambda\hat{a}_1^{\dagger\rm out}\hat{a}_1^{\rm out} = \frac{\lambda}{2}(\alpha_{\rm LO}^* + \hat{a}_{\rm sig}^{\dagger\rm in})(\alpha_{\rm LO} + \hat{a}_{\rm sig}^{\rm in}), \tag{2.81}$$

$$\hat{i}_2 = \lambda\hat{a}_2^{\dagger\rm out}\hat{a}_2^{\rm out} = \frac{\lambda}{2}(\alpha_{\rm LO}^* - \hat{a}_{\rm sig}^{\dagger\rm in})(\alpha_{\rm LO} - \hat{a}_{\rm sig}^{\rm in}), \tag{2.82}$$

and the difference between the two yields

$$\hat{i} = \hat{i}_1 - \hat{i}_2 = \lambda(\alpha_{\rm LO}^*\hat{a}_{\rm sig} + \alpha_{\rm LO}\hat{a}_{\rm sig}^\dagger). \tag{2.83}$$

Writing the complex amplitude of the local oscillator as $\alpha_{\rm LO} = |\alpha_{\rm LO}|e^{i\phi}$ we obtain

$$\begin{aligned} \hat{i}_\phi &= \lambda|\alpha_{\rm LO}|(e^{-i\phi}\hat{a}_{\rm sig} + e^{i\phi}\hat{a}_{\rm sig}^\dagger) \\ &= 2\lambda|\alpha_{\rm LO}|\hat{X}_{\rm sig}(\phi), \end{aligned} \tag{2.84}$$

where clearly by setting $\phi = 0$ and $\phi = \pi/2$ we are in fact measuring the canonical observables $\hat{X}$ and $\hat{P}$ respectively. The probability distribution for the $\hat{X}$ quadrature measurements of a coherent state is given by the normalized position space wavefunction [51]

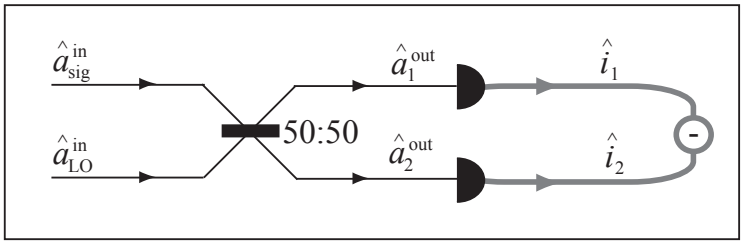

Figure 2.5: The physical setup for a homodyne measurement of the signal input mode. After having been mixed on a 50:50 beam splitter with a strong local oscillator, the two outgoing modes are absorbed in the photodetectors in which their intensities are translated into photocurrents. The quadrature measurement is then given by taking the difference between the photocurrents.

$$\langle x|\alpha\rangle = \left(\frac{2}{\pi}\right)^{1/4} \exp\left[-\left(\text{Im}[\alpha]\right)^2 - (x-\alpha)^2\right]. \tag{2.85}$$

By symmetry, the probability distribution for a $\hat{P}$ quadrature measurement can be obtained from the above expression with the coherent state $|\alpha\rangle$ rotated by an angle $\pi/2$ in phase space to $|i\alpha\rangle$. When trying to distinguish between two coherent states through a homodyne measurement, the error in the measurement is given by the overlap of their respective measurement probability distributions. This overlap diminishes exponentially with the distance between the two states. This will become clearer when we discuss measurements in the qubus scheme. Now we move on to consider the interaction of a single mode field with a single two level atom. Such a fine interaction can be obtained in an optical cavity and forms part of the field of cavity quantum electrodynamics (CQED).

2.2.5 The Jaynes-Cummings model

Here we consider an atom with two energy levels corresponding to different electronic configurations, the ground state $|g\rangle$ and the excited state $|e\rangle$ (see Fig. 2.6). The difference in energy between the two we denote by $\hbar\omega_A$, and fixing the zero point energy halfway between them, the free atomic Hamiltonian reads

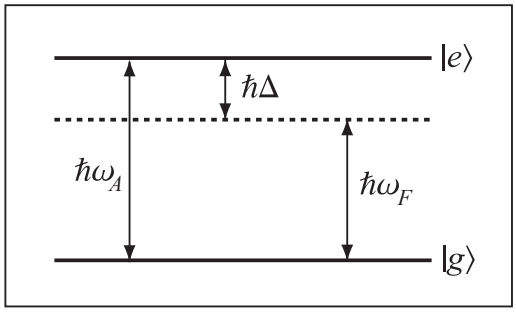

Figure 2.6: Energy level diagram of the atom and single mode. The energy difference between the ground ($|g\rangle$) and excited ($|e\rangle$) states of the atom is given by $\hbar\omega_A$ and the single mode energy by $\hbar\omega_F$. The detuning Δ corresponds to $\omega_A - \omega_F$.

$$\hat{H}_A = \frac{1}{2}\hbar\omega_A\hat{\sigma}_z, \tag{2.86}$$

with $\hat{\sigma}_z = |e\rangle\langle e| - |g\rangle\langle g|$ being the inversion operator. The free Hamiltonian for a single mode of frequency ω_F without the zero point energy is

$$\hat{H}_F = \frac{1}{2}\hbar\omega_F\hat{a}^\dagger\hat{a}. \tag{2.87}$$

If we consider this mode evaluated at the position of the atom (set to the origin), the solution to the Maxwell equations can be written as

$$\hat{\mathbf{E}} = i\mathbf{e}^\lambda\sqrt{\frac{\hbar\omega_F}{2\epsilon_0 V}}(\hat{a} + \hat{a}^\dagger). \tag{2.88}$$

where the time dependence has been absorbed into the annihilation and creation operators ($\hat{a}(t) = \hat{a}(0)e^{i\omega_F t}$). The interaction between the field and the atom is a dipole interaction with a corresponding interaction Hamiltonian [52]

$$\hat{H}_{int} = -\hat{\mathbf{d}}\cdot\hat{\mathbf{E}} = \hat{d}p(\hat{a} + \hat{a}^\dagger), \tag{2.89}$$

with

$$p = -i\sqrt{\frac{\hbar\omega_F}{2\epsilon_0 V}}, \quad \text{and} \quad \hat{d} = \hat{\mathbf{d}}\cdot\mathbf{e}^\lambda. \tag{2.90}$$

$\hat{\mathbf{d}}$ is the operator corresponding to the classical dipole moment $\mathbf{d} = -e\mathbf{r}$ (here e is the electron charge). Along with the atomic inversion operator defined above, we introduce the transition operators

$$\hat{\sigma}_+ = |e\rangle\langle g|, \quad \text{and} \quad \hat{\sigma}_- = |g\rangle\langle e|. \tag{2.91}$$

Similarly to the annihilation and creation operators, the transition operators are rotating and evolve as $\hat{\sigma}_\pm(t) = \hat{\sigma}_\pm(0)e^{\pm i\omega_A t}$. The dipole operator $\hat{d}$ is a 2×2 matrix, however as the diagonal elements $\langle e|\hat{d}|e\rangle = \langle g|\hat{d}|g\rangle = 0$, it may be written as

$$\hat{d} = d(\hat{\sigma}_+ + \hat{\sigma}_-), \tag{2.92}$$

where $d = \langle e|\hat{d}|g\rangle$ is assumed to be real. The total Hamiltonian then becomes

$$\begin{aligned} \hat{H}_T &= \hat{H}_A + \hat{H}_F + \hat{H}_{int} && (2.93) \\ &= \frac{1}{2}\hbar\omega_A\hat{\sigma}_z + \frac{1}{2}\hbar\omega_F\hat{a}^\dagger\hat{a} + \hbar g(\hat{a}\hat{\sigma}_+ + \hat{a}^\dagger\hat{\sigma}_-), && (2.94) \end{aligned}$$

with $g = dp/\hbar$. This expression is known as the Jaynes-Cummings Hamiltonian [53]. To arrive at this result, the rotating wave approximation is used, removing the terms $\hat{\sigma}_-\hat{a}$ and $\hat{\sigma}_+\hat{a}^\dagger$ oscillating at large frequency $e^{i(\omega_A+\omega_F)t}$ and keeping the terms $\hat{\sigma}_+\hat{a}$ and $\hat{\sigma}_-\hat{a}^\dagger$ oscillating at frequency $e^{i(\omega_A-\omega_F)t}$. One can understand the interaction part of the Jaynes-Cummings Hamiltonian as characterizing the absorption of a photon as the atom goes from the ground state to the excited state and the emission of a photon as the atom goes from the excited state to the ground state.

We now outline the procedure for obtain the dispersive limit of the Jaynes-Cummings Hamiltonian [52,54]. Using expression (2.94), the Schrödinger equation reads

$$i\hbar\frac{\partial|\psi(t)\rangle}{\partial t} = (\hat{H}_A + \hat{H}_F + \hat{H}_{int})|\psi(t)\rangle. \tag{2.95}$$

We now transform to the interaction picture via the operator $U_0 = e^{i(\hat{H}_A+\hat{H}_F)t/\hbar}$, in which the state vector becomes $|\tilde{\psi}(t)\rangle = U_0^{-1}|\psi(t)\rangle$ ($|\tilde{\psi}(0)\rangle = |\psi(0)\rangle$). The corresponding Schrödinger equation is

$$i\hbar\frac{\partial|\tilde{\psi}(t)\rangle}{\partial t} = \hat{H}_I(t)|\tilde{\psi}(t)\rangle, \tag{2.96}$$

with

$$\begin{aligned}\hat{H}_I(t) &= U_0^{-1}\hat{H}U_0 - i\hbar U_0^{-1}\frac{\partial U_0}{\partial t} \\ &= \hbar g(\hat{a}\hat{\sigma}_+ e^{i\Delta t} + \hat{a}^\dagger\hat{\sigma}_- e^{-i\Delta t}),\end{aligned} \tag{2.97}$$

where $\Delta = \omega_A - \omega_F$ is the detuning which we will assume to be large. The formal solution to (2.96) can be written

$$\begin{aligned}|\tilde{\psi}(t)\rangle &= \hat{T}\left[\exp\left(-\frac{i}{\hbar}\int_0^t dt'\hat{H}_I(t')\right)\right]|\tilde{\psi}(0)\rangle, \\ &= \hat{T}\left[1 - \frac{i}{\hbar}\int_0^t dt'\hat{H}_I(t') - \frac{1}{2\hbar^2}\int_0^t dt'\int_0^t dt''\hat{H}_I(t')\hat{H}_I(t'') + ...\right]|\tilde{\psi}(0)\rangle\end{aligned} \tag{2.98}$$

where $\hat{T}$ is the time ordering operator, which insures that $\hat{H}_I(t'')$ acts after $\hat{H}_I(t')$ for $t'' > t'$. After time ordering and to second order in the expansion we have

$$|\tilde{\psi}(t)\rangle \cong \left[1 - \frac{i}{\hbar}\int_0^t dt'\hat{H}_I(t') - \frac{1}{\hbar^2}\int_0^t dt'\hat{H}_I(t')\int_0^{t'} dt''\hat{H}_I(t'')\right]|\tilde{\psi}(0)\rangle. \tag{2.99}$$

Assuming a large detuning and a reasonable number of photons $\bar{n}$ (not too large) in the cavity mode, that is $g\sqrt{\bar{n}}/\Delta << 1$, the second term in the expansion can be neglected. After having integrated the third term and applied the rotating wave approximation we obtain

$$|\tilde{\psi}(t)\rangle \cong \left[1 - i\hat{H}_{disp}t/\hbar\right]|\tilde{\psi}(0)\rangle, \tag{2.100}$$

where the effective Hamiltonian is given by

$$\hat{H}_{disp} = \hbar\chi(\hat{\sigma}_+\hat{\sigma}_- + \hat{a}^\dagger\hat{a}\hat{\sigma}_z), \tag{2.101}$$

with $\chi = g^2/\Delta$. This is the dispersive limit of the interaction Hamiltonian $\hat{H}_{int}$ in the interaction picture. In this limit the photon absorption is neglected and instead a relative phase between the atomic states is produced. This particular interaction will be relied on extensively in the rest of this work, and so are the effects of dissipation, which we investigate next.

2.2.6 Dissipation and the master equation

So far we have only considered closed quantum systems, be it fields or single atoms. In reality such physical systems are continuously interacting with an environment or 'bath'. Entanglement occurs naturally between the two and this leads to decoherence effects, causing initially pure states to become mixed states. In turn this means that the evolution of these individual systems is no longer unitary. In the case of optical fields, such effects can consist in photon loss, or equivalently photon absorption of the environment.

The analysis of the evolution of an open system usually begins with a Hamiltonian of the general form [46, 55, 56]

$$\hat{H} = \hat{H}_S + \hat{H}_B + \hat{H}_{int}, \tag{2.102}$$

where $\hat{H}_S$ and $\hat{H}_B$ are the Hamiltonians of the system and the bath respectively, and $\hat{H}_{int}$ represents the interaction Hamiltonian between the two. For the damped harmonic oscillator which is our main concern here, they are

$$\begin{aligned} \hat{H}_S &= \hbar\omega_S \hat{a}^\dagger \hat{a}, \\ \hat{H}_B &= \hbar \sum_j \omega_j \hat{b}_j^\dagger \hat{b}_j, \\ \hat{H}_{int} &= \hbar \sum_j (c_j^* \hat{a} \hat{b}_j^\dagger + c_j \hat{a}^\dagger \hat{b}_j). \end{aligned} \tag{2.103}$$

The $\hat{b}_j$ ($\hat{b}_j^\dagger$) are the annihilation (creation) operators acting on the bath modes and the c_j are coupling constants. Thus the bath is assumed to be composed of harmonic oscillators and the interaction consists in exchanges of single photons between them and the system. Note here that different modes of the bath are not correlated (they do not interact with each other).

The starting point of most derivations of the master equation, governing the non-unitary evolution of an open system is the Schrödinger equation of motion in the interaction picture, reading

$$\frac{\partial \tilde{\nu}}{\partial t} = -\frac{i}{\hbar}\left[\tilde{H}_{int}, \tilde{\nu}\right], \tag{2.104}$$

with $\tilde{O} = e^{i(\hat{H}_S+\hat{H}_B)t/\hbar}\hat{O}e^{-i(\hat{H}_S+\hat{H}_B)t/\hbar}$. $\tilde{\nu}$ is the density matrix for the system and bath, which are initially uncorrelated, so we can write $\tilde{\nu}(0) = \tilde{\rho}_S(0) \otimes \tilde{\rho}_B(0)$. At later times, the system density matrix is obtained by

tracing out the bath as $\tilde{\rho}_S(t) = \mathrm{tr}_B\left[\tilde{\nu}(t)\right]$ and as such through integration we obtain the master equation

$$\frac{\partial\tilde{\rho}_S}{\partial t} = -\frac{1}{\hbar^2}\int_0^t dt' \mathrm{tr}_B\left[\tilde{H}_{int}(t), \left[\tilde{H}_{int}(t'), \tilde{\nu}(t')\right]\right]. \tag{2.105}$$

This expression is rather involved and can be simplified through the Born and the Markov approximations consecutively. The Born approximation relies on the weakness of the coupling between system and bath, enabling us to neglect terms higher than second order in $\tilde{H}_{int}$. This means $\tilde{\nu}(t')$ is replaced by $\tilde{\rho}_S(t') \otimes \tilde{\rho}_B(0)$ in the above expression. In the Markov approximation we assume that the state of the system at future times only depends on its present state, further replacing $\tilde{\rho}_S(t')$ with $\tilde{\rho}_S(t)$. These approximations being made, the master equation can be explicitly calculated for a zero-temperature bath using the Hamiltonians (2.103), yielding

$$\frac{\partial\rho}{\partial t} = -\frac{i}{\hbar}\left[\hat{H}_{int}, \rho\right] - \gamma(2\hat{a}\rho\hat{a}^\dagger - \hat{a}^\dagger\hat{a}\rho - \rho\hat{a}^\dagger\hat{a}), \tag{2.106}$$

ρ being the system density matrix and γ the damping rate. There are more complete expressions involving thermal baths (non-zero temperature) or even squeezed baths, however the above expression is widely used in the analysis of dissipative quantum optical systems. It provides a very good approximation for fields with wavelengths bellow the micrometer range and will suffice for the work presented in this thesis.

In this quantum optics section we have seen how quantum states of the eletromagnetic field could be characterized and manipulated. We considered the essential interaction of a single mode with a single atom, constituting the Jaynes-Cummings model and saw how the evolution of an open system could be approximated. In the next section we apply some of these concepts to the encoding and processing of quantum information and give an overview of known results.

2.3 Optical quantum computing

The physical realization of a quantum computer constitutes one of the main research drives of the field of quantum information science. New proposals come to light in practically every issue of journals concerned with the field. However there are some requirements which are independent of the chosen physical support, and they have been condensed into a set of seven fundamental criteria as enunciated by DiVincenzo [57]. The first five are concerned with the requirements for a single localized processor:

- Well characterized qubits.
- The ability to initialize the qubits in a standard state such as $|00...0\rangle$.
- Decoherence times much larger that gate operation times.
- A universal set of quantum gates.
- Single qubit measurement.

The last two criteria deal with the importance of communication and distributed applications:

- The ability to interconvert stationary and flying qubits.
- The faithful transmission of the flying qubits between chosen locations.

In this section we review some essential optical QIP proposals all the while keeping in mind these criteria.

2.3.1 Single photons and nonlinearities

One of the earliest proposal for a physical implementation of QIP was to use single photons. Without mentioning qubits, Milburn [58] proposed a quantum optical Fredkin gate (controlled SWAP) to realize reversible logic, without any energy dissipation. The gate acts on three bits encoded in the positions of three single photons and the essential interaction the gate relies on is a cross phase modulation occurring in a nonlinear optical Kerr medium. The interaction Hamiltonian is written

$$H_K = -\hbar\chi\hat{a}_1^\dagger\hat{a}_1\hat{a}_2^\dagger\hat{a}_2, \tag{2.107}$$

where $\hat{a}_1^\dagger$ and $\hat{a}_2^\dagger$ are the creation operators acting on the two optical modes propagating through the medium and χ is proportional to the third order nonlinear susceptibility coefficient $\chi^{(3)}$ of the medium. If each mode contains one or no photons it is easy to see that the resulting unitary operation on the two modes $U_K = \exp[i\chi t\hat{a}_1^\dagger\hat{a}_1\hat{a}_2^\dagger\hat{a}_2]$ will induce a conditional phase on the state corresponding two one photon in each mode $U_k|11\rangle = \exp[i\chi t]|11\rangle$ while leaving all other states ($|00\rangle, |01\rangle$ and $|10\rangle$) unchanged.

In Milburn's gate, the logical states correspond to the photon being in either one of two modes, with associated states $|10\rangle$ and $|01\rangle$. This encoding has come to be known as the dual-rail encoding for qubits and was used by Chuang and Yamamoto [59] to describe a complete quantum computer based on beam splitters, phase shifters and nonlinearities. Beam splitters and phase shifters (as defined in the previous section) are sufficient to implement arbitrary operations on a single qubit $|\psi\rangle = c_0|01\rangle + c_1|10\rangle$. The cross phase modulation then enables us to directly implement entangling gates between two qubits propagating in four different modes. The simplest example is

that of a CZ gate; in this case one simply needs to have one mode from each qubit going through the Kerr medium for a time $t = \pi/\chi$. A similar setup can be used with a polarization encoding of the qubits ($|\psi\rangle = c_0|H\rangle + c_1|V\rangle$), noting that polarizing beam splitters enable us to go from one encoding to the other.

All single photon proposals present several attributes, the main one being the long coherence time of well defined photonic qubits, be it in polarization or spatial encodings. This addresses directly the first three DiVincenzo criteria. Also the single qubit operations rely only on passive linear optical elements which are commonplace on standard optical tables and no interface with communication systems is needed. However photons do not interact easily and the strength of the nonlinearity required to induce a π phase between two single photons is far out of reach of current technology.

A more recent proposal by Franson *et al.* [60] makes use of the Zeno effect to implement entangling gates. The CZ gate here consists in a pair of modes weakly coupled and doped with two-photon absorbing atoms. The absorbers suppress the two photons per mode components through what is called the Zeno effect. After a given interaction time (distance), a complete swap of the two modes is achieved. At this point the two modes return to regular optical fibers and are manually swapped back. The switching from one mode into the other induces a π phase shift (similar to a single component of a beam splitter operation), relative to the other two qubit states. For a strong quantum Zeno effect the gate performs near deterministically, however again there is a significant gap with currently available technology and in consequence, due to photon loss, the gate does fail. Recent encoding [61] and distillation schemes [62] are helping to reduce this gap.

2.3.2 Measurement induced nonlinearities

The nonlinearities described above are not indispensable and it was shown in a paper by Knill, Laflamme and Milburn (KLM) [34] that passive linear optical elements along with single ancillary photons and photon number resolving detectors are sufficient for universal quantum computation. This striking result has triggered considerable amounts of research in linear optical quantum computing (LOQC). For detailed reviews of the field we point the interested reader to [49, 50] while a broad overview and perspective is given in [63]. Due to the fact that single photons hardly interact, the CZ gate unveiled in the KLM scheme is a probabilistic, heralded gate, whose successful outcome depends on a set of measurements. The building block of this gate is another gate, working on a smaller scale, the nonlinear sign

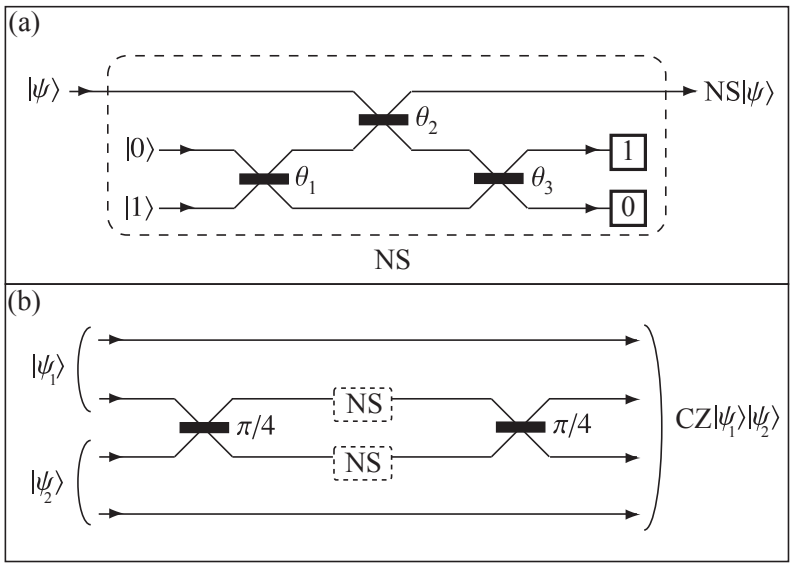

Figure 2.7: Optical circuit representations of two fundamental KLM gates. (a) The nonlinear sign gate, with an ancillary photon and three beam splitters. The reflectivities of the first and last beam splitters are the same ($\theta_1 = \theta_3$). The gate succeeds when a single photon is detected in the top ancillary mode. (b) Combining two NS gates and two 50:50 beam splitters leads to a CZ gate on two incoming qubits $|\psi_1\rangle$ and $|\psi_2\rangle$ in the dual rail encoding.

(NS) gate. It acts on a single optical mode as follows

$$\mathrm{NS}(c_0|0\rangle + c_1|1\rangle + c_2|2\rangle) = c_0|0\rangle + c_1|1\rangle - c_2|2\rangle, \tag{2.108}$$

applying a π phase shift on the two-photon component. The NS gate is illustrated in Fig. 2.7(a) and as we see it requires a single ancillary photon and two photodetectors. Measuring a single photon in the top detector indicates that the gate succeeded. This occurs with probability 1/4. Combining two of these gates and the photon bunching effect observed in the previous subsection, a full CZ gate working with success probability $1/4 \times 1/4 = 1/16$ is devised (see Fig. 2.7(b)). Since the initial paper, simplifications have been proposed, notably the NS gate of Ralph *et al.* [64], and an improvement on the success probability of the CZ gate to 2/27 was found by Knill [65], in a gate making use of two ancillary photons.

Entangled ancillary photons can further increase the success probability

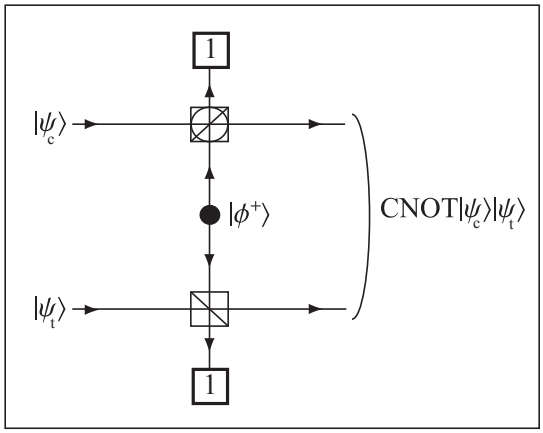

Figure 2.8: The CNOT gate designed by Pittmann *et al.* works with polarization encoded qubits. The ancillary photons form a Bell state $|\phi^+\rangle = (|HH\rangle + |VV\rangle)/\sqrt{2}$. The gate succeeds when both the top and bottom detectors detect a single photon. The parity checks work with probability 1/2 and thus the gate success probability is 1/4.

of a two-qubit entangling gate to 1/4, as illustrated by Pittmann *et al.* [66] and Koashi *et al.* [67]. The Franson type CNOT gate shown in Fig. 2.8 functions in the polarization encoding and consists in two parity checks (one on each input) with an ancillary Bell state of the form $|\phi^+\rangle = (|HH\rangle + |VV\rangle)/\sqrt{2}$. A parity check or gate can be simply composed of a polarizing beam splitter and a detector on one of the outgoing modes. It allows one to verify whether or not the two incoming photons have the same polarization.

The KLM scheme is very attractive and seemingly simple, however the probabilistic aspect of the two-qubit gates is problematic. The probability of successfully implementing a quantum circuit containing n of these of these gates will scale as p^n, where p is the success probability of an individual gate. That is on average we will have to attempt the circuit p^{-n} times. This number increases exponentially with the size of the circuit and becomes intractable for small p, eliminating any improvement the quantum computer may have had over its classical counterpart.

2.3.3 Gate teleportation and optical cluster states

The KLM approach potentially overcomes this obstacle of probabilistic gates by pushing it into an off-line preparation scheme. What we mean by this

is that the two-qubit gates are not used during the computation itself, but in the preparation of a resource to be used during the computation. The possibility to do so was first pointed out by Gottesman and Chuang [68] and the process is now referred to as gate teleportation. The example they give is that of a teleported CZ gate. A single qubit can be teleported by using a Bell state as a resource. The standard protocol consists in performing a joint measurement in the Bell basis of the input qubit and one half of the Bell pair. This procedure maps the input qubit to the other half of the Bell pair, up to a known unitary operation given by the measurement results. In the case of gate teleportation, the two input qubits each have one half of their own Bell pair ready for the teleportation, but before the measurements are performed, a CZ gate is attempted between the two other halves of each Bell state (the recipients of the teleportations). Due to the fact that the CZ gate commutes with the possible single qubit corrections required, it is imprinted onto the teleported qubits. Now all one needs is to be able to reliably prepare and store this entangled two-Bell state resource and the online implementation of the gate is assured to be deterministic.

Unfortunately the problem is not completely solved for LOQC applications, as the Bell basis measurements themselves only succeed with a maximum probability of 1/2 [69]. Eisert [70] provided a method based on semidefinite programming to find strict success probability upper bounds on linear optical gates, verifying this Bell state measurement probability and fixing the maximum success probability of an NS gate to 1/4 (no possible improvements over the initial gate). Thus given the resource state, the success probability for the single gate teleportation remains limited to 1/4. The entangled resources can be increased so as to increase the success probability of the qubit teleportations themselves. With n ancillary photons in $2n$ modes the resulting probability is $n/(n+1)$, rapidly becoming near deterministic. However the complete resource needed for the the near deterministic teleportation of a CZ gate is significant, estimated at 10^4 operations [71]. The resource cost of a single gate now being fixed, one can argue that the KLM scheme is scalable; the resources (modes, optical devices and detectors) scale polynomially instead of exponentially, with the number of gates composing a quantum circuit. However this approach cannot be scalable in a practical sense.

Further improvements were found by turning to cluster states. The first proposals in that direction was that of linked photon quantum computation by Yoran and Reznik [72]. In this scheme both the path and polarization degrees of freedom of each photon are used so as to enable a deterministic teleportation as described by Popescu [73]. Then each logical qubit is

represented by a chain of photons linked in path and polarization degrees of freedom alternatingly. CZ gates applied between chains before the teleportation procedure begins are imprinted onto the logical qubits as they are transmitted, through local measurements, as in the cluster state model. This proposal came roughly at the same time as the conventional photonic cluster state adaptation by Nielsen [74], reducing the number of operations per logical gate to order 10^2. The CZ gate is not necessary for the generation of cluster states and so further simplifications were given by Browne and Rudolph [75], based on a polarization entangled photon source, polarizing beam splitters and redundant encoding. The entangling gates then simply consist in a parity gate (type I fusion), used to grow linear chains, and an incomplete Bell state measurement (type II fusion), used to link up chains into a 2-dimensional lattice without breaking them up in case of failure. The latter requires an X measurement prior to each fusion attempt, to create a redundantly encoded qubit, very similar to the 'dangling' bond approach proposed by Barrett and Kok [43]. This simplified method brings the average cost of an individual two-qubit gate down to 52 Bell pairs instead of 54 8-photon entangled states in Nielsen's scheme.

Single photons seem to be good candidates for the realization of cluster state quantum computing. On the few-photon scale, many experiments have already been done, the most famous to date being the 4-photon cluster state demonstrated by Walther *et al.* [76], now surpassed by the 6-photon cluster state created by Lu *et al.* [77]. However as the cluster increases in size, the complexity of the circuits and the optical switching required constitute a tremendous technical challenge. A more intuitive way of viewing a cluster state is as being composed of static qubits. This was the initial picture Raussendorf and Briegel had in mind. LOQC provides the tools to do so as we will see next.

2.3.4 Distributed approaches

The idea of entangling atoms in the same cavity via the 'non-detection' of emitted photons was first mentioned by Plenio *et al.* [78]. Later Duan and Kimble proposed a scheme to entangle atoms in separate cavities [79], through the detection of cavity decay with single photon detectors. Each atom is driven by a classical laser pulse from their ground state to an excited state before decaying into one of two logical states (corresponding to $|0\rangle$ and $|1\rangle$) through the emission of a horizontally or a vertically polarized photon. The cavity outputs are mixed on a polarizing beam splitter to erase the which path information before being measured. Conditional on the

detection of a photon at each one of the beam splitter outputs, occurring with probability 1/2, the atoms are projected to the maximally entangled singlet state $(|01\rangle + |10\rangle)\sqrt{2}$.

Even though efficient, this scheme is not a parity check because the atoms are initialized in a known state. In order to be able to leave the coherence of the atoms untouched, a different setup is needed. Such a modified setup constitutes Barrett and Kok's proposal [43], where they consider two optical cavities containing single atoms coupled to outgoing modes mixed on a regular beam splitter this time. The individual atomic qubits comprise of two low-lying (qubit basis) states and a single excited state with a selection rule linking it to just one of the qubit states. Applying a π pulse leaves one of the low lying states unchanged, while making the other move up to the excited state. Decay leads to the emission of a single photon for this amplitude. So if, after applying the π pulse to both qubits, a single photon is detected after the beam splitter, the qubits are projected into the singlet state. A double-heralding procedure is used to remove mixture, generated if non-photon-number resolving detection is used. This method was combined with another result obtained by Lim *et al.* [80], where the implementation of a CZ gate is achieved through repeated measurements of the two atomic qubits in a mutually unbiased basis. The combination of the two proposals [81] leads to some saving in qubit resources during the generation of the cluster states. The scaling of these resources will be taken as a comparative in chapter 4.

2.3.5 Detectors and sources

Linear optics based approaches constitute attractive physical realizations indeed. The logical circuits are built up of passive linear optical elements and as we mentioned earlier, for all optical setups the coherence times of the qubits is not an obstacle. The experimental difficulty now lies in the single photon (or entangled pair) generation and photon number resolving detection. Increasing the efficiency of devices working in this regime constitutes a significant technological challenge, which is being taken on by many research groups worldwide. Such devices will not only serve LOQC but also all photon level communication systems, quantum or classical.

Real photo-detectors are subject to two types of errors. The first is photon loss, exemplified when the device detects fewer photons than the signal actually contained. The second is referred to as dark counts, when the device detects too many photons. Current experiments in general use avalanche photo-diodes which are commonly called bucket detectors, in that they are

not photon-number resolving. The measurement only tells us if there were photons in the signal mode, with a typical efficiency on the order of 80%. Devices can be cooled down so as to reduce the dark counts and allow for photon number resolution [82]. For example superconducting transition-edge detectors operating at temperatures in the milli Kelvin range [83] work with an efficiency of 88% at a wavelength of 1550nm. Quantum nondemolition measurements are also potential candidates [84] and we will see in the next section how the qubus scheme provides a natural implementation [85]

Turning to the generation of single photons, a crude approach is to use an attenuated laser source, producing weak coherent states containing only a single photon with a high probability. However such a source is not heralded and we never know with certainty whether or not the pulse contains 0, 1 or even 2 photons. There are currently mainly two schemes for a more precise generation, the first of which is conditional parametric down conversion, the most commonly used in LOQC experiments. This method involves sending photons with a fixed frequency ω_0 through a nonlinear optical medium which generates pairs of photons of frequency $\omega_1 + \omega_2 = \omega_0$. When one of these two outgoing photons is detected, we know with certainty that there is another single photon propagating, due to momentum conservation. Being able to conditionally open or close a filter based on the measurement result provides us with a heralded single photon source, but still not an on-demand source. The second type of schemes, addressing this issue, are cavity based and essentially rely on single photon emission of some matter qubit as it spontaneously decays from an excited state to a lower lying state [86]. The experiments are very complex and so far efficiencies remain on the order of a few percent (see [87] for a review on potential technologies).

Experiments can still be undertaken with low efficiency devices as the outcomes of interest are post-selected. But for scalable online quantum computation, serious progress will have to be made, in single photon sources, detectors and quantum memories, as emphasized in [63].

2.4 The Qubus Scheme

In the previous section we mentioned the concept of distributed QIP, in which the logical qubits used in the computation do not interact directly. Such an approach, combining stationary and flying [57] qubits presents many advantages [88]. To begin with it allows us to overcome the difficulty of implementing direct coherent interactions between logical qubits, thus enabling well isolated, low decoherence qubits. Another obvious attribute is the ex-

tendibility of the architecture, which constitutes a challenge for conventional static qubit architectures. The ancillary system(s) used to mediate interactions we will from now on refer to as quantum buses. These buses need not however be the propagating systems. In CQED applications, the logical qubits and the buses may be the photonic and the atomic qubits or vice versa. The case we mentioned in the previous section was that of single photons mediating interactions between atomic qubits. The other possibility is to use an atom to mediate the interaction between photonic qubits, as was demonstrated early on by Turchette et al. [89]. In this experiment, a conditional phase shift in polarization space was observed between pairs of single photons as they pass through a cavity containing a single atom. The effect is analogous to a cross-phase modulation obtained in a Kerr medium, but here it is amplified by the strong coupling of photons with the atom, due to the cavity.

A scalable setup was proposed by Duan and Kimble [79], in which single photons successively bounce off a cavity containing a single atom, implementing a conditional phase gate between the single photons. The atom-photon interaction takes place in the dispersive regime (no absorption). This interaction has also been achieved experimentally by Schuster et al. [90] for a superconducting qubit coupled to photons in a microwave transmission line. This same interaction also forms the basis of the 'photonic module' developed by Devitt et al. [91], which allows for the efficient generation of large scale stabilizer states, an essential resource for quantum applications. In this scheme the issue of storage is also potentially overcome through the continuous measurement of a cluster state as it is being produced by the modules.

As we saw in the previous section, the use of photonic qubits is confronted with serious technological challenges, in the design of efficient single photon sources and detectors. In the distributed setting, where the logical qubits are static, the thought of using a more robust mediating bus naturally springs to mind. The brings us to the idea of a continuous variable bus, which is the topic of this section.

2.4.1 Hybrid quantum information processing

Most of the results in quantum information theory were developed by making use of qubits or qudits. However even though single qubit operations are not so much of an issue, the level of control required to physically implement entangling gates between individual qubits and measure them within realistic coherence times is tremendous, limiting the experimental realizations.

The initial theoretical proposals were rapidly adapted to a continuous variable (CV) setting, where CV QIP was shown to be possible by Lloyd and Braunstein [92]. A detailed review is given by Braunstein and van Loock in [48]. Also recently the cluster state model was translated into a CV setting [93]. CV implementations may be more accessible in some respects, with simple measurements and entangling operations. Despite these advantages, this framework is limited by the nonlinearity available experimentally, making single system operations difficult, and the fact that even in theory, protocols cannot work perfectly. Combining the exactness of discrete variables and the robustness of continuous variables is therefore a natural route to take.

The term 'hybrid' was first coined by Lloyd [94] to describe quantum information processes featuring both discrete and continuous variables. The ability to switch on and off the set of interaction Hamiltonians of the type $\{\pm Z_{qubit}X_{osc}, \pm Z_{qubit}P_{osc}\}$ (where the first Pauli operator acts on the qubit and the second quadrature operator acts on the oscillator) enables one to simulate single qubit operations and quantum logical gates on discrete systems. The reverse is also true, that is these Hamiltonians allow for arbitrary logical gates on CV systems. Multi-qubit extensions were rapidly undertaken in generalizations [95,96]. The initial observation made by Lloyd came at the same time as Milburn's proposal to simulate interactions between trapped ions by coupling them to a common vibrational mode [97], constituting a direct physical realization of a hybrid quantum computer. This approach was used to entangle up to four ions experimentally [98]. A hybrid quantum computer could potentially be more versatile than its strictly discrete counterpart, providing simple algorithms to compute eigenvectors and eigenvalues [94] or implementing Grover's search algorithm in a direct way [95].

2.4.2 Conditional rotations and displacements

In this thesis we will consider two types of interactions, coupling discrete systems with CV systems. The first we refer to as the conditional rotation, described by the effective interaction Hamiltonian

$$\hat{H}_R = -\hbar\chi\hat{a}^\dagger\hat{a}\hat{\Lambda} \tag{2.109}$$

where $\hat{a}(\hat{a}^\dagger)$ are the annihilation (creation) operators acting on the CV probe mode and $\hat{\Lambda} = \sum_n \lambda_n|n\rangle\langle n|$. In the case of a cross-Kerr interaction, $\hat{\Lambda} = \hat{b}^\dagger\hat{b}$ the number operator acting on the signal (subsystem) mode ($\hat{\Lambda}|n\rangle = \lambda_n|n\rangle = n|n\rangle$) and χ is proportional to the third order nonlinear susceptibility of the

medium. In a CQED setting involving a two level atom interacting with the cavity mode which is far detuned, we observe the effective Hamiltonian seen earlier [52] in which $\hat{\Lambda} = Z$ where Z is the Pauli operator acting on the atomic qubit ($\hat{\Lambda}|n\rangle = \lambda_n|n\rangle = (-1)^n|n\rangle$) and χ is the atom-light coupling strength. In both the cross phase and the CQED settings we have a hybrid interaction between the continuous quadrature variables of the probe field and the discrete degrees of freedom of the subsystem. Initiating the probe in a coherent state $|\alpha\rangle$ and applying the interaction for a time t yields

$$e^{-i\hat{H}_R t/\hbar}\sum_n c_n|n\rangle|\alpha\rangle = \sum_n c_n|n\rangle|\alpha e^{i\lambda_n\chi t}\rangle. \tag{2.110}$$

The probe mode is in effect being conditionally rotated in phase space by an angle proportional (in the two cases we consider) to χt. We will denote the conditional rotation by

$$R(\theta\hat{\Lambda}) = e^{i\theta\hat{a}^\dagger\hat{a}\hat{\Lambda}}, \tag{2.111}$$

with $\theta = \chi t$.

The second interaction we consider is the conditional displacement. The interaction Hamiltonian producing the interaction is

$$\hat{H}_D = -\hbar\chi\hat{X}(\phi)\hat{\Lambda}, \tag{2.112}$$

where $\hat{X}(\phi) = (\hat{a}e^{-i\phi} + \hat{a}^\dagger e^{i\phi})/2$, the generalized quadrature operator. The resulting unitary operation after an interaction time t we refer to as a conditional displacement

$$\begin{aligned} e^{-i\hat{H_D}t/\hbar} &= e^{(\beta\hat{a}^\dagger - \beta^*\hat{a})\hat{\Lambda}} \\ &= \sum_n |n\rangle\langle n|e^{(\beta\hat{a}^\dagger - \beta^*\hat{a})\lambda_n} \\ &= D(\beta\hat{\Lambda}) \end{aligned} \tag{2.113}$$

with $\beta = i\chi t e^{i\phi}/2$. By changing the phase ϕ, the field or oscillator interacting with the subsystem can be conditionally displaced in different directions in phase space. In the present thesis we will only work with qubits as subsystems and thus mostly we will have $\hat{\Lambda} = Z$.

This particular interaction occurs in different physical setups. The first is in superconducting qubits, more specifically superconducting charge qubits coupled dispersively to an optical bus mode. This was realized experimentally by Wallraff et al. [99,100] who realized a coherent coupling of the qubit

with a microwave bus mode, enabling a dispersive readout of the qubit state via a homodyne measurement on this bus mode. A superconducting charge qubit essentially consists in a superconducting island connected to a large superconducting reservoir through a Josephson junction [101]. The two logical states correspond to the near degenerate quantum states with zero or one excess Cooper pairs on the island. If a composite junction made up of two parallel junctions is constructed, one can control the tunneling between the island and the reservoir via a magnetic flux threading the junction itself. Given such a setup a coupling of the form (2.112) naturally occurs between the qubit and the electromagnetic field surrounding the junction [102, 103]. Superconducting flux qubits also enable this type of coupling, implemented experimentally by Chiorescu et al. [104].

It is also possible to realize the Hamiltonian (2.112) in an ion trap with adapted driving fields [105, 106]. In this case the ions are coupled to a common vibrational mode (phonon), acting as a CV bus. This single vibrational mode approximation holds if the ions are well isolated from the environment, avoiding thermalization, and if they are sufficiently cool, so as to make the one dimensional harmonic approximation valid [40]. Once these criteria are fulfilled, the entire linear chain of trapped ions moves as one body, and the transition to the next higher energy state is made through the absorption of a center of mass phonon.

At this point it is worth noticing some differences between conditional rotations and displacements. First, conditional rotations commute with each other, in contrast with conditional displacements. Second, conditional rotations are energy conserving, while conditional displacements require an external energy input or output. Each one of these interactions will allow us to develop a distinct approach to qubus computation. The sole use of conditional rotations without displacements will call for bus measurements whereas the use of conditional displacements will enable measurement free operations. We begin with the latter and the use of the geometric phases in phase space.

2.4.3 Observing the geometric phase

Coming back to the geometric phase $D(\beta)D(\alpha) = e^{i\mathrm{Im}[\alpha^*\beta]}D(\alpha+\beta)$ generated by a pair of displacements, an interesting sequence to consider is one in which the oscillator returns to it's initial state in phase space, for example

$$D(-\beta)D(-\alpha)D(\beta)D(\alpha) = e^{2i\mathrm{Im}[\alpha^*\beta]}D(0). \tag{2.114}$$

The resulting state can be viewed as the same state up to a global phase. Considering a general closed loop $D_{\circlearrowleft}$ in phase space, characterized by a sequence of displacements of amplitudes $\{\alpha_j, j = 1, .., N\}$ with $\sum_{j=1}^{N} \alpha_j = 0$, then

$$D_{\circlearrowleft} = \prod_{j=1}^{N} D(\alpha_j) = e^{i\Theta}. \tag{2.115}$$

Given the relation between the coherent state amplitude α and the quadrature expectation values, $\mathrm{Re}[\alpha] = \langle \hat{X} \rangle = x$ and $\mathrm{Im}[\alpha] = \langle \hat{P} \rangle = p$, the resulting phase for an arbitrary loop which can be attained as $N \to \infty$ becomes [107]

$$\Theta = \oint (xdp - pdx). \tag{2.116}$$

This is nothing else but the area enclosed by the trajectory, independent of it's shape, size or of the speed at which it is completed. For these reasons it can be called a geometric phase [96]. The direction of the trajectory gives the sign of the phase, which is positive for anticlockwise loops.

In order to be able to observe this geometric phase, the displacements need to be conditional on the quantum state of another system. Luis [107] introduced this observation in the Schrödinger picture, here we will simply give the equivalent observation in the Heisenberg picture. Let us take a qubit which conditionally displaces a CV probe through the interaction $D(\beta Z)$. Then the $X = |0\rangle\langle 1| + |1\rangle\langle 0|$ qubit observable evolves to

$$\begin{aligned} X &\to D(\beta Z) X D^{\dagger}(\beta Z) = D(\beta Z) X D(-\beta Z) \\ &= \left\{ \frac{D(2\beta) + D(-2\beta)}{2} \right\} X + i \left\{ \frac{D(2\beta) - D(-2\beta)}{2} \right\} Y. \end{aligned} \tag{2.117}$$

At this point the qubit and probe are entangled, as indicated by the new observables. Completing a conditional loop enclosing an area Θ in phase space, noting that $D^{\dagger}_{\circlearrowleft} = D^{*}_{\circlearrowleft}$, the final X observable is

$$\begin{aligned} X &\to e^{i\Theta Z} X e^{-i\Theta Z} \\ &= \cos(2\Theta) X - \sin(2\Theta) Y. \end{aligned} \tag{2.118}$$

Thus the geometrical phase can be observed through an X measurement on a qubit initially in the $|+\rangle$ state as $\langle +|\cos(2\Theta)X|+\rangle - \langle +|\sin(2\Theta)Y|+\rangle =$

$\cos(2\Theta)$. This process can be used to implement arbitrary single qubit rotations, as long as the qubit can induce conditional loops in phase space resulting in both $e^{i\Theta Z}$ and $e^{i\Theta X}$ unitary operations. What can be done if we consider different qubits interacting with the same oscillator?

2.4.4 Multi-qubit interactions

The sequence (2.114) can be generalized to the conditional case by inserting a pair of commuting operators $\hat{A}$ and $\hat{B}$

$$D(-\beta\hat{B})D(-\alpha\hat{A})D(\beta\hat{B})D(\alpha\hat{A}) = e^{2i\Theta\hat{A}\hat{B}}, \tag{2.119}$$

where $\Theta = \mathrm{Im}[\alpha^*\beta]$. Here we have in effect simulated a Hamiltonian of the form $\hat{A}\hat{B}$. Now if these two operators act on the same composite system, one can simulate very useful Hamiltonians. For example if the composite system is a set of N qubits, then setting $\hat{A} = \hat{B} = \hat{J}_z = \sum_{n=1}^{N} Z_n$ enables the simulation of the highly useful nonlinear Hamiltonian $\hat{J}_z^2$.

Another way for the $\hat{A}$ and $\hat{B}$ operators to commute, is if they act on different subsystems. This leads us to the simulation of the essential two-qubit Ising interaction, which leads directly to the two qubit (a and b) conditional phase gate [97]

$$D(-\beta_b Z_b)D(-\beta_a Z_a)D(\beta_b Z_b)D(\beta_a Z_a) = e^{2i\Theta Z_b Z_a}. \tag{2.120}$$

Setting $\Theta = \mathrm{Im}[\beta_a^*\beta_b] = \pi/8$ yields a gate locally equivalent to the CZ gate as defined in section (2.1.3)

$$\mathrm{CZ} = e^{i\frac{\pi}{4}(1-Z_a)(1-Z_b)} = e^{i\frac{\pi}{4}Z_aZ_b}e^{-i\frac{\pi}{4}Z_a}e^{-i\frac{\pi}{4}Z_b}, \tag{2.121}$$

up to a global phase. This gate circuit is illustrated in Fig. 2.9 and the phase space trajectories of the probe in Fig. 2.10, taking β_a and β_b pure real and imaginary respectively. The sequence (2.119) is particularly relevant to situations in which the qubits are in different locations and do not interact simultaneously with the CV bus. Of course such a gate can also be implemented in the case in which the two qubits interact simultaneously with the bus, with $\hat{A} = \hat{B} = Z_a + Z_b$.

A conditional rotation based CZ gate was proposed by Spiller et al. [108],

$$R(\theta Z_1)D(-\beta)R(\theta Z_2)D(-i\beta)R(\theta Z_1)D(\beta)R(\theta Z_2)D(i\beta) \approx \mathrm{CZ}, \tag{2.122}$$

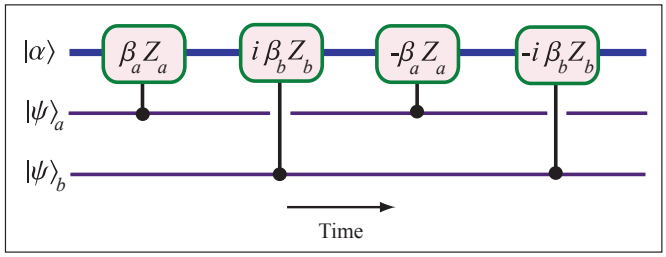

Figure 2.9: The circuit representation of the CZ gate described in the text, each rectangle is a conditional displacement, induced by the qubit onto the probe initiated in the coherent state $|\alpha\rangle$.

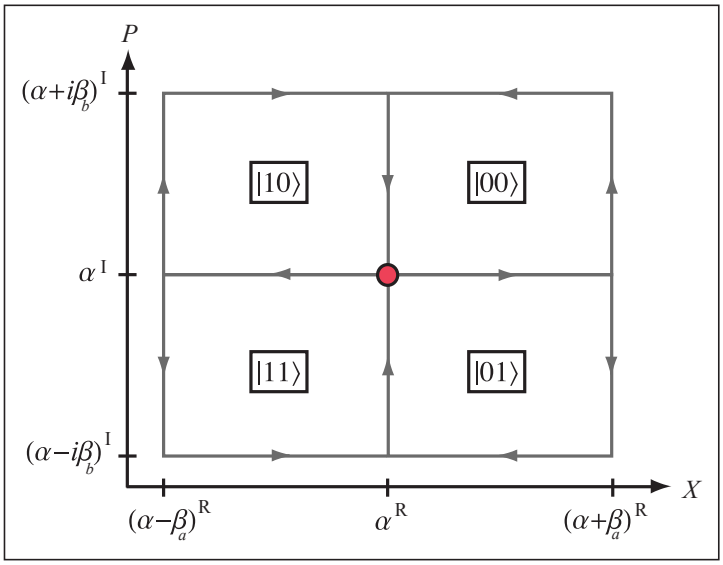

Figure 2.10: The four trajectories in phase space of the CV bus, corresponding to the four two-qubit states. Here we assume orthogonal displacements by taking β_a and β_b real. The 'R' and 'I' exponents represent the real and imaginary parts respectively.

setting the conditional two qubit phase $|\beta\theta|^2 = \pi/4$. However the bus doesn't fully disentangle from the qubits, leading to a systematic decoherence effect on them. The error scales as $|\beta|\theta^2$ and can be made small in the limit of large β and small θ. To obtain an exact conditional rotation based

CZ gate, we must use an important property of rotation operations, that is [109]

$$e^{\theta\hat{a}^\dagger\hat{a}} f\left(\hat{a},\hat{a}^\dagger\right) e^{-\theta\hat{a}^\dagger\hat{a}} = f\left(\hat{a}e^{-\theta},\hat{a}^\dagger e^{\theta}\right), \tag{2.123}$$

where f can be expanded in a power series. Then the conditional displacement can be realized with the following sequence [110]

$$D(\alpha\cos\theta)R(-\theta Z)D(-2\alpha)R(\theta Z)D(\alpha\cos\theta) = D\left(2i\alpha\sin\theta Z\right), \tag{2.124}$$

with α real. Based on these conditional displacements, an exact CZ gate can be constructed. The gate itself can be simplified by using conditional displacements of the form $D(\beta e^{i\theta Z})$ obtained through the removal of the first and last displacements in (2.124). The sequence becomes

$$D(-i\beta_b e^{i\theta Z_b})D(-\beta_a e^{i\theta Z_a})D(i\beta_b e^{i\theta Z_b})D(\beta_a e^{i\theta Z_a}) = e^{2i\beta_a\beta_b\sin^2\theta Z_1 Z_2}. \tag{2.125}$$

The size of the conditional phase is equal to the difference between the area enclosed by the even ($|00\rangle, |11\rangle$) and odd ($|01\rangle, |10\rangle$) qubit states. The areas are $\beta_a\beta_b$ and $\beta_a\beta_b\cos2\theta$ respectively, leading to a conditional phase $\Theta = \beta_a\beta_b(1-\cos2\theta) = 2\beta_a\beta_b\sin^2\theta$. The trajectories are shown in Fig. 2.10. An interesting distinction can be made between gates which use trajectories with opposite directions (e.g. (2.120)) and gates which use relative area difference like the one above.

It can easily be seen that the product of displacements conditioned on a set of qubits will ultimately lead to the simulation of at most two-body Hamiltonians of the form $\sum_{i,j} Z_i Z_j$. In order to directly simulate many-body interactions, single qubit conditional displacements are no longer sufficient. Then the conditional rotation allows us to overcome this issue and build up conditional displacements containing several qubit operators. Let us for example consider the three-qubit interaction $Z_a Z_b Z_c$, to simulate it we need a conditional displacement containing a product of operators, for example $D(\mu Z_a Z_c)$. This can be obtained through the sequence

$$R(\theta Z_c)D(\nu Z_a)R(-\theta Z_c) = D(\nu Z_a e^{i\theta Z_c}) = D(\nu\cos\theta Z_a + i\nu\sin\theta Z_a Z_c). \tag{2.126}$$

Based on this, the three-qubit interaction can be directly simulated as [96]

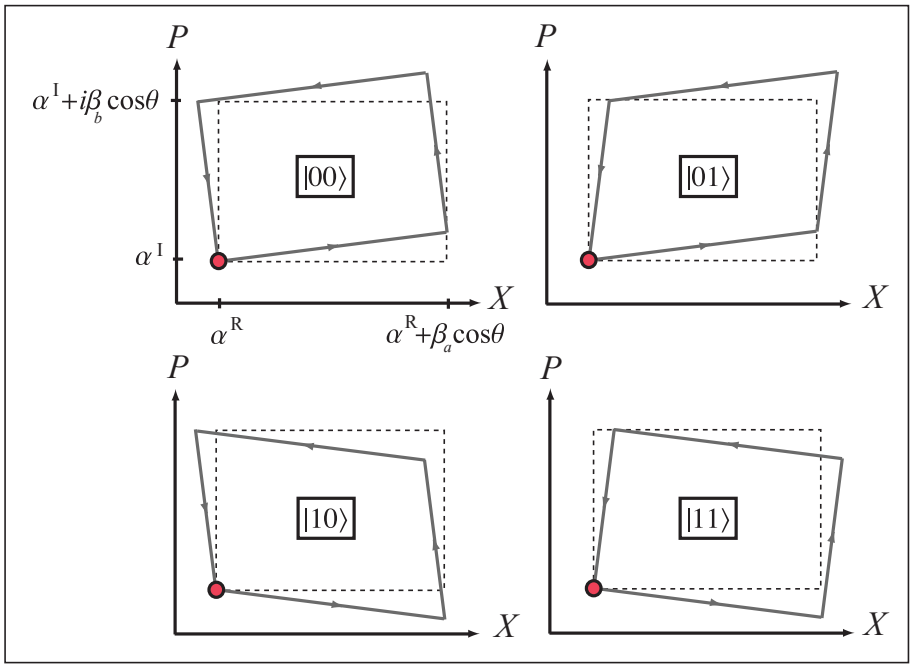

Figure 2.11: The four trajectories in phase space of the CV bus, for the exact CZ gate based on conditional rotations (2.125). We can see that the even and odd parities lead to different enclosed areas.

$$D(-\beta_b Z_b)D(-\beta_a Z_a e^{i\theta Z_c})D(\beta_b Z_b)D(\beta_a Z_a e^{i\theta Z_c}) = e^{-i\tau Z_a Z_b \sin(\theta Z_c+\varphi)}, \tag{2.127}$$

with $\tau = |\beta_a\beta_b|$ and $\varphi = \arg(\beta_a) - \arg(\beta_b)$. By setting $\varphi = 0$, the Hamiltonian $\lambda Z_a Z_b Z_c$ is obtained, and based on a variant of this the three-qubit Toffoli gate can be implemented. Wang and Zanardi extended this procedure to more systems and also to gates on encoded qubits [96].

The use of conditional geometric phases in phase space is very attractive, as the gates are implemented deterministically, without the need for post-selection or feed-forward. However they require at least two interactions per subsystem, one to couple the subsystem with the CV bus, generating a geometric phase, the second to decouple the two. Depending on the physical system envisaged, and in particular for distributed systems, this may be very complex to implement. If we are dealing with qubits in different locations, this means the CV bus will have to be dynamically switched and rerouted

every time we wish to apply a gate between two different qubits. One way of overcoming these issues is to design an adapted architecture, which can be scaled up in a practical way. The other way is to introduce bus measurements.

2.4.5 Qubus measurement-based gates

The simplest measurement one can think of is a single qubit measurement. This can be achieved through the qubus scheme with the same interactions utilized above, and is traditionally referred to in the quantum optics literature as a quantum non-demolition (QND) measurement [111, 112]. Let us consider the measurement in the computational basis (Z basis) of a single qubit initially in the state $|\psi\rangle = c_0|0\rangle + c_1|1\rangle$. This qubit can then either conditionally displace or conditionally rotate a CV bus in state $|\alpha\rangle$ as

$$D(\beta Z)|\psi\rangle|\alpha\rangle = c_0|0\rangle|\alpha+\beta\rangle + c_1|1\rangle|\alpha-\beta\rangle,$$

$$R(\theta Z)|\psi\rangle|\alpha\rangle = c_0|0\rangle|\alpha e^{i\theta}\rangle + c_1|1\rangle|\alpha e^{-i\theta}\rangle, \tag{2.128}$$

where we have chosen α and β to be real for simplicity. Of course we can also use a photonic qubit and the number operator $\hat{n}$ instead of the Pauli Z operator [113]. In any case, after the interaction, the probe state lies in one of two positions in phase space as illustrated in Fig. 2.12 and Fig. 2.13. Discriminating between them through a measurement will in turn implement a Z measurement on the qubit. This can be done via a homodyne detection, as described in section 2.2. In the first case, the two positions lie along the X quadrature axis and thus a projection onto this axis is optimal in discriminating the two. There is a measurement outcome probability distribution associated with each position

$$|\langle x|\alpha \pm \beta\rangle|^2 = \sqrt{\frac{2}{\pi}} e^{-2(x-\alpha\mp\beta)^2}. \tag{2.129}$$

Now choosing all measurement outcomes larger than the midpoint between the two distributions (α) to correspond to the qubit state $|0\rangle$ and all measurement outcomes smaller than the midpoint to correspond to the qubit state $|1\rangle$, the intrinsic error probability E_{beta} of our qubit measurement becomes

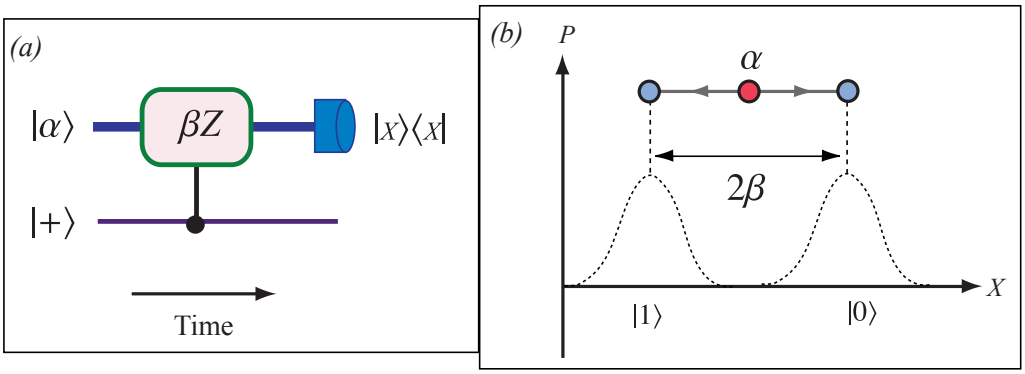

Figure 2.12: The displacement based single qubit measurement. (a) The circuit representation, in which the interaction is followed by an X quadrature measurement. (b) The phase space representation of the probe mode states, starting with an arbitrary α conditionally displaced by a real amount β. The curves on the X quadrature axis represent the measurement outcome probability distributions.

$$\begin{aligned} E_\beta &= \frac{1}{2}\sqrt{\frac{2}{\pi}}\int_{-\infty}^{0} e^{-2(x-\beta)^2}dx + \frac{1}{2}\sqrt{\frac{2}{\pi}}\int_{0}^{\infty} e^{-2(x+\beta)^2}dx \\ &= \frac{1}{\sqrt{\pi}}\int_{\beta/\sqrt{2}}^{\infty} e^{-x^2}dx \\ &= \frac{1}{2}\mathrm{erfc}\left[\frac{\beta}{\sqrt{2}}\right]. \end{aligned} \tag{2.130}$$

We have used the fact that this error is independent of the initial real amplitude and set $\alpha = 0$. In the case of the conditional rotation, for a small angle θ it is optimal to perform a P quadrature measurement. The error probability can again be calculated through an $|X\rangle\langle X|$ projection after having rotated the state in phase space through $e^{i\pi/2}$

$$\begin{aligned} E_\theta &= \frac{1}{2}\int_{-\infty}^{0} |\langle x|i\alpha e^{-i\theta}\rangle|^2 dx + \frac{1}{2}\int_{0}^{\infty} |\langle x|i\alpha e^{i\theta}\rangle|^2 dx \\ &= \frac{1}{2}\mathrm{erfc}\left[\frac{\alpha\sin\theta}{\sqrt{2}}\right]. \end{aligned} \tag{2.131}$$

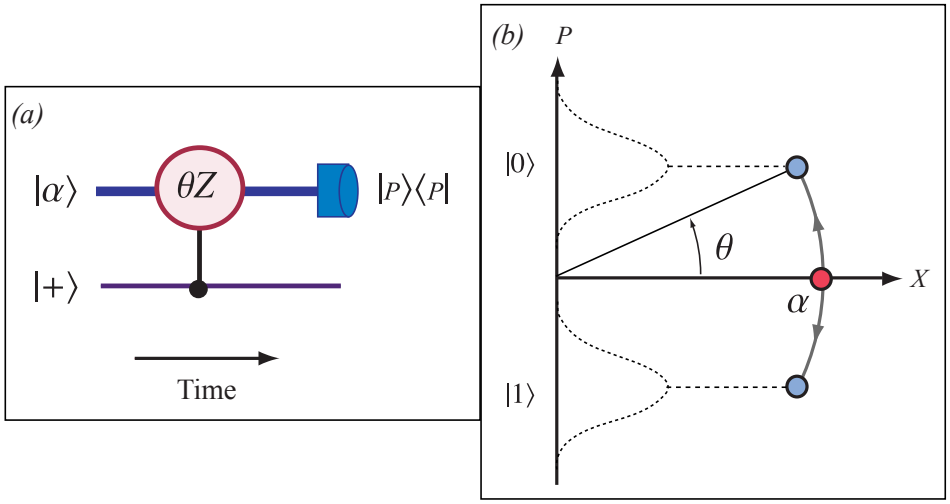

Figure 2.13: The rotation based single qubit measurement. (a) This time the interaction is followed by a P quadrature measurement. (b) In phase space the initial real amplitude in rotated in one of two directions. Again we observe measurement outcome probability distributions.

From these two results one can see that given one of two coherent states at distance d from each other in phase space, the optimal discriminating homodyne measurement will have an intrinsic error of $\mathrm{erfc}[d/2\sqrt{2}]/2$. One aspect of the conditional rotation is that even if the strength θ of the nonlinearity is small, these two states can be made as distinguishable as needed by increasing the amplitude α of the probe. This is easy to see because the projected distance between the two coherent states $|\alpha e^{i\theta}\rangle$ and $|\alpha e^{-i\theta}\rangle$ is $2\alpha\sin\theta \approx 2\alpha\theta$ for small θ. The small θ regime is referred to as the weak nonlinearity regime.

We note here that if instead of measuring the bus we measure the qubit in the $|\pm\rangle$ basis, we produce a coherent superposition of two coherent states: a cat state. Using a conditional displacement on a vacuum bus, the state after the interaction we saw is $c_0|0\rangle|\beta\rangle + c_1|1\rangle|-\beta\rangle$. The qubit measurement will then project the bus to the state $\mathcal{N}(c_0|\beta\rangle \pm c_1|-\beta\rangle)$, where $\mathcal{N} = 1/(1+2e^{-2\beta^2}\mathrm{Re}[c_0^* c_1])^{1/2}$ is a normalization factor. To some extent, the state of the qubit is mapped onto the CV bus. This approximate bit teleportation is used by Myers et al. [114] to implement quantum error correction within the qubus setting.

Now letting the bus interact with two qubits consecutively, supposing

they are initiated in the $|+\rangle$ state

$$D(\beta Z_b)D(\beta Z_a)|++\rangle|\alpha\rangle = \frac{1}{\sqrt{2}}|\psi^+\rangle|\alpha\rangle + \frac{1}{2}|00\rangle|\alpha+2\beta\rangle + \frac{1}{2}|11\rangle|\alpha-2\beta\rangle,$$
$$R(\theta Z_b)D(\theta Z_a)|++\rangle|\alpha\rangle = \frac{1}{\sqrt{2}}|\psi^+\rangle|\alpha\rangle + \frac{1}{2}|00\rangle|\alpha e^{2i\theta}\rangle + \frac{1}{2}|11\rangle|\alpha e^{-2i\theta}\rangle, \tag{2.132}$$

where $|\psi^+\rangle = (|01\rangle + |10\rangle)/\sqrt{2}$ as defined in section (2.1.3). Thus the bus is left in three possible states as show in Fig. 2.14, one of which ($|\alpha\rangle$) corresponds to an entangled state ($|\psi^+\rangle$) of the two qubits. Being able to discriminate the state $|\alpha\rangle$ from the other possibilities will in effect implement a parity gate with success probability 1/2. One option is to use homodyne detection, in which case it is reasonable to group the measurement outcomes into three bins, corresponding to the three possible states. In the conditional displacement case, the three bins will be

$$\begin{aligned} x(|\alpha-2\beta\rangle) &= [-\infty, \alpha-\beta[, \\ x(|\alpha\rangle) &= [\alpha-\beta, \alpha+\beta], \\ x(|\alpha+2\beta) &=]\alpha+\beta, \infty], \end{aligned} \tag{2.133}$$

meaning the intrinsic error probability when post-selecting the $|\alpha\rangle$ measurement outcome becomes

$$\begin{aligned} E_\beta &= \frac{1}{4}\int_{-\beta}^{\beta} e^{-2(x+2\beta)^2}dx + \frac{1}{4}\int_{-\beta}^{\beta} e^{-2(x-2\beta)^2}dx \\ &= \frac{1}{2}\int_{-\beta}^{\beta} e^{-2(x+2\beta)^2}dx. \end{aligned} \tag{2.134}$$

This error can be made small by increasing β, we already have $E_\beta \sim 7\times10^{-4}$ for $\beta = 3$. A similar analysis can be made for the conditional rotation based parity gate illustrated in Fig. 2.14, where now the distance β is simply replaced by $\alpha\sin2\theta/2$ with a P quadrature measurement.

Another possibility for the discrimination of the bus states is to resort to photon number detection. In this case the probe has to be unconditionally displaced by an amount $-\alpha$, prior to the measurement. Or equivalently the probe can be initiated in the vacuum state. For an ideal projection $|n\rangle\langle n|$ onto the number basis, the state of the two qubits becomes

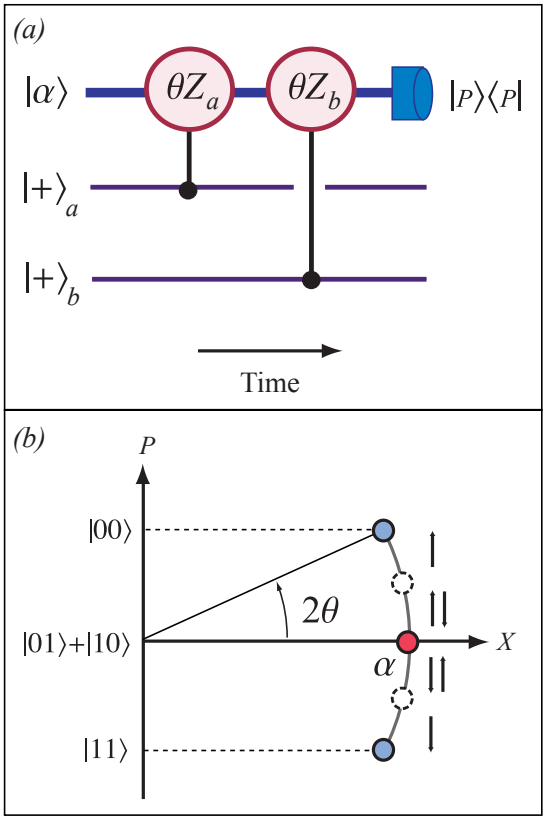

Figure 2.14: The conditional rotation based parity gate. (a) Both qubits a and b, initially prepared in $|+\rangle$ states, interact consecutively with the bus, before it undergoes homodyne detection. (b) The probe can end in one of three positions in phase space. The $|\alpha\rangle$ position now corresponds to an odd parity of the qubits. Post-selecting this state through a P quadrature measurement projects the qubits the odd parity Bell state

$$\begin{aligned} |\varphi_f\rangle &= (|01\rangle + |10\rangle)/\sqrt{2} \qquad \text{for } n = 0, \\ |\varphi_f\rangle &= (|00\rangle + (-1)^n|11\rangle)/\sqrt{2} \qquad \text{for } n > 0. \end{aligned} \tag{2.135}$$

Each outcome will occur with the same probability, though there is an intrinsic error of $e^{-4\beta^2}$ in the measurement due to the overlap between any coherent state with the vacuum state. This error can be made very small for suitable β.

Yet another option illustrates one potential advantage of using conditional rotations. The final states of the bus in (2.132) are $|\alpha\rangle$, $|\alpha e^{2i\theta}\rangle$ and $|\alpha e^{-2i\theta}\rangle$. Now because these three coherent states differ only in phase we can distinguish the inner state ($|\alpha\rangle$) from the two outer states ($|\alpha e^{2i\theta}\rangle$,$|\alpha e^{-2i\theta}\rangle$) without further knowledge on which one of these two outer states. This can be achieved through an X quadrature measurement, and in effect realizes a complete parity measurement on the qubits, as the state prior to measurement can be written

$$|\varphi\rangle = \frac{1}{\sqrt{2}}\langle x|\alpha\rangle|\psi^+\rangle + \frac{1}{2}\langle x|\alpha\cos 2\theta\rangle(e^{i\phi(x)}|00\rangle + e^{-i\phi(x)}|11\rangle), \qquad (2.136)$$

with $\phi(x) = \exp[2x\alpha\sin 2\theta - \alpha^2\sin 4\theta]$. We now have two distinct probability distributions each corresponding to a certain parity. Similarly to the single qubit measurement, we attribute all measurements to the left of the midpoint ($x = \alpha(1-\cos 2\theta)/2$) to the even parity state ($(e^{i\phi(x)}|00\rangle + e^{-i\phi(x)}|11\rangle)/\sqrt{2}$) and all those to the right we attribute to the odd parity ($|\psi^+\rangle$). Each one will occur with equal probability, however the error now becomes $E_\theta = \mathrm{erfc}[\alpha\sin^2\theta/\sqrt{2}]$, which is significantly larger than the error occurring in a post-selected P quadrature measurement. In the weak nonlinearity regime, this error is of the order 10^{-5} for $\alpha\theta^2 > 9$, thus again it can be made small by increasing the probe amplitude α.

Based on this near deterministic parity check, Nemoto and Munro devised a Franson type CNOT gate [115] by using an ancillary qubit. In this gate, both the signal and target qubits go through such a parity gate with the same ancillary qubit, but in different bases. Three feed-forward steps are needed, one for each parity gate and one after the measurement of the ancillary qubit, guaranteeing the simulation of a unitary gate on the two inputs. A particularly well suited candidate system for measurement-based qubus schemes would be Nitrogen vacancy centers in diamond [116] within individual cavities. They could operate at optical wavelengths, insuring efficient homodyne measurements, and have exhibited coherence times of up to several microseconds at room temperature.

Different variants of the parity gate can be found in [108], where conditional rotations and displacements are used, so as to increase the separation of the probe states in phase space and enable gates functioning with a smaller intrinsic error. However, in view of a full analysis of the gate, one must also factor in the number of interactions and thus the time taken. The crucial effects of dissipation in the bus are the topic of the next chapter.

Chapter 3

Loss in hybrid qubit-bus couplings and gates

One attribute of distributed approaches to quantum computing, as mentioned earlier, is the potential for low decoherence and extendible storage regions for qubits. Now assuming such a high quality storage is achieved, the most important source of noise to consider lies in the bus itself. As it interacts and travels between qubits, decoherence effects acting upon the bus will be transmitted to all the qubits which are coupled to it. Thus it becomes crucial to understand and characterize this indirect source of decoherence, before envisaging any strategies to suppress it or protect against it. In this chapter we investigate the effects of what is one of the major sources of decoherence in the qubus scheme; bus dissipation.

As pointed out in the previous chapter, the physical circumstances in which one can envisage a hybrid coupling between a CV and discrete variable system have been extensively investigated. Possible realizations for the qubus scheme include that of atomic qubits interacting dispersively with a cavity mode (optical or vibrational in the case of trapped ions), superconducting charge qubits coupled to a microwave bus mode and single photons interacting with a strong probe in a Kerr medium.

Decoherence effects during such interactions have been explored in the past, for example in the case of a two-level atom interacting dispersively with an optical mode in a dissipative cavity [117–120]. This dispersive type of interaction forms the basis for most qubus schemes and dissipation effects during the interaction on an entangling gate between two qubits can potentially be overcome through an iterative procedure, as shown by Barrett and Milburn [121]. A symmetrization technique to develop resilience

to both dissipation and thermal fluctuations was also proposed by Cen and Zanardi in an ion trap setting [122]. There the authors took advantage of the invariance under time reversal of the action of the gate, noticing that the combination of an interaction sequence with its time reversed version canceled out, to some extent, the effects of dissipation. Even though they are effective, these methods focus on a pair of qubits within the same cavity or trap and decoherence due to inter-cavity communication remains to be addressed. In addition to this they propose interaction sequences which have to be iterated many times before any significant improvement in gate fidelity can be appreciated. In the context of cross phase modulation, Jeong approximated the effects of decoherence along with their impact on optical quantum information processing using weak nonlinearities [123, 124]. He showed that dissipation effects in a two-qubit parity gate can be minimized if one can implement a photon number measurement on the bus. In the absence of such a technology, the exact effect on the photonic qubits remains to be evaluated and possibly overcome.

The chapter is structured as follows. In the first section we focus on loss during interactions, extending Jeong's results by considering an arbitrary input in what we call the sliced approximation, for which interaction and dissipation are successively applied and summed over. We then proceed to solving exactly the master equation during the interaction for both the dispersive cavity QED and the all optical cross phase situations and apply the results to different probe states. After this we follow the entanglement and coherence dynamics of a qubit and the CV as they interact with each other. A trade off between the entanglement generated and the required precision in interaction time is observed.

In section 2 we carry our attention over to loss in between interactions, distinguishing at first the effects of loss on conditional rotation and conditional displacement entangled qubit-bus states. Then we give a simple scheme for the purification of a particular type of mixed qubit-bus state, using only a two-qubit gate, a beam splitter and non-photon resolving detectors. At the end of the section we discuss the effects of transmission loss on a parity gate.

Finally in section 3 we move our attention to hybrid gates themselves starting with the simulated conditional displacement gate followed by the CZ gate. By adding dissipation between interactions we obtain the quantum operations undergone by the qubits and discuss gate fidelity. We provide a simple iteration scheme to simplify the operation down to a perfect CZ gate followed by independent single qubit dephasing. At last we investigate one approach to probe state engineering in order to overcome dissipation effects.

3.1 Loss during interactions

In this section we consider the effects of loss in the bus during a dispersive interaction represented by the conditional rotation operation $R(\theta\hat{\Lambda})$, as defined in the previous chapter. The process is pictorially represented in Fig. 3.1. We first extend previous work approximating the process in discrete time steps. It is a very intuitive approach, which converges numerically as the time steps become smaller. We then verify the validity of the approach by solving the dynamics in continuous time via the master equation.

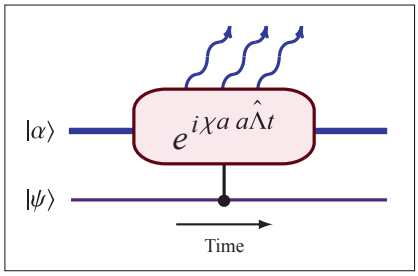

Figure 3.1: Loss in the probe mode during the coupling between the discreet system $|\psi\rangle$ and the CV prepared in the coherent state $|\alpha\rangle$.

3.1.1 The sliced approximation

Here we focus on the all optical situation encountered by Jeong [123, 124], but this time taking a signal mode of arbitrary dimension interacting with a probe mode in a Kerr medium. The two-level input can easily be mapped to the CQED setting. If we only recognize loss in the probe beam $|\alpha\rangle$ during the interaction, then a possible approach to expressing the effect of loss is to let the interaction $R(\theta\hat{\Lambda})$ and the linear loss occur at different times. That is one may assume that the interaction occurs for a short time Δt, then the loss takes place, and they keep taking turns in the nonlinear medium. For small Δt this turns out to be a very good approximation as we will see later.

The most common way of introducing linear loss in an optical mode is to insert a beam splitter with a vacuum input and then trace out the loss mode. Thus let us begin with the first level of approximation, that of a single interaction followed by a beam splitter (see Fig. 3.2(a)). The input state reads

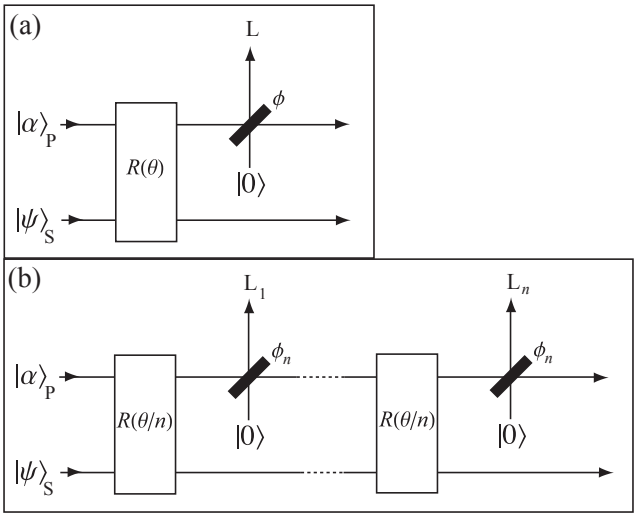

Figure 3.2: Schematic representation of the sliced approximation. (a) the first level of approximation, in which the signal and probe interact once, before the probe undergoes loss in the form of a beam splitter, whose output loss mode is traced out. (b) The n^{th} level of approximation, with n interactions and beam splitters.

$$|\psi_i\rangle = \sum_n c_n |n\rangle_{\rm S} \otimes |\alpha\rangle_{\rm P} \otimes |0\rangle_{\rm L}, \tag{3.1}$$

where the initial states of the signal, probe and loss modes are $\sum_n c_n|n\rangle_{\rm S}$, $|\alpha\rangle_{\rm P}$ and $|0\rangle_{\rm L}$ respectively. The combined state then evolves to

$$|\psi_f\rangle = \sum_n c_n |n\rangle_{\rm S} \otimes |\alpha {\rm cos}\phi e^{in\theta}\rangle_{\rm P} \otimes |\alpha {\rm sin}\phi e^{in\theta}\rangle_{\rm L}, \tag{3.2}$$

where cosϕ represents the transmittivity of the beam splitter. The reduced state of the signal-probe system is then obtained by tracing out the loss mode as

$$\begin{aligned} \rho_{\rm SP}^{(1)} &= {\rm Tr}_{\rm L}\left[|\psi_f\rangle\langle\psi_f|\right] & (3.3)\\ &= \sum_{n,m} c_{nm} |n\rangle\langle m| \otimes |\alpha {\rm cos}\phi e^{in\theta}\rangle\langle\alpha {\rm cos}\phi e^{im\theta}| \times {\rm I}_{\rm L}, & (3.4) \end{aligned}$$

with $c_{nm} = c_n c_m^*$ and

$$\mathrm{I_L} = \frac{1}{\pi}\int d\beta \langle\beta|\alpha \mathrm{sin}\phi e^{in\theta}\rangle\langle\alpha \mathrm{sin}\phi e^{im\theta}|\beta\rangle \tag{3.5}$$

$$= e^{-\alpha^2 \mathrm{sin}^2\phi(1-e^{i(n-m)\theta})}. \tag{3.6}$$

The next level of approximation consists in two interactions of strength $\theta/2$ and two identical beam splitters with reflectivity $\mathrm{sin}\phi$ with associated loss modes $\mathrm{L_1}$ and $\mathrm{L_2}$, leading to a final signal-probe state

$$\rho_{\mathrm{SP}}^{(2)} = \mathrm{Tr}_{\mathrm{L_1,L_2}}\left[|\psi_f\rangle\langle\psi_f|\right] \tag{3.7}$$

$$= \sum_{n,m} c_{nm}|n\rangle\langle m| \otimes |\alpha \mathrm{cos}^2\phi e^{in\theta}\rangle\langle\alpha \mathrm{cos}^2\phi e^{im\theta}| \times \mathrm{I_{L_1}I_{L_2}}, \tag{3.8}$$

with

$$\mathrm{I_{L_1}I_{L_2}} = \frac{1}{\pi}\int d\beta \langle\beta|\alpha \mathrm{sin}\phi e^{in\theta/2}\rangle\langle\alpha \mathrm{sin}\phi e^{im\theta/2}|\beta\rangle \tag{3.9}$$

$$\times \frac{1}{\pi}\int d\beta \langle\beta|\alpha \mathrm{cos}\phi \mathrm{sin}\phi e^{in\theta}\rangle\langle\alpha \mathrm{cos}\phi \mathrm{sin}\phi e^{im\theta}|\beta\rangle \tag{3.10}$$

$$= e^{-\alpha^2 \mathrm{sin}^2\phi(1-e^{i(n-m)\theta/2}+\mathrm{cos}^2\phi(1-e^{i(n-m)\theta}))}. \tag{3.11}$$

Iterating this procedure N times (see Fig. 3.2(a)) we obtain

$$\rho_{\mathrm{SP}}^{(N)} = \sum_{n,m} c_{nm}|n\rangle\langle m| \otimes |\alpha \mathrm{cos}^N\phi e^{in\theta}\rangle\langle\alpha \mathrm{cos}^N\phi e^{im\theta}| \times \mathrm{I_T} \tag{3.12}$$

with

$$\mathrm{I_T} = \prod_{k=1}^{N} \mathrm{I_{L}}_k = \mathrm{exp}\left[-\alpha^2 \mathrm{sin}^2\phi \sum_{k=1}^{N} \mathrm{cos}^{2(k-1)}\phi(1-e^{ik(n-m)\theta/N})\right]. \tag{3.13}$$

The individual transmission coefficient $\mathrm{cos}\phi$ is matched to the total expected transmission $\mathrm{cos}\phi_{\mathrm{tot}}$, in function of the number of iterations, i.e. we fix $\mathrm{cos}\phi = \mathrm{cos}^{1/N}\phi_{\mathrm{tot}}$. As can be observed in Fig. 3.3(a), this approximation tends rapidly to the continuous solution derived next.

3.1.2 Solving the master equation

Starting from the interaction Hamiltonian $H_{int} = -\hbar\chi\hat{a}^\dagger\hat{a}\hat{\Lambda}$ previously defined, we can evaluate the effects of dissipation in the probe mode during the interaction continuously by solving the optical Linblad master equation [51]

$$\frac{\partial\rho(t)}{\partial t} = -\frac{i}{\hbar}\left[H_{int}, \rho(t)\right] + \gamma(2\hat{a}\rho(t)\hat{a}^\dagger - \hat{a}^\dagger\hat{a}\rho(t) - \rho(t)\hat{a}^\dagger\hat{a}) \tag{3.14}$$

where we have assumed a zero temperature bath (a good approximation in the visible light regime). The damping factor γ quantifies the dissipation in the probe mode as mentioned in the background chapter. If we consider a general input density matrix element $|n\rangle\langle m| \otimes |\alpha\rangle\langle\alpha|$ in which the probe and the signal are disentangled, we can find the equation of motion for this particular element by looking at the operator $\rho_{nm}(t) = \langle n|\rho(t)|m\rangle$. Due to the disentangled form of the initial state we have $\rho_{nm}(0) = |\alpha\rangle\langle\alpha|$ for all n and m. The equation of motion for each element is given by

$$\begin{aligned}\frac{\partial\rho_{nm}(t)}{\partial t} &= i\chi\lambda_n\hat{a}^\dagger\hat{a}\rho_{nm}(t) + -i\chi\lambda_m\rho_{nm}(t)\hat{a}^\dagger\hat{a} \\ &+\gamma(2\hat{a}\rho_{nm}(t)\hat{a}^\dagger - \hat{a}^\dagger\hat{a}\rho_{nm}(t) - \rho_{nm}(t)\hat{a}^\dagger\hat{a}).\end{aligned} \tag{3.15}$$

As before, λ_n represent the eigenvalues of the qudit operator $\hat{\Lambda}|n\rangle = \lambda_n|n\rangle$. Following the method used in [117], we use the super-operators $\mathcal{M}(\cdot) = \hat{a}^\dagger\hat{a}(\cdot)$, $\mathcal{P}(\cdot) = (\cdot)\hat{a}^\dagger\hat{a}$ and $\mathcal{J}(\cdot) = \hat{a}(\cdot)\hat{a}^\dagger$ to rewrite the above equation as

$$\begin{aligned}\frac{\partial\rho_{nm}(t)}{\partial t} &= \left\{i\chi(\lambda_n\mathcal{M} - \lambda_m\mathcal{P}) + \gamma(2\mathcal{J} - \mathcal{M} - \mathcal{P})\right\}\rho_{nm}(t) \\ &\equiv \mathcal{L}_{nm}\rho_{nm}(t),\end{aligned} \tag{3.16}$$

The formal solution to (3.16) is then $\rho_{nm}(t) = e^{\mathcal{L}_{nm}t}\rho_{nm}(0)$. The super-operators realize an algebra obeying the commutation relations $[\mathcal{J}, \mathcal{M}] = [\mathcal{J}, \mathcal{P}] = \mathcal{J}$ for which decomposition theorems have been derived [125] (see Appendix A), leading to

$$\begin{aligned}\exp[\mathcal{L}_{nm}t] &= \exp\left[\frac{2\gamma(e^{(2\gamma - i(\lambda_n - \lambda_m)\chi)t} - 1)}{2\gamma - (\lambda_n - \lambda_m)\chi}\mathcal{J}\right] \\ &\times \exp\left[(i\lambda_n\chi - \gamma)\mathcal{M}t\right] \\ &\times \exp\left[(-i\lambda_m\chi - \gamma)\mathcal{P}t\right].\end{aligned} \tag{3.17}$$

Now applying this result to our initial element $\rho_{nm}(0) = |\alpha\rangle\langle\alpha|$ we obtain:

$$\rho_{nm}(t) = \zeta_{nm}|\alpha e^{(-\gamma + i\lambda_n\chi)t}\rangle\langle\alpha e^{(-\gamma + i\lambda_m\chi)t}| \tag{3.18}$$

with

$$\zeta_{nm} = \exp\left[-|\alpha|^2\left\{1 - e^{-2\gamma t} - \frac{1 - e^{(-2\gamma + i(\lambda_n - \lambda_m)\chi)t}}{1 - i(\lambda_n - \lambda_m)\chi/2\gamma}\right\}\right]. \tag{3.19}$$

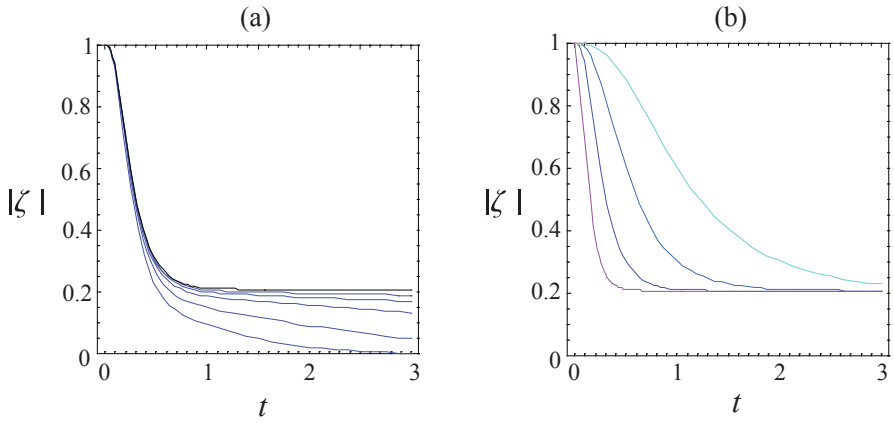

Figure 3.3: (a) Plots of the real part of the coherence parameter $|\zeta| = |\zeta_{01}|$ for different N in the sliced approximation, with $\alpha = 100$,$\gamma = 4$ and $\chi = 0.1$. Starting from the bottom curve, we have $N = 10, 20, 50, 100$ and 200 in blue. The top black curve corresponds to the closed form. We see that the approximation rapidly converges, for reasonable N. In comparing the curves, we equated $t = N\Delta t$ and $\cos\phi = e^{-\gamma t/N}$. (b) Time evolution of $|\zeta|$ with fixed $\alpha = 100$ and $\chi/\gamma = 0.025$. From top to bottom, $\gamma = 1, 2, 4$ and 8. We see that all the curves tend to the same limit and as expected the larger γ is, the quicker $|\zeta|$ tends to that limit.

The coefficient derived above is the closed expression for the parameter $\mathrm{I_T}$ obtained in the previous section as the number of iterations N tends to infinity. We can see from Fig. 3.3(a) that the sliced approximation in fact rapidly converges to the exact solution. We have $\zeta_{nm} = \zeta^*_{mn}$ and so $|\zeta_{nm}| = |\zeta_{mn}|$ as well as $\zeta_{nn} = 1$. We also quickly notice from (3.19) that this coherence parameter does not tend to 0 as t tends to infinity for a fixed α. We have

$$|\zeta_{nm}|_{t\to\infty} = \exp\left[-|\alpha|^2 \frac{(\lambda_n - \lambda_m)^2}{4(\gamma/\chi)^2 + (\lambda_n - \lambda_m)^2}\right]. \tag{3.20}$$

This is illustrated in Fig. 3.3(b) for ζ_{01} with $\hat{\Lambda} = \hat{n}$. One way of understanding this is that the probe undergoes loss as it couples to the signal, thus reducing the coherence in the signal. But eventually the probe returns to the vacuum state (the time it takes depends on the initial amplitude and the damping factor), disentangling itself and leaving some coherence in the signal. However the larger the amplitude, the larger the effective interaction time, the less coherence remains in the signal.

In the CQED setting, it will not be possible to observe this limiting behavior in cavities with very high quality factors, as the atomic decay rate far exceeds the cavity decay rate γ. However the aim of the qubus scheme is to entangle qubits in separate cavities via shared optical modes. Thus the regime of moderate coupling is appropriate, in which $g \sim \gamma$, where g is the Rabi frequency of the atom. A particularly promising system is Nitrogen-vacancy (NV) centers embedded in a photonic crystal such as diamond. For this system, the parameters are of the order of $g \sim 10^4$ MHz and $\gamma \sim 10^3$ MHz, meaning an interaction time on the scale of nanoseconds, while the typical atomic decay time lies in the hundreds of nanoseconds [91, 126]. As we are working in the dispersive limit, we require a small absorption rate quantified by $\alpha^2 g^2/\Delta^2 \sim 10^{-2}$, where Δ is the detuning between the atomic transition and cavity mode frequencies. With $\chi \sim g^2/\Delta$, these parameters yield a ratio $\gamma/\chi \sim 10^2$, leading to a limiting coherence parameter $|\zeta_{01}|_\infty \sim 0.37$ with a probe amplitude $\alpha = 100$.

As time progresses, the process can be viewed as a unitary operation between the signal and the damped probe in addition to a dephasing effect on the signal. To view this more clearly, let us write the output density matrix using $\hat{\Lambda} = Z$, $\theta = \chi t$ and defining $z_n \equiv (-1)^n$,

$$\rho(t) = \sum_{n,m=0,1} c_{nm}\zeta_{nm}|n\rangle\langle m| \otimes |\alpha e^{-\gamma t + i z_n \theta}\rangle\langle \alpha e^{-\gamma t + i z_m \theta}|. \tag{3.21}$$

Writing $\zeta_{nm} = e^{f_{nm}}$, we can separate the exponent into it's real and imaginary parts $\mathrm{Re}[f_{nm}] + i\mathrm{Im}[f_{nm}]$. The real part reads

$$\begin{aligned} e^{\mathrm{Re}[f_{nm}]} &= \exp[-\frac{|\alpha|^2}{2(\gamma^2+\chi^2)}(\chi^2(1-e^{-2\gamma t}) \\ &- 2\gamma^2 e^{-2\gamma t}\sin^2\chi t - \chi\gamma e^{-2\gamma t}\sin 2\chi t) \\ &\times (1 - z_n z_m)], \end{aligned} \tag{3.22}$$

representing the decay of the off-diagonal components of the density matrix. It takes the form $e^{-\epsilon(1-z_n z_m)}$ and applying this type of operation to a qubit

density matrix $\rho = \sum_{n,m=0,1} c_{nm}|n\rangle\langle m|$ yields directly the phase flip channel [40]

$$\begin{aligned} e^{\mathrm{Re}[f_{nm}]}\rho &= e^{-\epsilon(1-z_n z_m)}\rho \\ &= e^{-\epsilon}(\mathrm{cosh}\epsilon + z_n z_m \mathrm{sinh}\epsilon)\rho \\ &= \frac{1+e^{-2\epsilon}}{2}\rho + \frac{1-e^{-2\epsilon}}{2} Z\rho Z. \end{aligned} \tag{3.23}$$

In the limit of large interaction times (3.23) leads to a fixed dephasing effect

$$e^{\mathrm{Re}[f_{nm}]}_{t\to\infty} = \exp\left[-\frac{|\alpha|^2}{2(1+(\gamma/\chi)^2)}(1-z_n z_m)\right], \tag{3.24}$$

which can be recovered from (3.20). The imaginary part of the exponent is

$$e^{\mathrm{Im}[f]} = \exp\left[\frac{i\gamma|\alpha|^2}{2(\gamma^2+\chi^2)}(\chi(1-e^{-2\gamma t}\mathrm{cos}2\chi t) - \gamma \mathrm{sin}2\chi t)(z_n - z_m)\right], \tag{3.25}$$

corresponding to a single qubit phase acquired in the process. It is known and can be corrected for if needed; it is not an intrinsic source of noise. However the level of precision required to undo this phase, which can be affected by fluctuations in the coupling and damping parameters, in particular for large α, represents a significant challenge.

3.1.3 Different probe states

So far we have considered arbitrary states of the signal and a coherent state of the probe mode. This coherent state has the property that it does not decohere into a mixture in the presence of loss. However other probe inputs that do decohere in the presence of dissipation, can easily be investigated using the same techniques. Here we apply the results obtained above on states of interest to illustrate their usefulness.

To begin with we can consider a probe having been prepared in a normalized superposition of coherent states (cat states) $\sum_k d_k|\alpha_k\rangle$. If the subsystem and probe mode begin disentangled, our initial density matrix reads

$$\rho_{\mathrm{cat}}(0) = \sum_{n,m} c_{nm}|n\rangle\langle m|_{\mathrm{S}} \otimes \sum_{k,l} d_{kl}|\alpha_k\rangle\langle\alpha_l|_{\mathrm{P}}. \tag{3.26}$$

Solving the equations of motion for each element $\rho_{nm}(0) = \sum_{k,l} d_{kl}|\alpha_k\rangle\langle\alpha_l|$ we obtain

$$\rho_{\rm cat}(t) = \sum_{n,m} c_{nm}|n\rangle\langle m| \otimes \sum_{k,l} d_{kl}\zeta_{nm}^{kl}|\alpha_k e^{(-\gamma+i\lambda_n\chi)t}\rangle\langle\alpha_l e^{(-\gamma+i\lambda_m\chi)t}|, \quad (3.27)$$

with

$$\zeta_{nm}^{kl} = \exp\left[-\left(\frac{|\alpha_k|^2+|\alpha_l|^2}{2}\right)(1-e^{-2\gamma t}) - \frac{\alpha_k\alpha_l^*(1-e^{(-2\gamma+i(\lambda_n-\lambda_m)\chi)t})}{1-i(\lambda_n-\lambda_m)\chi/2\gamma}\right]. \quad (3.28)$$

Here, in addition to the dephasing process, we observe the decoherence of the cat state itself, as it interacts with the signal. Unlike in the case of a single coherent state input, which stays pure under dissipation, here loss changes the shape of the probe mode state, which will eventually become a statistical mixture, before returning to the vacuum state.

Another probe input could be a pure entangled state $\sum_n c_n|n\rangle|\alpha_n\rangle$, one which may be produced by a perfect interaction or some purification. In a manner very similar to the previous example, our output density matrix after time t becomes:

$$\rho_{ent}(t) = \sum_{n,m} c_{nm}\zeta_{nm}^{nm}|n\rangle\langle m| \otimes |\alpha_n e^{-(\gamma+in\chi)t}\rangle\langle\alpha_m e^{-(\gamma+im\chi)t}|, \quad (3.29)$$

where n and m (the subscripts for the initial coherent states) simply replace k and l in (3.27). We will stop here with the consideration of other probe states, but the results of the previous section can be applied to any probe state, provided it can be conveniently expressed in the coherent state basis. Now we return to the simple coherent state probe and look at the behavior of entanglement.

3.1.4 Entanglement and coherence dynamics

One expects the issue of coherence to be intimately linked to the entanglement shared between the signal and the probe systems. In order to observe the dynamics of this entanglement we restrict the signal to being a qubit and will continue to use $\hat{\Lambda} = Z$. Equation (3.18) provides us with a time dependent density matrix and having our input signal in the state $(|0\rangle + |1\rangle)/\sqrt{2}$, it reads

$$\begin{aligned}\rho(t) &= \frac{1}{2}\{|0\rangle\langle 0| \otimes |\alpha_0\rangle\langle\alpha_0| + \zeta_{01}|0\rangle\langle 1| \otimes |\alpha_0\rangle\langle\alpha_1| \\ &+ \zeta_{10}|1\rangle\langle 0| \otimes |\alpha_1\rangle\langle\alpha_0| + |1\rangle\langle 1| \otimes |\alpha_1\rangle\langle\alpha_1|\}, \end{aligned} \quad (3.30)$$

with $\alpha_0 = \alpha e^{(-\gamma+i\chi)t}$ and $\alpha_1 = \alpha e^{(-\gamma-i\chi)t}$. The entanglement being invariant under local unitary operations we allow ourselves for simplicity to apply the conditional phase $|0\rangle\langle 0| + e^{i\mathrm{Im}[\alpha_0\alpha_1^*]}|1\rangle\langle 1|$ on the qubit. Then we redefine the bus probe states as $|\alpha_0\rangle$ and $|\alpha_1'\rangle = e^{i\mathrm{Im}[\alpha_0\alpha_1^*]}|\alpha_1\rangle$ so that the overlap between the two is real: $\langle\alpha_0|\alpha_1'\rangle = |\langle\alpha_0|\alpha_1\rangle|$. This allows us to express them in an orthogonal basis $\{|x\rangle, |y\rangle\}$ as [127]

$$\begin{aligned} |\alpha_0\rangle &= a|x\rangle + b|y\rangle, \\ |\alpha_1'\rangle &= a|x\rangle - b|y\rangle. \end{aligned} \tag{3.31}$$

Taking a and b real without loss of generality, normalization leads to

$$a = \sqrt{\frac{1+\delta}{2}}, \quad b = \sqrt{\frac{1-\delta}{2}}, \tag{3.32}$$

with $\delta = e^{-\alpha^2 e^{-2\gamma t}(1-\cos(2\chi t))}$. At this point we can write our locally equivalent density matrix in the orthonormal basis $\{|0\rangle|x\rangle, |0\rangle|y\rangle, |1\rangle|x\rangle, |1\rangle|y\rangle\}$ as follows

$$\rho(t) = \frac{1}{2}\begin{pmatrix} a^2 & ab & \zeta_{01}a^2 & -\zeta_{01}ab \\ ab & b^2 & \zeta_{01}ab & -\zeta_{01}b^2 \\ \zeta_{10}a^2 & \zeta_{10}ab & a^2 & -ab \\ -\zeta_{10}ab & -\zeta_{10}b^2 & -ab & b^2 \end{pmatrix}. \tag{3.33}$$

We have now managed to express the qubit and CV composite state in the form of a two qubit state. Given the resulting two-qubit density matrix, there are several entanglement measures to choose from, including the logarithmic negativity and the relative entropy of entanglement [128]. Here we will work with the concurrence as defined by Wooters [129,130] which can be computed easily. To do so we first need to calculate $\bar{\rho}(t)$, the corresponding density matrix having undergone complex conjugation in the 'magic basis' as

$$\bar{\rho} = (Y \otimes Y)\rho^*(Y \otimes Y). \tag{3.34}$$

Each Pauli Y operator acts on one of the two qubits forming the state ρ. Then the concurrence

$$C(\rho(t)) = \max\{0, \lambda_1 - \lambda_2 - \lambda_3 - \lambda_4\}, \tag{3.35}$$

where the λ_is are the eigenvalues, in decreasing order, of the Hermitian matrix $R \equiv \sqrt{\sqrt{\rho(t)}\bar{\rho}(t)\sqrt{\rho(t)}}$. We then plot the concurrence as a function of the scaled time χt for particular choices of parameters α and γ/χ (Fig. 3.4).

As the qubit and the field initially start in a product state, and eventually for large times should return to a product state when the probe field doesn't contain anymore photons, we would expect the entanglement to peak at some point in time.

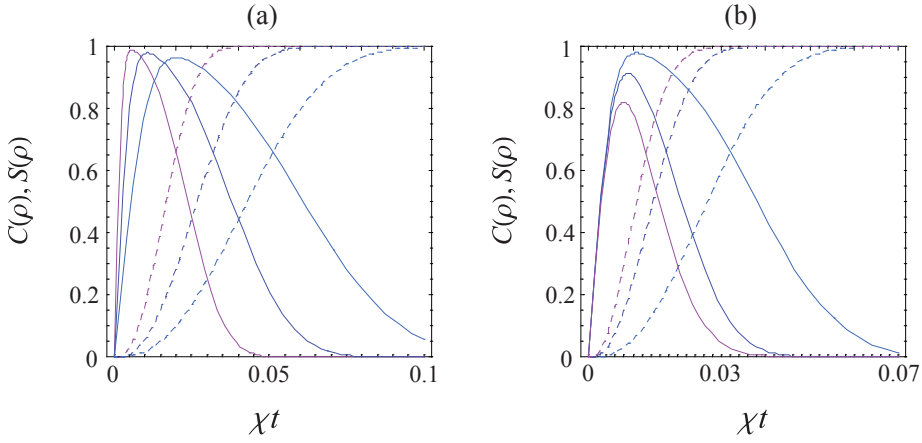

Figure 3.4: Plots of the concurrence $C(\rho)$ (solid) and the von Neumann entropy $S(\rho) = -\mathrm{tr}(\rho \log \rho)$ (dashed) of the combined state of the CV mode and qubit as a function of the scaled time χt. (a) From left to right α=200,100 and 50 with a fixed ratio of damping rate to nonlinearity $\gamma/\chi = 1$. (b) The amplitude α is fixed to 100 and from highest to lowest peaking curves γ/χ=1, 7 and 21.

This is verified in the plots of Fig. 3.4. In Fig. 3.4(a) we can observe how the amplitude of the field α affects the behavior of entanglement in time. The larger α is, the larger the maximum entanglement. This may be explained by the fact that the separation between the possible states of the field in phase space increases with α as $2\alpha \sin \chi t$, thus making them more distinguishable. For large α the maximum concurrence tends naturally to 1, however the peaking of the entanglement also becomes sharper. It is quickly generated, but also quickly destroyed. This is illustrated by the von Neumann entropy $S(\rho)$ characterizing the decoherence. Fig. 3.4(b) shows us how the maximum achievable entanglement depends on the ratio γ/χ, as did the limit of the coherence parameter in the previous section. The larger the relative damping γ, the lower and the quicker the entanglement peaks in time. In both plots $S(\rho)$ tends to 1, meaning the qubit is left in a maximally mixed state, disentangled from the probe. However this is not always the

case and in general the larger the ratio γ/χ is, the smaller the amount of entanglement generated, the lower the final entropy of the qubit becomes.

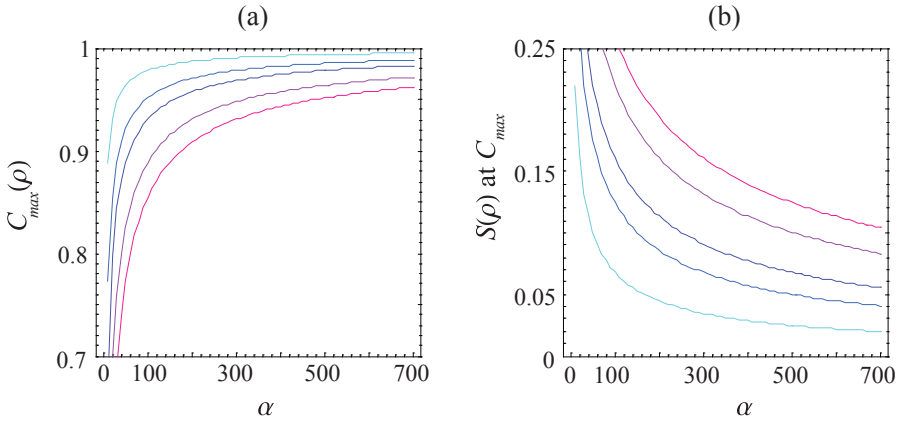

Figure 3.5: (a) The maximum concurrence as a function of the amplitude α of the probe with $\gamma/\chi = 1$, 3, 5, 10 and 15 from top to bottom. (b) The von Neumann entropy of the combined state at the entanglement peaking time with the same values for γ/χ in decreasing order from top to bottom.

In view of a QND measurement on a single qubit [111, 112], only the entanglement with the probe needs to be taken into account, as decoherence in the process will not affect the measurement statistics. However, when the application becomes cat state generation or multiqubit gates [123, 124], decoherence becomes a crucial issue which has to be weighted against the entanglement. In such applications one wishes to produce coherent superpositions of single or multiple quantum systems. Thus it is important to view the behavior of the entropy of the combined state at the time at which the entanglement is maximized. This behavior is illustrated in Fig. 3.5(a), showing the expected limiting behavior of the maximum entanglement as α increases. In Fig. 3.5(b) the corresponding entropy of the combined outgoing state is seen to decrease asymptotically for all choices of the parameter γ/χ. In consequence one can simply reduce the amount of decoherence by increasing the strength of the probe. This is in part due to the fact that the interaction time becomes shorter, reducing the effective decoherence time.

The success of such an approach to minimize the decoherence will then depend on the loss incurred in between interactions. The reason being that the larger the amplitude α is, the larger the amount of dephasing incured by the qubits coupled to the probe mode during these time intervals will

be. This will become clear in the next section. In consequence we observe a similar trade-off of as that encountered in schemes such as the hybrid quantum repeater proposed in [120]. If the transit time and conditions are appropriate, the approach is indeed effective. For example taking $\gamma/\chi = 5$ and a moderate amplitude $\alpha = 10^4$ we obtain a maximum concurrence of 0.998 for a von Neumann entropy of 10^{-2}.

So the higher the entanglement we want to measure or couple out of the cavity if we are dealing with cavity QED systems, the larger the probe amplitude and the more precise the timing of the interaction will have to be. Clearly, these issues of coherence and entanglement will have to be combined in order to optimize quantum gates in which different qubits interact with the same probe mode.

3.2 Loss between interactions

In this section we look at dissipation in the bus mode after it has interacted with a subsystem. This will allow us to see a potential advantage in using conditional displacements instead of conditional rotations. Then we look at a simple purification scheme for a particular entangled qubit-bus state and finally see the effects of loss in transmission on a parity gate.

3.2.1 Distinguishing rotations from displacements

Without any ongoing interaction, dissipation in the probe can be estimated by solving the optical master equation

$$\frac{\partial\rho(t)}{\partial t} = \gamma(2\hat{a}\rho(t)\hat{a}^\dagger - \hat{a}^\dagger\hat{a}\rho(t) - \rho(t)\hat{a}^\dagger\hat{a}) \equiv \mathcal{L}\rho(t), \tag{3.36}$$

where $\mathcal{L}$ is the corresponding Liouvillian and γ is the damping constant. Following the same notation as in the previous section [117], we have

$$\mathcal{L} = \gamma(2\mathcal{J} - \mathcal{M} - \mathcal{P}), \tag{3.37}$$

The formal solution again can be written $\rho(t) = e^{\mathcal{L}t}\rho(0)$. Using a similar decomposition as before, the effect of this linear loss on a matrix element $|\alpha\rangle\langle\beta|$ is given by

$$e^{\mathcal{L}t}|\alpha\rangle\langle\beta| = e^{-(1-e^{-2\gamma t})(|\alpha|^2/2+|\beta|^2/2-\alpha\beta^*)}|\alpha e^{-\gamma t}\rangle\langle\beta e^{-\gamma t}|. \tag{3.38}$$

This result was initially derived by Walls and Milburn [131] using time ordering techniques. One can identify the expression for the overlap between

the coherent states $\langle\beta|\alpha\rangle$ in the coefficient and thus the result can be written as

$$e^{\mathcal{L}t}|\alpha\rangle\langle\beta| = \langle\beta|\alpha\rangle^{\eta}|\alpha e^{-\gamma t}\rangle\langle\beta e^{-\gamma t}|, \tag{3.39}$$

with $\eta = 1 - e^{-2\gamma t}$. As we can see, the smaller the overlap is, the larger the decoherence effect.

Now let us assume an ideal qubit-bus entangled state generated through a conditional rotation

$$\rho_i = \sum_{n,m=0,1} c_{nm}|n\rangle\langle m| \otimes |\alpha e^{i\theta z_n}\rangle\langle\alpha e^{i\theta z_m}|. \tag{3.40}$$

Dissipation in the bus will lead to a combined state

$$\mathcal{L}\rho_i = \sum_{n,m=0,1} c_{nm}\xi_{nm}|n\rangle\langle m| \otimes |\alpha e^{-\gamma t+i\theta z_n}\rangle\langle\alpha e^{-\gamma t+i\theta z_m}| \tag{3.41}$$

with

$$\begin{aligned} \xi_{nm} &= \langle\alpha e^{i\theta z_m}|\alpha e^{i\theta z_n}\rangle^{\eta} && (3.42)\\ &= e^{-\eta\alpha^2\sin^2\theta(1-z_n z_m)}e^{i\eta\alpha^2\sin 2\theta(z_n-z_m)/2}. && (3.43) \end{aligned}$$

As before, the first term represents phase flip channel and the second a single qubit phase. This phase can be problematic to undo or keep track of, as α and θ need to be large enough so as to allow any useful measurements. Now this phase only vanishes for $\theta = 0$ or π, in which case the bus and qubit are not entangled, or for $\theta = \pm\pi/2$. In the latter case, the probe is in one of two diametrically opposed states. Interestingly it is at this point that the entanglement between the qubit and bus is maximized. However the larger the separation between the two coherent states, the stronger the effect of the phase flip channel. Thus both for technological reasons and for qubit coherence preservation, θ will have to be reasonably small (the trade-off is investigated in detail by Ladd et al. [120]), and this phase linked to dissipation will have to be controlled, which represents a serious challenge.

If on the other hand we are using weak conditional displacements, this phase problem can suppressed, as long as we have sufficient control of the direction of the displacements. For example taking the same real initial probe amplitude α, an entangled qubit-bus state generated through a conditional displacement of real amplitude β will evolve to

$$\mathcal{L}\rho_i = \sum_{n,m=0,1} c_{nm}\xi_{nm}|n\rangle\langle m| \otimes |(\alpha+\beta z_n)e^{-\gamma t}\rangle\langle(\alpha+\beta z_m)e^{-\gamma t}|, \quad (3.44)$$

with

$$\begin{aligned} \xi_{nm} &= \langle \alpha+\beta z_m|\alpha+\beta z_n\rangle^{\eta} & (3.45)\\ &= e^{-\eta\beta^2(1-z_n z_m)}. & (3.46) \end{aligned}$$

No phase accompanies the phase flip channel. This is an important distinction between conditional rotations and displacements, showing a potential advantage in using the latter.

One interesting question which follows from this is: how can we purify such a noisy qubit-bus state? A particular case is discussed in the next section.

3.2.2 Purifying a qubit-bus state

Protocols for the purification of entangled states have been studied extensively since Bennett et al. [132] pointed out the possibility of purifying (increasing the entanglement content) of two-qubit entangled states. In an optical setting, the purification of entangled cat states has been investigated by Jeong and Kim [133]. However the natural question of whether one can purify a noisy qubit-bus entangled state, pointed to in [127], remains unaddressed. Such an approach may present advantages in entanglement distribution via the qubus parity gate. Instead of purifying the resulting two-qubit states, it may be more efficient to first purify the pair of qubit-bus states, and then let the resulting bus interact with a new qubit. This could potentially reduce the qubit resources from four to three, for a single purification round.

Assuming arbitrary operations on both sides of the pairs, purification can be achieved for general states by combining the standard methods in [132,133]. However here we choose a particular type of state which does not require any nonlinearities on the side of the bus and in that sense is similar to the example given in [133]. This allows us to give a first explicit hybrid qubit-bus purification scheme. The state is

$$\rho = F|\phi^+\rangle\langle\phi^+| + (1-F)|\psi^+\rangle\langle\psi^+|, \quad (3.47)$$

with

$$|\phi^+\rangle = \frac{1}{\sqrt{2}}(|0,\alpha\rangle + |1,-\alpha\rangle), \tag{3.48}$$

$$|\psi^+\rangle = \frac{1}{\sqrt{2}}(|0,-\alpha\rangle + |1,+\alpha\rangle). \tag{3.49}$$

The target state here being $|\phi^+\rangle$, the fidelity F of the given noisy state is then $F = \langle\phi^+|\rho|\phi^+\rangle$. We also notice that $|\psi^+\rangle = X|\phi^+\rangle$, so the noisy state corresponds to the target state whose qubit has undergone a bit flip channel, applying an X error with a certain probability. This is a key feature of the state which will allow us to perform the purification without resorting to nonlinearities on the buses.

This particular state is all the more interesting to us because it is, up to local operations on the qubits, the state obtained through applying linear loss to the bus. Recall (3.23) that dissipation in the bus affects an initial hybrid state ρ as $\rho \to \lambda\rho + (1-\lambda)Z\rho Z$, equivalent to the qubit having undergone a phase-flip channel. Thus we can either follow the qubit in the $|\pm\rangle$ basis or apply Hadamard transformations on the qubit before and after dissipation in the bus takes place, yielding exactly the state (3.47), with an initial pure qubit-bus state $|\phi^+\rangle$.

Now we assume we are given two such noisy qubit-bus states

$$\begin{aligned}\rho &= \rho_1 \otimes \rho_2 \\ &= F^2|\phi^+\rangle\langle\phi^+|_1 \otimes |\phi^+\rangle\langle\phi^+|_2 + (1-F)^2|\psi^+\rangle\langle\psi^+|_1 \otimes |\psi^+\rangle\langle\psi^+|_2 \\ &+ F(1-F)\left\{|\phi^+\rangle\langle\phi^+|_1 \otimes |\psi^+\rangle\langle\psi^+|_2 + |\psi^+\rangle\langle\psi^+|_1 \otimes |\phi^+\rangle\langle\phi^+|_2\right\}.\end{aligned} \tag{3.50}$$

The protocol, illustrated in Fig. 3.6 then goes as follows. On one side a CNOT gate is applied to the qubits, with qubit 1 as control and on the other the buses are mixed on a 50:50 beam splitter whose outputs we write as

$$|\alpha\rangle_1|\alpha\rangle_2 \to |\sqrt{2}\alpha\rangle_1|\text{vac}\rangle_2, \tag{3.51}$$

$$|\alpha\rangle_1|-\alpha\rangle_2 \to |\text{vac}\rangle_1|\sqrt{2}\alpha\rangle_2, \tag{3.52}$$

$$|-\alpha\rangle_1|\alpha\rangle_2 \to |\text{vac}\rangle_1|-\sqrt{2}\alpha\rangle_2, \tag{3.53}$$

$$|-\alpha\rangle_1|-\alpha\rangle_2 \to |-\sqrt{2}\alpha\rangle_1|\text{vac}\rangle_2, \tag{3.54}$$

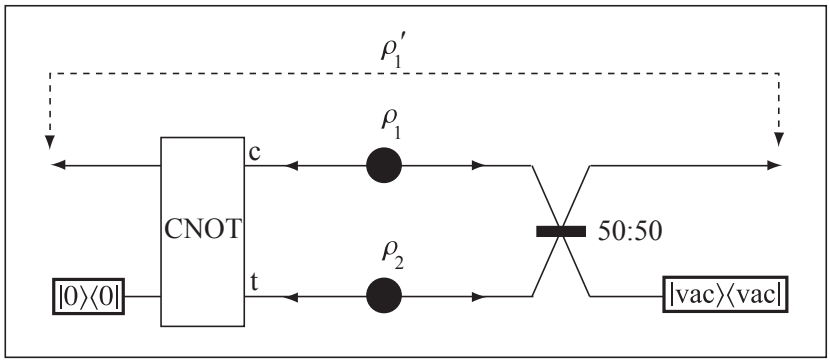

Figure 3.6: Schematic representation of the purification scheme described in the text. The two states ρ_1 and ρ_2 are composed of a qubit propagating to the left and a mode propagating to the right. A CNOT gate is applied to the two qubits, with qubit 1 as control and the two modes go through a 50:50 beam splitter. Upon the measurement results $|0\rangle$ on qubit 2 and $|\text{vac}\rangle$ on mode 2, qubit 1 and mode 1 are left in a state with increased fidelity.

where $|\text{vac}\rangle$ stands for the vacuum state, to avoid confusion with the logical qubit states. This maps the possible states as follows

$$\begin{aligned}
|\phi^+\rangle_1|\phi^+\rangle_2 &\to \frac{1}{\sqrt{2}}|\phi^{+'}\rangle_1|0,\text{vac}\rangle_2 + \frac{1}{2}|0,\text{vac}\rangle_1|1,\alpha'\rangle_2 + \frac{1}{2}|1,\text{vac}\rangle_1|1,-\alpha'\rangle_2,\\
|\psi^+\rangle_1|\psi^+\rangle_2 &\to \frac{1}{\sqrt{2}}|\psi^{+'}\rangle_1|0,\text{vac}\rangle_2 + \frac{1}{2}|0,\text{vac}\rangle_1|1,-\alpha'\rangle_2 + \frac{1}{2}|1,\text{vac}\rangle_1|1,\alpha'\rangle_2,\\
|\phi^+\rangle_1|\psi^+\rangle_2 &\to \frac{1}{\sqrt{2}}|\phi^{+'}\rangle_1|1,\text{vac}\rangle_2 + \frac{1}{2}|0,\text{vac}\rangle_1|0,\alpha'\rangle_2 + \frac{1}{2}|1,\text{vac}\rangle_1|0,-\alpha'\rangle_2,\\
|\psi^+\rangle_1|\phi^+\rangle_2 &\to \frac{1}{\sqrt{2}}|\psi^{+'}\rangle_1|1,\text{vac}\rangle_2 + \frac{1}{2}|0,\text{vac}\rangle_1|0,-\alpha'\rangle_2 + \frac{1}{2}|1,\text{vac}\rangle_1|0,\alpha'\rangle_2,
\end{aligned} \tag{3.55}$$

with $|\phi^{+'}\rangle = ((|0,\alpha'\rangle + |1,-\alpha'\rangle)/\sqrt{2}$ (similarly for $|\psi^{+'}\rangle$) and $\alpha' = \sqrt{2}\alpha$. Now measuring qubit 2 in the computational basis and applying a bucket detector to mode 2 will, conditional on the measurement result $|0,\text{vac}\rangle_2$, result in the new state

$$\rho_1' = F'|\phi^{+'}\rangle\langle\phi^{+'}|_1 + (1-F')|\psi^{+'}\rangle\langle\psi^{+'}|_1, \tag{3.56}$$

with

$$F' = \frac{F^2}{F^2 + (1-F)^2}. \tag{3.57}$$

The intrinsic error in the bucket measurement is of order $e^{-\alpha^2/2}$ and can be neglected for suitable α. Now we notice that $F' > F$ for $F > 1/2$, meaning that the fidelity has been increased, probabilistically. One also notices the increase in amplitude of the bus mode, which can be seen both as a nuisance and an advantage. In one way it makes the coherence qubit-bus pair more sensitive to dissipation effects on the bus, and in the other it further increases the net entanglement between the two.

A more general mixed qubit-bus state would require random bilateral rotations, meaning bus operations of the form $|\alpha\rangle \to \mathcal{N}(|\alpha\rangle + |-\alpha\rangle)$, which in turn rely on nonlinearities possibly implemented through a further interaction of the buses with ancillary qubits [133]. However as explained previously, this example suffices to show that noisy qubit-bus pairs caused by bus loss can indeed be purified without further nonlinearities on the bus. This is an important new result.

On the topic of qubit-bus pairs we will stop here, nonetheless this constitutes an interesting area of research in its own right. Chen *et al.* looked at the nonlocality of such hybrid entangled states states and showed that although they can contain exactly one ebit of entanglement, they cannot be maximally entangled [134]. There remains a lot to be understood about this type of discrete-continuous variable entanglement and its quantification in general cases (mixed states for example) is still an open question.

3.2.3 Effects in the two-qubit parity gate

Returning to dissipation in the probe mode, a first step to take in understanding its effects on qubus gates is to consider the parity gate. For this we come back to (3.58), set $\alpha = 0$ and add a second qubit (b), which then conditionally displaces the damped probe by a complementary amplitude $\beta e^{-\gamma t}$ to that of the first qubit (a), leading to

$$\rho_f = \frac{1}{2} \sum_{a,a',b,b'=0,1} \xi_{aa'} |ab\rangle\langle a'b'| \otimes |\beta e^{-\gamma t}(z_a + z_b)\rangle\langle \beta e^{-\gamma t}(z_{a'} + z_{b'})|, \tag{3.58}$$

where both qubits were initiated in the $|+\rangle$ state. For clarity we rewrite this state as

$$\rho_f = F_{\text{trans}} |\varphi\rangle\langle\varphi| + (1 - F_{\text{trans}}) Z_a |\varphi\rangle\langle\varphi| Z_a, \tag{3.59}$$

where $F_{\text{trans}} = (1 + e^{-2\eta\beta})/2$ and

$$|\varphi\rangle = \frac{1}{\sqrt{2}}|\psi^+\rangle|0\rangle + \frac{1}{2}|00\rangle|2\beta e^{-\gamma t}\rangle + \frac{1}{2}|11\rangle|-2\beta e^{-\gamma t}\rangle. \tag{3.60}$$

At this point we perform a P quadrature measurement so as to project the qubits to the entangled state $|\psi^+\rangle = (|01\rangle + |10\rangle)/\sqrt{2}$. As we know from the previous section, we post-select measurements close to $P = 0$, with an associated fidelity

$$F_{\text{meast}} = 1 - E_{\beta e^{-\gamma t}} = 1 - \frac{1}{4}\text{erf}\left[\frac{\beta e^{-\gamma t}}{\sqrt{2}}, \frac{3\beta e^{-\gamma t}}{\sqrt{2}}\right]. \tag{3.61}$$

So the final, post-selected fidelity of the entangled state becomes

$$F_{\text{fin}} = F_{\text{trans}} F_{\text{meast}}. \tag{3.62}$$

One important point to note here is that F_{trans} is given by the distance and the type of medium the bus travels through to get from the first to the second qubit and in practice cannot be reduced. However F_{meast} can be increased to some extent, by choosing the size of the acceptable measurement window, to the expense of the success probability of the entangling gate. As the bin size around the value $P = 0$ diminishes, the output fidelity increases and the success probability decreases. The ability to tune these parameters is crucial attribute of the qubus scheme, in particular for quantum repeater applications [119].

From the results of this section, one sees that loss in the transmission can be quantified through the overlaps of probe states, and we now extend this method to a two-qubit measurement free gate.

3.3 Loss in the measurement-free CZ gate

The present section is divided into three parts. We first investigate dissipation effects in simulating the building block interaction which is the conditional displacement, through conditional rotations. After this we proceed with the full CZ gate and in the last part we attempt to engineer the probe so as to increase the performance of the gate.

3.3.1 The conditional displacement

We begin by reminding ourselves of the conditional displacement sequence

$$D(\alpha\cos\theta)R(-\theta Z)D(-2\alpha)R(\theta Z)D(\alpha\cos\theta) = D(2i\alpha\sin\theta Z), \qquad (3.63)$$

with α real (see Fig. 3.7), and reminding ourselves of the phases induced by consecutive displacements $D(\beta)D(\alpha) = e^{i\mathrm{Im}(\alpha^*\beta)}D(\alpha+\beta)$ and consequently $D^\dagger(\alpha)D^\dagger(\beta) = e^{-i\mathrm{Im}(\alpha^*\beta)}D^\dagger(\alpha+\beta)$ as $D^\dagger(\delta) = D(-\delta)$. Displacements and rotations acting on the density matrix we will denote by $\mathcal{D}(\alpha)\rho = D(\alpha)\rho D^\dagger(\alpha)$ and $\mathcal{R}(\theta)\rho = R(\theta)\rho R^\dagger(\theta)$.

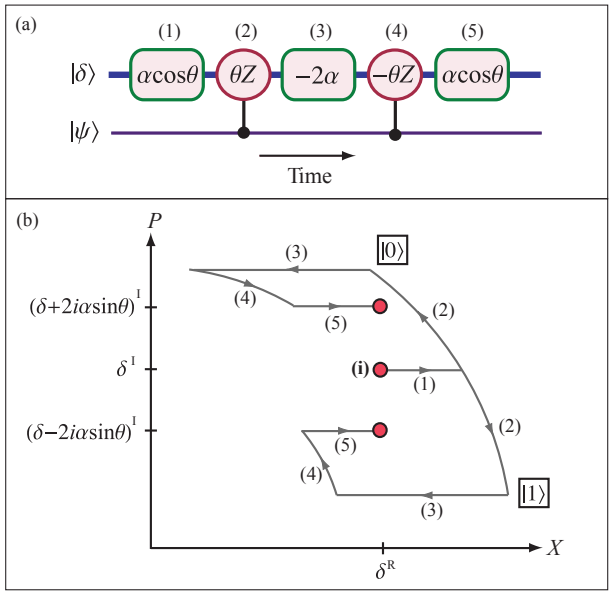

Figure 3.7: (a) The interaction sequence for the the simulation of the conditional displacement gate. (b) The two possible trajectories of the probe in phase space, the upper and lower paths corresponding to the qubit states $|0\rangle$ and $|1\rangle$ respectively. Here as in the text, we assume α to be real. The 'R' and 'I' exponents denote the real and imaginary parts of the probe amplitude δ at each time step. As we can see, the two possible final positions of the probe in phase space correspond to an effective conditional displacement.

In order to characterize loss in an interaction sequence, we will simply introduce dissipation in the probe mode between and during each interaction. Dissipation during the interactions is due to loss in the nonlinear material or cavity system used to to mediate the interaction, whereas dissipation in

between each interaction is due to fiber loss, mode mismatch and other effects. As mentioned earlier, the qubus scheme calls for cavities operating in the moderate coupling regime, such that the bus mode can rapidly couple in to the cavity, pick up the phase shift and couple out back into a waveguide for example. Most of the loss occurs at these coupling stages and can be quantified by the collection efficiency of the cavity, that is the amount of photons which exit the cavity in the correct mode. Consequently different loss parameters should arise. However, all types of loss result in a dephasing of the qubit(s) and their effects can thus be combined into a single effective loss parameter.

We will also assume the effective amount of loss is the same in each segment. We will use the notation $\mathcal{L}|\alpha\rangle\langle\beta| \rightarrow \langle\beta|\alpha\rangle^{\eta}|\dot{\alpha}\rangle\langle\dot{\beta}|$ with $\eta = 1 - e^{-2\gamma t}$. The fixed amount of loss between each interaction is $l = \gamma t$ and we represent the attenuated coherent state by $\dot{\alpha} \equiv \alpha e^{-l}$ such that the number of dots will determine the number of attenuations i.e. $\ddot{\alpha} \equiv \alpha e^{-2l}$. The quantum operations on the qubits will be obtained by calculating these state-dependent overlaps.

Now let us consider the effects of dissipation in the whole interaction sequence (3.63). For generality we will keep the amplitudes of the three displacements as free real variables α_1, α_2 and α_3. The first step in the sequence is a displacement so taking our probe initially in the vacuum state we have

$$\begin{aligned} \mathcal{D}(\alpha_1)\rho &= \sum_{a,a'=0,1} c_{aa'}|a\rangle\langle a'| \otimes D(\alpha_1)|0\rangle\langle 0|D^{\dagger}(\alpha_1) \\ &= \sum_{a,a'=0,1} c_{aa'}|a\rangle\langle a'| \otimes |\alpha_1\rangle\langle\alpha_1|, \end{aligned} \tag{3.64}$$

where $\{|a\rangle, a = 0, 1\}$ represents the basis states of the qubit and the state of the probe mode is kept to the right. Loss in the probe mode at this point will decrease the amplitude of the coherent state to $|\dot{\alpha}_1\rangle$, without affecting the qubit. Proceeding to the second step which is a conditional rotation we have

$$\mathcal{R}(\theta Z)\mathcal{L}\mathcal{D}(\alpha_1)\rho = \sum_{a,a'=0,1} c_{aa'}|a\rangle\langle a'| \otimes |\dot{\alpha}_1 e^{i\theta z_a}\rangle\langle\dot{\alpha}_1 e^{i\theta z_{a'}}|. \tag{3.65}$$

Now we introduce loss in the probe mode, leading to

$$\begin{aligned} \mathcal{L}\mathcal{R}(\theta Z)\mathcal{D}(\alpha_1)\rho &= \sum_{a,a'=0,1} c_{aa'}|a\rangle\langle a'| \otimes |\ddot{\alpha}_1 e^{i\theta z_a}\rangle\langle\ddot{\alpha}_1 e^{i\theta z_{a'}}| \\ &\times \langle\dot{\alpha}_1 e^{i\theta z_{a'}}|\dot{\alpha}_1 e^{i\theta z_a}\rangle^{\eta}. \end{aligned} \tag{3.66}$$

Continuing in this fashion and completing the sequence

$$\mathcal{D}(\alpha_3)\mathcal{L}\mathcal{R}(-\theta Z)\mathcal{L}\mathcal{D}(\alpha_2)\mathcal{L}\mathcal{R}(\theta Z)\mathcal{L}\mathcal{D}(\alpha_1)\rho$$

$$= \sum_{a,a'=0,1} c_{aa'}|a\rangle\langle a'| \otimes |\dddot{\alpha}_1 + \ddot{\alpha}_2 e^{-i\theta z_a} + \alpha_3\rangle\langle z_a \to z_{a'}|$$
$$\times \exp[i\sin\theta(\ddot{\alpha}_2\alpha_3 - \ddot{\alpha}_1\alpha_2)(z_a - z_{a'})] \times (\xi_1\xi_2\xi_3)^\eta, \tag{3.67}$$

with the ξ's representing the three loss terms (overlaps). The notation $z_a \to z_{a'}$ means the contents of the bra are the same as in the previous ket replacing z_a with $z_{a'}$. In order to simulate a conditional displacement (with dephasing on the qubit), we require the state of the probe mode to be of the form $|\gamma z_a\rangle\langle\gamma z_{a'}|$. This is achieved by setting $\dddot{\alpha}_1 + \ddot{\alpha}_2\cos\theta + \alpha_3 = 0$. Combining the loss terms we obtain

$$\xi_1\xi_2\xi_3 = \exp[-S(1 - z_a z_{a'})] \times \exp[iT(z_a - z_{a'})], \tag{3.68}$$

with$T = \sin\theta(\ddot{\alpha}_1\alpha_2 + \dddot{\alpha}_1\dot{\alpha}_2 + (\dot{\alpha}_1^2 + \ddot{\alpha}_1^2 + \dot{\alpha}_2^2)\cos\theta)$ and $S = \sin^2\theta(\dot{\alpha}_1^2 + \ddot{\alpha}_1^2 + \dot{\alpha}_2^2)$. Here as in the evaluation of the coherence parameter (3.19) in section 3.1.2, the exponent can be separated into real and imaginary parts. The former is characterized by S, representing the amount of dephasing incurred by the qubit, which can be decomposed into a bit-flip channel as in (3.23). The latter constitutes the known phase acquired by the qubit in the process, characterized by T. Interestingly, this overall conditional phase can be tuned at will by adapting the amplitudes of the displacements, leading to the exact simulation of a conditional displacement. In other words, in this sequence we can limit the effects of dissipation to a dephasing on the qubit, producing nonetheless the correct combined output state. Previously also, loss during the interaction had led to single qubit dephasing effects which can be factored in here. We now move on to examine a two qubit gate in the presence of probe loss.

3.3.2 The CZ gate

Based on four of these conditional displacements induced by a pair of qubits on the same probe mode, a gate locally equivalent to the CZ gate can be built. An interaction sequence leading to this unitary operation is $\hat{U} = D(-\beta_b Z_b)D(-\beta_a Z_a)D(\beta_b Z_b)D(\beta_a Z_a) = e^{2iIm\{\beta_a^*\beta_b\}Z_a Z_b}$ with $\beta_a^*\beta_b = i\pi/8$ where Z_a and Z_b act on qubits a and b respectively. Here we use the same method as before, introducing dissipation between each interaction, as illustrated in Fig. 5.8. We will assume the probe starts off in the vacuum state,

but the same result is obtained if we initialize it in any coherent state (this will become clear in the next subsection). The initial density matrix reads

$$\rho = \sum_{a,a',b,b'=0,1} c_{aa'bb'} |ab\rangle\langle a'b'| \otimes |0\rangle\langle 0|. \tag{3.69}$$

At this point it is worth noting that even though the probe undergoes amplitude damping, it can nonetheless be perfectly disentangled from the qubits coupled to it whatever the amplitude of the coherent state it starts off in (it may not be the case for other optical states). This is done by tuning the second (opposite) conditional displacement, in function of the known loss parameter l into which loss during the interaction has also been factored. Thus the amplitude of the second conditional displacement will be reduced by a factor of e^{-2l}, the damping undergone by the probe since the last coupling. Resolving the whole gate sequence (see Fig. 3.8 and 3.9) and choosing β_a and β_b to be real we obtain

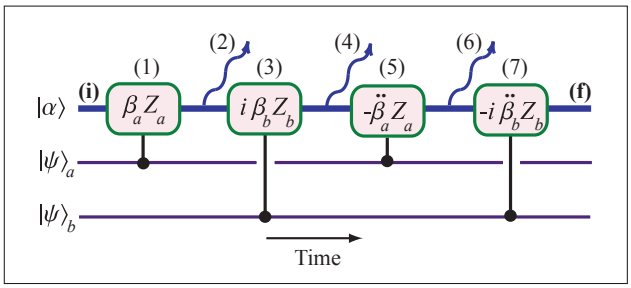

Figure 3.8: The interaction sequence for the CZ gate with loss. Between each one of the four conditional displacements (1,3,5,7) the probe undergoes dissipation (2,4,6).

$$\mathcal{D}(-i\ddot{\beta}_b Z_b)\mathcal{L}\mathcal{D}(-\ddot{\beta}_a Z_a)\mathcal{L}\mathcal{D}(i\beta_b Z_b)\mathcal{L}\mathcal{D}(\beta_a Z_a)\rho =$$

$$\sum_{a,a',b,b'=0,1} c_{aa'bb'} |ab\rangle\langle a'b'| \otimes |0\rangle\langle 0| \times (\xi_1\xi_2\xi_3)^\eta$$
$$\times \exp[i(\dot{\beta}_a\beta_b + \ddot{\beta}_a\dot{\beta}_b)(z_a z_b - z_{a'} z_{b'})]. \tag{3.70}$$

First we notice the geometrical phase represented by the last term. This is precisely the form of a two-qubit conditional phase having been applied to

the density matrix. Ignoring the other terms, if we can set $\dot{\beta}_a\beta_b + \ddot{\beta}_a\dot{\beta}_b = \pi/4$ then we have simulated a CZ gate. However the dephasing effects are included in the three ξ overlaps. The first and third lead to single qubit dephasing

$$\xi_1 = \langle \beta_a z_{a'} | \beta_a z_a \rangle = \exp[-\beta_a^2(1 - z_a z_{a'})],$$

$$\xi_3 = \langle i\dot{\beta}_b z_{b'} | i\dot{\beta}_b z_b \rangle = \exp[-\dot{\beta}_b^2(1 - z_b z_{b'})], \tag{3.71}$$

while the second overlap corresponds to loss in the probe mode when it holds information on both qubits

$$\begin{aligned} \xi_2 &= \langle \dot{\beta}_a z_{a'} + i\beta_b z_{b'} | \dot{\beta}_a z_a + i\beta_b z_b \rangle \\ &= \exp[-(\dot{\beta}_a^2 + \beta_b^2) + (\dot{\beta}_a z_a + i\beta_b z_b)(\dot{\beta}_a z_{a'} - i\beta_b z_{b'})]. \end{aligned} \tag{3.72}$$

In order to be able to express the resulting quantum operation in a closed form, we first arrange the terms in the exponential such that when writing the expansion we obtain an accessible closed algebra. Symmetrizing the terms we have

$$\xi_2^\eta = \exp[-x_0 + x_1 z_a z_{a'} + x_2 z_b z_{b'} + x_3(z_a + iz_b)(z_{a'} - iz_{b'})], \tag{3.73}$$

with $x_0 = \eta(\dot{\beta}_a^2 + \beta_b^2)$, $x_1 = \eta\dot{\beta}_a(\dot{\beta}_a - \beta_b)$, $x_2 = \eta\beta_b(\beta_b - \dot{\beta}_a)$ and $x_3 = \eta\dot{\beta}_a\beta_b$. Focusing first on the x_3 term, we can write out the expansion of that particular exponential acting on the density matrix as

$$\sum_{n=0}^{\infty} \frac{(x_3)^n (Z_a + iZ_b)^n \rho (Z_a - iZ_b)^n}{n!}. \tag{3.74}$$

Now we define the two-qubit operators

$$\begin{aligned} J &= Z_a + iZ_b, \\ K &= Z_a Z_b. \end{aligned} \tag{3.75}$$

Then grouping the terms in the expansion we obtain the following unnormalized operation

$$e^{x_3(z_a + iz_b)(z_{a'} - iz_{b'})}\rho = c_+\rho + c_- K\rho K + s_- J\rho J^\dagger + s_+ J^\dagger \rho J, \tag{3.76}$$

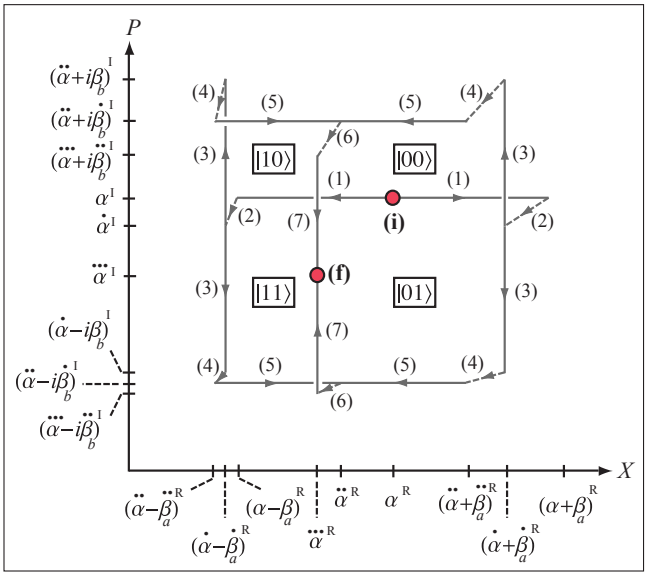

Figure 3.9: The trajectories of the probe state in phase space. All four paths start and end at the same amplitudes α and $\ddot{\alpha}$ respectively, insuring that the probe disentangles from the qubits.

with

$$\begin{aligned} c_{\pm} &= (\cosh 2x_3 \pm \cos 2x_3)/2, \\ s_{\pm} &= (\sinh 2x_3 \pm \sin 2x_3)/4. \end{aligned} \tag{3.77}$$

Now we have to factor in the other terms x_0, x_1 and x_2 of ξ_2^{η}. Further identifying

$$\begin{aligned} e_0 &= \cosh x_1 \cosh x_2, \quad e_1 = \cosh x_1 \sinh x_2, \\ e_2 &= \sinh x_1 \cosh x_2, \quad e_3 = \sinh x_1 \sinh x_2, \end{aligned} \tag{3.78}$$

and $K' = i + K$ we obtain the final normalized operation

$$\begin{aligned} \xi_2^{\eta}\rho &= e^{-x_0}\{(c_+e_0 + c_-e_3)\rho + (c_+e_2 + c_-e_1)Z_a\rho Z_a \\ &+ (c_+e_1 + c_-e_2)Z_b\rho Z_b + (c_+e_3 + c_-e_0)K\rho K \\ &+ (s_+e_1 + s_-e_2)K'\rho K'^{\dagger} + (s_+e_2 + s_-e_1)K'^{\dagger}\rho K' \\ &+ (s_+e_3 + s_-e_0)J\rho J^{\dagger} + (s_+e_0 + s_-e_3)J^{\dagger}\rho J\}, \end{aligned} \tag{3.79}$$

on the two-qubit state. Setting $\beta_b = \dot{\beta}_a = \beta$ removes the single qubit terms Z_a and Z_b and also the K' terms, yielding the operation

$$\xi_2^{\eta}\rho = e^{-2\eta\beta^2}(c_+\rho + c_- K\rho K + s_- J\rho J^\dagger + s_+ J^\dagger \rho J) \tag{3.80}$$

with $x_3 = \eta\beta^2$. Focusing on the low loss regime, we can assume a small η between each interaction. Truncating to second order in η the expansion (3.74) leading to the above operation we have

$$\begin{aligned} \rho &\rightarrow \rho + \eta\beta^2(Z_a + iZ_b)\rho(Z_a - iZ_b) \\ &= \rho + \eta\beta^2 Z_a\rho Z_a + \eta\beta^2 Z_b\rho Z_b \\ &+ i\eta\beta^2(Z_b\rho Z_a - Z_a\rho Z_b). \end{aligned} \tag{3.81}$$

Let us assume we are in a quantum error correction (QEC) setting where ancilla qubits are being used. Once the ancilla systems have undergone projective measurements, syndromes are extracted for each logical qubit, indicating whether or not it has been subject to a Z error. The last two terms however will lead to cross terms of syndrome states which cannot be observed in the measurement process and thus they are removed from the resulting density matrix [135]. That is the measurement of the syndrome projects the system to one of two known states, one with a Z error which can be corrected for, and one withtout any error. This leaves us with single qubit errors on a and b with equal probability. So for small loss we are only observing single qubit errors throughout the gate (at each one of the three dissipation stages) which can be corrected for via QEC.

Correlated errors represented by the operator K appearing in higher order terms are quantified by the coefficient c_- in the normalized operation (3.79). In Fig. 3.10(a) we can see how this part scales with loss in comparison to uncorrelated errors. The general quantum operations we have obtained are of great importance for error correction. They provide us with the error syndromes and their associated probabilities which in turn can be directly fed into fault tolerance calculations. This will ultimately allow us to compare the qubus scheme with other proposed implementations of quantum information processing.

To appreciate the effect of loss on the whole gate we look at the fidelity of the output state with regards to the ideal output, for a two qubit input state $|+\rangle|+\rangle$. Such an equally weighted superposition input state provides a good general indication as to the gates performance in addition to the fact that the ideal output is a useful resource, locally equivalent to a Bell state or two-qubit cluster state. A plot of the fidelity against the relative intensity

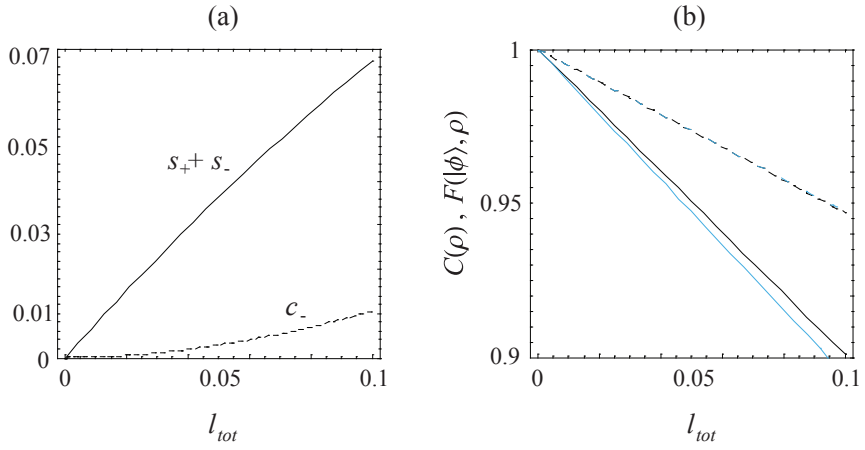

Figure 3.10: (a) The scaling of the normalized correlated (c_-) and uncorrelated errors ($s_+ + s_-$) against the loss l_{tot} as defined in the text. Dissipation occurs three times, once between each interaction, in equal amounts. (b) The fidelity (dashed) $F(|\phi\rangle, \rho) = \langle\phi|\rho|\phi\rangle$ of the two qubit output state, where $|\phi\rangle = e^{i\pi Z_1 Z_2/4}|+\rangle_1|+\rangle_2$ constitutes the ideal output state and the concurrence (solid), both for the single (black) and the iterated sequences (light). We observe the same fidelity for both of them while the outputted concurrence is lower for the iterated sequence.

decrease of the probe through dissipation defined as $l_{tot} = 1 - (\exp[-3l])^2$ is shown in Fig. 3.10(b). This can be understood in that if the probe is initiated in a coherent state with amplitude α, then at the end of the gate it disentangles from the qubits and is left with an amplitude αe^{-3l}. In computing the fidelity we use

$$\beta_a = \beta_b = \frac{1}{2}\sqrt{\frac{\pi}{e^{-l} + e^{-3l}}} \tag{3.82}$$

so as to make the phase represented by the last term in (3.70) that of an ideal CZ gate. We find that even for an intensity decrease of up to 80% in the probe mode (corresponding to 8 dB loss in total), the output fidelity remains above 0.5, allowing for purification. In the moderate loss regime, both the fidelity and the entanglement remain high; for example taking $l_{tot} = 0.05$ corresponding to a decrease of 5% in probe intensity (0.22 dB loss) results in an output with $F \sim 0.97$ and a concurrence of ~ 0.95.

Finally we now show how a simple repetition scheme can significantly

simplify full gate operation. The first point to notice is similar in spirit to the observation made in [122] that the ideal (loss-free) operation is invariant under time reversal. That is if we reverse the order of the interactions, we obtain the same conditional geometric phase. However in the case of separate cavities, a time reversed iteration does not help fight decoherence for a coherent state probe. The reason for this is that the single qubit error linked to the transfer between each cavity scales in the same way as the geometrical phase (of order $2\beta^2$). The observation we make here is that the gate is also invariant under a swapping of the displacement directions. That is the same geometrical phase is obtained, again in the loss free case, if now qubit a conditionally displaces the probe in the imaginary direction in 3.70) and qubit b displaces it in the real direction. Let us denote the two different sequences, this time in a dissipative setting as

$$\begin{aligned}\mathcal{S} &= \mathcal{D}(-i\ddot{\beta}_b Z_b).\mathcal{L}.\mathcal{D}(-\ddot{\beta}_a Z_a).\mathcal{L}.\mathcal{D}(i\beta_b Z_b).\mathcal{L}.\mathcal{D}(\beta_a Z_a)\\ \tilde{\mathcal{S}} &= \mathcal{D}(-\ddot{\beta}_b Z_b).\mathcal{L}.\mathcal{D}(-i\ddot{\beta}_a Z_a).\mathcal{L}.\mathcal{D}(\beta_b Z_b).\mathcal{L}.\mathcal{D}(i\beta_a Z_a).\end{aligned} \tag{3.83}$$

We have

$$\begin{aligned}\mathcal{S} &= e^{i\kappa(z_a z_b - z_{a'} z_{b'})}(\xi_1\xi_2\xi_3)^\eta \mathcal{D}(0)\\ \tilde{\mathcal{S}} &= e^{i\kappa(z_a z_b - z_{a'} z_{b'})}(\xi_1\tilde{\xi}_2\xi_3)^\eta \mathcal{D}(0),\end{aligned} \tag{3.84}$$

with $\kappa = \dot{\beta}_a\beta_b + \ddot{\beta}_a\dot{\beta}_b$. Now we notice that the effects of the two sequences differ only in the central overlap terms ξ_2 and $\tilde{\xi}_2$ which contain the correlated errors. It is straightforward to see that their combined effect yields

$$\begin{aligned}\tilde{\xi}_2\xi_2 &= \langle i\dot{\beta}_a z_{a'} + \beta_b z_{b'}|i\dot{\beta}_a z_a + \beta_b z_b\rangle\langle\dot{\beta}_a z_{a'} + i\beta_b z_{b'}|\dot{\beta}_a z_a + i\beta_b z_b\rangle\\ &= e^{-2\beta_b^2(1-z_b z_{b'})}e^{-2\dot{\beta}_a^2(1-z_a z_{a'})},\end{aligned} \tag{3.85}$$

which are just single qubit phase flip channels. Thus the combination of the two sequences gives the operation

$$\begin{aligned}\tilde{\mathcal{S}}\mathcal{S} &= e^{2i\kappa(z_a z_b - z_{a'} z_{b'})}\\ &\times\ e^{-2\eta(\beta_b^2+\dot{\beta}_b^2)(1-z_b z_{b'})}e^{-2\eta(\beta_a^2+\dot{\beta}_a^2)(1-z_a z_{a'})}\\ &\times\ \mathcal{D}(0),\end{aligned} \tag{3.86}$$

where the first term is the unitary conditional two-qubit phase and the next two are single qubit dephasing terms. The corresponding operation undergone by the qubits, omitting the conditional phase is

$$\begin{aligned}\tilde{\mathcal{S}}\mathcal{S}\rho &= (1-p_a)(1-p_b)\rho + p_a(1-p_b)Z_a\rho Z_a \\ &+ (1-p_a)p_b Z_b\rho Z_b + p_a p_b Z_a Z_b \rho Z_b Z_a, \end{aligned} \tag{3.87}$$

where

$$p_\nu = \frac{1-e^{-4\eta(\beta_\nu^2+\dot{\beta}_\nu^2)}}{2}, \tag{3.88}$$

the probability that each qubit incured a Z error, with $\nu = a,\ b$. Clearly these dephasing processes are independent, leading to a very simple operation, in contrast with the partial operations (3.79) or even (3.80) obtained in the single interaction sequence. Due to the fact that the geometrical phase and the qubit dephasing both double for a single iteration of the gate, there is no advantage to further reducing the sizes of the displacements and increasing the number of iterations.

The output state fidelity and entanglement of this sequence are plotted in Fig. 3.10(b), setting $\beta_a = \beta_b = \sqrt{\pi/8(e^{-l}+e^{-3l})}$. The fidelity is very similar while the concurrence is slightly reduced, compared to the single sequence. So for entanglement distribution in view of communication applications, which only follow the purification of an entangled state up to an acceptable level, the iterated scheme is penalizing, as it requires twice the amount of time and reduces the entanglement. But in view of full blown quantum computation with quantum error correction, the iterated scheme may present a serious advantage, simplifying errors at the gate level.

At this point we would like to note that the method used throughout this section is very broad and could be applied to general bus mediated quantum information processing schemes. Loss of coherence in the bus will automatically result in dephasing on the qubits coupled to it at that time. If several qubits are simultaneously coupled then correlated errors will arise. These will have to be minimized in order to efficiently correct for errors. However the peculiarity of the qubus scheme is that we are using non-orthogonal states of the bus to encode information held by the subsystems. Surprisingly, in the absence of loss, perfect multiqubit gates can be implemented this way. In a dissipative setting, this non-orthogonality leads to overlap calculations which are very likely to arise in general non-orthogonal bus schemes.

Following the above results, there are two main directions for additional work. The first is to find a way of dealing with the single qubit phases accumulated throughout qubus gates. Simply undoing them would require considerable precision and this may not be a realistic option. The second is to investigate possible schemes to reduce dephasing effects, possibly by engineering the probe itself. An attempt at doing so is outlined in the next subsection.

3.3.3 An attempt at probe engineering

According to the previous section, qubit dephasing is related to the overlap (at least in terms of coherent states) between intermediary states of the bus. Thus one way of approaching the problem would be to make these overlaps as large as possible, reducing the distinguishability of bus states and in turn reducing qubit dephasing. The possibility of such an approach is due to the fact that the geometrical phase is built up from the conditional displacements, independently of the actual state of the bus. So for example, using a mixed probe or a thermal state still allows for the building up of conditional geometrical phases. Interestingly enough, preparing the probe in a mixed state of the form $\frac{1}{N}\sum_{i=1}^{N}|\alpha_i\rangle\langle\alpha_i|$ does not worsen the performance of the gate, compared to the use of a pure state $|\alpha\rangle\langle\alpha|$. This means that to some degree we need coherent superposition to increase the overlaps.

The operation that we want to be able to hide in some sense into the bus, is a conditional displacement. The first state of the bus one might think of is a squeezed state, squeezed in the direction of the displacement. However we need to keep in mind the fact that we will want to protect both qubits, while each one displaces the bus in a different direction, so as to generate phases. In that case, a squeezed probe may to some extent protect one qubit, but it will penalize the other. The candidate states we consider here are cat states. To appreciate the potential effect of this approach, let us begin with a cat state of real amplitudes

$$|\mathcal{C}_d\rangle = \frac{1}{\mathcal{N}}\sum_{n=0}^{d-1}|2n\beta\rangle, \tag{3.89}$$

with the normalization

$$\mathcal{N}^2 = \sum_{n,m=0}^{d-1} e^{-2\beta^2(n-m)^2}. \tag{3.90}$$

The combined state of the probe and qubit we write as

$$\rho = \sum_{a,a'=0,1} c_{aa'}|a\rangle\langle a'| \otimes \left\{ \frac{1}{\mathcal{N}^2} \sum_{n,m=0}^{d-1} |2n\beta\rangle\langle 2m\beta| \right\}. \tag{3.91}$$

A good indicator of the protective action of the bus is to let it interact through a conditional displacement with the qubit and then trace it out

$$\begin{aligned}
\rho' &= \mathrm{Tr}_{\mathrm{bus}}\left[\mathcal{D}(\beta Z)\rho\right] \\
&= \mathrm{Tr}_{\mathrm{bus}}\left[\sum_{a,a'=0,1} c_{aa'}|a\rangle\langle a'| \otimes \left\{ \frac{1}{\mathcal{N}^2} \sum_{n,m=0}^{d-1} |(2n+z_a)\beta\rangle\langle (2m+z_{a'})\beta| \right\} \right] \\
&= \sum_{a,a'=0,1} c_{aa'}|a\rangle\langle a'| \left\{ \frac{1}{\mathcal{N}^2} \sum_{n,m=0}^{d-1} \langle (2m+z_{a'})\beta|(2n+z_a)\beta\rangle \right\}.
\end{aligned} \tag{3.92}$$

Resolving the sum of overlaps we obtain

$$\rho' = \sum_{a,a'=0,1} c_{aa'}\xi_{aa'}|a\rangle\langle a'|, \tag{3.93}$$

with

$$\xi_{aa'} = e^{-\beta^2(1-z_a z_{a'})} \frac{d + 2\sum_{n=1}^{d-1}(d-n)e^{-2n^2\beta^2}\cosh(2n\beta^2(z_a - z_{a'}))}{d + 2\sum_{n=1}^{d-1}(d-n)e^{-2n^2\beta^2}}. \tag{3.94}$$

One recognizes the first term as the usual overlap obtained if the probe was initiated in a simple coherent state. We see $\xi_{aa'} = 1$ for $a = a'$ as required. The second term contributes to increasing the overlap and this can be appreciated by taking the limit of large β for which

$$\xi_{a\neq a'} \to \frac{d-1}{d} \qquad \text{as} \qquad \beta \to \infty. \tag{3.95}$$

Increasing d reduces the effect of tracing out the probe, as could have been expected. Thus we are really only concerned here with the overlap between a particular cat state and it's displaced version and the above result is quite intuitive. The overlap in the above case is plotted for different values of d in Fig. 3.11(a).

As we pointed to before, the bus will be displaced in two different directions, dependent on each qubit. We will choose these to be orthogonal, and

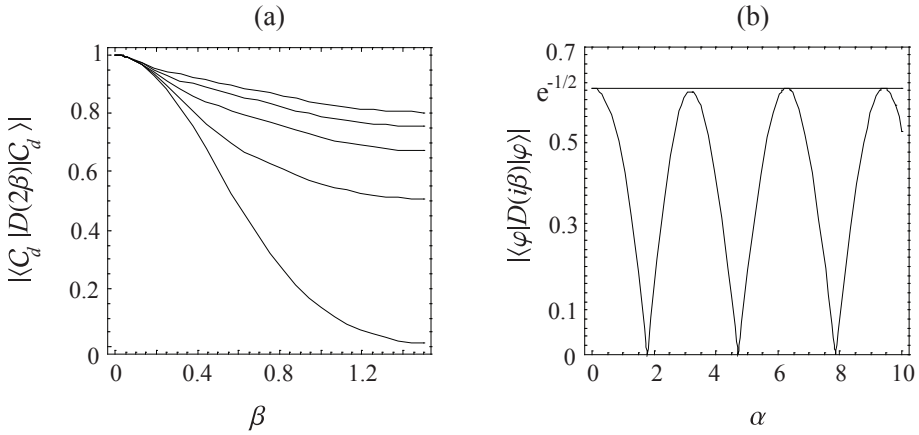

Figure 3.11: (a) Plots of the overlaps between a linear cluster $|\mathcal{C}_d\rangle$ and its displaced version, for $d = 1, .., 5$ from top to bottom. (b) The overlap between $|\varphi\rangle = \frac{1}{\mathcal{N}}(|0\rangle + |\alpha\rangle)$ and its displaced version as a function of α, with $\beta = 1$. The horizontal line corresponds to the overlap $|\langle\alpha|D(i\beta)|\alpha\rangle| = e^{-\beta^2/2}$ for a simple coherent state.

so a linear cat state will most certainly only protect one qubit. To overcome this we propose the use of a cat state in the form of a square grid or lattice, as illustrated in Fig. 3.12. We refer to this type of state as a grid state which takes the form

$$|\mathcal{G}_d\rangle = \frac{1}{\mathcal{N}} \sum_{n,m=0}^{d-1} |(n + im)\beta\rangle, \tag{3.96}$$

with

$$|\mathcal{N}|^2 = \sum_{n,m,p,q=0}^{d-1} e^{-\beta^2(n^2+m^2+p^2+q^2-2(n+im)(p-iq))}. \tag{3.97}$$

The overlap between the grid state and its displaced version is equal to $\langle\mathcal{G}_d|D(\beta)|\mathcal{G}_d\rangle$. The full expression is rather complicated, but taking the limit of large β again, we have

$$|\langle\mathcal{G}_d|D(\beta)|\mathcal{G}_d\rangle| \to \frac{d-1}{d} \qquad \text{as} \qquad \beta \to \infty. \tag{3.98}$$

The result can be understood geometrically as a proportional area overlap,

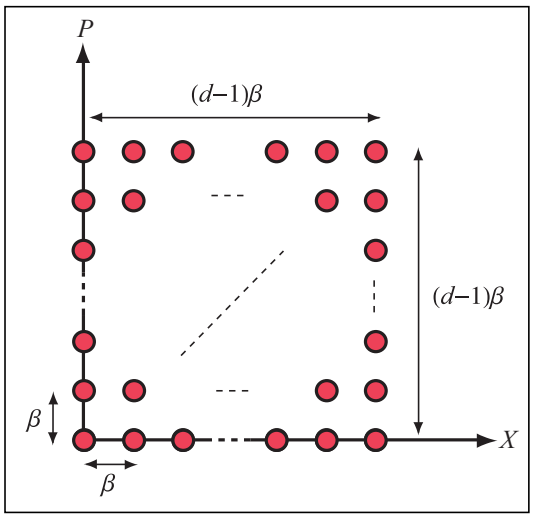

Figure 3.12: Phase space picture of the regular grid state $|\mathcal{G}_d\rangle$.

in number of coherent states in phase space. Thus we see that the overlap is increased through increasing d, and this time the same result holds for an orthogonal displacement, i.e. $|\langle\mathcal{G}_d|D(i\beta)|\mathcal{G}_d\rangle| \to \frac{d-1}{d}$ in the limit of large β. We note here that if we wanted to look at the overlap between the two possible grid states after a conditional displacement $D(\beta Z)$ we would have to insert a factor of two in the amplitudes, as in the linear cat state example. For the time being we are only verifying if such a state would be of any use and so we are not concerned with its preparation.

Before we start looking at the full gate, it is worth mentioning a potentially damaging feature of cat states. To illustrate the observation, let us take a typical cat state $|\varphi\rangle = (|0\rangle + |\alpha\rangle)/\mathcal{N}$ with α real. The overlap between the original state and a version displaced by $i\beta$ is then

$$|\langle\varphi|D(i\beta)|\varphi\rangle| = \frac{e^{-\beta^2/2}(2 + 4e^{-\alpha^2} + 2\cos 2\alpha\beta + 8e^{-\alpha^2/2}\cos\alpha\beta)^{1/2}}{2 + 2e^{-\alpha^2/2}}. \quad (3.99)$$

This oscillating function is plotted in Fig. 3.11(b), and as we can see there, the two states (original and displaced) can be perfectly orthogonal for some values of α and β. This could potentially exacerbate the dephasing incured by qubits having conditionally displaced the probe by these amounts and will probably play a role in the viability of the cat state probe approach.

Now let us move to the dissipative CZ gate and write our initial two-qubit and probe state as

$$\rho_i = \sum_{a,a',b,b'=0,1} c_{aa'bb'}|ab\rangle\langle a'b'| \otimes \frac{1}{\mathcal{N}}\sum_{i,j}|\alpha_i\rangle\langle\alpha_j|. \tag{3.100}$$

Applying the same sequence as in the previous section, with $\beta_a = \beta_b = \beta$ for simplicity, we obtain

$$\begin{aligned}\rho_f &= \sum_{a,a',b,b'=0,1} c_{aa'bb'}|ab\rangle\langle a'b'|e^{i(\dot{\beta}\beta+\ddot{\beta}\dot{\beta})(z_a+z_b-z_{a'}z_{b'})} &(3.101)\\ &\otimes \frac{1}{\mathcal{N}}\sum_{i,j}|\ddot{\alpha}_i\rangle\langle\ddot{\alpha}_j|P_a^{ij}P_b^{ij}(\xi_1^{ij}\xi_2^{ij}\xi_3^{ij})^\eta, &(3.102)\end{aligned}$$

where we have extra single qubit phases

$$P_a^{ij} = \exp\left[i\beta(e^{-4l}-1)(\mathrm{Im}[\alpha_i]z_a - \mathrm{Im}[\alpha_j]z_{a'})\right], \tag{3.103}$$

$$P_b^{ij} = \exp\left[i\beta(e^{-5l}-e^{-l})(\mathrm{Re}[\alpha_i]z_b - \mathrm{Re}[\alpha_j]z_{b'})\right], \tag{3.104}$$

and the three overlaps per probe matrix element

$$\xi_1^{ij} = \langle\alpha_j + \beta z_{a'}|\alpha_i + \beta z_a\rangle, \tag{3.105}$$

$$\xi_2^{ij} = \langle\dot{\alpha}_j + \dot{\beta}z_{a'} + i\beta z_{b'}|\dot{\alpha}_i + \dot{\beta}z_a + i\beta z_b\rangle, \tag{3.106}$$

$$\xi_3^{ij} = \langle\ddot{\alpha}_j + i\dot{\beta}z_{b'}|\ddot{\alpha}_i + i\dot{\beta}z_b\rangle. \tag{3.107}$$

We note that even though we have compensated the displacements, the probe and qubits remain entangled, as indicated by these extra phases which cancel out for $\alpha_i = \alpha_j$. The impact of a grid state probe on the gate performance is evaluated by looking at the fidelity $\langle\phi|\rho_{ab}|\phi\rangle$ (with $|\phi\rangle = (|0\rangle|+\rangle + |1\rangle|-\rangle)/\sqrt{2}$) of the reduced two-qubit state

$$\begin{aligned}\rho_{ab} &= \mathrm{Tr}_{\mathrm{bus}}[\rho_f] &(3.108)\\ &= \frac{1}{4}\sum_{a,a',b,b'=0,1}|ab\rangle\langle a'b'|e^{i(\dot{\beta}\beta+\ddot{\beta}\dot{\beta})(z_a+z_b-z_{a'}z_{b'})} &(3.109)\\ &\times \frac{1}{\mathcal{N}}\sum_{i,j}\langle\ddot{\alpha}_j|\ddot{\alpha}_i\rangle P_a^{ij}P_b^{ij}(\xi_1^{ij}\xi_2^{ij}\xi_3^{ij})^\eta, &(3.110)\end{aligned}$$

obtained with a pure input $|+\rangle_a|+\rangle_b$. For the numerical analysis, we define a new variable r which allows us to modulate the spacing of the input grid state, i.e. $|\mathcal{G}_d\rangle = \frac{1}{\mathcal{N}} \sum_{n,m=0}^{d-1} |r(n+im)\beta\rangle$, so as to be able to search for an optimal spacing, given a particular inter-coupling loss coefficient l which we set to 0.1 in the calculations. The results are displayed in Fig. 3.13.

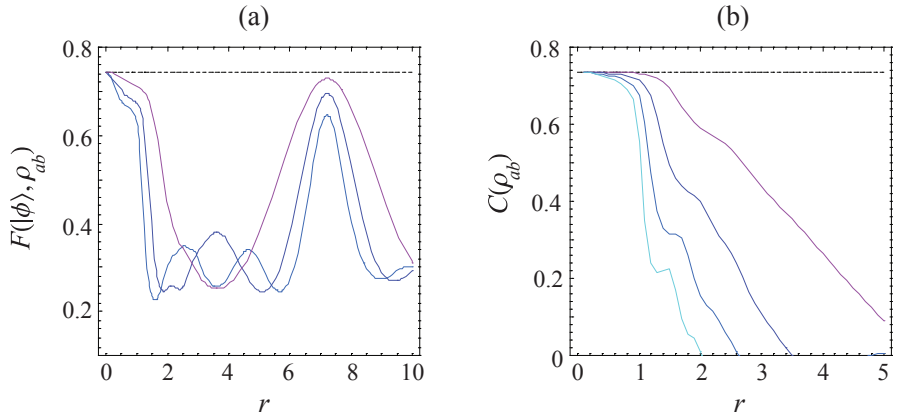

Figure 3.13: (a) The fidelity of the two-qubit output state $F(|\phi\rangle, \rho_{ab}) = \langle\phi|\rho_{ab}|\phi\rangle$, as a function of the lattice spacing r. The loss l is fixed to 0.1 between each interaction and the top horizontal line represents the fidelity achieved using a simple coherent state. Then from the highest peaking curve to the lowest we have $d = 2, 3$ and 4. (b) The entanglement generated between the two qubits, in the form of the concurrence, as a function of r with $l = 0.1$. The horizontal line again represents the concurrence achieved with a coherent state. From top to bottom we have $d = 2, 3, 4$ and 5.

In Fig. 3.13(a) we have plotted the fidelity of the output state as a function of the spacing between coherent states in the lattice. We observe significant variations as r changes however the standard fidelity is never exceeded and it would seem that increasing d worsens the overall performance of the gate. Plots of the concurrence, shown in Fig 3.13(b) confirm the observation. It seems like after all, the entire process is dominated by the mixing of the probe state, which is transmitted to the pair of qubits. The increased overlap is not sufficient in this case to protect the coherence of the qubits.

As the probe and qubits are still entangled at the end of the gate, one may suggest that tracing out the probe is the principal source of decoherence. To verify this we applied a time reversal to the sequence in order to decouple

the probe as much as possible from the qubits. This does slightly increase the performance of the gate but it remains bellow the results obtained in the single coherent state case, in all the range of l, r and d explored.

At this point one can really begin to appreciate the particularity of the coherent state and its usefulness in the qubus scheme. As it undergoes linear loss it remains pure and so it can always be perfectly decoupled from the qubits. Whether or not there exists a quantum state which can outperform the coherent state in such applications is still an open and interesting question. If there is not, then the last option that might be explored is to find optimal displacement sequences and paths in phase space, generating the required geometric phase and reducing the dephasing incured by the qubits. Attempts have so far been unsuccessful.

If we restrict ourselves to simple parity gates with small dissipation, the qubus scheme can be used directly to build cluster states in a distributed fashion. This constitutes the topic of the next chapter.

Chapter 4

The probabilistic generation of cluster states

As explained in the introduction, measurement-based quantum computing is a very promising alternative to the circuit model of quantum computing. It only requires the preparation of a highly entangled multi-qubit state, the cluster state, alongside arbitrary single qubit measurements and feed-forward. The efficient generation of the cluster state is crucial to the viability of measurement-based quantum computing. In the first section of this chapter we propose a truly scalable approach to building cluster states of matter qubits in a distributed fashion, using the qubus scheme. The key advantage being an increase in probability of success of the entangling operation, these results call for the quantification of the performance of different growth strategies over a complete range of success probabilities. Novel approaches to treating this issue and finding optimal strategies are proposed in the second section of the chapter.

4.1 The efficiencies generation of cluster states via the qubus scheme

The cluster state approach was quickly applied [72, 74, 75, 136, 137] to linear optics quantum computing [34] and was experimentally demonstrated on the scale of several qubits (see the review [50] for a full set of references). This scenario as we saw contains a significant scaling problem in practice, due to the probabilistic nature of the logical gates. However, the cluster state method enables this problem to be pushed into the off-line preparation of the cluster [72, 74, 75], at a lower cost in resources than gate teleportation

methods. Many different schemes have been proposed to efficiently generate the photonic cluster states, because of the simplicity of the interactions and the appealing coherence time of the photons. Photon loss can be treated efficiently through 'indirect measurements' and a more elaborate preparation of the cluster [138] but at a significant cost in terms of the qubit dephasing [139]. There remains an issue concerning storage though. Initially, each photon will be flying down an optical fibre (or two [72]), meaning there is a need for an adaptive quantum memory. Reliable and efficient single photon sources and detectors are a further issue for single photon approaches as we saw earlier.

The qubus scheme [85, 115, 140–144] was developed in an attempt to overcome the scaling properties of linear optics QIP. This scheme is non-destructive and not limited by the beam-splitters' optimal success probability of 1/2. Already at this point, one can notice the usefulness of the parity gate discussed at the end of chapter 2 for photonic cluster state approaches. A near deterministic entangler is all that is required to grow cluster states efficiently, be it in Browne and Rudolph's [75] or in Yoran and Reznik's model [72]. The effective CZ gates can be obtained through entanglement and local operations alone. However, as pointed out before, choosing photons as a support for one-way quantum computing may not be the best option. Solid state or matter systems may be more compact and easy to deal with in this application and constituted the initial proposed system, when cluster states were first developed [41]. In many of the solid state qubit systems proposed to date, the multi-qubit gates arise from direct interactions between the qubits. Adding extra qubits to a computation therefore leads to changes in the required control fields and to the Hamiltonian of the whole system. As a consequence, the required setup becomes increasingly more complicated as the number of qubits in the computational system increases. A further issue is that in order for some solid state qubits to interact directly, they may need to be in such close proximity that application of individual control fields and measurements becomes infeasible.

Distributed QIP potentially overcomes these problems. Many proposals make use of single photons to effectively mediate interactions between matter qubits [79,145–149]. Having interacted with matter qubits, the photons then interact with each other in a linear optical setup before being measured, thus projecting the matter qubits into the required state without them having interacted directly. It has been shown that entanglement and logical operations can be generated in this way. However, once again there are probabilistic limits in these approaches due to the fact that simple linear optics is inherently non-deterministic.

The next step was to use these probabilistic entangling schemes to prepare cluster states of matter qubits [43, 80, 81, 150, 151]. Barrett and Kok looked at this problem [43] and proposed the use of a double-heralding probabilistic entangling procedure in order to build cluster states. This method has been further developed in a second paper, using a repeat until success method proposed by Lim et al. [80], where implementation of a conditional phase gate is proposed, using a mutually unbiased basis [81]. This enables some saving of qubit resources during the generation of the graph or cluster states. However, a further very interesting aspect of this proposal is that there are now three possible outcomes to the measurement. Along with the usual success and failure outcomes, there is an insurance outcome, in which the qubits are left in a known product state, up to local operations. This means that, following the insurance outcome, a new attempt to implement the gate is possible. The corresponding scaling properties of the average number of required entangling operations follow from the various outcome probabilities for the entangling operation.

This entangling operation requires a rather elaborate measurement scheme, which may be tough to implement experimentally. Furthermore, as the scheme involves the detection of two photons, the success probability has a quadratic dependence on the detector efficiency. Therefore on top of the inherently probabilistic aspect of linear optics, the detector efficiencies dramatically affect the scaling of the resources (even for the highest reported efficiencies). It should be noted that the scheme is robust against photon loss due to the fact that this is a heralded source of error [1], so the fidelity of successful operation doesn't suffer. Nevertheless, the reduction in success probability of the gate requires a significant increase in resource overhead, which in turn increases the weight of unheralded errors in the cluster state itself. So single photon measurement has its limits in realizing entangling operations on matter qubits. However, homodyne measurements on coherent light fields can be made much more efficient than photon detection. In this section we will show how this and other factors make continuous variables a very powerful tool for growing cluster states.

4.1.1 The three-qubit entangling gate

There are quite a number of well studied systems where one has a natural interaction between a matter qubit and the electromagnetic field. These

[1] This of course assumes no dark counts in the detection process. Dark counts are generally an unheralded error and unfortunately tend to be larger in the higher efficiency detectors.

include atoms (real and artifical) in cavity QED (both at the optical and telecom wavelengths) [152], NV-centers in diamond [153], quantum dots with a single excess electron [154], trapped ions [30] and SQUIDs [101] to name only a few. All these systems are likely to be suitable candidates for the two qubit gate explained in chapter 2.

We saw previously how a simple two-qubit gate could be built with a pair of controlled bus rotation and a subsequent measurement of the probe. If we are in the optical wavelength range, this measurement works with an efficiency of at over 99% [155]. For cluster state generation the simplest option is an efficient momentum ($P = X(\pi/2)$) quadrature homodyne measurement (given the probe starts off in a coherent state $|\alpha\rangle$ of real amplitude, which will be the case in the rest of this chapter), yielding a success probability close to 1/2. We will note here that this is the most accessible and robust qubus scheme so far proposed, using a single interaction per qubit. Would it be possible to further improve the success probability all the while maintaining a highly efficient measurement?

Within the same framework of conditional rotations, one can envisage three qubits interacting with a single probe beam initially in the coherent state $|\alpha\rangle$. If we limit ourselves again to efficient P quadrature measurements (which scale as $\alpha\theta$), we could consider the generation of three qubit states. GHZ states are for instance one particularly useful state [75]. One way of projecting the qubits onto GHZ-type states is to vary the strength of the interactions between the qubits and the probe beam. Let us as before represent a rotation of the coherent probe beam by $R(\theta) = \exp(i\theta\hat{a}^\dagger\hat{a})$. Now no $R(\pm\theta Z_1)R(\pm\theta Z_2)R(\pm\theta Z_3)|\alpha\rangle$ combination will lead to the required GHZ end states in the case that we implement a P quadrature measurement. However having one of the qubits interact twice as much with the probe beam will yield the correct paths in phase space. Consider the sequence $R(\theta Z_1)R(\theta Z_2)R(-2\theta Z_3)|\alpha\rangle$ which we depict in Fig. 4.1. The peak centered on the origin will then correspond to the GHZ state $(|000\rangle + |111\rangle)\sqrt{2}$ (after being detected). This will happen with a probability of 1/4. Next the two peaks having been rotated through $\pm 2\theta$ will correspond to the qubit states $(|01\rangle_{1,2} + |10\rangle_{1,2})|1\rangle_3/\sqrt{2}$ and $(|01\rangle_{1,2} + |10\rangle_{1,2})|0\rangle_3/\sqrt{2}$ respectively. Now in both of these possible outcomes we obtain the same Bell state on qubits 1 and 2, disentangled with qubit 3. So overall we obtain a GHZ state with probability of 1/4 and a Bell state with probability of 1/2 (on two qubits of our choice), heralded by the probe beam P quadrature measurement outcome. The other two outcomes project the qubits to two different known product states $|001\rangle$ or $|110\rangle$. Consequently, if all we want to do is entangle a pair of qubits, we can now do this with probability of 3/4.

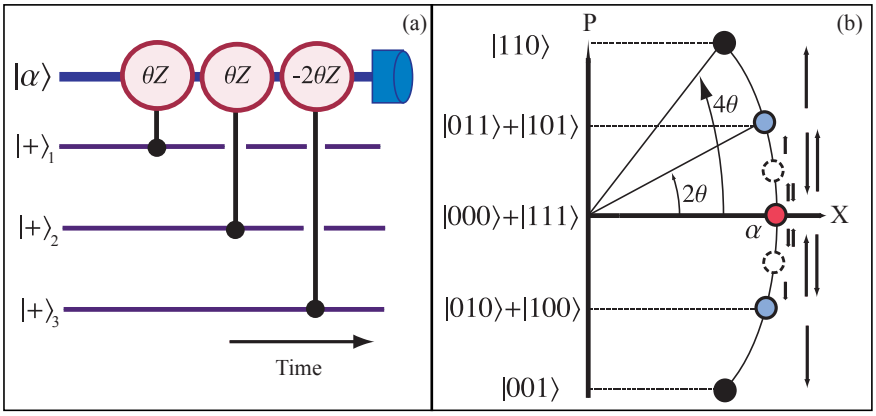

Figure 4.1: Schematic diagram (a) of a three qubit entangling operation. In (b) the possible probe trajectories caused by the three conditional rotations. There are five different end-states. Upon measurement, three of these will project the qubits to entangled states of interest.

It may seem like increasing the number of qubits taking part will further raise the success probability. This claim turns out to be valid if we allow for more and more interactions as we add extra qubits. Considering for example the 4 qubit case. The optimal combination then becomes $R(\theta Z_1)R(\theta Z_2)R(2\theta Z_3)R(-4\theta Z_4)|\alpha\rangle$. We now have 16 possible paths in phase space with 9 different end states. All of these apart from two, under detection, will project the qubits to Bell states and GHZ states. Focusing solely on qubits 1 and 2 (these can be any two qubits which we choose to have interact only once with the probe beam), they will be entangled with probability $p = 7/8$. Following this method for larger numbers of qubits, $R(\theta Z_1)R(\theta Z_2)R(2\theta Z_3)R(4\theta Z_4)...R(-2^{n-2}\theta Z_n)|\alpha\rangle$ the success probability in entangling a specific pair of qubits (here 1 and 2) scales as $p = 1 - 2^{1-n}$. We don't necessarily have to view these extra $n-2$ qubits as ancillas. They can become (if they aren't already) useful elements ('dangling bonds') for future operations when we consider the generation of 2D cluster states. However there are drawbacks to using this generalization. The setup and measurement process will become increasingly complicated. The probe beam will have to travel and interact a lot more, rapidly accentuating the errors that we could have had initially. Another essential point to note, is that the gate operation time will grow exponentially with the number of qubits we are willing to use. If we only have access to a fixed interaction strength θ,

the gate operation time will double every time we add an extra qubit. So depending on the situation we are in, a compromise will have to be made between the time we are willing to take and the success probability we want to achieve. The 3-qubit gate minimizes the ratio of operation time over probability and we shall use this 3/4 probability in the remainder of the paper.

4.1.2 Scaling

We now consider how this entangling scheme may be used for generating cluster states of matter qubits. The usual cluster state is a rectangular 2D lattice of qubits. Building chains is a possible basis for generating cluster states. If the chains are efficiently generated, then simple schemes can be developed to combine them to form a 2D cluster, required for quantum computing [74,75,156]. Given a parity check operation, the simplest growing technique involves taking one qubit (prepared in a superposition state $(|0\rangle + |1\rangle)/\sqrt{2}$) at a time and linking it on the end of the chain. Once this is done, a Hadamard transform is performed on this new end qubit, before the next one is added. In case of failure, the initial end qubit is left in an unknown state. Thus it needs to be measured and adaptive feed forward on its nearest neighbour then enables recovery of the cluster state. So the chain shrinks by one qubit in this case. This constitutes the basic sequential approach to building chains. Clearly for success probabilities smaller than 1/2, the chain will shrink on average; for a success probability of exactly 1/2, it will remain the same length.

We can immediately appreciate benefits from the relatively high probabilities achieved in our two entangling procedures. The first two-qubit procedure already constitutes the limit of simple linear optics approaches. The second one, involving a 3 qubit interaction, can already be used in a sequential fashion, ensuring fast average growth and thus limited resource consumption.

In the case of lower probabilities, small chains are to be built inefficiently before joining them to the main chain. The process of linking chains with an entangling operation is described in Fig. 4.2, using the stabilizer notation. We can see that even though we are not obliged to measure out one qubit, the actual length of the resulting chain is the sum of the two initial ones minus one qubit. A convenient way of representing this operation with states is used in [43]. And in Fig. 4.3, we can see how the three qubit gate allows us to directly join three chains into a 'T' piece, as well as joining two chains together. In case of failure, the end qubits need to be measured out

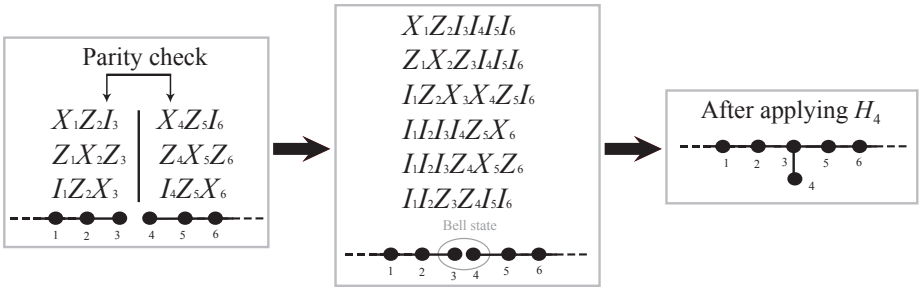

Figure 4.2: Applying a parity check projects the two involved qubits to a state stabilized by the operator Z_3Z_4, removing all the operators anti-commuting with it. Here we apply a Hadamard transform on qubit 4 after the operation, thus producing a dangling bond.

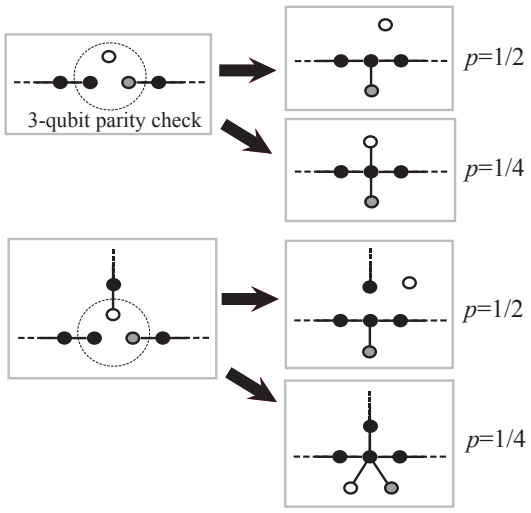

Figure 4.3: Using the 3-qubit gate, we can first attempt to join a pair of chains. This will work 3/4 of the time, producing one or two dangling bonds centred on the same qubit, allowing for repeated trials at linking chains to form two dimensional clusters. Three chains can also been linked up in a similar fashion to produce a 'T' shape.

and each chain shrinks by one element. Then the procedure is repeated. Supposing we start off with two chains of equal length L (following previous analysis [156], L is defined as the number of qubits constituting the linear

cluster), then the average size of the resulting chain is:

$$L_f = \sum_{i=0}^{L} 2(L - 1/2 - i)p(1-p)^i \approx 2L - 1 - 2(1-p)/p \,, \tag{4.1}$$

p being the success probability of the entangling operation. This approximation isn't meaningful for small chains as we will see in the following section. But nonetheless we use it here for the sake of direct comparison with previous work. We can immediately identify a critical length, above which there is growth:

$$L > L_c = 1 + 2(1-p)/p \,. \tag{4.2}$$

This critical length varies between different entangling operations. If an actual logical gate can be immediately implemented, then $L_c = 2(1-p)/p$ for example. Or if this logical gate requires the qubits from the cluster to interact directly (non-distributive approach) then $L_c = 4(1-p)/p$ [156]. So our minimal size chain, ensuring growth is L_0 and $L_0 > L_c$ (the next integer greater than L_c).

Following strategies previously developped, these minimal chains are grown in a divide and conquer fashion (in parallel, without recycling) starting from individual qubits before being merged together. This yields scaling relations for the average time taken $T[L]$ and the average number of entangling operations $N[L]$ to grow a chain of length L:

$$T[L] = t \sum_{i=1}^{\log_2(L_0-1)+1} (1/p)^i + (t/p)\log_2\left(\frac{L-L_c}{L_0-L_c}\right) \tag{4.3}$$

$$N[L] = \frac{\left(1/2\sum_{i=1}^{\log_2(L_0-1)+1}(2/p)^i + 1/p\right)(L-L_c)}{L_0-L_c} - \frac{1}{p} \tag{4.4}$$

where t denotes the time taken per entangling operation.

For our first entangling procedure (2-qubit gate) $p = 1/2$, $L_c = 3$ and thus $L_0 = 4$. Growing this 4-chain will require 14 entangling operations on average leading to $N[L] = 16L - 50$. This is already the theoretical limit for simple single photon applications. In the repeat until success method [81], for a failure probability of 0.6 (and equal success and insurance probabilities, on all results), the scaling is $N[L] = 185L - 1115$ and for a failure probability of 0.4 it becomes $N[L] \simeq 16.6L - 47.7$. Now if we switch to our 3 qubit gate, then $L_0 = 2$. We will notice that $L_c = 5/3$ meaning the $L_0 - L_c$ factor will contribute more than before, because we chose this difference to be unity (also note that here this difference tends to unity as the success probability

increases). The average number of entangling operations required then simply becomes $N_0 = 1/p = 4/3$, giving us a scaling $N[L] = 8L - 44/3$. This is a vast improvement over previous proposals.

We shall extend this scaling comparison to the generation of 2D cluster states. Using the redundant encoding method described in [75], we can give the average number of qubits consumed in the creation of a vertical link. Each trial to establish this link costs two qubits (per chain), because we first need to create dangling bonds. If we succeed in linking the two dangling bonds, we need to measure the first dangling qubit in order to establish the CZ gate then measure the next one, to have a direct link between the two chains. The fact that we can only implement a simple entangling operation and not the logical gate means we lose an additional qubit, which may be used later for additional vertical links or error correction. But if we concentrate on the task of making a single vertical link, the number of qubits consumed is:

$$V = 2(1/p + 1) \, . \tag{4.5}$$

We can see that this converges to 4 as p tends to unity (this corresponds to the qubit cost of a single trial). Then the average number of entangling operations required to make the vertical bond is given by:

$$N_V = 2N[V] + 1/p \, . \tag{4.6}$$

Using the linear optics scheme proposed in [81], for failure probabilities of 0.6, 0.4 and 0.2 respectively, $N_V = 3334$, 191.2 and 32.5. The latter failure probability would however be very difficult to implement physically. With our two and three qubit entangling procedures we obtain $N_V = 70$ and 46.7 respectively. We can see that the efficiency of these schemes generalizes to the creation of 2D cluster states in a straightforward manner. Our gates can also be used to build cluster states in a 'tree' like fashion, as proposed by Bodiya and Duan in [157]. The method relies on the observation that GHZ-type states are locally equivalent to star shaped cluster states. A parity check is all that is needed here.

We now turn back to the time scaling. Solving T for $p = 1/2$ we end up with:

$$T[L] = 14 + 2\log_2(L - 3) \, . \tag{4.7}$$

Of course this is only valid for $L \geq 4 = L_c$. The above result is obtained with a $T_0 = 14$ corresponding to the average time needed to build a 5-qubit chain without recycling (this is due to the form of the sum). It is pretty clear that if we allow for entangling operations to be made in parallel, alongside

additional resources, this T_0 can be minimized. For $p > 1/2$ we have $L_0 = 2$, meaning we only keep the first term in the sum for T_0. This results in a general closed expression for T:

$$T[L] = (t/p)\left(1 + \log_2\left(\frac{L - L_c}{L_0 - L_c}\right)\right) . \tag{4.8}$$

We can compare this with the time taken by a sequential adding and building, as we now have access to probabilities higher than 1/2. Adding one qubit at a time, via an entangling procedure, gives the recursion relation $L_{k+1} = L_k + 2p - 1$ for the length, leading to the number of rounds $k = (L-1)/(2p-1)$. So for our 3 qubit gate, on average the chain grows by one unit every two trials. The time being sequential too, $T_{L+1} = T_L + t/p$, the general form for T becomes:

$$T[L] = (L - 1)t/p . \tag{4.9}$$

Thus time now scales linearly with the length of the chain in contrast with the logarithmic dependence we had above.

4.1.3 Optimizing time and resources

For the two-qubit entangling gate, we essentially stand at the same point as the photonic cluster state approaches. Optimizing the resources boils down to finding the optimal strategies in combining elements of cluster states. Though this is a classical analysis, relying on probabilistic gates, it is a very complex task. Obtaining bounds or comparing different strategies requires computing assistance. In their recent paper, Kieling, Gross, and Eisert [158,159] investigate these issues in significant detail. They analyse essential methods and derive bounds for the globally optimal strategy, based on an entangling operation working with probability 1/2.

For higher probabilities however, the critical length insuring average growth simply doesn't exist anymore and additional truly scalable approaches are at hand. We shall go over the obvious ones. From previous works on generating cluster states [43, 156], we know that the simplest way to grow short chains with probabilistic gates is through a 'divide and conquer' approach. It also turns out to be much quicker than a sequential adding, as we allow for many gates to operate in parallel. As described earlier on, this technique attempts to link up chains of equal length on each round, and discards the chains which failed to do so.

This approach can be extended to growing large chains in the aim of saving time. In this context we can work out some important *average* quantities, starting off with the time taken:

$$T[L] = 1 + \log_2(L-1) = k \; . \tag{4.10}$$

Here k represents the number of rounds and can easily be worked out, as we saw above, from the given chain length. Thus we will only use k in the following expressions. Next we can give the number of chains, at a particular round k ($L = 1$ for $k = 0$), having started off with n qubits:

$$C[k] = n(p/2)^k \; . \tag{4.11}$$

Then the number of remaining qubits on that round is given by:

$$Q[k] = C[k] \times L = n(p/2)^k(2^{k-1} + 1) \; . \tag{4.12}$$

Following this we can work out the number of wasted qubits $W[k] = n - Q[k]$. Finally, when discussing the necessary resources we need the overall cumulative number of entangling operations:

$$G[k] = \sum_{j=1}^{k-1} \frac{C[j,m]}{2} = \frac{n}{2}\left(\frac{1-(p/2)^{k-1}}{2/p-1}\right) \; . \tag{4.13}$$

In order to have a first comparison with the method described in the previous section, we can set the value of $C[k]$ to unity. Or alternatively, we can use the ratio $N_{\rm dc}[k] = G[k]/C[k]$ which will give the average number of entangling operations required to produce a single chain:

$$N_{\rm dc}[k] = \frac{\sum_{j=1}^{k-1} C[j]}{2C[k]} \; . \tag{4.14}$$

Expressing this ratio in function of $L = 2^{k-1} + 1$ we obtain:

$$N_{\rm dc}[L] = \frac{(2/p)^{\log_2(L-1)} - 1}{2-p} \; . \tag{4.15}$$

From the initial strategy, with $m \geq 2$ we reached a value linear in L:

$$N[L] = \left(\frac{2}{p}\right)\frac{L-1-2(1-p)/p}{1-2(1-p)/p} - \frac{1}{p} \; . \tag{4.16}$$

Obviously this will scale better with L, but surprisingly enough, the threshold above which it becomes more advantageous is very high. As observed in

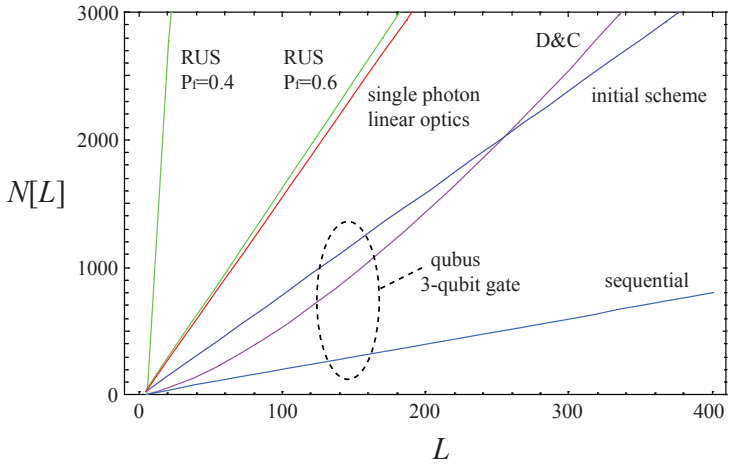

Figure 4.4: Comparison of entangling operation requirements for chain production, using our 3-qubit gate. Clearly for chains smaller than 250 qubits the full divide and conquer approach is more advantageous than the linear scaling obtained through the initial merging technique. The savings in the number of entangling operations are most significant around lengths of 100 to 120 qubits. However, the sequential adding scheme is significantly more efficient still, as expected. With this we achieve much lower scalings in comparison with those obtained through the repeat until success (RUS) scheme, P_f representing the failure probability. The 'linear optics' curve corresponds to a success probability of 1/2 using the divide and conquer strategies [156]. This is the theoretical limit of conventional linear optical schemes, ignoring all detector and source inefficiencies.

Fig. 4.4 (for our 3 qubit gate), up till lengths of 250 qubits, the full divide and conquer approach requires less entangling operations. This is due to the fact that the probabilities we are dealing with are significantly higher than in previous schemes, which were undertaken in two steps, the building of minimal elements L_0 and then their merging, in order to be scalable.

We can compare this with the sequential adding method for which we have:

$$N_{\rm seq}[L] = (L-1)/(2p-1)\ . \tag{4.17}$$

Obviously this represents a considerable saving, as can be verified in Fig. 4.4. Overall we find that the three-qubit gate allows for a far more efficient cluster state generation that linear optics based proposals.

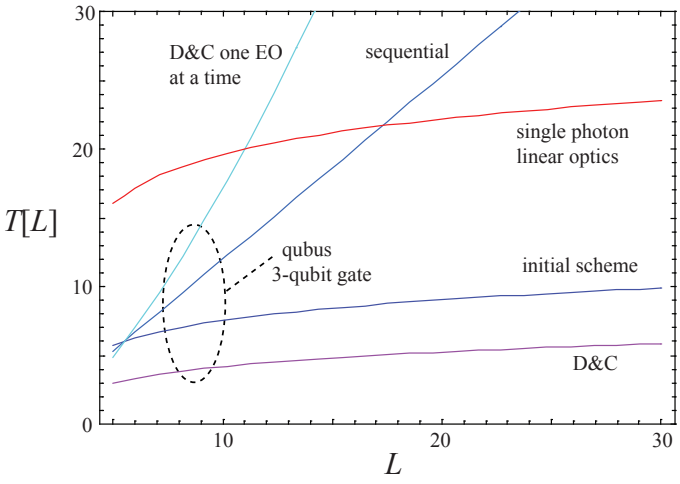

Figure 4.5: Comparison of time requirements for chain production, for various strategies, as a function of the chain length. The divide and conquer approach, as expected, saves significant amounts of time. The linear time dependence of sequential adding does not compare, for long chains. However we can see the difference in work required if we only allow one entangling operation at a time. Again we can observe the theoretical limit for linear optics.

We can also compare the time scaling of these various strategies, in units of time t corresponding to a single measurement. For the complete divide and conquer scheme we simply have:

$$T_{\mathrm{dc}}[L] = t\,(1 + \log_2(L-1)) \ . \tag{4.18}$$

and for the initial scheme:

$$T[L] = \frac{t}{p}\left(1 + \log_2\left(\frac{L - L_c}{L_0 - L_c}\right)\right) \ . \tag{4.19}$$

For the sequential adding, the cumulative time obeys $T_{L+1} = T_L + t/p$, and the general form for T becomes:

$$T_{\mathrm{seq}}[L] = t(L-1)/p \ . \tag{4.20}$$

Thus time now scales linearly with the length of the chain, in contrast with the logarithmic dependence we had above.

The first two approaches have a logarithmic dependence on the length L, however $T_{\rm dc}$ is significantly lower as might have been expected (see Fig. 4.5). Overall we see that there is a clear advantage to divide the task up and to run parallel entangling operations. The decrease in generation time over the single photon linear optics proposals is not as striking as the savings in entangling resources, however it remains considerable. We can appreciate the drastic impact of a heightened success probability on the scalability of cluster state generation. This provides a significant incentive to pursue the weak nonlinearity schemes even though at the present time they are much harder to implement experimentally that single photon linear optical schemes.

We note that the resources in qubits become quite large, in the absence of recycling. The amount of wasted qubits for the full divide and conquer approach grows very quickly as can be seen from the expression for $W[k]$. One could envisage in this case a form of partial recycling, to save on the qubit resources whilst still retaining the time speed up. Then we would allow for two or three trials before discarding the chains (the initial scheme set no limit on the number of trials). However the protocol now becomes more elaborate unless we are willing to wait between each round (of discarding) because some chains will link on the first trial while others will link on the second (supposing we allow two trials). So it seems like savings in time could be made if we are able to manage and organize chains of different lengths.

The linear time scaling for the sequential method is due to the fact that operations cannot be undertaken in parallel during its growth. If we didn't have access to simultaneous entangling operations, the time scaling for the divide and conquer methods would be equivalent to $N_{dc}[L]$ which is sub-exponential. One needs to keep in mind that by adopting a sequential method, the whole procedure is simplified considerably and would be more accessible to physical implementations. Divide and conquer methods require a lot of work in parallel and should in practice involve the moving about and reordering of qubits or even small cluster states. Unless the actual edges linking up the vertices in the graph states can be displaced via entanglement swapping strategies, we will most probably have to physically move some vertices in order to implement additional entangling operations. Adding qubits sequentially should solve some architectural problems which may arise. For example, the qubits could be perfectly static and the measuring system (including the ancillary qubit which can be reused) would travel along the chain 'zipping' it up. Of course the measuring system would go back and forth, with a frequency related to the success probability of a single operation. But essentially the qubits constituting the chain wouldn't have

to move. This seems significantly more practical than moving the qubits and chains around or having to change the measuring setup every time so as to implement the operation between qubits in various places. However many of these problems may be solved by more advanced protocols making use of percolation phenomena as developed in [160].

All this brings us to view the cluster state as having active regions in which it is being built or measured in the computation (both can be undertaken simultaneously) and regions in which the qubits are simply waiting. Now this waiting can be minimized in the building itself, through the appropriate protocols, and in the measurement process. That is, the cluster can be built only a few layers in advance, so that the qubits have less waiting to do, between the building and the actual measurement. In any case, there will be some waiting. Therefore the lowest decoherence support would be preferred, but it may not be the easiest to manipulate. Thus we may envisage having two different physical realizations constituting the cluster state. For example, we could use single electron spins initially in building the cluster. Once the links are made between one site and its nearest neighbours, the qubit could be switched into a nuclear spin state which has a significantly longer coherence time, via a swap operation or some other coherent write and read actions. Most of the waiting would be done in the long-lived state, before being swapped again for the readout [33, 119]. This follows the same scenario as using a second physical system to mediate the interaction and make the measurements, in distributed quantum computing.

In the present proposal, we use a continuous variable bus and homodyne measurements to generate the links. This physical system shows itself to be very efficient in this application. Then, for example, electron spins or superconducting charge qubits could then be the matter realization interacting with the bus and serving for the final readout. These systems provide the useful static aspect required, they interact well with the mediating bus and ensure good single qubit measurements. Finally a low decoherence realization such as nuclear spin could be envisaged, mainly as a storage medium. The swapping or write and read procedure should have a high fidelity for this storage to be beneficial. On the whole, we see that optimization will depend directly on the physical realization(s) we have chosen to work with. For systems with long dephasing times we would give priority to sequential adding approaches, as we have some freedom in the time scaling and thus we can make significant savings in resources. But for realizations with short dephasing times, we would probably want to divide the task up and run operations in parallel, in order to accelerate the fabrication of the cluster state, at the expense of extra resources.

4.1.4 The measurement-free approach

Looking at our entangling gates, we have seen that if we utilize four non-linear interactions and three qubits the success probability is dramatically increased. Within the framework of four non-linear interactions, another option presents itself to us [108]. In the spirit of the initial proposal of Wang and Zanardi [96] this can easily be extended to the simulation of many-body interactions. The interactions required to build a cluster state are pairwise thus conditional displacements are sufficient.

By having the probe interact with more qubits and adapting the direction of the displacements, we can pick out the qubits we want to couple through the state-dependent geometrical phases. In that way one could start from a general sequence of the form:

$$\prod_{n=1}^{N} D(-\beta_n Z_n) \prod_{n=1}^{N} D(\beta_n Z_n) = \exp\left[2i\mathrm{Im}\left\{\sum_{n=1}^{N-1}\left(\beta_n^* Z_n \sum_{p=n+1}^{N} \beta_p Z_p\right)\right\}\right]. \tag{4.21}$$

But here we are simulating interactions between all qubits and from this sequence one cannot directly generate linear or grid-like cluster states. That is we need to adjust the β_n so as to choose which qubits we want to interact. We can use such a sequence to directly generate useful graph states such as star shaped graphs (locally equivalent to GHZ states). For example, taking β real and the displacement from qubit 1 orthogonal to all the others we have

$$\prod_{n=2}^{N} D(-\beta Z_n) D(-i\beta Z_1) \prod_{n=2}^{N} D(\beta Z_n) D(i\beta Z_1) = \exp\left[-2i\beta^2 Z_1 \left\{\sum_{n=2}^{N} Z_n\right\}\right]. \tag{4.22}$$

Clearly if we set $\beta = \sqrt{\pi/8}$ we will obtain a star shaped graph of our N qubits, centered on qubit 1 (Fig. 4.6(a)). We note that from this condition on β and the conditional displacement simulation sequence (3.63), the scaling and magnitude requirements for $\alpha\theta$ here are comparable to those of the measurement-induced entangling schemes. To generate a linear cluster we need to switch to another interaction sequence. We need to disentangle the probe with the qubits as the sequence evolves so as not to create extra links. Coming back to our conditional phase operation $\hat{U}$ we notice that after the third interaction the probe becomes disentangled from qubit 1. Furthermore by setting $\beta_1 = i\beta_2$ the entirety of the geometric phase is al-

ready acquired (by the corresponding two-qubit state) at this point. Along with this observation and a correct ordering of the displacements we can propose a sequence of the form

$$D(-\beta Z_N)D(-i\beta Z_{N-1})...D(\beta Z_4)D(-\beta Z_2)D(i\beta Z_3)D(-i\beta Z_1)D(\beta Z_2)D(i\beta Z_1)$$
$$= \exp\left[2i\beta^2 \sum_{n=1}^{N-1}(-1)^n Z_n Z_{n+1}\right] \tag{4.23}$$

Again setting $\beta = \sqrt{\pi/8}$ all the couplings are locally equivalent to conditional phase gates, yielding a linear cluster state (see Fig. 4.6(b)). We can view the probe as creating the links as it travels along the chain.

The main advantage with these generalizations is the reduced number of interactions per qubit. If we were to use the simple conditional phase sequence $\hat{U}$ then the number of interactions per qubit would be $2d$ where d is the degree of the qubit in the graph state. In other words, to build a N qubit star shaped graph, the center qubit would have to interact $2(N-1)$ times at most, or with local operations to swap the center qubit as the star is being generated we could bring this down to four interactions per qubit. As we see from our generalized sequence each qubit would only need to interact twice with the probe mode. Now if we think of a grid-like structure, the qubits inside the graph will have $d = 4$, thus using $\hat{U}$ would mean we require 8 interactions for each of these qubits. But here again if we switch to the linear cluster sequence each one of these qubits would interact 4 times only, twice in each of the two chains that go through it.

These multi-qubit approaches could be envisaged in different contexts. For example we may view it as an expensive resource (be it in time or work) alongside a cheaper one such as probabilistic two qubit parity gates. Many schemes make use of a basic building block such as star shaped graphs. For instance this approach could be used to directly generate the building blocks needed in the percolation techniques derived in [160], then easier measurement based gates would take on from there, following the same methods. When we begin to think of loss in the probe mode however, this star shaped graph sequence is a lot less robust than the linear graph sequence. The reason being that halfway through the interactions the probe holds information about all qubits, meaning that correlated errors will be quite significant. Whereas in the linear graph sequence, the probe holds information about at most two elements because it is constantly disentangling from the previous ones. Meaning that the correlated errors will be limited to pairs of qubits.

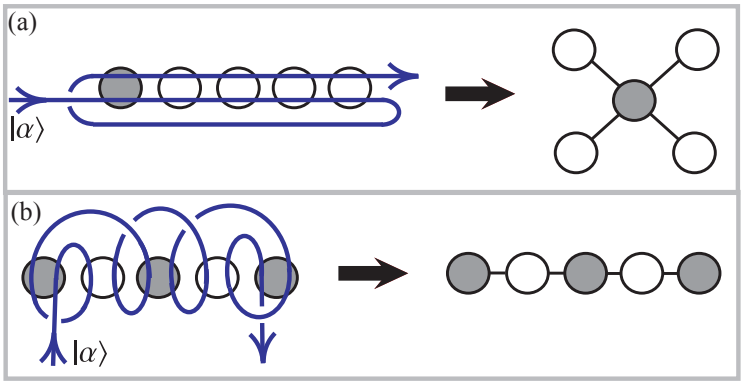

Figure 4.6: Schematic representation of two different interaction sequences derived in the text. The gray and the white qubits lead to a pure imaginary and pure real conditional displacement of the probe mode α. The first and second interaction, for each qubit, are in opposite directions in phase space. In (a) we have the sequence leading to a star shape while in (b) the one leading to a linear graph, both on 5 qubits. For larger numbers of qubits we have the same patterns.

In that sense the simplest and apparently most robust procedure for building a grid like structure is to generate chains that would then overlap at the intersections. In any case we can compensate for the loss in the probe and make sure it disentangles from the qubits. This will leave us with weighted graphs and some dephasing on the qubits. We can then resort to purification protocols such as those proposed in [161].

The important aspect of this measurement free approach is that it is significantly quicker. Also it does precisely simulate the two qubit gates required for generating the cluster state, unlike the measurement based gates which are simple parity checks. This means that no feed-forward or local operations are required. But this comes to a price. The constraints for the strength of the interactions are greater, that is they are now fixed, in contrast with our parity gates for which there simply was a lower bound needed for the distinguishability of the measurement outcomes.

Now given these near deterministic operations, the number of interactions required to build a certain cluster state becomes fixed. The question of time then simply reduces to the number of gates we can implement in parallel. Looking at the process in a dynamical way, we can see now that the size of the cluster state at a certain time during the computation is

significantly reduced. This 'buffer' region of the cluster state may still be a couple of layers, but the off-line part of the cluster, which isn't attached yet, can be made very small. Previously, the size of the buffer that is yet to be linked up was dictated by the success probabilities of the entangling operations [43]. The bigger this off-line prepared buffer is, the more time it takes to build it and the more time it takes to attach it. In other words the more errors it contains. Now depending on the amount of near deterministic gates we can implement in parallel, this off-line buffer only needs to consist in a couple of layers, freshly built, purified and attached. As a matter of fact we may not even need this off-line aspect anymore. The individual qubits could be added directly to the existing cluster as it is being measured. This represents huge savings in the number of qubits we are dealing with and minimizes the error they may have picked up, as they spend a minimal time inside a cluster state. The issues raised at the end of the last section are still of concern here. There always will be *some* waiting, between the building and the readout, so change in support during that time, from electron spin to nuclear spin for example, in order to minimize the dephasing, is still an important idea.

In this section we have considered the efficiencies of the qubus scheme for the generation of matter qubit cluster states, enabling us to work in the success probability regime of $p \geq 1/2$. Being able to overcome the critical probability of $1/2$ opens up a whole range of different possibilities which previous results in the field do not account for. The probability of $3/4$ obtained in our three qubit gate drastically reduces the cost in resources, providing a significant improvement over single photon proposals. Practical effects such as mismatched coupling rates and bus loss were investigated in [162]. The two-qubit parity gate was shown to be quite resilient against mismatched coupling rates (up to a bias in the projection), however the overall requirements are demanding, calling for further work to overcome these issues.

We also examined different growth strategies and noticed the impact they had on resource usage. Developing efficient strategies then becomes essential to the viability of measurement-based computation. In particular we need to be able to characterize the performance of different strategies over the whole range of success probabilities, as we have now been able to overcome the $p = 1/2$ limit. The topic of the next section is to try to look at the exact average growth or rate of production yielded by different strategies within different resource settings, with the aim of finding optimal strategies.

4.2 Two regimes in probabilistic cluster state growth

The analysis of the probabilistic growth of cluster states does not involve any quantum elements. The process at hand is a simple stochastic process, however evaluating the exact resource requirements is very challenging. Even more challenging is to define and find the optimal strategy. In trying to answer such questions, one can identify two main routes taken in previous work. The first is the use of computer simulations such as Monte Carlo simulations, to evaluate the performance of different strategies [163]. The strategy in this case consists in a set of rules, applied to a population at each time step. The simulations are interesting and are certainly a requirement in such studies, however they need to be completed by some form of analytical approximation, so that one can gain an intuitive understanding of what is observed.

The second route is that of analytical results [43, 134, 156] in which a strategy is not population dependent. The average performance is calculated directly through crude approximations such as Eq. 4.1 and many resources are discarded. For example the divide and conquer strategy discards all chains which fail to fuse, independent of their length, so as to ease calculations. Another issue with this approach is that many operations are run in parallel, meaning that in the end one is necessarily presented with a trade-off between time and work, which makes it hard to compare different strategies. One attribute of the comparative simulations in [163] is that they only allow for one entangling operation per time step. This simplification we will make in the second part of this section.

A thorough study involving both approaches was undertaken by Gross *et al.* [159]. In their setting, one starts with a finite pool of minimal elements (entangled pairs) and then tries to maximize the expected length of the final chain. This work is by far the most complete in understanding the resource requirements and limits of cluster state generation with probabilistic gates. However in this section we look at the issue of cluster state generation through another perspective, that of maximizing the production rate, given on demand resources. Such a setting may be conceived of in a large scale quantum computer. It makes the problem more tractable analytically and may be very much related to the approach taken in [159].

In the first part of this section we investigate the large scale generation of cluster states, assuming large populations and entangling resources. We then apply this method to vast purification schemes, illustrating another one of its application. In the third part we come back to the individual chain picture and introduce absorbing Markov chains as a valuable tool for

growth analysis. We note here that we will focus on the production of linear cluster states only, as they form the basis for most 2D generation strategies [134, 156, 159].

4.2.1 Steady state generation of cluster states

In order to investigate the large scale production of linear clusters we will adopt a model somewhat similar to previous work relying on computer simulations [163]. In this model we assume that at any given time step we have a pool of chains of various lengths, all arranged into bins corresponding to a particular length. By fixing a maximum length L we can represent the population distribution through the population vector

$$\mathbf{n} = (n_1, n_2, .., n_L)^T, \tag{4.24}$$

where n_i represents the qubit content of the i^{th} bin. The qubit content of the entire distribution is then given by

$$\sum_{i=1}^{L} n_i = N. \tag{4.25}$$

The first assumption we will make is that of large N, sufficiently large for us to ignore issues of parity, allowing us to take arbitrary fractions of the n_i. Such an approximation is sometimes made in queuing theory, and is known as the fluid approximation [164]. We now define the normalized population vector as

$$\bar{\mathbf{n}} = (\bar{n}_1, \bar{n}_2, .., \bar{n}_L)^T \equiv \lim_{N\to\infty} \frac{1}{N}\mathbf{n}, \tag{4.26}$$

with

$$\sum_{i=1}^{L} \bar{n}_i = 1. \tag{4.27}$$

Secondly we assume an on demand supply of fresh qubits. The result is equivalent to assuming infinite population in the length 1 bin, as is the case in [163]. In this context, a strategy defines how one should pair up all the elements (chains of different lengths) of the population distribution. As we also allow for large parallel entangling resources, a strategy arranges all the elements into pairs and attempts to fuse them all in parallel, at each time step. In contrast to the definition used in [159], here a strategy is a fixed

pairing which is repeatedly applied to the population and thus time ordering is no longer necessary.

Within this framework, we define the output of the system as the number of chains produced per time step which exceed the maximum length L, normalized over their qubit content. To be able to tract the dynamics analytically and for this output to be constant, we require the strategies to lead to steady state behavior. That is the population vector $\bar{\mathbf{n}}$ should remain constant. For this to hold, we automatically inject the qubit content of the outputed chains into the single qubit bin. Also whenever there is a failure outcome, the free qubits generated are transfered to the length one bin. This in effect closes the system, even though we have a constant input of qubits and a constant output of chains exceeding length L.

As the process at hand is a fusion process, we need introduce a new object, which we will refer to as the pairing matrix $\mathbf{Q}$, fully defining a strategy. This pairing matrix tells us in which proportions chains of different lengths are to be paired up, under the constraint that this repeated pairing leads to steady state dynamics. It is worth emphasizing here how useful an attribute it is for a strategy to yield a constant output. The pairing matrix is a square $L \times L$ matrix

$$\mathbf{Q} = \begin{pmatrix} Q_{11} & Q_{12} & \cdots & Q_{1L} \\ Q_{21} & Q_{22} & \cdots & Q_{2L} \\ \vdots & \vdots & \ddots & \vdots \\ Q_{L1} & Q_{L2} & \cdots & Q_{LL} \end{pmatrix}, \tag{4.28}$$

where the element Q_{ij} represents the (normalized) number of pairs of chains of length i and j involved in the parallel fusion process. Clearly we have $Q_{ij} = Q_{ji}$, so $\mathbf{Q}$ is a symmetric matrix and thus there are only $N(N+1)/2$ different variables, the contents of a triangular matrix. For convenience we define

$$\tilde{\mathbf{Q}} = \begin{pmatrix} 2Q_{11} & Q_{12} & \cdots & Q_{1L} \\ Q_{21} & 2Q_{22} & \cdots & Q_{2L} \\ \vdots & \vdots & \ddots & \vdots \\ Q_{L1} & Q_{L2} & \cdots & 2Q_{LL} \end{pmatrix}, \tag{4.29}$$

and

$$\mathbf{R} = \begin{pmatrix} 1 & 0 & \cdots & 0 \\ 0 & 2 & \cdots & 0 \\ \vdots & \vdots & \ddots & \vdots \\ 0 & 0 & \cdots & L \end{pmatrix}. \tag{4.30}$$

This allows us to relate the population vector and pairing matrix as

$$T[\mathbf{Q}] = \mathbf{R}\tilde{\mathbf{Q}}\,\mathbf{e} = \bar{\mathbf{n}}, \tag{4.31}$$

where $\mathbf{e}^T = (1, .., 1)$ is the unit vector of length L. The normalization constraint on the pairing matrix itself can simply be written as

$$\mathrm{Tr}\left[\mathbf{R}\tilde{\mathbf{Q}}\,\mathbf{e}\right] = 1. \tag{4.32}$$

For simplicity we will use the conventional CZ gate as our entangling gate, such that if we try joining two chains of length l_1 and l_2, we will obtain with probability p (the success probability of the gate) a single chain of length $l_1 + l_2$, and with probability $1 - p$ the two chains having shrunk by one qubit $l_1 - 1$ and $l_2 - 1$ (for $l_1, l_2 > 1$). This configuration would occur in a distributive CZ gate, where in case of failure, the affected qubits are left in an unknown state and have to be measured out in order to retrieve the cluster state on the rest of the chain. We can now visualize the effect of the fusion processes in terms of the pairing matrix elements. For successful fusions, the map S maps the paring matrix to another pairing matrix $S : \mathbf{Q} \to \mathbf{Q}^{(s)}$ according to

$$Q_{i,j} \to \begin{cases} \frac{1}{2} Q^{(s)}_{i+j,i+j} & \text{if } i + j \leq L, \\ \\ \frac{i+j}{2} Q^{(s)}_{1,1} & \text{if } i + j > L, \end{cases} \tag{4.33}$$

where we have added commas in the subscripts for clarity. The first situation corresponds to the standard successful fusion of two chains. Note here that we have some freedom in how we choose to express these transitions because we are requiring steady state behavior, i.e. conditioning on the population vector itself. Thus we are free to write the transitions as we wish to, making sure that normalization in conserved and the corresponding population vector remains constant. Here the successful fusion leads to 'half a pair' $Q^{(s)}_{i+j,i+j}$. The second situation corresponds to a chain being outputted and its qubit content being reinjected into the first bin. In case of failure the map $F : \mathbf{Q} \to \mathbf{Q}^{(f)}$ is applied, acting as

$$Q_{i,j} \rightarrow \begin{cases} Q^{(f)}_{i-1,j-1} + Q^{(f)}_{1,1} & \text{if } i,j > 1, \\ Q^{(f)}_{i,j-1} + \frac{1}{2}Q^{(f)}_{1,1} & \text{if } i = 1, j > 1, \\ Q^{(f)}_{i-1,j} + \frac{1}{2}Q^{(f)}_{1,1} & \text{if } i > 1, j = 1, \\ Q^{(f)}_{1,1} & \text{if } i = j = 1. \end{cases} \tag{4.34}$$

The outgoing elements are again chosen so as to conserve qubit number. Given the two possible transitions, the steady state condition can be written as

$$T[\mathbf{Q}] = T[p\mathbf{Q}^{(s)} + (1-p)\mathbf{Q}^{(f)}]. \tag{4.35}$$

This leads to a set of linear equations relating the elements $Q_{i,j}$. At this point we can write the output per cycle as

$$\text{Out}[\mathbf{Q}] = p\sum_{j=1}^{N}\sum_{i=1}^{j} Q_{i,j}(i+j) \quad \text{with} \quad i+j > N. \tag{4.36}$$

Now to clarify the process again in words; to each pairing matrix (strategy), is associated a single normalized population vector. This pairing matrix is applied repeatedly, producing an average output per cycle. The whole problem of finding the optimal strategy $\mathbf{Q}_o$ (and consequently its associated optimal population vector $\bar{\mathbf{n}}_o$), can then be stated as follows:

Find $\mathbf{Q}_o$ such that

$$\text{Out}[\mathbf{Q}_o] = \max \text{Out}[\mathbf{Q}], \tag{4.37}$$

subject to

$$T[\mathbf{Q}_o] = T[p\mathbf{Q}_o^{(s)} + (1-p)\mathbf{Q}_o^{(f)}], \tag{4.38}$$

and

$$\text{Tr}\left[\mathbf{R}\tilde{\mathbf{Q}}_o\,\mathbf{e}\right] = 1. \tag{4.39}$$

Let us consider the simplest case of two bins, the first one containing single qubits and the second containing entangled pairs. The pairing matrix in this case is

$$\mathbf{Q} = \begin{pmatrix} Q_{1,1} & Q_{1,2} \\ Q_{2,1} & Q_{2,2} \end{pmatrix}, \tag{4.40}$$

with the associated population vector given by

$$\bar{\mathbf{n}} = \begin{pmatrix} 2Q_{1,1} + Q_{1,2} \\ 4Q_{2,2} + 2Q_{1,2} \end{pmatrix}, \tag{4.41}$$

and the output by

$$\mathrm{Out}[\mathbf{Q}] = p(3Q_{1,2} + 4Q_{2,2}). \tag{4.42}$$

There are only three parameters to optimize over, as $Q_{1,2} = Q_{2,1}$. Maximizing the output yields a strategy in which we we do not pair chains of length 2 (i.e. $Q_{(o)2,2} = 0$). Now of course if we were only quantifying the output through the number of chains leaving the system, then intuitively the optimal approach would be to produce the shortest length. This would in turn mean that in this example, it would be a waste of resources to produce chains of length 4. But it is important to stress at this point that producing larger chains is valued because we quantify the output in terms of numbers of qubits. So in this sense it is not entirely obvious what the optimal strategy is. As we said previously, the proportions are fixed by the success probability and the steady-state conditions, in this case we obtain simply $Q_{(o)1,2} = pQ_{(o)1,1}$. The normalization condition then yields $Q_{(o)1,1} = 1/(2 + 3p)$. There are no other steady state strategies in which $Q_{2,2} = 0$ (i.e. different proportions). The output for the optimal strategy is $3p^2/(2 + 3p)$. We can compare this output with another obvious strategy, that of pairing within each bin only; $Q_{1,2} = 0$. Then we obtain a steady output of $2p^2/(2 + 2p)$, which is lower for all $0 \leq p \leq 1$.

Applying this method to larger numbers of bins yields interesting results. The first observation we make is that for a given number of bins, the vanishing elements of the optimal strategy seem to be independent of p. However the values of the non-vanishing elements have to be functions of p as they are related to the population vector. The second observation is that even though we normalize the output in terms of qubits, the optimal strategies always produce the shortest length. That is if we have L bins, the optimal strategy will always output chains of length $L + 1$ only. So making the produced chains as small as possible insures a maximum qubit output. Also in general there is a branching out of the pairing when the chains to be paired approach $L/2$. What we mean by this is that there are several pairings which produce this target length of $L + 1$. In Fig. 4.7 is displayed

how this branching evolves with the number of bins, in a rather irregular fashion. Given this number which remains relatively low with the size of the system, we see that the optimal strategies keep large numbers of bins empty, a little less than $L/2$ of them.

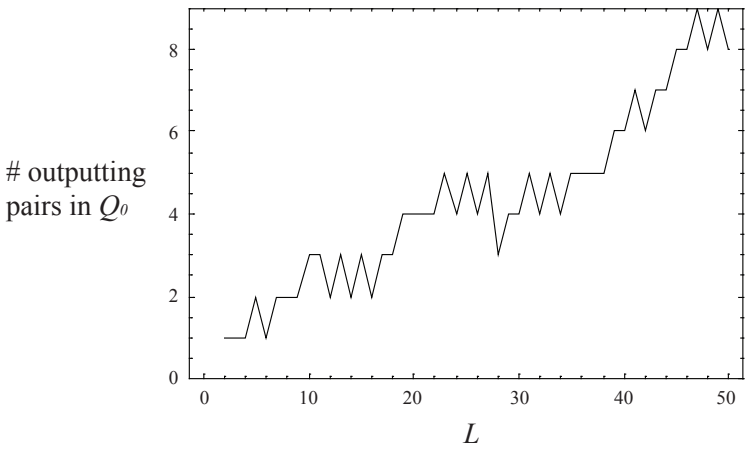

Figure 4.7: This plot follows the number of different parings (non-zero elements in the paring matrix) which contribute to the output. That is the number of different non-zero elements $Q_{i,j}$ for which $i + j > L$. We can see this number has a complicated evolution with L, but there are a few observations to be made. Comparatively, odd numbers of bins tend to have a larger number of outputting pairs, within small differences in number of bins. Also the outputting number of pairs for odd L seems to at least stagnate or increase, whereas for some even L, there is a decrease. Overall, the average evolution of this outputting number is not linear with the number of bins.

One aspect of optimal strategies which is interesting to keep track of is the pairing within bins, that is the terms of the form $Q_{i,i}$. As we look at the optimal strategies for increasing L, one easily notices how for small bin numbers at least, it becomes optimal to pair elements of same length. There are two possible ways of viewing this. The first way is to simply record whether particular $Q_{i,i}$ terms are part of the optimal strategy. This is illustrated in Fig. 4.8(a) and clearly shows how these terms become predominant in low bin numbers. The second, more precise way, is to record whether for a particular length, the optimal strategy *only* pairs elements of this same length together. That is one keeps track of the non-zero $Q_{(o)i,i}$ terms with

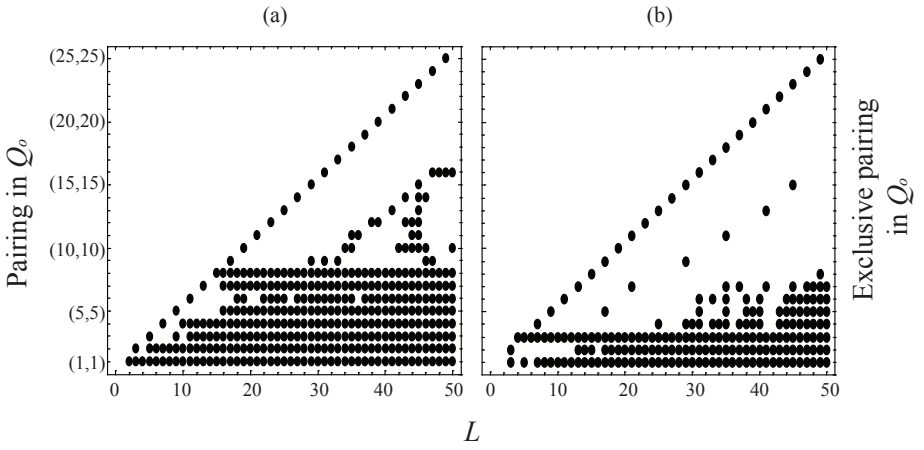

Figure 4.8: These graphs shows with the use of points, whether a particular $Q_{i,i}$ (denoted by (i,i) along the vertical axis) term is present in the optimal strategy, for a given number of bins L. In (a) one can see whether or not such a pairing is part of the strategy at all. In (b) is shown the presence of exclusive pairing $Q_{i,i}$, as defined in the text.

$Q_{(o)i,j} = Q_{(o)j,i} = 0$ for all j. We refer to this as exclusive pairing, illustrated in Fig. 4.8(b). And again, a similar but stronger observation can be made; it is advantageous to pair elements of the same length only, within this lower set of bins. This result is interesting, as it was observed in the simulations run in [163], that the strategy pairing chains of the same length outperformed other proposed strategies.

The fact that the strategy is directly associated with a population distribution poses an initial question: is it always possible to reach the optimal steady state population? If one allows for a selective pairing, in which chains can be put aside and not be involved in fusion attempts, then it is obviously the case that the optimal population distribution can be attained in time. One way of proceeding may be to first populate the upper most bin L as much as possible and then populate lower bins by breaking up these large chains through Z measurements, as explained in chapter 2, until the right proportions are obtained. This of course means that the entangling resources will not be used at their full capacity, but this is simply a proof of principle. A more interesting result would be to develop an extended framework in which a strategy is not only defined for the optimal steady state population, but also for a whole set of transient populations. Then the optimal strategy

would become the strategy which converges fastest to the optimal steady state, starting with a population vector $\bar{\mathbf{n}} = (1, 0, .., 0)$. We have not yet been able to define and find converging strategies which use all the entangling resources available at each time step. However we have used a step by step optimization and found convergence for small L. In that case the problem can be stated at each time step as:

Find $\mathbf{Q}_t$ such that

$$D[T[\mathbf{Q}'_t], \bar{\mathbf{n}}_o] = \min D[T[\mathbf{Q}'], \bar{\mathbf{n}}_o], \tag{4.43}$$

over all $\mathbf{Q}$ for which $T[\mathbf{Q}] = \bar{\mathbf{n}}_{\text{in}}$, with $\mathbf{Q}' = p\mathbf{Q}^{(s)} + (1-p)\mathbf{Q}^{(f)}$. Here $\bar{\mathbf{n}}_{\text{in}}$ is the population vector at that particular time step and D is some distance measure. This step by step optimization is very demanding numerically and the convergence for $L = 4$ is illustrated in Fig. 4.9. In this case we used $D[\mathbf{a}, \mathbf{b}] = \text{Tr}|\mathbf{a} - \mathbf{b}|$ and it is clear that the population rapidly converges, within 10 time steps. Numerical extension to larger L has so far failed, but this example provides a positive expectation of convergence in general.

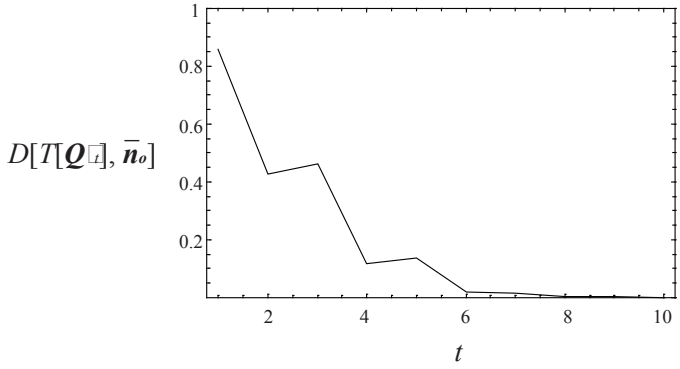

Figure 4.9: Plot of the distance between the population distribution at time step t and the optimal distribution $\bar{\mathbf{n}}_o$ (for $L = 4$), with an initial distribution $(1, 0, 0, 0)$.

4.2.2 Steady state purification protocols

Now we will quickly discuss the application of a similar model to vast purification protocols [165]. In such systems the quality (the quantity whose evolution is followed) is no longer the length of the cluster state, but the

fidelity of an entangled state. By combining pairs of different fidelities, one can probabilistically produce pairs of higher fidelities [129], via entangling gates and parity measurements. Thus two pairs will either produce a single pair of a higher fidelity, or both be destroyed. This is the first difference with the dynamics involved in cluster state growth, where the quality of particular elements can increase or decrease. Note here that now the pairs are shared between two physically distant parties.

As before, we will assume a continuous population, an on demand supply of pairs of a minimal fidelity (f_0) and a maximum fidelity (f_c) above which elements are taken out of the production line. This again enables us to simulate a closed system and look for steady state dynamics. The aim being to produce as many pairs above that threshold, per time step. These pairs could then be of a high enough fidelity so as to be used in teleportation or entanglement swapping. First let us look at a particular example and then give guidelines on how to generalize this to more complicated cases. Consider that we have a supply of entangled states of rank two (similar to the hybrid states discussed in the previous chapter), reducible through random bilateral rotations to a state of the form

$$\rho = f|\psi\rangle\langle\psi| + (1-f)|\phi\rangle\langle\phi|, \tag{4.44}$$

with $|\psi\rangle = (|01\rangle + |10\rangle)/\sqrt{2}$ and $|\phi\rangle = (|00\rangle + |11\rangle)/\sqrt{2}$. Assuming our target state is $|\psi\rangle$ and we have two pairs, each with fidelity f_1 and f_2, our initial combined state in the basis $\{|\psi\rangle_1|\psi\rangle_2, |\psi\rangle_1|\phi\rangle_2, |\phi\rangle_1|\psi\rangle_2, |\phi\rangle_1|\phi\rangle_2\}$ is given by

$$\rho_1 \otimes \rho_2 = \begin{pmatrix} f_1 f_2 & f_1(1-f_2) \\ (1-f_1)f_2 & (1-f_1)(1-f_2). \end{pmatrix} \tag{4.45}$$

With the qubits in pair 1 being the targets, a bilateral CNOT operation will lead to the state

$$\rho_1 \otimes \rho_2 \rightarrow \begin{pmatrix} f_1(1-f_2) & f_1 f_2 \\ (1-f_1)f_2 & (1-f_1)(1-f_2). \end{pmatrix} \tag{4.46}$$

Selecting even parity measurement outcomes on pair 2, we obtain the output state of pair 1

$$\rho_{out} = F(f_1, f_2)|\psi\rangle\langle\psi| + (1 - F(f_1, f_2))|\phi\rangle\langle\phi|, \tag{4.47}$$

with

$$F_{1,2} \equiv F(f_1, f_2) = \frac{f_1 f_2}{f_1 f_2 + (1-f_1)(1-f_2)}, \tag{4.48}$$

the denominator being the probability of the successful purification (we will interchangeably use f_i and i)

$$p_{1,2} = f_1 f_2 + (1 - f_1)(1 - f_2). \tag{4.49}$$

This leads to two differences with the cluster state generation process. Firstly, now the quality of the successful output of the fusion of two elements isn't simply the sum of their respective qualities (lengths), it is a more elaborate function of them (the input fidelities). One could envisage generalizing to different classes of functions describing the fusion process at hand. Maybe this could also be applied to other complex systems involving the fusion of elements in a population, observed in some biological systems for example. The second difference is that there isn't a fixed success probability throughout the system, it now depends on the qualities themselves; the larger the initial fidelities, the larger the success probability. So in a way there is an acceleration of the process as the fidelities increase (again there may be other systems with different quality dependent probabilities).

Concerning the ordering or numbering of the bins, there may be a few subtleties, but these are only relevant to the algorithmic implementation. The issue is that given an on demand supply of pairs with fidelity f_0, the number of accessible fidelities one can produce, bellow some threshold f_c grows very quickly. Ignoring the threshold for the time being and defining a round as a recombination of every element generated so far, including with itself, the number of accessible fidelities grows as 2,4,12,108 and 10476 from rounds 1 to 5. Here we will just give an outline of how one could proceed in building the accessible population.

Starting from f_0, at each round we combine all elements of the previous set together (including with themselves), generating a new set, to which we add the previous set. Then we remove all elements exceeding f_c and proceed to the next round. Repeat this until all the new combinations yield fidelities above f_c. This will give us the set of all accessible fidelities. The next step is to order or number the bins in a particular way, so as to make the transition rule easy to program, in an iterative way. This brings us to the transition rules for this purification process

$$Q_{i,j} \to \begin{cases} \frac{1}{2} p_{i,j} \left\{ Q^{(s)}_{F_{i,j},F_{i,j}} + Q^{(s)}_{0,0} \right\} & \text{if } F_{i,j} \leq f_c; \\ \\ p_{i,j} Q^{(s)}_{0,0} & \text{if } F_{i,j} > f_c, \end{cases} \tag{4.50}$$

In case of failure we have the simple replacement rule

$$Q_{i,j} \to (1 - p_{i,j}) Q^{(f)}_{0,0}. \tag{4.51}$$

Then again we superpose these two transitions $\mathbf{Q} \to \mathbf{Q}^{(s)} + \mathbf{Q}^{(f)}$ and solve for the steady-state, normalizing over the number of pairs. One issue now lies in the definition or the quantification the output. The qubit content of the output was rather obvious in the cluster state case, but here we might want to give a different type of weighting on possible fidelities produced, this may depend on the actual protocol or architecture at hand. For simplicity here we will just weigh them proportionally to the produced fidelity itself

$$\text{Out}[\mathbf{Q}] = \sum_{j=1}^{N} \sum_{i=1}^{j} p_{i,j} F_{i,j} Q_{i,j} \quad \text{with} \quad F_{i,j} > f_c. \tag{4.52}$$

To illustrate these ideas let us consider an example which doesn't involve too many accessible fidelities. Suppose we set $f_0 = 0.7$, $f_c = 0.98$ and use the purification function in (4.48). Then we have access to 4 different fidelities bellow the threshold: one is f_0, the second is $F_{0,0} = f_1$, the third is $F_{0,1} = f_2$ and the last is $F_{0,2} = F_{1,1} = f_3$, in increasing fidelities. Notice here that we have overlap between different 'paths' of purification, these features will depend entirely on the purification function. All other combinations (six of them) will produces pairs exceeding the threshold. Thus the output becomes:

$$\begin{aligned} \text{Out}[\mathbf{Q}] &= p_{0,3} F_{0,3} Q_{0,3} + p_{1,2} F_{1,2} Q_{1,2} \\ &+ p_{1,3} F_{1,3} Q_{1,3} + p_{2,2} F_{2,2} Q_{2,2} \\ &+ p_{2,3} F_{2,3} Q_{2,3} + p_{3,3} F_{3,3} Q_{3,3}. \end{aligned} \tag{4.53}$$

Maximizing this output, with the steady-state condition yields the optimal strategy which doesn't rely on the use of elements of fidelity f_3 and has the pairings $Q_{0,0}$=0.316456, $Q_{0,1}$=0.112059, $Q_{1,2}$=0.0714857 with a net output per cycle of 0.055986. This is a rather trivial example but it nevertheless provides us with a strategy which can't easily be arrived at intuitively. We believe the real challenge in this particular application is to be able to find an algorithm for generalizing to arbitrary purification functions and accessible fidelities.

The flow approximation used in these results is very useful in queuing theory and may very well be applicable to large scale cluster state production and purification schemes. However the effects of discreteness remain

to be investigated and an interesting result would be to find a threshold qubit content N bellow which this approach collapses. Having covered the large scale production regime, we now return to the discrete case of single chain growth with one entangling operation per time step and reveal another powerful approach.

4.2.3 Production rates and absorbing Markov chains

In this subsection we focus on single chain growth, with one entangling operation per time step. This apparently simple framework will lead to a whole range of possible strategies, involving at each time step an actual distribution of chains of various lengths. To do this we use Markov chains (and from now on we will use the words linear cluster, or simply cluster, instead of using the word chain when referring the quantum systems, so as to avoid confusion). A Markov chain is a stochastic process involving a set of random variables $\{X_t\}_{t=0}^{\infty}$ obeying the Markov property [166, 167]

$$P(X_{t+1} = s_j | X_t = s_{i_t}, X_{t-1} = s_{i_{t-1}}, .., X_0 = s_{i_0}) = P(X_{t+1} = s_j | X_t = s_{i_t}), \tag{4.54}$$

where the possible values of X_t form a countable set $S = \{s_1, s_2, .., s_n\}$ called the state space of the chain. In words, the Markov property states that the process is memoryless, meaning the state of the chain at the next time period only depends on its present state and not its past history. The value $P_{ij}(t) = P(X_t = s_j | X_{t-1} = s_i)$ is the probability of being in state s_j at time t given that the chain was in state s_i at time $t-1$. It is refered to as the transition probability of moving from s_i to s_j at time t. Collecting all these transition probabilities leads to the stochastic matrix $\mathbf{P}(t) = [P_{ij}(t)]$.

When the transition probabilities are constant in time ($P_{ij}(t) = P_{ij}$), the chain is said to be homogeneous and is fully described by the constant stochastic matrix $\mathbf{P} = [P_{ij}]$, called the transition matrix. The state of the chain on the other hand is characterized by a probability distribution vector $\mathbf{p}^T = (p_1, p_2, .., p_n)$ with $\sum_i p_i = 1$. Now if the initial state of the chain is $\mathbf{p}(0)$, then it will evolve to $\mathbf{p}(k) = \mathbf{P}^k \mathbf{p}(0)$ after k time steps. For this reason the (i, j)-entry in $\mathbf{P}^k$ represents the probability of moving from s_i to s_j in exactly k steps (this results from the Markov property).

A Markov chain can also be represented by a directed graph, in which each node corresponds to a particular state and each edge to a possible transition, with an associated probability. If all states are connected, i.e. if there is a path connecting all nodes to one another, then the chain is said to be irreducible.

Now the application of this Markov chain formalism to linear cluster growth is straightforward. In our case, the state space represents the length of the cluster we are focusing our attention on. As we try to fuse it with chains of different lengths, it can increase or decrease in length, in discrete time steps. Now in order to incorporate a target or threshold length in our framework, we require *absorbing* states, states such that once they are entered, they are never left. Thus if s_l is an absorbing state, then $P_{ll} = 1$ (the (ll)-entry of the transition matrix $\mathbf{P}$). This in turn means that a chain containing absorbing states is reducible, not irreducible.

The transition matrix $\mathbf{P}$ of a reducible Markov chain can be made to assume the canonical form [167]

$$\mathbf{P} = \begin{pmatrix} \mathbf{T}_{11} & \mathbf{T}_{12} \\ \mathbf{0} & \mathbf{T}_{22} \end{pmatrix}, \tag{4.55}$$

where $\mathbf{0}$ represents a matrix with entries 0 only. In the case of an absorbing Markov chain, $\mathbf{T}_{22}$ becomes the identity matrix $\mathbf{I}$ and the canonical form of $\mathbf{P}$ reads

$$\mathbf{P} = \left(\begin{array}{ccc|ccc} P_{1,1} & \cdots & P_{1,m} & P_{1,m+1} & \cdots & P_{1,m+n} \\ \vdots & & \vdots & \vdots & & \vdots \\ P_{m,1} & \cdots & P_{m,m} & P_{m,m+1} & \cdots & P_{m,m+n} \\ \hline 0 & \cdots & 0 & 1 & \cdots & 0 \\ \vdots & & \vdots & \vdots & \ddots & \vdots \\ 0 & \cdots & 0 & 0 & \cdots & 1 \end{array}\right), \tag{4.56}$$

where we have m transient states and n absorbing states. From this transition matrix we will be able to calculate all that we need for our study. First we can obtain the average number of times the chain passes through the state s_j given that it started off in state s_i [167]

$$E_i[j] = [(\mathbf{I} - \mathbf{T}_{11})^{-1}]_{ij}. \tag{4.57}$$

The matrix $(\mathbf{I} - \mathbf{T}_{11})^{-1}$ is often referred to as the fundamental matrix of a Markov chain. Summing the above expectation value over all transient states we obtain the expected time to absorption, having started in state s_i

$$t_i = [(\mathbf{I} - \mathbf{T}_{11})^{-1}\mathbf{e}]_i. \tag{4.58}$$

Finally, the probability of absorption into state s_{m+j}, having started in state s_i is given by

$$p_i[m+j] = [(\mathbf{I} - \mathbf{T}_{11})^{-1}\mathbf{T}_{12}]_{ij}. \tag{4.59}$$

Now we have all the tools in hand to start looking at the growth of linear clusters. Throughout this study we assume an on demand supply of single qubits, and the aim is to generate a cluster exceeding a given length L as fast as possible. This means $\mathbf{T}_{11}$ is now an $L \times L$ matrix and we will always initiate the chain in state s_1, that of a linear cluster of length one (a single qubit). The performance of a strategy is evaluated as the rate of production of clusters exceeding length L given in terms of their qubit content. This rate is then normalized, such that we obtain the average qubit output per entangling operation. This will be stated mathematically after some examples. We note here that we will use the same type of entangling gate as in the previous section, working with probability p.

To begin with, let us consider the growth of our main cluster, through single qubit adding. We will call the repeated addition of a standard cluster length as pumping. So in this first case, we are considering the strategy of single qubit pumping, which we mentioned in the previous section. However here we are not making any approximation on the main cluster length. The transition matrix for the corresponding chain is a tridiagonal matrix

$$\mathbf{P} = \left(\begin{array}{ccccccc|c} 1-p & p & & & & & & \\ 1-p & 0 & p & & & & & \\ & 1-p & 0 & p & & & & \\ & & \ddots & \ddots & \ddots & & & \\ & & & 1-p & 0 & p & & \\ & & & & 1-p & 0 & p & \\ \hline & & & & & & & 1 \end{array}\right), \tag{4.60}$$

For this simple strategy we can easily calculate the time to absorption which we will denote by $t[1, L]$. As there is a single absorbing state, the rate of production is $1/t[1, L]$ and the average qubit output per entangling operation is $L/t[1, L]$. This quantity corresponds to the performance $\mathrm{Perf}(S[1], L)$ of the single qubit pumping strategy $S[1]$. The next obvious strategy to consider is two-qubit pumping $S[2]$, in which the transition matrix for the main cluster growth process now becomes

$$\mathbf{P} = \left(\begin{array}{cccccc|cc} 1-p & 0 & p & & & & & \\ 1-p & 0 & 0 & p & & & & \\ & 1-p & 0 & 0 & p & & & \\ & & \ddots & \ddots & \ddots & \ddots & & \\ & & & 1-p & 0 & 0 & p & \\ & & & & 1-p & 0 & 0 & p \\ \hline & & & & & & 1 & \\ & & & & & & & 1 \end{array}\right), \tag{4.61}$$

and the underlying preparation of the pump corresponds to the transition matrix $\left(\begin{array}{c|c} 1-p & p \\ \hline 0 & 1 \end{array}\right)$. So we are in effect following two Markov chains, where the length of the time step for the main chain is modulated by the time to absorption of the underlying chain. The graph representation of both strategies is illustrated in Fig. 4.10. Now for the pump preparation we have $t[1,2] = 1/p$ and we observe two absorbing states for the main chain: s_{L+1} and s_{L+2} each occurring with probability c_1 and c_2 ($c_1 + c_2 = 1$). These probabilities can be computed via expression (4.59). Collecting all these parameters we can now give the performance of this two-qubit pumping strategy $S[2]$ as

$$\mathrm{Perf}(S[2], L) = \frac{c_1 L + c_2(L+1)}{t[2,L](t[1,2]+1)}. \tag{4.62}$$

The performance of the single and the two-qubit pumping strategies are plotted in Fig. 4.11. We can see that over the whole range of p, two-qubit pumping is advantageous. This holds for different values of L. One fact to stress here is that we are no longer running parallel entangling operations, as was the case in the divide and conquer strategies. All we are doing is applying entangling operations sequentially, on different linear clusters. An approximation to the performance can be analytically calculated through the expected growth speed of the main cluster, when its length is large enough. This is in fact the approximation made in qubus cluster state generation section. In the case of single qubit pumping, this growth speed is simply $p(+1) + (1-p)(-1) = 2p - 1$. For two-qubit pumping, the main chain growth speed is $3p - 1$, with the time $1/p$ to prepare the pump, yielding a total growth speed $(3p-1)/(1/p+1)$.

As we can see in the plots of Fig. 4.11, the approximations only start to become useful for large L. But in general it seems like they can be taken as lower bounds on the actual performance of the strategy.

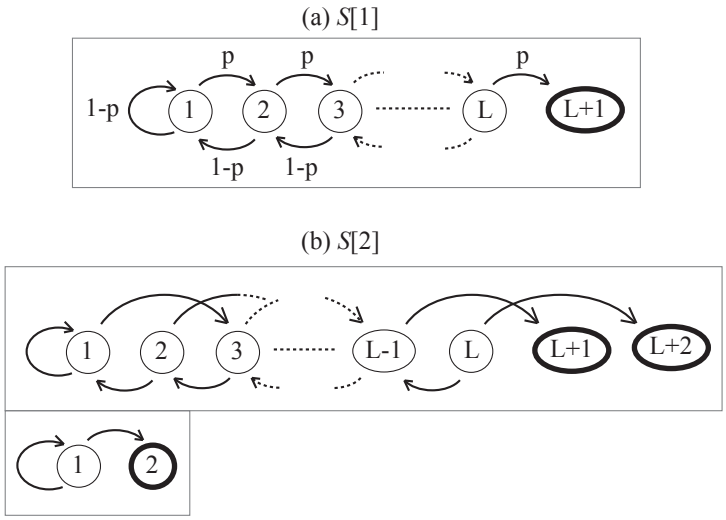

Figure 4.10: Schematic representations of the single and two-qubit pumping strategies $S[1]$ and $S[2]$. Absorbing states are represented by thick borders. In (b) is also shown the underlying pump preparation process for $S[2]$.

Following the method for two-qubit pumping, we can now consider a whole family of strategies in which a pump of a certain size r is prepared through single qubit adding: $S[r]$. The performance of these strategies is given by

$$\mathrm{Perf}(S[r], L) = \frac{\sum_{i=1}^{r} c_i(L+i-1)}{t[r,L](t[1,r]+1)}, \tag{4.63}$$

where the c_i correspond to the absorption probability for the state corresponding to $L+i$. The -1 added to lengths in the summation accounts for the fact that the cluster starts with $L=1$. This guarantees that the the performance tends to 1 as p tends to 1.

These performances are plotted for $r = 1, 2, 3$ and 4 in Fig. 4.12. We can see that two-qubit pumping is more efficient for a wide range of p, but increasing the pump size allows for an improvement in production rate for small p.

Now that we are using larger pumps, we no longer need to produce the pumps through single qubit adding, whose performance rapidly becomes negligible for $p < 1/2$. The three-qubit pump cannot be produced more efficiently, as decomposing the corresponding Markov chain into two processes

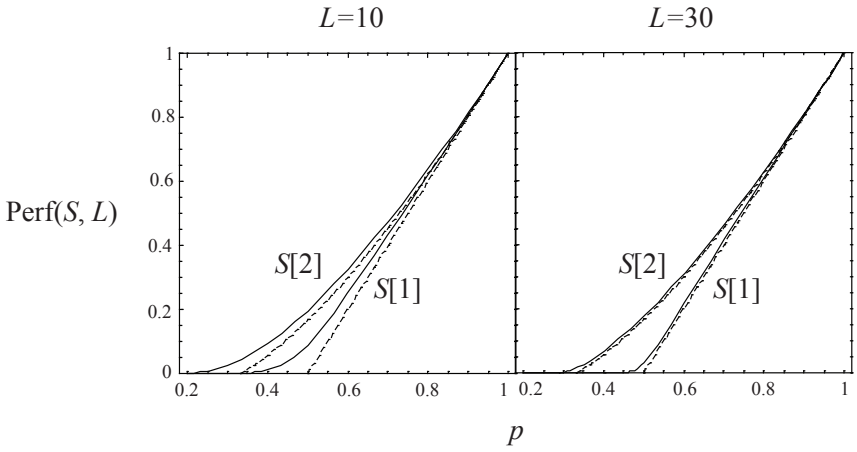

Figure 4.11: Plots of the performances of single and two-qubit pumping strategies $S[1]$ and $S[2]$ (solid) along with their analytical approximations (dashed). Both for $L = 10$ and $L = 30$ we observe a higher performance of $S[2]$ over all p. Though quite good in the case of $L = 30$, the analytical approximations are are very rough in the case of $L = 10$.

does not increase the efficiency. This means that $S[4]$ is the first pump size which we can layer, that is we can produce the pump with another pump larger than one qubit. In this case, the process layering proceeds as follows. First we produce pairs. With these pairs we produce the pump. And with this pump we increase the size of the main cluster.

Calculating the performance for this strategy is slightly more involved. The whole system now contains three different processes. The first is pair generation, with as before the transition matrix $\mathbf{M}_1 = \left(\begin{array}{c|c} 1-p & p \\ \hline 0 & 1 \end{array}\right)$. Next the growth of the four qubit pump, from pairs, has the following transition matrix

$$\mathbf{M}_2 = \left(\begin{array}{ccc|cc} 1-p & 0 & p & & \\ 1-p & 0 & 0 & p & \\ 0 & 1-p & 0 & & p \\ \hline & & & 1 & \\ & & & & 1 \end{array}\right), \tag{4.64}$$

and finally the growth of the main cluster from the above produced pump is characterized by

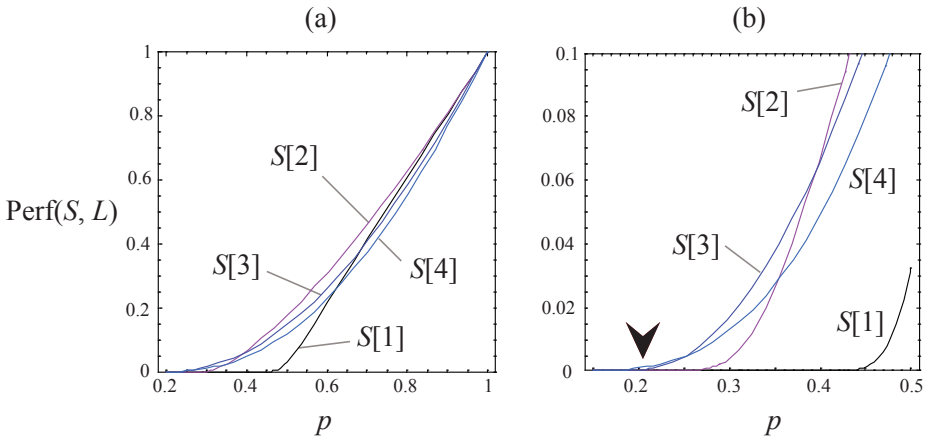

Figure 4.12: Plots of the performances of the one, two, three and four-qubit pumping strategies $S[1], S[2], S[3]$ and $S[4]$, with $L = 30$. For high p the strategies converge as shown in (a). On the whole two-qubit pumping seems optimal for this type of strategy, however we observe an improvement in using a larger pump for small p. This can be seen in plot (b), where $S[2]$ is overtaken by $S[3]$ which itself is overtaken by $S[4]$, as indicated by the arrow.

$$\mathbf{M}_3 = \left(\begin{array}{ccccccccc} 1-p & 0^3 & c_1p & c_2p & & & & & \\ 1-p & 0 & 0^3 & c_1p & c_2p & & & & \\ & \ddots & \ddots & \ddots & \ddots & \ddots & & & \\ & & 1-p & 0 & 0^3 & c_1p & c_2p & & \\ & & & \ddots & \ddots & \ddots & \ddots & \ddots & \\ & & & & 1-p & 0 & 0^3 & c_1p & c_2p \\ \hline & & & & & & \multicolumn{3}{c}{\mathbf{I}_{5\times 5}} \end{array}\right), \quad (4.65)$$

where 0^3 stands for three 0 entries. A graphic representation of this layered strategy, which we will denote by $S_3[4]$ is illustrated in Fig. 4.13. The comparative performance with the simpler $S[4]$ strategy is shown in Fig. 4.14(a). As expected, preparing the four-qubit pump with pairs accelerates the production rate.

As we can see from this example, the production (lengths and associated probabilities) of each process has to be taken into the transition matrix for the next process. Now for convenience we redefine the absorption time t as

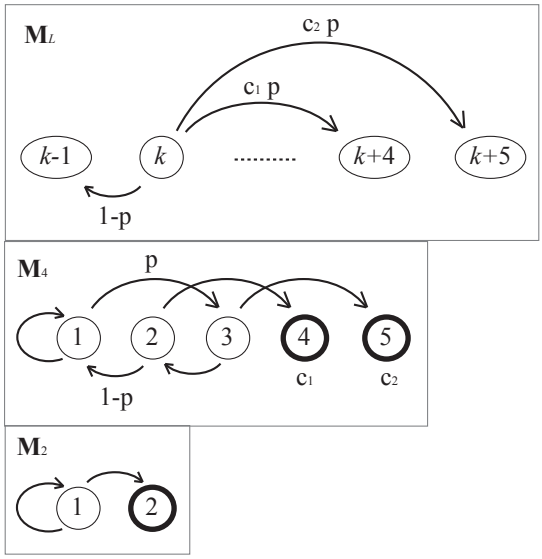

Figure 4.13: Graphic representation of the four-qubit pumping layered strategy. Each Markov chain corresponds to a different process and a different transition matrix. The main cluster growth is characterized by $\mathbf{M}_3$. Here we have illustrated the possible transitions of a typical transient state (length) $1 < k \leq L$.

a function of a given transition matrix $t[\mathbf{M}]$, so as to be able to express the performance of a strategy involving n separate processes as

$$\mathrm{Perf}(S_n) = \frac{\sum_{i=1}^{r} c_i(L+i-1)}{t[\mathbf{M}_n](t[\mathbf{M}_{n-1}](t[\mathbf{M}_{n-2}](...)+1)+1)}, \tag{4.66}$$

here each transition matrix $\mathbf{M}_j$ depends on $\mathbf{M}_{j-1}$. Obviously there are many directions to take, based on this result, however we have so far only obtained results for the four-qubit pumping strategy, which are positive. Within this framework, a systematic optimization will clearly have to begin by fixing the probability p and the maximum length L, before searching through different layerings.

One essential type of strategy which remains to be formulated in this Markov chain setting is insistent strategies, where all the entanglement generated in different processes is used up entirely. That is we repeatedly attempt to fuse the main cluster and the pump until one or the other sees all its entanglement consumed. Such a type of strategy was mentioned earlier

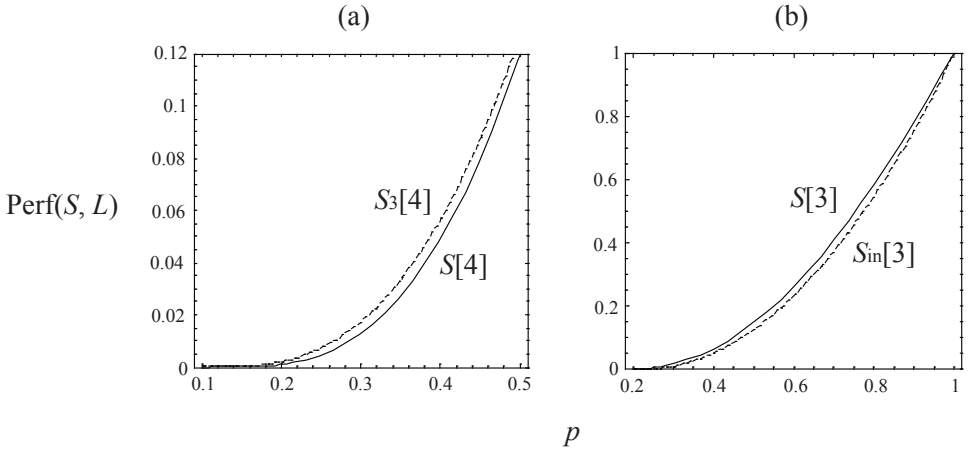

Figure 4.14: (a) Comparative performance of $S[4]$ and $S_3[4]$ as defined in the text. We observe a clear improvement in layering more processes. (b) The lower bound of the performance of the insistent three-qubit pumping strategy $S_{\text{in}}[3]$ and the expected performance of the non-insistent strategy $S[3]$.

on in the chapter at which point we followed previous work and made a significant approximation. Here we come back to this calculation, where we repeatedly attempt to join two linear clusters of lengths l_1 and l_2, as in [159]. The expected final length is given by

$$l_f = l_1 + l_2 - \langle T \rangle. \tag{4.67}$$

$\langle T \rangle$ represents the average number of qubits consumed in the process and writing $l_{\min} = \min(l_1, l_2)$ we have

$$\begin{aligned} \langle T \rangle &= 2p \sum_{n=0}^{l_{\min}-2} n(1-p)^n + (1-p)^{l_{\min}-1}(2l_{\min}-1) \\ &= \frac{2(1-p)}{p} - (1-p)^{l_{\min}-1}\left(1 + \frac{2(1-p)}{p}\right). \end{aligned} \tag{4.68}$$

Thus we can see how the limiting value for this quantity, with p fixed, tends to $2(1-p)/2$ as $l_{\min}$ tends to infinity. Individual terms in this summation give us the transition probabilities for a particular cluster being grown through insistent fusion. However different transitions take different amounts of time.

Thus in fact we are no longer in a homogeneous Markov chain setting. We propose to average out this time difference by using the average transition time or the average number of fusion attempts

$$\begin{aligned}\langle N\rangle &= p\sum_{n=0}^{l_{\min}-2}(n+1)(1-p)^n + (1-p)^{l_{\min}-1}(l_{\min}-1)\\ &= \frac{1}{p} - \frac{(1-p)^{l_{\min}-1}}{p},\end{aligned} \tag{4.69}$$

and then using this average as a fixed time step value. Let us look at the case of three-qubit pumping for example. The insistent strategy will allow for two attempts at fusing the main cluster with the pump, because in a case of an initial failure, there remains entanglement in the pump. Thus if we consider a transient state $3 \leq k \leq L$, then $\langle N\rangle = p(1) + (1-p)(2) = 2-p$. This value, alongside the pump preparation time, will modulate the time to absorption for the main Markov chain with possible transitions $P_{k,k+3} = p$, $P_{k,k+1} = p(1-p)$ and $P_{k,k-2} = (1-p)^2$. So as not to waste resources, the transient state $k = 1$ can only progress along the chain and the state $k = 2$ cannot decrease. However the transition times for both of these states are $N = 1$, so in some sense we can view the above averaging as giving us a lower bound on the performance of the insistent strategy $S_{\text{in}}[3]$. As shown in plot (b) of Fig. 4.14, the resulting performance is lower than for the non-insistent strategy for all p.

This result is not very satisfying and points to the weakness of the approximation. In order to really analyze this type of strategy, one would need to introduce controlled Markov chains, in which an overarching chain represents a decision process (the control space). To each state of this chain is associated a transition matrix, which is applied to the system we are actually looking at. Such an approach would also enable us to investigate context-dependent strategies [163], where the chosen fusion attempt depends on the distribution of chain lengths at each time step. It is worth noting here however that in some instances, these strategies become fixed strategies. An example is the greedy strategy as defined by Rohde and Barrett [163], which attempts to fuse the two largest chains at each time step. Due to the fact that they start off with a pool of single qubits, this strategy is nothing but single qubit pumping, for which we obtained the exact performance without resorting to computer simulation. In any case, these decision based strategies are far more difficult and interesting to investigate, and will constitute the theme of further research.

We began this chapter by applying the qubus scheme to the generation of cluster states of matter qubits and found significant improvements over previous proposals. In the process we noticed the importance of strategies for the probabilistic growth of cluster states in general. We approached this issue in the second section from two different perspectives and observed interesting results. In particular Markov chains, and potentially controlled Markov chains seem to be a promising framework for the representation of growth strategies. We managed to reproduce previous results obtained through computer simulations and were able to give a general exact formula for arbitrarily complicated fixed strategies, without recycling. For a large range of success probabilities, two-qubit pumping seems to be optimal. The introduction of recycling led us to understand the limits of fixed strategies. The next level of analysis will require controlled Markov chains, which are known to provide optimal strategies for the control of stochastic processes.

Throughout the chapter we have assumed the possibility of fusing any two clusters being part of our pool at a given time. This can be done in one of two ways. Either he physical clusters can be stationary and the distribution of entanglement mobile, or the clusters can be transported to different locations. The latter may not seem this relevant at the cluster generation stage, but as will most certainly be the case, the preparation and measurement of the cluster during computation will be done in different locations. In that sense the ability to move whole clusters (or their correlations) to other locations is crucial. This constitutes one of the applications of the composite system transfer protocols devised in the next chapter.

Chapter 5

A qudit bus for data transmission and quantum information processing

Many of the proposed quantum computer architectures include spatially distinct regions that perform the roles of memory and interaction [168–172]. Such a distributed approach presents several advantages which we pointed at earlier on, including decoherence suppression in well-isolated memories and extendibility of the system. There is potential for simplifying and concentrating the level of control needed, and mitigating the effects of cross-talk, by restricting the number of control elements in the processing regions. Also a level of defect-tolerance can be incorporated by routing around defective regions.

In this context an efficient transfer of information from the memory areas to the processing areas is crucial [57]. To achieve this information transfer, current proposals include the use of mobile qubits [170–173] and flying qubits with an interconversion to stationary qubits [79, 174, 175]. Other possible frameworks for data transfer are spin chains [176–178] and qubus schemes [108, 119]. Teleportation can also be used in quantum computer architectures [68, 179] to provide effective communication and computation channels. Also, as mentioned at the end of the previous chapter, the efficient transfer of cluster states from preparation locations to measurement locations will be crucial for a fast one-way quantum computer.

Given an interface between stationary and flying systems, one natural question is: how could higher dimensional buses be used in such data transfer schemes? This constitutes the central theme of this chapter. For example

we might want to transmit a pair of qubits with a single use of a quantum channel. In general, the efficient use of qudits can optimize the Hilbert space of the system's degrees of freedom [180]. Most of the qubit realizations proposed and used are actually embedded in a qudit structure already with the non-computational states seen as sources of potential error to be quantified and mitigated [181].

The study of qudits in information processing and communication has generated many results [182–185], defining generalized gates, teleportation protocols and finding feasible physical implementations [186]. Additionally, the transient occupation of higher dimensional states can greatly reduce the complexity of certain gates, for example Ralph *et al.* have shown that the efficiency of synthesising the Toffoli gate can be improved by using a qutrit subspace [187]. Yet the issue of data transfer between arbitrary dimensional systems through a single higher dimensional qudit bus has not been considered. Such a qudit bus would constitute a generic resource, enabling the distribution of entanglement and data over different groups of systems in a flexible fashion. This will result in a physical compression of the information, reducing the number of controlled physical systems and the number of quantum channels required across the processor.

In this chapter we show protocols for high dimensional quantum transfer employing a passive mediating bus. By keeping this mediator passive (fixing it as the target to all qudit gates and avoiding local operation on it), we simplify the interactions and reduce the level of control needed. The information held by an arbitrary composite system can either be transfered or teleported via the bus to a recipient system in another location, through entangling operations, measurements and feed-forward. We focus initially on a composite system made up of two subsystems of equal dimension and then generalize to arbitrary numbers of subsystems. To illustrate our scheme we describe in detail the cases of two-qubit and two-qutrit composite systems, where a qutrit represents a three level system. As the composite system is being transmitted, non-trivial operations may also be applied. At the end of the chapter we will see how the qubus scheme provides a potential physical realization.

5.1 Protocols

Our protocols enable quantum communication between two parties, Alice and Bob, via a passive bus. We assume initially that Alice has two subsystems (qudits) of equal dimension that she wishes to send to Bob, who

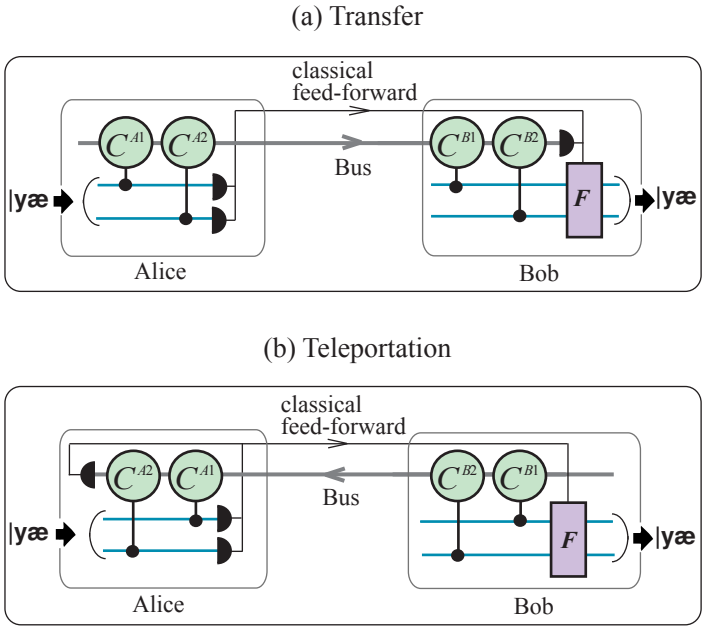

Figure 5.1: Schematic representation of the two variants of the protocol. In a) Alice first couples her input state $|\psi\rangle$ with the passive bus via conditional unitary operations and measures out her two subsystems in a conjugate basis. She sends the bus and the measurement results to Bob. On his side, Bob has prepared the recipient state of two subsystems and on receiving the bus, couples his subsystems to the bus via conditional unitary operations. After measuring the bus, Bob performs feed-forward (denoted by a unitary operation F) on his state to reconstruct Alice's input. In b) Bob first couples his recipient state to the bus and sends it to Alice. Upon receiving the bus she couples her input state with it and then proceeds with the measurements as in the transfer protocol. All the results are then communicated to Bob who performs the adapted feed forward, effecting qudit teleportation.

also has two qudits of the same dimension as Alice (see Fig. 5.1). Initially Alice holds two d-dimensional systems $A1$ and $A2$ in an arbitrary state $|\psi\rangle_A = \sum_{i,j=0}^{d-1} x_{ij}|i\rangle_{A1}|j\rangle_{A2}$. Initiating the transfer protocol, Alice couples her composite system to the d^2-dimensional bus via conditional unitary operations. These can be written as

$$C^{Aj} = \sum_{i=0}^{d-1} |i\rangle\langle i| \otimes U_i^{Aj}, \tag{5.1}$$

where the projectors $|i\rangle\langle i|$ act on subsystem Aj (here $j = 1, 2$) and the unitary operations U_i act on the bus state. An appropriate set of operations for each subsystem will produce a one-to-one mapping between the basis states of the composite system and the basis states of the bus (always to the right, with basis states $|\varphi_{ij}\rangle$), guaranteeing a complete mapping of the x_{ij} coefficients. The resulting combined state we write as

$$\begin{aligned} |\xi\rangle &= \sum_{i,j=0}^{d-1} x_{ij}|i\rangle_{A1}|j\rangle_{A2}|\varphi_{ij}\rangle, \\ &\text{with} \quad \langle\varphi_{i'j'}|\varphi_{ij}\rangle = \delta_{ii'}\delta_{jj'}, \end{aligned} \tag{5.2}$$

at which point the bus is then sent to Bob through a quantum channel.

Before receiving the bus, Bob prepares his two d-dimensional recipient qudits in the equally weighted superposition $|\psi'\rangle_B = \frac{1}{d}\sum_{k,l=0}^{d-1}|k\rangle_{B1}|l\rangle_{B2}$. Then he couples each one of them to the encoded bus via interactions of the form of Eq. (5.1), leading to a combined state

$$C|\psi'\rangle|\xi\rangle = \frac{1}{d}\sum_{i,j,k,l=0}^{d-1} x_{ij}(|k\rangle|l\rangle)_B(|i\rangle|j\rangle)_A U_l^{B2}U_k^{B1}|\varphi_{ij}\rangle, \tag{5.3}$$

with $C = C^{B2}C^{B1}$. To transfer the input state, Alice measures her subsystems in a conjugate basis (one can be obtained through a Fourier transform of the computational basis). This can be done at any time after sending the bus, removing $|i\rangle|j\rangle$ from the above expression up to known phases. The results will be sent as classical information used in the final feed-forward applied by Bob.

To complete the transfer, Bob measures the mediator and *for all measurement results* retrieves Alice's state up to a known correction (unitary two-qudit operation, denoted by F in Fig. 5.1). Complete quantum information transfer places requirements on the unitary operations, $\left\{U_k^{B1}, k = 0, 1, .., d-1\right\}$

and $\left\{U_l^{B2}, l = 0, 1, .., d-1\right\}$ that must be fulfilled. These requirements can be expressed thus

$$\mathrm{Tr}\left[\left(U_l^{B2}U_k^{B1}\right)\left(U_{l'}^{B2}U_{k'}^{B1}\right)^\dagger\right] = d^2\delta_{kk'}\delta_{ll'}, \tag{5.4}$$

for all k, k', l and l'. The above expression states that any ordered combination made up of a single unitary operation from each set needs to result in an operation orthogonal to all other combinations, in terms of the Hilbert-Schmidt inner product, defined on operators $\hat{V}$ and $\hat{W}$ as $\mathrm{Tr}(\hat{V}\hat{W}^\dagger)$.

Reversing the order of the coupling to the mediator allows qudit quantum teleportation to be performed (Fig. 5.1(b)). In this case, Bob first entangles his subsystems (prepared in an equally weighted superposition, as before) with the mediating bus, and sends the mediator to Alice. Alice then entangles her state with the mediator. The entanglement and subsequent measurement enables the completion of a qudit teleportation protocol between Alice and Bob. Keeping the indices used above, the final state after these interaction is precisely that of Eq. (5.3), switching i and j for k and l. Thus a deterministic transfer of the quantum information held by Alice's composite system is obtained if the unitary operations contained in her interactions obey the relation in Eq. (5.4). In other words we have flexibility in the direction in which we want to use the quantum channel, leading to two different protocols, serving essentially the same purpose and requiring the same type of interactions.

Now we must identify the sets of unitary operations that satisfy Eq. (5.4), and for this we focus on a particular class of unitary operators namely permutation operators. They will provide us with an intuitive understanding of the problem and allow us to straightforwardly see the feasibility of the protocol. These operators we define as $P \equiv \sum_{s=0}^{m-1} |p(s)\rangle\langle s|$ where p is a permutation mapping an ordered set of elements to itself, written as $p(s) = s'$. A compact expression for describing permutations is provided by the cycle notation [188]

$$\begin{pmatrix} 1 & 2 & 3 & 4 & 5 \\ 2 & 3 & 1 & 5 & 4 \end{pmatrix} \equiv (123)(45), \tag{5.5}$$

where each pair of brackets contains a cycle which is read from left to right. The effect of p on an element can for example be written as $p(4) = 5$. The operator corresponding to Eq. (5.5) is then $P = |1\rangle\langle 3| + |2\rangle\langle 1| + |3\rangle\langle 2| + |4\rangle\langle 5| + |5\rangle\langle 4|$ and the associated permutation p entirely specifies the operator P.

Having chosen and defined the class of permutation operators, we proceed to writing down the two sets of operators $\left\{P_k^{B1}, k = 0, 1, .., d-1\right\}$ and $\left\{P_l^{B2}, l = 0, 1, .., d-1\right\}$, for each subsystem. In addition to the orthogonality requirements, by choosing one of the permutations in each set (P_0^{B1} and P_0^{B2}) to be the identity, the expression in Eq. (5.4) implies that all non-trivial combinations must correspond to *complete* permutations (derangements). This can be expressed as $P_l^{B2} P_k^{B1} |s\rangle \neq |s\rangle$ for all k and l except when $k = l = 0$. The simplest case occurs for d=2, which we explore in detail in the next section.

5.2 Transmitting two qubits

To illustrate our transfer protocol we consider the transmission of a two-qubit state. To effect transmission, Alice and Bob require a four dimensional bus. There is a total of $n!$ permutations on n elements, of which $!n = n! \sum_{k=0}^{n} (-1)^k / k!$ correspond to complete permutations [189]. In consequence, given the present dimensionality, we have $!4 = 9$ permutation operators to choose from. We define the bus basis states $\{|s\rangle, s = 0, .., 3\}$. The full interaction between Alice's two qubits and the bus we write as

$$\begin{aligned} C^{A2} C^{A1} = &\left(|0\rangle_{A2}\langle 0| \otimes I^{A2} + |1\rangle_{A2}\langle 1| \otimes P^{A2}\right) \\ &\times \left(|0\rangle_{A1}\langle 0| \otimes I^{A1} + |1\rangle_{A1}\langle 1| \otimes P^{A1}\right), \end{aligned} \tag{5.6}$$

where, the identity I and the permutation operators P^{A1} and P^{A2} act on the bus. We will arrange the possible operators into two groups, one consisting of pairwise swap operations and the other of cyclic permutations. They are represented schematically in Fig. 5.2. There are 3 distinct pairwise swap permutations which in the cycle notation we write as $q_1 = (01)(23)$ (corresponding to the permutation operator $Q_1 = |1\rangle\langle 0| + |0\rangle\langle 1| + |3\rangle\langle 2| + |2\rangle\langle 3|$), $q_2 = (02)(13)$ and $q_3 = q_1 q_2 = (03)(12)$. The 6 cyclic permutations are given by $r_1 = (0123)$, $r_2 = (0132)$, $r_3 = (0213)$ and their inverses. We begin with the first type of interaction in which both Alice and Bob make use of pairwise swap operators. Proceeding with the first part of the transfer protocol, Alice starts with her two qubits in an arbitrary state with the bus initiated in the $|0\rangle$ state, leading to a combined state

$$|\psi\rangle = \left(x_0|00\rangle + x_1|01\rangle + x_2|10\rangle + x_3|11\rangle\right)_A |0\rangle. \tag{5.7}$$

Setting $P^{A1} = Q_1$, $P^{A2} = Q_3$ she entangles her state with the bus,

$$C|\psi\rangle = x_0|00\rangle_A|0\rangle + x_1|01\rangle_A|3\rangle + x_2|10\rangle_A|1\rangle + x_3|11\rangle_A|2\rangle, \tag{5.8}$$

with $C = C^{A2}C^{A1}$. Then she measures out her qubits in the $|\pm\rangle$ basis and up to phase corrections depending on the measurement outcomes, Alice sends the disentangled bus to Bob, which is in state

$$|\xi\rangle = x_0|0\rangle + x_1|3\rangle + x_2|1\rangle + x_3|2\rangle. \tag{5.9}$$

The phase corrections are sent as classical information and kept until then end of protocol when Bob performs the feed-forward operation on his two-qubit state.

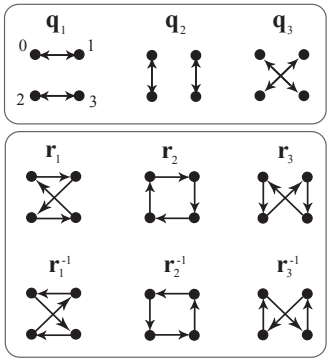

Alice		Bob		Type of mapping
$A1$	$A2$	$B1$	$B2$	
$\mathbf{q}_i$	$\mathbf{q}_j$	$\mathbf{q}_i$	$\mathbf{q}_j$	local
$\mathbf{q}_i$	$\mathbf{q}_j$	$\mathbf{q}_j$	$\mathbf{q}_i$	
$\mathbf{q}_i$	$\mathbf{q}_j$	$\mathbf{q}_i$	$\mathbf{q}_k$	entangling
$\mathbf{q}_i$	$\mathbf{q}_j$	$\mathbf{q}_k$	$\mathbf{q}_i$	
$\mathbf{r}_i$	$\mathbf{q}_{i+1}$	$\mathbf{r}_j$	$\mathbf{q}_{j+1}$	combined
$\mathbf{r}_i$	$\mathbf{q}_{i+1}$	$\mathbf{q}_{j+1}$	$\mathbf{r}_j$	

Figure 5.2: A schematic representation of the nine possible derangements on four elements represented here by dots. The table indicates whether the state that is mapped out by Bob before the feed forward is applied is locally equivalent to the initial two-qubit state Alice sent, or whether Bob must perform entangling operations on his two-qubit state to reconstruct the transmitted state. This depends on the derangement chosen for each subsystem 1 and 2, and the bus measurement outcomes. Within the two stages of the protocol, the choice of permutations must obey the orthogonality requirements. This explains why we specify the q_{i+1}, as it is the only one satisfying the requirements of Eq. (5.4), given that r_i was chosen. The table is not exhaustive but gives the main observations.

In the second part of the protocol, Bob prepares a pair of qubits $B1$ and $B2$ in $|+\rangle = (|0\rangle + |1\rangle)/\sqrt{2}$ states. Upon receiving the bus, he lets the two qubits interact consecutively with it, keeping the same interaction

$C = C^{B2}C^{B1}$,

$$\begin{aligned} C|+\rangle|+\rangle|\xi\rangle = \frac{1}{2}\{&|00\rangle_B(x_0|0\rangle + x_1|3\rangle + x_2|1\rangle + x_3|2\rangle) \\ &+|01\rangle_B(x_0|3\rangle + x_1|0\rangle + x_2|2\rangle + x_3|1\rangle) \\ &+|10\rangle_B(x_0|1\rangle + x_1|2\rangle + x_2|0\rangle + x_3|3\rangle) \\ &+|11\rangle_B(x_0|2\rangle + x_1|1\rangle + x_2|3\rangle + x_3|0\rangle)\}. \end{aligned} \tag{5.10}$$

To complete the protocol Bob measures the mediating bus in the computational basis. To view the results of different measurement outcomes the above combined state can be written in a matrix form which we term the *pre-measurement matrix*. The pre-measurement matrix contains the possible unitary operations the initial two-qubit state will undergo as it is transmitted in function of the measurement outcomes. Thus defining the projector $\lambda_n = |n\rangle\langle n|$, we rewrite Eq. (5.10) as

$$M_{\text{loc}}, = \begin{pmatrix} \lambda_0 & \lambda_3 & \lambda_1 & \lambda_2 \\ \lambda_3 & \lambda_0 & \lambda_2 & \lambda_1 \\ \lambda_1 & \lambda_2 & \lambda_0 & \lambda_3 \\ \lambda_2 & \lambda_1 & \lambda_3 & \lambda_0 \end{pmatrix}. \tag{5.11}$$

So for example if Bob measures the bus in the state $|3\rangle$ (corresponding to λ_3), he has reproduced Alice's initial two-qubit state up to the (known) unitary operation

$$M_{\text{loc},|3\rangle} = \begin{pmatrix} 0 & 1 & 0 & 0 \\ 1 & 0 & 0 & 0 \\ 0 & 0 & 0 & 1 \\ 0 & 0 & 1 & 0 \end{pmatrix}. \tag{5.12}$$

Measuring the mediating bus in any one of the states $|0\rangle$, $|1\rangle$, $|2\rangle$, or $|3\rangle$ yields the initial two-qubit state up to the unitary operations $I_{B1}I_{B2}$, $X_{B1}I_{B2}$, $X_{B1}X_{B2}$ and $I_{B1}X_{B2}$ applied to it respectively, where X is the qubit Pauli matrix $X = |1\rangle\langle 0| + |0\rangle\langle 1|$. This means the feed-forward operation F only consists of local unitary operations on the qubits and is therefore a *local mapping*.

In contrast, if Alice uses the two permutation operators $P^{A1} = Q_1, P^{A2} = Q_3$ and Bob uses $P^{B1} = Q_2, P^{B2} = Q_3$, he then obtains the pre-measurement matrix

$$M_{\text{ent}} = \begin{pmatrix} \lambda_0 & \lambda_3 & \lambda_1 & \lambda_2 \\ \lambda_3 & \lambda_0 & \lambda_2 & \lambda_1 \\ \lambda_2 & \lambda_1 & \lambda_3 & \lambda_0 \\ \lambda_1 & \lambda_2 & \lambda_0 & \lambda_3 \end{pmatrix}. \tag{5.13}$$

In this case all measurement outcomes require a non-local feed-forward operation F, so we call this an *entangling mapping*. The mapped out state is locally equivalent to Alice's input state with a CNOT gate applied to it, for all outcomes.

The second type of interaction makes use of cyclic permutations. We note here that Alice and Bob cannot choose their two permutation operators from the cyclic permutations alone, as they will not fulfill the requirements of Eq. (5.4). An example of a valid choice is to set $P^{A1} = P^{B1} = R_1$ and $P^{A2} = P^{B2} = Q_2 = R_1^2$, then we obtain the pre-measurement matrix

$$M_{\text{com}} = \begin{pmatrix} \lambda_0 & \lambda_2 & \lambda_1 & \lambda_3 \\ \lambda_2 & \lambda_0 & \lambda_3 & \lambda_1 \\ \lambda_1 & \lambda_3 & \lambda_2 & \lambda_0 \\ \lambda_3 & \lambda_1 & \lambda_0 & \lambda_2 \end{pmatrix}. \tag{5.14}$$

Here what we see is that the measurement outcomes $|1\rangle$ and $|3\rangle$ lead to a local mapping while the $|0\rangle$ and $|2\rangle$ measurement outcomes lead to an entangling mapping. For arbitrary states, each mapping occurs with equal probability in this case, we term this measurement dependent case a *combined mapping*. It is worth noting here that either way, the quantum information is left intact, meaning a repeat-until-success scheme [80] can be envisaged. If the aim of the protocol is to entangle the two transmitted qubits through a CNOT gate, and the permutation operators at hand are those used to generate the output in Eq. (5.14), then we can repeat the protocol (on average twice), until the desired entangled output state is obtained.

By searching through different combinations we see that local and entangling mappings can only be achieved if both Alice and Bob choose their permutations from the pairwise Q_1, Q_2 and Q_3 operators. Using the same permutations will yield a local mapping, whereas changing them will yield an entangling mapping. Another important point is that independent of Alice's choice of interaction, Bob using an element R_i will yield a combined mapping.

As the subsystem dimension increases, finding sets of permutation operators satisfying (5.4) and observing the feed-forward operations for different measurement outcomes rapidly becomes intractable. Also the entangling power of the resulting unitary operations applied to the transmitted state (before the feed-forward) can vary, unlike in the two-qubit case [190]. In spite of these difficulties, the general methods given in the next section allow us to systematically investigate higher dimensions.

5.3 Building interactions with permutations

We can generalize the previous discussion, keeping the concepts of local, entangling and combined mappings. To effect these mappings for arbitrary subsystem dimension d, we find two different types of interactions based on conditional permutation operators. The first type of interaction makes use of the commuting operators H and V whose corresponding permutations in the cycle notation are

$$\begin{aligned} h = \quad & (0,1,..,d-1) \\ & (d,d+1,..,2d-1) \\ & \vdots \\ & (d^2-d,d^2-d+1,..,d^2-1), \end{aligned}$$

$$\begin{aligned} v = \quad & (0,d,..,d^2-d) \\ & (1,d+1,..,d^2-d+1) \\ & \vdots \\ & (d-1,2d-1,..,d^2-1), \end{aligned} \tag{5.15}$$

acting on d^2 elements representing the bus basis states. As we can see h and v consist in cycles of length d where each element is included in only one cycle from each. We now identify them with q_1 and q_2 for $d = 2$ respectively. Extending the representation in Fig. 2 we see that if we arrange the elements into a $d \times d$ square lattice, h groups the elements composing the cycles in a horizontal way whereas v groups them in a vertical way. Arbitrary combinations $V^l H^k$ lead to orthogonal permutation operators satisfying Eq. (5.4) and thus we can arrange them into the two sets

$$\begin{aligned} &\{P_k^{B1} | P_k^{B1} = H^k, k = 0,..,d-1\}, \\ &\{P_l^{B2} | P_l^{B2} = V^l, l = 0,..,d-1\}. \end{aligned} \tag{5.16}$$

These operators based on permutations with d-cycles allow for a transmission of Alice's state without the need for nonlocal operations at the feed-forward stage. This can be seen by first rewriting the bus basis states $|s\rangle$ as $|\mathrm{MOD}_d(s), \lfloor s/d \rfloor\rangle$ so that the above operators act according to $V^l H^k |m,n\rangle = |\mathrm{MOD}_d(m+k), \mathrm{MOD}_d(n+l)\rangle$. By initiating the bus in the state $|0,0\rangle$, Alice and Bob can choose their sets so that the final state in Eq. (5.3) before the

bus measurement reads

$$\frac{1}{d}\sum_{i,j,k,l=0}^{d-1} x_{ij}\left(|k\rangle|l\rangle\right)_B\left(|i\rangle|j\rangle\right)_A V^{d-l}H^{d-k}V^jH^i|0,0\rangle$$
$$=\frac{1}{d}\sum_{i,j,k,l=0}^{d-1} x_{ij}\left(|k\rangle|l\rangle\right)_B\left(|i\rangle|j\rangle\right)_A$$
$$\otimes|\mathrm{MOD}_d(i-k),\mathrm{MOD}_d(j-l)\rangle. \tag{5.17}$$

Alice measuring her subsystems in the conjugate basis and Bob measuring the bus in the $|m,n\rangle$ state will result in Bobs composite system being in the state

$$\sum_{i,j=0}^{d-1} x_{ij}|\mathrm{MOD}_d(i-m)\rangle|\mathrm{MOD}_d(j-n)\rangle = X^{-m}\otimes X^{-n}|\psi\rangle, \tag{5.18}$$

up to local phase corrections induced by Alice's measurements (no entangling operation can arise from the measurements, as shown in Appendix B). $|\psi\rangle$ is the initial state of Alice's composite system and X is the generalized Pauli operator [191] defined by its action on the basis states: $X|s\rangle \equiv |\mathrm{MOD}_d(s+1)\rangle$. With this interaction we can also choose to deterministically entangle the subsystems in the transmission, directly processing information, as observed in the previous section.

The second type of conditional permutation operator is the simplest and makes use of the cyclic permutation on d^2 elements $x = (0,1,...d^2-1)$ corresponding to the generalized Pauli X operator acting on d^2 basis states (modulo d^2). Because X^n operations commute, Eq. (5.4) becomes a set of simultaneous modulo inequations on different values of n. It is always possible to find two sets satisfying these requirements; in the first set, conditioned on the first subsystem we choose

$$\{P_k^{B1}|P_k^{B1}=X^k, k=0,..,d-1\}. \tag{5.19}$$

Based on this choice, we can adapt the second set so that no two combinations induce the same shift operation:

$$\{P_l^{B2}|P_l^{B2}=X^{ld}, l=0,..,d-1\}. \tag{5.20}$$

Using this type of permutation again leads to deterministic transfer of Alice's composite system up to a known two-qudit operation. However whether or not Bob's state before the feed-forward is locally equivalent to Alice's

input state will depend on the measurement result. We note here that this controlled interaction can be assimilated to the hybrid version of the SUM gate [183] (acting on qudits of different dimension), the qudit extension of the CNOT gate.

This cyclic permutation approach can be applied to the generalized case of transmitting m subsystems via a d^m-dimensional bus. In this case there are m sets of d permutations (including the identity), each defining the interaction of a particular subsystem with the bus. The main idea behind Eq. (5.4) is conserved: any ordered combination of permutations from the sets (one from each set), must result in a permutation orthogonal to all the other combinations in terms of the Hilbert-Schmidt inner product

$$\mathrm{Tr}\left[\prod_{Bj=1}^{m} P_{k_{Bj}}^{Bj}\left(\prod_{Bj=1}^{m} P_{l_{Bj}}^{Bj}\right)^{\dagger}\right] = d^m \prod_{Bj=1}^{m} \delta_{k_{Bj}l_{Bj}}, \tag{5.21}$$

for all Bj, k and l, where Bj numbers the subsystems. Following on from the previous case we can use the sets

$$\begin{aligned}\{P_{k_{Bj}}^{j} | P_{k_{Bj}}^{j} = X^{k_{Bj}d^{Bj-1}}, Bj = 1,..,m,\\ \text{and} \quad k_{Bj} = 0,..,d-1,\},\end{aligned} \tag{5.22}$$

with $X = \sum_{i=0}^{d^m-1} |\mathrm{MOD}_{d^m}(i+1)\rangle\langle i|$, ensuring deterministic data transfer for all m and d. The order in which the permutation operators are arranged within the sets will define the feed-forward operation applied by Bob. Thus we have found two types of interactions allowing for the successful transfer of composite systems, with or without entanglement generation. This constitutes a generic resource for quantum data transfer.

5.4 Transmitting two qutrits

To illustrate the method developped above, let us consider the case of two qutrits. Alice holds two qutrits initially unentangled with the bus, with basis states $\{|0\rangle, |1\rangle, |2\rangle\}$ for each qutrit and $\{|s\rangle, d = 0, 1, .., 8\}$ for the bus. The three systems are coupled via the consecutive interactions

$$\begin{aligned}\hat{C} = &\left(|0\rangle\langle 0| \otimes I^{A2} + |1\rangle\langle 1| \otimes P_1^{A2} + |2\rangle\langle 2| \otimes P_2^{A2}\right)\\ &\times \left(|0\rangle\langle 0| \otimes I^{A1} + |1\rangle\langle 1| \otimes P_1^{A1} + |2\rangle\langle 2| \otimes P_2^{A1}\right),\end{aligned} \tag{5.23}$$

where qutrit $A1$ interacts with the bus before qutrit $A2$. We now must find sets of permutations $\{I, P_1, P_2\}^{A1}$ and $\{I, P_1, P_2\}^{A2}$ which satisfy the requirements for complete information transfer (5.4).

Following the first type of interaction proposed in the previous section, we identify nine orthogonal permutation operators including the identity. The two operators G and H generating all nine of them when combined, correspond to the derangements

$$g = (012)(345)(678) \text{ and } h = (036)(147)(258). \tag{5.24}$$

We write the permutation operators as $Y_{n,m} = H^n G^m$ with $n, m = 0, 1, 2$. By combining them correctly we can satisfy the relations (5.4) and thus realize a deterministic transfer of the two-qutrit state. We illustrate this with a first example, in which Alice couples her input composite system to the bus via the operators $\{I, Y_{0,1}, Y_{0,2}\}^{A1}$ and $\{I, Y_{1,0}, Y_{2,0}\}^{A2}$. After Alice measures out her two qutrits the bus is in the state

$$\begin{aligned} |\xi\rangle = x_0|0\rangle + x_1|3\rangle + x_2|6\rangle + x_3|1\rangle + x_4|4\rangle \\ + x_5|7\rangle + x_6|2\rangle + x_7|5\rangle + x_8|8\rangle \end{aligned} \tag{5.25}$$

up to phase corrections. Bob then prepares two blank qutrits each in the superposition $(|0\rangle + |1\rangle + |2\rangle)/\sqrt{3}$ and couples them to the bus via the inverse permutations $\{I, Y_{0,2}, Y_{0,1}\}^{B1}$ and $\{I, Y_{2,0}, Y_{1,0}\}^{B2}$. This yields the pre-measurement matrix

$$M = \left(\begin{array}{ccc|ccc|ccc} \lambda_0 & \lambda_3 & \lambda_6 & \lambda_1 & \lambda_4 & \lambda_7 & \lambda_2 & \lambda_5 & \lambda_8 \\ \lambda_6 & \lambda_0 & \lambda_3 & \lambda_7 & \lambda_1 & \lambda_4 & \lambda_8 & \lambda_2 & \lambda_5 \\ \lambda_3 & \lambda_6 & \lambda_0 & \lambda_4 & \lambda_7 & \lambda_1 & \lambda_5 & \lambda_8 & \lambda_2 \\ \hline \lambda_2 & \lambda_5 & \lambda_8 & \lambda_0 & \lambda_3 & \lambda_6 & \lambda_1 & \lambda_4 & \lambda_7 \\ \lambda_8 & \lambda_2 & \lambda_5 & \lambda_6 & \lambda_0 & \lambda_3 & \lambda_7 & \lambda_1 & \lambda_4 \\ \lambda_5 & \lambda_8 & \lambda_2 & \lambda_3 & \lambda_6 & \lambda_0 & \lambda_4 & \lambda_7 & \lambda_1 \\ \hline \lambda_1 & \lambda_4 & \lambda_7 & \lambda_2 & \lambda_5 & \lambda_8 & \lambda_0 & \lambda_3 & \lambda_6 \\ \lambda_7 & \lambda_1 & \lambda_4 & \lambda_8 & \lambda_2 & \lambda_5 & \lambda_6 & \lambda_0 & \lambda_3 \\ \lambda_4 & \lambda_7 & \lambda_1 & \lambda_5 & \lambda_8 & \lambda_2 & \lambda_3 & \lambda_6 & \lambda_0 \end{array}\right). \tag{5.26}$$

This is a local mapping, i.e. Bob obtained Alice's two-qutrit input state up to local operations, independent of the measurement outcome. By using this set of permutation operators, we can also achieve an entangling mapping. Starting with the same interactions on Alice's side but switching to $\{Y_{0,1}, Y_{0,2}\}^{B1}$ and $\{I, Y_{2,2}, Y_{1,1}\}^{B2}$ on Bob's side we obtain the pre-

measurement matrix

$$M = \left(\begin{array}{ccc|ccc|ccc} \lambda_0 & \lambda_3 & \lambda_6 & \lambda_1 & \lambda_4 & \lambda_7 & \lambda_2 & \lambda_5 & \lambda_8 \\ \lambda_8 & \lambda_2 & \lambda_5 & \lambda_6 & \lambda_0 & \lambda_3 & \lambda_7 & \lambda_1 & \lambda_4 \\ \lambda_4 & \lambda_7 & \lambda_1 & \lambda_5 & \lambda_8 & \lambda_2 & \lambda_3 & \lambda_6 & \lambda_0 \\ \hline \lambda_1 & \lambda_4 & \lambda_7 & \lambda_2 & \lambda_5 & \lambda_8 & \lambda_0 & \lambda_3 & \lambda_6 \\ \lambda_6 & \lambda_0 & \lambda_3 & \lambda_7 & \lambda_1 & \lambda_4 & \lambda_8 & \lambda_2 & \lambda_5 \\ \lambda_5 & \lambda_8 & \lambda_2 & \lambda_3 & \lambda_6 & \lambda_0 & \lambda_4 & \lambda_7 & \lambda_1 \\ \hline \lambda_2 & \lambda_5 & \lambda_8 & \lambda_0 & \lambda_3 & \lambda_6 & \lambda_1 & \lambda_4 & \lambda_7 \\ \lambda_7 & \lambda_1 & \lambda_4 & \lambda_8 & \lambda_2 & \lambda_5 & \lambda_6 & \lambda_0 & \lambda_3 \\ \lambda_3 & \lambda_6 & \lambda_0 & \lambda_4 & \lambda_7 & \lambda_1 & \lambda_5 & \lambda_8 & \lambda_2 \end{array}\right). \tag{5.27}$$

Each measurement outcome will simulate an entangling operation on the transmitted state. Clarisse *et al.* [190] derived criteria for identifying maximally entangling permutation matrices (acting on two systems of equal dimension), which we review here. The matrix corresponding to a permutation operator P is maximally entangling over all unitary operations if it satisfies the following conditions: every block contains a single nonzero entry; all blocks are different; nonzero entries in the same block-row are in different subcolumns; nonzero entries in the same block-column are in different subrows. In the case of two qubits, the CNOT operation constitutes a maximally entangling permutation.

From these criteria it can be seen that the above resulting matrix is *not* maximally entangling (for all measurement outcomes), because it fails to fulfill one of the requirements: one identifies identical blocks. However with a judicious choice of permutations, one can achieve a maximally entangling mapping. For example Alice choosing the sets $\{I, Y_{0,1}, Y_{0,2}\}^{A1}$, $\{I, Y_{1,0}, Y_{2,0}\}^{A2}$, and Bob the sets $\{I, Y_{2,1}, Y_{1,2}\}^{B1}$ and $\{I, Y_{2,2}, Y_{1,1}\}^{B2}$ results in the pre-measurement matrix

$$M_{\max} = \left(\begin{array}{ccc|ccc|ccc} \lambda_0 & \lambda_3 & \lambda_6 & \lambda_1 & \lambda_4 & \lambda_7 & \lambda_2 & \lambda_5 & \lambda_8 \\ \lambda_8 & \lambda_2 & \lambda_5 & \lambda_6 & \lambda_0 & \lambda_3 & \lambda_7 & \lambda_1 & \lambda_4 \\ \lambda_4 & \lambda_7 & \lambda_3 & \lambda_5 & \lambda_8 & \lambda_2 & \lambda_3 & \lambda_6 & \lambda_0 \\ \hline \lambda_7 & \lambda_1 & \lambda_4 & \lambda_8 & \lambda_2 & \lambda_5 & \lambda_6 & \lambda_0 & \lambda_3 \\ \lambda_3 & \lambda_6 & \lambda_0 & \lambda_4 & \lambda_7 & \lambda_1 & \lambda_5 & \lambda_8 & \lambda_2 \\ \lambda_2 & \lambda_5 & \lambda_8 & \lambda_0 & \lambda_3 & \lambda_6 & \lambda_1 & \lambda_4 & \lambda_7 \\ \hline \lambda_5 & \lambda_8 & \lambda_2 & \lambda_3 & \lambda_6 & \lambda_0 & \lambda_4 & \lambda_7 & \lambda_1 \\ \lambda_1 & \lambda_4 & \lambda_7 & \lambda_2 & \lambda_5 & \lambda_8 & \lambda_0 & \lambda_3 & \lambda_6 \\ \lambda_6 & \lambda_0 & \lambda_3 & \lambda_7 & \lambda_1 & \lambda_4 & \lambda_8 & \lambda_2 & \lambda_5 \end{array}\right). \tag{5.28}$$

Here all blocks are different and for each measurement outcome we have a

maximally entangling permutation operator and in consequence a maximally entangling unitary operation [190], acting on the transmitted qutrits.

Continuing with the second method of the previous section we now use the shift operation $X = \sum_{n=0}^{8} |n+m \pmod 9\rangle\langle n|$, the sets are of the form $\left\{I, X, X^2\right\}^{A1}$ and $\left\{I, X^3, X^6\right\}^{A2}$. If Alice uses the ordered combination above and Bob couples his two qutrits to the bus with the combination $\left\{I, X^8, X^7\right\}^{B1}$ and $\left\{I, X^6, X^3\right\}^{B2}$ (i.e. the inverse, which is also a solution of Eq. (5.4)) we obtain the pre-measurement matrix

$$M = \left(\begin{array}{ccc|ccc|ccc} \lambda_0 & \lambda_3 & \lambda_6 & \lambda_1 & \lambda_4 & \lambda_7 & \lambda_2 & \lambda_5 & \lambda_8 \\ \lambda_6 & \lambda_0 & \lambda_3 & \lambda_7 & \lambda_1 & \lambda_4 & \lambda_8 & \lambda_2 & \lambda_5 \\ \lambda_3 & \lambda_6 & \lambda_0 & \lambda_4 & \lambda_7 & \lambda_1 & \lambda_5 & \lambda_8 & \lambda_2 \\ \hline \lambda_8 & \lambda_2 & \lambda_5 & \lambda_0 & \lambda_3 & \lambda_6 & \lambda_1 & \lambda_4 & \lambda_7 \\ \lambda_5 & \lambda_8 & \lambda_2 & \lambda_6 & \lambda_0 & \lambda_3 & \lambda_7 & \lambda_1 & \lambda_4 \\ \lambda_2 & \lambda_5 & \lambda_8 & \lambda_3 & \lambda_6 & \lambda_0 & \lambda_4 & \lambda_7 & \lambda_1 \\ \hline \lambda_7 & \lambda_1 & \lambda_4 & \lambda_8 & \lambda_2 & \lambda_5 & \lambda_0 & \lambda_3 & \lambda_6 \\ \lambda_4 & \lambda_7 & \lambda_1 & \lambda_5 & \lambda_8 & \lambda_2 & \lambda_6 & \lambda_0 & \lambda_3 \\ \lambda_1 & \lambda_4 & \lambda_7 & \lambda_2 & \lambda_5 & \lambda_8 & \lambda_3 & \lambda_6 & \lambda_0 \end{array}\right). \tag{5.29}$$

The same observation as in the two qubit case can be made. Different measurement outcomes call for different types of feed forward. If we measure the states $|0\rangle$, $|3\rangle$ or $|6\rangle$ (which occurs with a probability 1/3) we obtain the initial state up to local operations on the two qutrits. However all other outcomes will lead to the initial state having undergone an entangling operation, though not a maximally entangling one. We now move on to consider the physical implementation of the proposed operations along with the coupling between the bus and the subsystems.

5.5 A continuous variable bus

The implementation of general qudit gates requires considerable control. However the second interaction with which we propose to implement our protocols only depends on the ability to perform a generalized X operation conditionally. The use of a CV bus may seem like a complication at first, but interestingly it provides a very natural way of realizing such a conditional operation. Given an interaction Hamiltonian of the form $H_{int} = -\hbar\chi\hat{n}_{\text{bus}}\hat{\Lambda}_{\text{sub}}$ where $\hat{\Lambda}_{\text{sub}} = \sum_{s=0}^{d-1} s|s\rangle\langle s|$ acts on the subsystem, we can approximate the conditional X by preparing the bus in a coherent state $|\alpha\rangle$. $\hat{n}_{bus}$ represents the number operator acting on the energy eigenstates of the harmonic oscillator, so in fact we are looking at a conditional rotation

type of interaction. After an interaction time t the combined state evolves as $e^{-iH_{int}t/\hbar}|s\rangle|\alpha\rangle = |s\rangle|\alpha e^{i\theta s}\rangle$ with $\theta = \chi t$. Thus we see that the possible states of the subsystem are encoded into the phase of the coherent state, as is the case in the qubus scheme. However here we assume an arbitrary interaction strength.

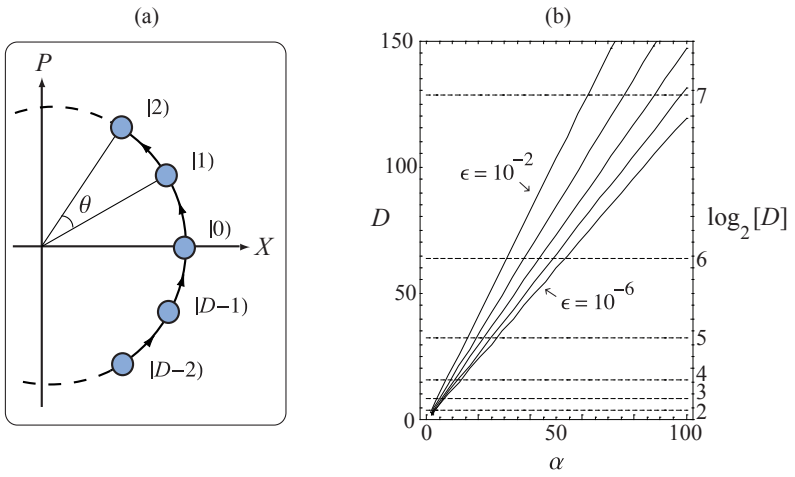

Figure 5.3: (a) A phase space picture of the cyclic effect of the shift operation $e^{i\theta\hat{N}}$ on the state of the CV bus, with $\theta = 2\pi/D$. As defined in the text, $|n) = |\alpha e^{in\theta}\rangle$. (b) The maximum dimension of the composite system to be transmitted as a function of the amplitude α, for a fixed overlap $\epsilon = 10^{-j}$ representing the error. From top to bottom we have $j = 2, .., 6$. The dashed horizontal lines represent the capacity of the channel in number of qubits that can be transferred.

Now given a D-dimensional composite system, the bus states we will write as $\{|n) \equiv |\alpha e^{i2n\pi/D}\rangle, n = 0, .., D-1\}$. It is worth noting here that this set of states is literally generated at the encoding stage, on Alice's side in the transfer protocol or on Bob's side in the teleportation protocol. Each subsystem interacts with the bus for a different amount of time, rotating the states of the bus in phase space by a different angle (see Fig. 5.3(a)). This is reminiscent of the three-qubit gate proposed in the previous chapter. Setting $\theta = 2\pi/D$, we can view the effect of a general interaction as

$$C^k|s\rangle|n) = |s\rangle|\mathrm{MOD}_D(n + ks)), \tag{5.30}$$

with $C = e^{i\theta\hat{n}_{\mathrm{bus}}\hat{\Lambda}_{\mathrm{sub}}}$. Thus we see that by repeating the interactions or

equivalently increasing the interaction time, we obtain all the conditional operations required to implement our protocol, even for arbitrary numbers of subsystems (Eq. (5.22)). This is achieved through the cyclic nature of the rotation operation $e^{i\theta\hat{n}}$ on the coherent state.

The bus states do not form an orthogonal basis $(n|m) \neq \delta_{nm}$, and so the dimension D of the transmitted composite system will be limited by the available amplitude α of the bus. For a fixed overlap $\epsilon = (n|n+1)$ which is deemed acceptable, the dimension of the composite system is bounded from above by

$$D \leq \frac{2\pi}{\cos^{-1}(\ln\epsilon/\alpha^2 + 1)}. \tag{5.31}$$

The behavior of this bound is illustrated in Fig. 5.3(b). We can see that the scaling is close to being linear and the capacity of the bus is large, even for ϵ as low as 10^{-5}. In this case the CV bus can potentially teleport up to 7 qubits with a moderate amplitude of $\alpha = 100$.

If we plan to use heterodyne detection to distinguish between the bus states, a more appropriate value to keep small will be the overlap of the Q functions [192]. Another option we have at our disposal is to trade the error probability for the probability of a failure outcome by employing unambiguous state discrimination (USD). Building on from a result by Chefles and Barnett [193], some work has already been done by van Enk [194] on the USD of symmetric coherent states using linear optics and photodetectors. These schemes are near optimal for small amplitudes and will be optimized for the transmission of large composite systems. In consequence we have a choice of measurements to implement on this CV bus which enable us to realize our transfer and teleportation protocols, given an arbitrary interaction strength.

Chapter 6

Summary and outlook

In this thesis we have investigated three areas related to the implementation of QIP. As a starting point we argued that distributed approaches constitute the most promising route toward a scalable quantum computer, already allowing for nontrivial applications to be realized experimentally at the time of writing. We also pointed at the potential advantages of the cluster state model for information processing. This set the framework for the results obtained.

Having chosen the qubus scheme as a physical realization, in the third chapter we looked at the effects of dissipation on the bus. First we generalized previous work on dissipation during dispersive interactions. These interactions led to the conditional rotation which is one of the center pieces of the qubus proposal. We found that as well as causing decoherence in the qubit interacting with the bus, dissipation induces a known conditional phase on the qubit. This problematic phase is a function of the amount of loss incurred by the probe as well as its initial amplitude. We followed the entanglement dynamics between the bus and the qubit and found that the larger the initial amplitude of the probe the larger the maximum entanglement and the lower the entropy of the combined state at the entanglement peaking time.

The decoherence process corresponds to a phase-flip channel which can be combined with the phase-flip channel induced by inter-cavity loss. This enabled us to characterize the effects of loss in the complete measurement-free CZ gate. We obtained the quantum operations induced and their effect on the fidelity and entanglement of output states. These operations are essential to the development of a large scale architecture containing levels of error correction. We found that in the presence of moderate loss the gate

operated with a high fidelity and that a simple reversal of the gate made the errors balance out to being independent single qubit phase-flip channels. This is the simplest quantum operation one could conceive of in this situation and could potentially simplify error correction on higher levels. Overall we find that dissipation in the bus leads to a well understood dephasing of the qubits and provide a general approach to characterizing decoherence effects in quantum bus schemes, through the calculation of overlaps.

In the fourth chapter we applied the qubus scheme to the distributed generation of cluster states of matter qubits. Keeping a simple homodyne measurement, we proposed a three qubit gate working with probability 3/4. This increase in probability past the 1/2 limit is crucial, as it allows us to generate cluster states in a truly scalable fashion. The improvements over previous proposals are significant. At this point we came to understand the importance of strategies for the probabilistic growth of cluster states. This led us to provide two new view points on cluster growth, independent of the physical realization. In the large flow approximation we obtained the optimal strategies for various cluster state lengths, which in other circumstances is a particularly tough problem solve. Coming back to the discrete growth of a single cluster we introduced absorbing Markov chains. We found that for a large range of p, two-qubit pumping was the optimal pumping strategy, however we also found that strategies could be layered to improve their performance. These results introduce new tools and perspectives to cluster growth studies and have the potential to be extended to context dependent strategies.

Finally in the fifth chapter we addressed the important issue of composite system transmission. This application is vital for distributed approaches to QIP and also for cluster state quantum computing in the case that the preparation and measurement regions are distinct. We provided simple protocols for the deterministic transfer of states of arbitrary dimension via a single bus. We discussed in detail the cases of two-qubit and two-qutrit transmission, finding the interactions leading to a maximally entangling mapping. As a closing point the qubus scheme, or the use of a CV bus, proved to be a natural framework for the physical realization of such protocols. Overall these results illustrate the potential applications of higher dimensional buses and points to their use in increasing the information processing power by accelerating data transfer and entanglement distribution.

The results obtained in this thesis provide a basis for many further topics of research. Concerning the first part of the results, on the effects of dissipation on the qubus CZ gate. We now have a rough model for one source of noise. It needs to be complemented by a realistic inherent decoherence

process of the qubits, before one has a complete noise model for the gate. Once this is achieved, the real question of a scalable architecture will come into play. First we should find out what the noise threshold for the system is, based on previous calculation methods. Then we will have to choose a computational model and design a full blown architecture which incorporates the required levels of error correction. This in itself would constitute an extension of the results presented here.

With regards to cluster state growth, further work can be divided into two areas. The first is the adaptation of a more involved mathematical framework, such as controlled Markov chains, to really obtain a context dependent optimal growth strategy, if such a strategy exists or can be stated with a set of directives. Maybe a deeper question would be to determine whether the questions of growth speed and the question of maximum expected length as addressed by Gross *et al.* [159] can be related and solved via the same mathematical approach. The second logical extension is the development and comparison of 2D cluster state growth strategies. A starting question would be whether or not it is possible to significantly increase the growth efficiency by not first generating linear clusters and then trying to connect them. There are already a number of 2D growth strategies in the literature which again assume large parallel entangling resources, making them hard to compare with each other. Setting the work and time as equal quantities might be a good start for this study.

Lastly, the protocols for composite system transfer could be incorporated into the design of a scalable architecture mentioned earlier. In addition to this, the protocols may be modified or extended so as to guarantee secure data transfer to different users via the same bus. This would enter into the area of research known as data hiding, and in this case quantum data hiding for multiple users.

Overall, the results presented in this thesis point to the strong potential of distributed applications, in particular using a robust higher dimensional quantum bus. These distributed applications constitute a natural approach to the preparation of the cluster state and the combination of the two forms a very promising route toward scalable quantum information processing. We hope the results contained in this work will contribute to the development of actual devices and will trigger new research in the field of quantum information processing.

Appendix A

Decomposition theorem

In this appendix we state the relevant decomposition theorem derived by Witschel in [125]. For an operator algebra obeying the commutation relation

$$[\hat{A}, \hat{B}] = y\hat{B}, \tag{A.1}$$

an exponentiation of the two operators can be decomposed as follows

$$\begin{aligned} \exp[\mu(\hat{A} + \nu\hat{B})] &= \exp[\mu\hat{A}] \exp[(\nu/y)(1 - e^{-\mu y}\hat{B})] & \text{(A.2)} \\ &= \exp[(\nu/y)(e^{\mu y} - 1)\hat{B}] \exp[\mu\hat{A}]. & \text{(A.3)} \end{aligned}$$

Coming back to our superoperators we have

$$\exp[\mathcal{L}_{nm}t] \equiv \exp[t(\hat{A} + \hat{B})], \tag{A.4}$$

with

$$\begin{aligned} \hat{A} &\equiv (i\chi\lambda_n - \gamma)\mathcal{M} + (-i\chi\lambda_m - \gamma)\mathcal{P}, \\ \hat{B} &\equiv 2\gamma\mathcal{J}. \end{aligned} \tag{A.5}$$

Noting that $[\mathcal{J}, \mathcal{M}] = [\mathcal{J}, \mathcal{P}] = \mathcal{J}$, we observe the commutation relation $[\hat{A}, \hat{B}] = y\hat{B}$ with $y = 2\gamma - i(\lambda_n - \lambda_m)\chi$. Then setting $\nu = 1$ in expression A.3 we straightforwardly obtain 3.17.

Appendix B

Alice's measurements in the qudit bus protocol

Here we show how Alice's measurements do not change the fact that Bob's final composite state is locally equivalent to the initial state $|\psi\rangle$. To see this we rewrite the full state of the bus with Alice's and Bob's composite systems, after all the interactions (5.17)

$$|\varphi_T\rangle = \frac{1}{d} \sum_{a_1,a_2,b_1,b_2=0}^{d-1} x_{a_1 a_2} \left(|b_1\rangle|b_2\rangle\right)_B \left(|a_1\rangle|a_2\rangle\right)_A \otimes|\mathrm{MOD}_d(a_1 - b_1), \mathrm{MOD}_d(a_2 - b_2)\rangle. \quad \text{(B.1)}$$

Measuring the bus in the $|m, n\rangle$ state leaves Alice's and Bob's qudits in the combined state

$$|m,n\rangle\langle m,n||\varphi_T\rangle = \sum_{a_1,a_2,b_1,b_2=0}^{d-1} x_{a_1 a_2} \left(|a_1 - m\rangle|a_2 - n\rangle\right)_B \left(|b_1 + m\rangle|b_2 + n\rangle\right)_A , \quad \text{(B.2)}$$

where we have omitted the MOD_d. One possible way of seeing the effect of Alice's measurement is to apply the discrete Fourier transform to her qudit states before a measurement in the computational basis. The transform is given by [40]

$$|k\rangle \to \frac{1}{\sqrt{d}} \sum_{l=0}^{d-1} e^{2i\pi lk/d} |l\rangle, \quad \text{(B.3)}$$

and applying it to (B.2) we obtain

$$\begin{aligned} &\frac{1}{d} \quad \sum_{a_1,a_2,b_1,b_2=0}^{d-1} x_{a_1 a_2} \left(|a_1 - m\rangle|a_2 - n\rangle\right)_B \\ &\otimes \quad \sum_{c_1,c_2=0}^{d-1} e^{2i\pi(c_1(b_1+m)+c_2(b_2+n))/d} \left(|c_1\rangle|c_2\rangle\right)_A . \end{aligned} \tag{B.4}$$

Now Alice measuring her qudits in the states $|s\rangle|t\rangle$ will leave Bob's composite system in the state

$$\begin{aligned} |\psi_f\rangle &= \sum_{a_1,a_2=0}^{d-1} x_{a_1 a_2} Z^s X^{-m} |a_1\rangle \otimes Z^t X^{-n} |a_2\rangle \\ &= Z^s X^{-m} \otimes Z^t X^{-n} |\psi\rangle, \end{aligned} \tag{B.5}$$

locally equivalent to the initial state, with Z being the generalized Pauli operator acting as $Z|j\rangle = e^{2i\pi j/d}|j\rangle$.

Bibliography

[1] M. Planck. On the law of distribution of energy in the normal spectrum. *Ann. Phys.*, 4:553, 1901.

[2] A. Einstein. On a heuristic viewpoint concerning the production and transformation of light. *Ann. Phys.*, 17:132, 1905.

[3] N. Bohr. On the constitution of atoms and molecules,. *Philosophical Magazine*, 6:26, 1913.

[4] N. Bohr. The spectra of helium and hydrogen. *Nature*, 92:231, 1914.

[5] L. de Broglie. Researches on the quantum theory. *Thesis, Paris*, 1924.

[6] W. Heisenberg. Quantum-theoretical re-interpretation of kinematic and mechanical relations. *Zeitschrift fr Physik*, 33:879, 1925.

[7] E. Schrödinger. An undulatory theory of the mechanics of atoms and molecules. *Phys. Rev.*, 28:1049, 1926.

[8] P.A.M. Dirac. The quantum theory of the electron. *Proc. R. Soc. A*, 117:610, 1928.

[9] M. Arndt, O. Nairz, J. Voss-Andreae, C. Keller, G. van der Zouw, and A. Zeilinger. Waveparticle duality of C60. *Nature*, 401:680, 1999.

[10] A. Einstein, B. Podolsky, and N. Rosen. Can quantum-mechanical description of physical reality be considered complete? *Phys. Rev.*, 47:777, 1935.

[11] J.S. Bell. On the Einstein Podolsky Rosen paradox. *Physics*, 1:195, 1964.

[12] A. Aspect, P. Grangier, and G. Roger. Experimental tests of realistic local theories via bell's theorem. *Phys. Rev. Lett.*, 47:460, 1981.

[13] A. Turing. On computable numbers, with an application to the Entscheidungsproblem. *Proc. Math. Soc.,Series 2*, 42, 1936.

[14] J. von Neumann. A universal Turing machine with two internal states. *Automata Studies, Princeton University Press*, page 157, 1956.

[15] J. von Neumann. First draft of a report on the electronic discrete variable automatic computer. 1945.

[16] C. E. Shannon. A mathematical theory of communication. *Bell System Tech. J.*, 27:379, 1948.

[17] G.E. Moore. Cramming more components onto integrated circuits. *The original paper is available at: http://www.intel.com/technology/mooreslaw/index.htm*, 1965.

[18] R. Feynman. Simulating physics with computers. *Int. J. of Theoretical Physics*, 21:467, 1982.

[19] S. Lloyd. Universal quantum simulators. *Science*, 273:1073, 1996.

[20] D. Deutsch. Quantum theory, the Curch-Turing principle and the universal quantum computer. *Proc. R. Soc. A*, 400:97, 1985.

[21] D. Deutsch and R. Jozsa. Rapid solutions of problems by quantum computation. *Proc. R. Soc. A*, 439:553, 1992.

[22] P.W. Shor. Polynomial-time algorithms for prime factorization and discrete logarithms on a quantum computer. *Proc. Annual Symposium on the Foundations of Computer Science*, 35:124, 1994.

[23] L. Grover. A fast quantum mechanical algorithm for database search. *Proc. Annual ACM Symposium on the Theory of Computing*, 28:212, 1996.

[24] C.H. Bennet and G. Brassard. Quantum cryptography. *Proceedings of IEEE International Conference on Computers, Systems and Signal Processing, New York*, page 175, 1984.

[25] C.H. Bennett and S.J. Wiesner. Communication via one- and two-particle operators on Einstein-Podolsky-Rosen states. *Phys. Rev. Lett.*, 69:2881, 1992.

[26] C.H. Bennett, G. Brassard, C. Crépeau, R. Jozsa, A. Peres, and W.K. Wootters. Teleporting an unknown quantum state via dual classical and Einstein-Podolsky-Rosen channels. *Phys. Rev. Lett.*, 70:1895, 1993.

[27] P.W. Shor. Scheme for reducing decoherence in quantum computer memory. *Phys. Rev. A*, 52:(R) 2493, 1995.

[28] A.M. Steane. Error correcting codes in quantum theory. *Phys. Rev. Lett.*, 77:793, 1996.

[29] A.R. Calderbank, E.M. Rains ans P.W. Shor, and N.J.A. Sloane. Quantum error correction via codes over GF(4). *IEEE Trans. Inform. Theory*, 44:1369, 1998.

[30] J.I. Cirac and P. Zoller. Quantum computations with cold trapped ions. *Phys. Rev. Lett.*, 74:4091, 1995.

[31] N. Gershenfeld and I.L. Chuang. Bulk spin resonance quantum computing. *Science*, 275:350, 1997.

[32] D. Loss and D.P. DiVincenzo. Quantum computation with quantum dots. *Phys. Rev. A*, 57:120, 1998.

[33] B.E. Kane. A silicon-based nuclear spin quantum computer. *Nature*, 393:133, 1998.

[34] E. Knill, R. Laflamme, and G.J. Milburn. A scheme for efficient quantum computation with linear optics. *Nature*, 409:46, 2001.

[35] E. Farhi, J. Goldstone, S. Gutmann, and M. Sipser. Quantum computation by adiabatic evolution. *preprint:quant-ph/0001106*, 2000.

[36] J. Preskill. Topological quantum computation. *Caltech Physics 219 lecture notes on quantum computation chapter 9, available at http://www.theory.caltech.edu/ preskill/ph229/.*

[37] P.A.M. Dirac. A new notation for quantum mechanics. *Proceedings of the Cambridge Philosophical Society*, 35:416, 1939.

[38] A.S. Holevo. Statistical problems in quantum physics. *Proceedings of the second Japan-USSR Symposium on Probability Theory*, pages 104, Springer–Verlag, 1973.

[39] W.K. Wootters and W.H. Zurek. A single quantum cannot be cloned. *Nature*, 299:802, 1982.

[40] M.A. Nielsen and I.L. Chuang. *Quantum Computation and Information*. Cambridge University Press, 2001.

[41] R. Raussendorf and H.-J. Briegel. A one-way quantum computer. *Phys. Rev. Lett.*, 86:5188, 2001.

[42] M. Hein, W. Dür, J. Eisert, R. Raussendorf, M. Van den Nest, and H.-J. Briegel. Entanglement in graph states and its applications. *Proceedings of the International School of Physics 'Enrico Fermi' on Quantum Computers, Algorithms and Chaos, Varenna, Italy, preprint quant-ph/0602096*, 2005.

[43] S.D. Barrett and P. Kok. Efficient high-fidelity quantum computation using matter qubits and linear optics. *Phys. Rev. A*, 71:060310(R), 2005.

[44] D. Gottesman. Stabilizer codes and quantum error correction. *PhD Thesis, California Insitute of Technology, quant-ph/9705052*, 1997.

[45] L.D. Landau and E.M. Lifshitz. *The classical theory of fields*. Elsevier Butterworth-Heinemann press, 4 edition, 2004.

[46] D.F. Walls and G.J. Milburn. *Quantum optics*. Springer, 2 edition, 2008.

[47] S.M. Barnett and J.A. Vaccaro. *The quantum phase operator; a review*. Taylor and Francis, 2007.

[48] S.L. Braunstein and P. van Loock. Quantum information with continuous variables. *Rev. Mod. Phys.*, 77:513, 2005.

[49] C.R. Myers and R. Laflamme. Linear optics quantum computation: an overview. *Proceedings of the International School of Physics 'Enrico Fermi' on Quantum Computers, Algorithms and Chaos, Varenna, Italy, preprint quant-ph/0512104*, 2006.

[50] P. Kok, W.J. Munro, K. Nemoto, T.C. Ralph, J.P. Dowling, and G.J. Milburn. Linear optical quantum computing with photonic qubits. *Rev. Mod. Phys.*, 79:135, 2007.

[51] C.W. Gardiner and P. Zoller. *Quantum Noise*. Springer, 2000.

[52] C.C. Gerry and P.L. Knight. *Introductory quantum optics*. Cambridge University press, 2005.

[53] E.T. Jaynes and F.W. Cummings. Comparison of quantum and semi-classical radiation theories with application to the beam maser. *Proc. IEEE*, 51:89, 1963.

[54] S. Schneider, A.M. Herkommer, U. Leonhardt, and W.P. Schleich. Cavity field tomography via atomic deflection. *J. Mod. Opt.*, 44:2333, 1997.

[55] H.J. Carmichael. *Statistical methods in quantum optics*. Springer, 2002.

[56] L. Mandel and E. Wolf. *Optical coherence and quantum optics*. Cambridge University press, 1995.

[57] D.P. DiVincenzo. The physical implementation of quantum computation. *Fortschr. Phys.*, 48:771, 2000.

[58] G.J. Milburn. Quantum optical Fredkin gate. *Phys. Rev. Lett.*, 62:2124, 1989.

[59] I.L. Chuang and Y. Yamamoto. Simple quantum computer. *Phys. Rev. A*, 52:3489, 1995.

[60] J.D. Franson, B.C. Jacobs, and T.B. Pittman. Quantum computing using single photons and the Zeno effect. *Phys. Rev. A*, 70:062302, 2004.

[61] C.R. Myers and A. Gilchrist. A photon loss tolerant Zeno CSIGN gate. *Phys. Rev. A*, 75:052339, 2007.

[62] P.M. Leung and T.C. Ralph. Improving the fidelity of optical Zeno gates via distillation. *Phys. Rev. A*, 74:062325, 2006.

[63] J.L. O'Brien. Optical quantum computing. *Science*, 318:1467, 2007.

[64] T.C. Ralph, A.G.White, W.J.Munro, and G.J. Milburn. Simple scheme for efficient linear optics quantum gates. *Phys. Rev. A*, 65:012314, 2002.

[65] E. Knill. Quantum gates using linear optics and postselection. *Phys. Rev. A*, 66:052306, 2002.

[66] T.B. Pittmann, B.C. Jacobs, and J.D. Franson. Probabilistic quantum logic operations using polarizing beam splitters. *Phys. Rev. A*, 64:062311, 2001.

[67] M. Koashi, T. Yamamoto, and N. Imoto. Probabilistic manipulation of entangled photons. *Phys. Rev. A*, 63:030301, 2001.

[68] D. Gottesman and I.L. Chuang. Demonstrating the viability of universal quantum computation using teleportation and single-qubit operations. *Nature*, 402:390, 1999.

[69] N. Lütkenhaus, J. Calsamiglia, and K.A. Suominen. Bell measurements for teleportation. *Phys. Rev. A*, 59:3295, 1999.

[70] J. Eisert. Optimizing linear optics quantum gates. *Phys. Rev. Lett.*, 95:040502, 2005.

[71] A.J.F. Hayes, A. Gilchrist, C.R. Myers, and T.C. Ralph. Utilizing encoding in scalable linear optics quantum computing. *J. Opt. B*, 6:533, 2004.

[72] N. Yoran and B. Reznik. Deterministic linear optics quantum computation with single photon qubits. *Phys. Rev. Lett.*, 91:037903, 2003.

[73] S. Popescu. An optical method for teleportation, preprint quant-ph/9501020. 1995.

[74] M.A. Nielsen. Optical quantum computation using cluster states. *Phys. Rev. Lett.*, 93:040503, 2004.

[75] D.E. Browne and T. Rudolph. Resource-efficient linear optical quantum computation. *Phys. Rev. Lett.*, 95:010501, 2005.

[76] P. Walther, K.J. Resch, T. Rudolph, H.Weinfurter, V. Vedral, M. Aspelmeyer, and A. Zeilinger. Experimental one-way quantum computing. *Nature*, 434:169, 2005.

[77] C.-Y. Lu, X.-Q. Zhou, O. Gühne, W.-B. Gao, J. Zhang, Z.-S. Yuan, A. Goebel, T. Yang, and J.-W. Pan. Experimental entanglement of six photons in graph states. *Nature Physics*, 3:91, 2007.

[78] M.B. Plenio, S.F. Huelga, A. Beige, and P.L. Knight. Cavity loss induced generation of entangled atoms. *Phys. Rev. A*, 59:2468, 1999.

[79] L.-M. Duan and H.J. Kimble. Efficient engineering of multiatom entanglement through single-photon detections. *Phys. Rev. Lett.*, 90:253601, 2003.

[80] Y.L. Lim, A. Beige, and L.C. Kwek. Repeat-until-success quantum computing. *Phys. Rev. Lett.*, 95:030505, 2005.

[81] Y.L. Lim, S.D. Barrett, A. Beige, P. Kok, and L.C. Kwek. Repeat-until-success quantum computing using stationary and flying qubits. *Phys. Rev. A*, 73:012304, 2006.

[82] E. Waks, K. Inoue, W.D. Oliver, E. Diamanti, and Y. Yamamoto. High-efficiency photon-number detection for quantum information processing. *IEEE: J. Sel. Top. Quantum Electron.*, 9:1502, 2003.

[83] D. Rosenberg, A.E. Lita, A.J. Miller, and S.W. Nam. Noise-free high-efficiency photon-number-resolving detectors. *Phys. Rev. A*, 71:061803, 2005.

[84] P. Grangier, J.A. Levenson, and J.P. Poizat. Quantum non-demolition measurements in optics. *Nature*, 396:537, 1998.

[85] K. Nemoto and W.J. Munro. Universal quantum computation on the power of quantum non-demolition measurements. *Phys. Lett A*, 344:104, 2005.

[86] C. Santori, D. Fattal, J. Vuckovic, G. Solomon, and Y. Yamamoto. Indistinguishable photons from a single-photon device. *Nature*, 419:594, 2020.

[87] B. Lounis and M. Orrit. Single-photon sources. *Rep. Prog. Phys.*, 68:1129, 2005.

[88] A. Beige. Quantum computing without qubit-qubit interactions. *Quantum Theory and Symmetries*, 4:22.

[89] Q.A. Turchette, C.J. Hood, W. Lange, H. Mabuchi, and H.J. Kimble. Measurement of conditional phase shifts for quantum logic. *Phys. Rev. Lett.*, 75:4710, 1995.

[90] D.I. Schuster, A.A. Houck, J.A. Schreier, A. Wallraff, J.M. Gambetta, A. Blais, L. Frunzio, B. Johnson, M.H. Devoret, S.M. Girvin, and R.J. Schoelkopf. Resolving photon number states in a superconducting circuit. *Nature*, 445:515, 2007.

[91] S.J. Devitt, A.D. Greentree, R. Ionicioiu, J.L. O'Brien, W.J. Munro, and L.C.L. Hollenberg. The photonic module: an on-demand resource for photonic entanglement. *Phys. Rev. A.*, 76:052312, 2007.

[92] S. Lloyd and S.L. Braunstein. Quantum computation over continuous variables. *Phys. Rev. Lett.*, 82:1784, 1999.

[93] N.C. Menicucci, P. van Loock, M. Gu, C. Weedbrook, T.C. Ralph, , and M.A. Nielsen. Universal quantum computation with continuous-variable cluster states. *Phys. Rev. Lett.*, 97:110501, 2006.

[94] S. Lloyd. Hybrid quantum computing. *preprint quant-ph/0008057*, 1999.

[95] X. Wang, A. Sørensen, and K. Mølmer. Multibit gates for quantum computing. *Phys. Rev. Lett.*, 86:3907, 2001.

[96] X. Wang and P. Zanardi. Simulation of many-body interactions by conditional geometric phases. *Phys. Rev. A*, 65:032327, 2002.

[97] G.J. Milburn. Simulating nonlinear spin models in an ion trap. *preprint quant-ph/9908037*, 1999.

[98] C.A. Sackett, D. Kielpinski, B.E. King, C. Langer, V. Meyer, C.J. Myatt, M. Rowe, Q.A. Turchette, W.M. Itano, D.J. Wineland, and C. Monroe. Experimental entanglement of four particles. *Nature*, 404:256, 2000.

[99] A. Wallraff, D.I. Schuster, A. Blais, L. Frunzio, J. Majer, M.H. Devoret, S.M. Girvin, and R.J. Schoelkopf. Approaching unit visibility for control of a superconducting qubit with dispersive readout. *Phys. Rev. Lett.*, 95:060501, 2005.

[100] A. Wallraff, D.I. Schuster, A. Blais, L. Frunzio, R.-S. Huang, J. Majer, S. Kumar, S.M. Girvin, and R.J. Schoelkopf. Circuit quantum electrodynamics: coherent coupling of a single photon to a cooper pair box. *Nature*, 431:162, 2004.

[101] A. Shnirman, G. Schön, and Z. Hermon. Quantum manipulations of small josephson junctions. *Phys. Rev. Lett.*, 79:2371, 1997.

[102] T.P. Spiller. Superconducting circuits for quantum computing. *Fort. Phys.*, 48:1075, 2000.

[103] Y. Makhlin, G. Schöen, and A. Shnirman. Quantum state engineering with josephson-junction devices. *Rev. Mod. Phys.*, 73:357, 2001.

[104] I. Chiorescu, P. Bertet, K. Semba, Y. Nakamura, C.J.P.M. Harmans, and J.E. Mooij. Coherent dynamics of a flux qubit coupled to a harmonic oscillator. *Nature*, 431:159, 2004.

[105] D.J. Wineland, C. Monroe, W.M. Itano, D. Leibfried, B.E. King, and D.M. Meekhof. Experimental issues in coherent quantum-state manipulation of trapped atomic ions. *Journal of Research of the National Institute of Standards and Technology*, 103:259, 1998.

[106] C. Monroe, D.M. Meekhof, B.E. King, , and D.J. Wineland. A 'Schrödinger cat' superposition state of an atom. *Science*, 272:1131, 1996.

[107] A. Luis. Quantum mechanics as a geometric phase: phase-space interferometers. *J. Phys. A*, 34:7677, 2001.

[108] T.P. Spiller, K. Nemoto, S.L. Braunstein, W. J. Munro, P. van Loock, and G.J. Milburn. Quantum computation by communication. *New J. Phys.*, 8:30, 2006.

[109] W.H. Louisell. *Quantum statistical properties of radiation.* Wiley Classics Library, 1990.

[110] P. van Loock, W.J. Munro, K. Nemoto, T.P. Spiller, T.D. Ladd, S.L. Braunstein, and G.J. Milburn. Hybrid quantum computation in quantum optics. *preprint quant-ph/0701057*, 2006.

[111] G.J. Milburn and D.F. Walls. State reduction in quantum-counting quantum nondemolition measurements. *Phys. Rev. A*, 30:56, 1984.

[112] N. Imoto, H.A. Haus, and Y. Yamamoto. Quantum nondemolition measurement of the photon number via the optical Kerr effect. *Phys. Rev. A*, 32:2287, 1985.

[113] W.J. Munro, K. Nemoto, R.G. Beausoleil, and T.P. Spiller. A high-efficiency quantum non-demolition single photon number resolving detector. *Phys. Rev. A*, 71:033819, 2005.

[114] C.R. Myers, M. Silva, K. Nemoto, and W.J. Munro. Stabilizer quantum error correction with quantum bus computation. *Phys. Rev. A*, 76:012303, 2007.

[115] K. Nemoto and W.J. Munro. Nearly deterministic linear optical controlled-NOT gate. *Phys. Rev. Lett.*, 93:250502, 2004.

[116] F. Jelezko, T. Gaebel, I. Popa, A. Gruber, and J. Wrachtrup. Observation of coherent oscillations in a single electron spin. *Phys. Rev. Lett.*, 92:076401, 2004.

[117] J.G.P. de Faria and M.C. Nemes. Dissipative dynamics of the Jaynes-Cummings model in the dispersive approximation: Analytical results. *Phys. Rev. A*, 59:3918, 1999.

[118] K.M.F. Romero and M. C. Nemes. Exact description of decoherence in optical cavities. *Physica A*, 325:333, 2003.

[119] P. van Loock, T.D. Ladd, K. Sanaka, F. Yamaguchi, K. Nemoto, W.J. Munro, and Y. Yamamoto. Hybrid quantum repeater using bright coherent light. *Phys. Rev. Lett.*, 96:240501, 2006.

[120] T.D. Ladd, P. van Loock, K. Nemoto, W.J. Munro, and Y. Yamamoto. Hybrid quantum repeater based on dispersive CQED interactions between matter qubits and bright coherent light. *New J. Phys.*, 8:164, 2006.

[121] S.D. Barrett and G.J. Milburn. Phys. rev. a. *Quantum-information processing via a lossy bus*, 74:060302(R), (2006).

[122] L.-X. Cen and P. Zanardi. Decoherence suppression for oscillator-assisted geometric quantum gates via symmetrization. *Phys. Rev. A*, 71:060307(R), 2005.

[123] H. Jeong. Using weak nonlinearity under decoherence for macroscopic entanglement generation and quantum computation. *Phys. Rev. A*, 72:034305, 2005.

[124] H. Jeong. Quantum computation using weak nonlinearities: Robustness against decoherence. *Phys. Rev. A*, 73:052320, 2006.

[125] W. Witschel. Ordered products of exponential operators by similarity transformations. *Int. J. Quantum Chem.*, 20:1233, 1981.

[126] A.D. Greentree, J. Salzman, S. Prawer, and L.C.L. Hollenberg. Quantum gate for Q switching in monolithic photonic-band-gap cavities containing two-level atoms. *Phys. Rev. A.*, 73:013818, 2006.

[127] P. van Loock, N. Lütkenhaus, W.J. Munro, and K. Nemoto. Quantum repeaters using coherent-state communication. *preprint quant-ph/0806.1153*, 2008.

[128] M.B. Plenio and S. Virmani. An introduction to entanglement measures. *Quant. Inf. Comp.*, 7:1, 2007.

[129] C.H. Bennet, D. P. DiVincenzo, J. Smolin, and W. K. Wooters. Mixed-state entanglement and quantum error correction. *Phys. Rev. A*, 54:3824, 1996.

[130] W.K. Wooters. Entanglement of formation of an arbitrary state of two qubits. *Phys. Rev. Lett.*, 80:2245, 1997.

[131] D.F. Walls and G.J. Milburn. Effect of dissipation on quantum coherence. *Phys. Rev. A*, 31:2403, 1985.

[132] C.H. Bennett, G. Brassard, S. Popescu, B. Schumacher, J.A. Smolin, and W.K. Wootters. Purification of noisy entanglement and faithful teleportation via noisy channels. *Phys. Rev. Lett.*, 76:722, 1996.

[133] H. Jeong and M.S. Kim. Purification of entangled coherent states. *Quant. Inf. Comp.*, 2:208, 2002.

[134] Z.-B. Chen, G. Huou, and Y.-D. Zhang. Quantum nonlocality and applications in quantum information processing of hybrid entangled states. *Phys. Rev. A*, 65:032317, 2002.

[135] S. Devitt. private communication.

[136] C.M. Dawson, H.L. Haselgrove, and M.A. Nielsen. Noise thresholds for optical quantum computers. *Phys. Rev. Lett.*, 96:020501, 2006.

[137] C.M. Dawson, H.L. Haselgrove, and M.A. Nielsen. Noise thresholds for optical cluster-state quantum computation. *Phys. Rev. A*, 73:052306, 2006.

[138] M. Varnava, D.E. Browne, and T. Rudolph. Loss tolerance in one-way quantum computation via counterfactual error correction. *Phys. Rev. Lett.*, 97:120501, 2006.

[139] P.P. Rohde, T.C. Ralph, and W.J. Munro. Error tolerance and trade-offs in loss- and failure-tolerant quantum computing schemes. *Phys. Rev. A*, 75:010302, 2007.

[140] G.D. Hutchinson and G.J. Milburn. Nonlinear quantum optical computing via measurement. *J. Mod. Opt.*, 51:1211, 2004.

[141] S.D. Barrett, P. Kok, K. Nemoto, R.G. Beausoleil, W.J. Munro, and T.P. Spiller. Symmetry analyzer for nondestructive Bell-state detection using weak nonlinearities. *Phys. Rev. A*, 71:060302(R), 2005.

[142] W.J. Munro, K. Nemoto, T.P. Spiller, S.D. Barrett, P. Kok, and R.G. Beausoleil. Efficient optical quantum information processing. *J. Opt. B: Quantum Semiclass. Opt.*, 7:S135, 2005.

[143] W.J. Munro, K. Nemoto, and T.P. Spiller. Weak nonlinearities: A new route to optical quantum computation. *New J. Phys.*, 7:137, 2005.

[144] F. Yamaguchi, K. Nemoto, and W.J. Munro. Quantum error correction via robust probe modes. *Phys. Rev. A*, 73:060302(R), 2006.

[145] S. Bose, P.L. Knight, M.B. Plenio, and V. Vedral. Proposal for teleportation of an atomic state via cavity decay. *Phys. Rev. Lett.*, 83:5158, 1999.

[146] C. Cabrillo, J.I. Cirac, P. Garcia-Fernandez, and P. Zoller. Creation of entangled states of distant atoms by interference. *Phys. Rev. A*, 59:1025, 1999.

[147] X.-L. Feng, Z.-M. Zhang, X.-D. Li, S.-Q. Gong, and Z.-Z. Xu. Entangling distant atoms by interference of polarized photons. *Phys. Rev. Lett*, 90:217902, 2003.

[148] D.E. Browne, M.B. Plenio, and S.F. Huelga. Robust creation of entanglement between ions in spatially separate cavities. *Phys. Rev. Lett.*, 91:067901, 2003.

[149] C. Simon and W.T.M. Irvine. Robust long-distance entanglement and a loophole-free Bell test with ions and photons. *Phys. Rev. Lett.*, 91:110405, 2003.

[150] S.C. Benjamin. Comment on 'efficient high-fidelity quantum computation using matter qubits and linear optics'. *Phys. Rev. A*, 72:056302, 2005.

[151] S.C. Benjamin, J. Eisert, and T.M. Stace. Optical generation of matter qubit graph states. *New J. Phys.*, 7:194, 2005.

[152] J.M. Raimond, M. Brune, and S. Haroche. Manipulating quantum entanglement with atoms and photons in a cavity. *Rev. Mod. Phys.*, 73:565, 2001.

[153] F. Jelezko, T. Gaebel, I. Popa, A. Gruber, and J. Wrachtrup. Observation of coherent oscillations in a single electron spin. *Phys. Rev. Lett.*, 92:076401, 2004.

[154] E. Pazy, E. Biolatti, T. Calarco, I. D'Amico, P. Zanardi, F. Rossi, and P. Zoller. Spin-based optical quantum gates via Pauli blocking in semiconductor quantum dots. *Europhys. Lett.*, 62:175, 2003.

[155] E.S. Polzik, J. Carri, and H.J. Kimble. Spectroscopy with squeezed light. *Phys. Rev. Lett.*, 68:3020, 1992.

[156] L.-M. Duan and R. Raussendorf. Efficient quantum computation with probabilistic quantum gates. *Phys. Rev. Lett.*, 95:080503, 2005.

[157] T.P. Bodiya and L.-M. Duan. Scalable generation of graph-state entanglement through realistic linear optics. *Phys. Rev. Lett.*, 97:143601, 2006.

[158] K. Kieling, D. Gross, and J. Eisert. Minimal resources for linear optical one-way computing. *J. Opt. Soc. Am. B*, 24:184, 2007.

[159] D. Gross, K. Kieling, and J. Eisert. Potential and limits to cluster-state quantum computing using probabilistic gates. *Phys. Rev. A*, 74:042343, 2006.

[160] K. Kieling, T. Rudolph, and J. Eisert. Percolation, renormalization, and quantum computing with non-deterministic gates. *Phys. Rev. Lett.*, 99:130501, 2007.

[161] C. Kruszynska, A. Miyake, H.J.Briegel, and W.Dür. Entanglement purification protocols for all graph states. *Phys. Rev. A*, 74:052316, 2006.

[162] P.P. Rohde, W.J. Munro, T.C. Ralph, P. van Loock, and Kae Nemoto. Practical effects in the preparation of cluster states using weak nonlinearities. *preprint quant-ph/0705.4522*, 2007.

[163] P.P. Rohde and S.D. Barrett. Strategies for the preparation of large cluster states using non-deterministic gates. *New J. Phys.*, 9:198, 2007.

[164] L. Kleinrock. *Queueing Systems. Volume 1: Theory.* Wiley-Interscience, 1975.

[165] R. Van Meter, T. D. Ladd, W.J. Munro, and K. Nemoto. System design for a long-line quantum repeater. *accepted in IEEE/ACM Transactions on Networking, preprint quant-ph/0705.4128*, 2007.

[166] A. Papoulis and S.U. Pillai. *Probability, random variables and stochastic processes.* McGraw-Hill Higher Education, 2002.

[167] C.D. Meyer. *Matrix analysis and applied linear algebra.* Society for Industrial and Applied Mathematics, 2000.

[168] D.D. Thaker, T.S. Metodi, A.W. Cross, I.L. Chuang, and F.T. Chong. Quantum memory hierarchies: Efficient designs to match available parallelism in quantum computing. *ACM Proc. International Symposium on Computer Architecture*, 33:378, 2006.

[169] R. Van Meter and M. Oskin. Architectural implications of quantum computing technologies. *ACM Journal on Emerging Technologies in Computing Systems*, 2(1), 2006.

[170] D. Kielpinksy, C. Monroe, and D.J. Wineland. Architecture for a large-scale ion-trap quantum computer. *Nature*, 417:709, 2002.

[171] J.M. Taylor, H.-A. Engel, W. Dür, A. Yacoby, C.M. Marcus, P. Zoller, and M.D. Lukin. Fault-tolerant architecture for quantum computation using electrically controlled semiconductor spins. *Nat. Phys.*, 1:177, 2005.

[172] L.C.L. Hollenberg, A.D. Greentree, A.G. Fowler, and C.J. Wellard. Two-dimensional architectures for donor-based quantum computing. *Phys. Rev. B*, 74:045311, 2006.

[173] A.J. Skinner, M.E. Davenport, and B.E. Kane. Hydrogenic spin quantum computing in silicon: A digital approach. *Phys. Rev. Lett.*, 90:087901, 2003.

[174] L.-M. Duan, J.I. Cirac, P. Zoller, and E.S. Polzik. Quantum communication between atomic ensembles using coherent light. *Phys. Rev. Lett.*, 85:5643, 2000.

[175] D.K.L. Oi, S.J. Devitt, and L.C.L. Hollenberg. Scalable error correction in distributed ion trap computers. *Phys. Rev. A.*, 74:052313, 2006.

[176] S. Bose. Quantum communication through an unmodulated spin chain. *Phys. Rev. Lett.*, 91:207901, 2003.

[177] S. Lloyd. Power of entanglement in quantum communication. *Phys. Rev. Lett.*, 90:167902, 2003.

[178] M. Friesen, A. Biswas, X. Hu, and D. Lidar. Efficient multiqubit entanglement via a spin bus. *Phys. Rev. Lett.*, 98:230503, 2007.

[179] R. Van Meter, K. Nemoto, and W.J. Munro. Communication links for distributed quantum computation. *IEEE Transactions on Computers*, 56:1643, 2007.

[180] A.D. Greentree, S.G. Schirmer, F. Green, L.C.L. Hollenberg, A.R. Hamilton, and R.G. Clark. Maximizing the Hilbert space for a finite number of distinguishable quantum states. *Phys. Rev. Lett.*, 92:097901, 2004.

[181] S.J. Devitt, S.G. Schirmer, D.K.L. Oi, J.H. Cole, and L.C.L. Hollenberg. Subspace confinement: How good is your qubit? *New J. Phys.*, 9:384, 2007.

[182] S.D. Bartlett, H. de Guis, and B.C. Sanders. Quantum encodings in spin systems and harmonic oscillators. *Phys. Rev. A*, 65:052316, 2002.

[183] J. Daboul, X. Wang, and B.C. Sanders. Quantum gates on hybrid qudits. *J. Phys. A: Math. Gen.*, 36(14):2525, 2003.

[184] D.P. O'Leary, G.K. Brennen, and S.S. Bullock. Parallelism for quantum computation with qudits. *Phys. Rev. A*, 74:032334, 2006.

[185] X.-H. Li, F.-G. Deng, and H.-Y. Zhou. Controlled teleportation of an arbitrary multi-qudit state in a general form with d-dimensional Greenberger-Horne-Zeilinger states. *Chin. Phys. Lett.*, 24:1151, 2007.

[186] D.Mc Hugh and J. Twamley. Trapped-ion qutrit spin molecule quantum computer. *New J. Phys.*, 7:174, 2005.

[187] T.C. Ralph, K.J. Resch, and A. Gilchrist. Efficient toffoli gates using qudits. *Phys. Rev. A*, 75:022313, 2007.

[188] P.H.E. Meijer. *Group Theory, The Application to Quantum Mechanics.* North-Holland Publishing, 1962.

[189] P.R. de Montmort. Essai d'analyse sur les jeux de hasard. *Paris*, 1708.

[190] L. Clarisse, S. Ghosh, S. Severini, and A. Sudbery. Entangling power of permutations. *Phys. Rev. A*, 72:012314, 2005.

[191] D. Gottesman. Fault-tolerant quantum computation with higher-dimensional systems. *Chaos, Solitons and Fractals*, 10:1749, 1999.

[192] K. Vogel M. Freyberger and W.P. Schleich. From photon counts to quantum phase. *Phys. Lett. A*, 176:41, 1993.

[193] A. Chefles and S.M. Barnett. Optimum unambiguous discrimination between linearly independent symmetric states. *Phys. Lett. A*, 250:223, 1998.

[194] S.J. van Enk. Unambiguous state discrimination of coherent states with linear optics: Application to quantum cryptography. *Phys. Rev. A*, 66:042313, 2002.